Analytical modelling of the water block phenomenon in oil and gas wells

THE UNIVERSITY of ADELAIDE

Saurabh Naik
Australian School of Petroleum
University of Adelaide

August, 2019

A thesis submitted for the degree of Doctor of Philosophy

To my parents for their continual patience and support
and my dearest twin brother, for always understanding.

Contents

Abstract

In oil or gas production wells, water can become trapped by capillary forces in the reservoir rock near to the wellbore or hydraulic fracture face. The trapped water dramatically reduces the production rate of oil or gas. The general term for wells suffering from productivity loss due to capillary trapped water is "water block". The severity of the water block is the result of the combined effects of wettability, capillary forces, viscous forces, fluid compressibility, hydraulic fracture length and various other reservoir and well properties. A numerical model can be used to evaluate all the effects for particular scenarios. However, for most oil or gas reservoirs, there is great uncertainty in many of the reservoir parameters. Evaluating enough scenarios numerically to account for all the uncertainty can be extremely time-consuming. Analysing the sensitivity to uncertain parameters is substantially faster and better served by analytical models. Historically, the impact of the end effects in production wells have been neglected in analytical models as the target reservoirs have generally had high permeability. Now, the development of petroleum fields involves targeting much lower permeability reservoirs. These reservoirs can exhibit high capillary pressures. Despite the significant capillary pressure effects, analytical models have yet to be developed for gas or oil well performance accounting for capillary end effects.

The goal of this thesis is to develop analytical models to include the effects of capillary forces near to the wellbore or the hydraulic fracture and to analyse the impact of fluid compressibility, wettability, capillary forces, viscous forces, porous media network characteristics and hydraulic fracture half-length. This thesis includes five journal papers, four of which have been published; the last one finished with intention to submit later this year. The thesis develops new analytical models to calculate the productivity index of gas wells. The new models account for viscous forces, capillary forces, inertial forces, wettability, compressibility, non-uniform flow into hydraulic fractures and capillary end effects near to the wellbore or hydraulic fracture. The analytical models are validated through matching with experimental data or numerical simulators. The forms of the capillary pressure and relative permeability curves are extremely important properties of the reservoir which impact the magnitude of the capillary end effect. The shape of the curves is significantly impacted by the characteristics of the pore network. A sophisticated mixed percolation model coupled

with effective medium theory is developed in the thesis. The novelty of the new percolation model is that it applies mixed bond-site percolation for the first time to the water-hydrocarbon drainage problem, while only bond or site percolation was applied in previous models. This thesis integrates the complex interaction between the viscous, capillary and inertial forces, water cut, hydraulic fracture length and the topology of the pore network. The study quantifies the impact of each of the aforementioned characteristics of two phase flow on the productivity of gas wells. The results of this thesis are critical in screening for economic well candidates for intervention.

Declaration

I certify that this work contains no material which has been accepted for the award of any other degree or diploma in my name, in any university or other tertiary institution and, to the best of my knowledge and belief, contains no material previously published or written by another person, except where due reference has been made in the text. In addition, I certify that no part of this work will, in the future, be used in a submission in my name, for any other degree or diploma in any university or other tertiary institution without the prior approval of the University of Adelaide and where applicable, any partner institution responsible for the joint-award of this degree. I acknowledge that copyright of published works contained within this thesis resides with the copyright holder(s) of those works. I also give permission for the digital version of my thesis to be made available on the web, via the University's digital research repository, the Library Search and also through web search engines, unless permission has been granted by the University to restrict access for a period of time. I acknowledge the support I have received for my research through the provision of an Australian Government Research Training Program Scholarship.

_____ _____

Candidate Signature Date

Acknowledgements

First and foremost, I would like to thank Professor Pavel Bedrikovetsky for providing me the opportunity to undertake this PhD. It has provided many valuable life lessons. During my time as a student I have developed substantially, and I am truly grateful to all the people I have met. This thesis would have been impossible to complete without them.

Developing my self-confidence has been a critical aspect which has allowed me to complete this thesis. I would like to thank my friend Dmitry, you taught me to truly value myself. You were the catalyst for a lot of the decisions I made after my trip to America, and I don't regret any of them. Thank you Matthew Woolley and David Marques, for being my mentor and teaching me to trust my technical capabilities and judgement. After working under you I feel more capable as an engineer and less like a student.

Thank you to all my fellow PhD students, Abdullah, Gabriel, Jack, Larissa, Maria, Mike, Sara, Shuyan, Tamineh, Thomas, Yulong. You were there to share all the difficulties of a PhD with. Thank you to all my friends from CDW, Cody, Josh, Ben, Kieran and Duncan. Drawing and painting was my first passion and it was difficult finding other people I connected with. I appreciate all the time we spent together and I look forward to much more.

Thank you to Bethany, Marija, Deanna and the voice house team for pushing me out of my comfort zone, and developing my confidence. Big thank you to all my dance teachers, Simon, Bermata, Sean, Bianca and Veronica. Dance has become one of the best additions to my life. It has no doubt positively impacted the way I interact with people, at the university, at work, and every other aspect of my life. Thank you to Ameen for founding and running the Adelaide University Salsa Mania Club. It has made me truly enjoy my time on campus and been one of the best social aspects during my time at the university.

Thank you to Mark O'Donoghue, for hosting your weekly meditation seminars and thank you Simon Holford and Kathryn Amos for your guidance and support throughout the turbulent later stage of my study. There were stressful periods that you helped me get through.

I have sincere gratitude towards Dr. Zhenjiang You, for always being available to talk to about my PhD. For all the time you spent carefully poring over my work. It was truly a blessing to have you as one of my supervisors. Thank you Kirill Gerke, for your contribution and collaboration. It was easy to work with you.

Thank you to my loving parents Neeta and Sunil, for supporting me while I undertook this long and difficult process. And lastly, I would like to thank my twin brother Kaustubh. For always being there and always being honest. Right from the beginning to the end, through all the ups and downs. You were always someone I could talk to, no matter the problem big or small.

Thesis by publication

Naik, S., You, Z. and Bedrikovetsky, P., 2015. Rate enhancement in unconventional gas reservoirs by wettability alteration. Journal of Natural Gas Science and Engineering, 26, pp.1573-1584.

Naik, S., You, Z. and Bedrikovetsky, P., 2015, November. Effect of Wettability Alteration on Productivity Enhancement in Unconventional Gas Reservoirs: Application of Nanotechnology. In SPE Asia Pacific Unconventional Resources Conference and Exhibition. Society of Petroleum Engineers.

Naik, S., You, Z. and Bedrikovetsky, P., 2016, October. Prevention of water-blocking formation damage in gas reservoirs wettability alteration, analytical modelling. In SPE Asia Pacific Oil & Gas Conference and Exhibition. Society of Petroleum Engineers.

Naik, S., You, Z. and Bedrikovetsky, P., 2018. Productivity index enhancement by wettability alteration in two-phase compressible flows. Journal of Natural Gas Science and Engineering, 50, pp.101-114.

Naik, S., Malgaresi, G., You, Z. and Bedrikovetsky, P., 2018. Well productivity enhancement by applying nanofluids for wettability alteration. The APPEA Journal, 58(1), pp.121-129.

Naik, S., Yang, S., Woolley, M. and Bedrikovetsky, P., 2019. Analytical modelling of the water block phenomenon in hydraulically fractured wells. Journal of Natural Gas Science and Engineering, 67, pp.56-70.

Naik, S., Gerke, K., You, Z., Bedrikovetsky, P., 2019. Application of Percolation theory, Critical Path Theory and Effective Medium Theory for calculation of two phase relative permeability. (To be submitted).

1. Contextual statement

1.1. Research background and rationale

The operation of drilling into a new formation, completing the wellbore and hydraulic fracturing can introduce non-native water into the reservoir. Generally, there is an attempt to produce back this introduced water. However, not all the water can be recovered. Simulation modelling results by Bahrami et al. (2012) and Li et al. (2014) and laboratory studies by Bazin et al. (2010), Kamath and Laroche (2003) and Mahadevan et al. (2009) show that the unrecovered water is trapped by capillary forces and that the trapped water impedes gas flow.

The behaviour of capillary trapped water has been replicated numerous times in the laboratory during two phase core flooding (Huang and Honarpour, 1998; Kyte and Rapoport, 1958; Pini and Benson, 2013; Richardson et al., 1952; Virnovsky et al., 1995), particularly when the core samples have low permeability. The build-up of water is caused by the capillary pressure difference between the core pore network and the core outlet. It is referred to as the capillary end effect. The capillary trapped water forms films over the pore throats and consequently impedes flow to the gas or oil phase.

Capillary end effects can occur in production wells as the capillary pressures are significantly lower in the wellbore than that in the reservoir. For reservoirs with low permeability and high capillary forces, flow impedance can become significant and the well can become "water blocked". Remediation may be required. A common technique for remediation is the application of some chemical for wettability alteration near to the wellbore.

There are numerous publications on the laboratory application of nano-fluids or surfactants and the impact they have on parameters such as interfacial tension or contact angle (Adibhatla et al., 2006; Al-Anazi et al. 2007; Alvarez et al, 2014; Bang et al., 2009; Bryant et al., 2006; Esmaeilzadeh et al., 2015; Giraldo et al., 2013; Karimi et al., 2012; Kathel and Mohanty, 2013; Li and Firoozabadi, 2000; Li and Torsaeter, 2015; Roustaei et al., 2012; Wu and Firoozabadi, 2010; Xie et al., 2009).

However, there is poor translation of this information to the final impact on the performance of the well. The laboratory studies all show some improvement in

gas flow performance for the conditions of the lab test. There is no proper model to apply the result of the laboratory test to calculate well productivity under reservoir conditions.

Xie et al. (2009) perform laboratory tests to quantify permeability increase as a result of surfactant application in core floods. Their results indicate that there could be 56% increase in gas deliverability through application of some surfactant. However their field trials on three gas storage wells, as published in Weiss and Xie (2009), failed to replicate the result. Two of these three wells produced around 33% increase in rate and one failed to show any improvement. Their method of calculating increase gas production rate in the well was multiplying the well rate by the ratio of permeability increase measured in the laboratory.

The magnitude of water block before and after chemical treatment will depend on various properties of the reservoir, the reservoir fluid, the well, the hydraulic fracture and the chemical treatment. Paterniti (2009) did a field trial of a micro emulsion (ME) additive surfactant on 34 wells and non-emulsifier (NE) surfactant on 32 wells. They split results in 3 groups: low Gas oil ratio (GOR), medium GOR and high GOR. They observed that the ME surfactant caused 38% more gas rate for the low GOR group, 11% less gas in the medium GOR group and 1% less gas in the high GOR group.

None of the few published case studies report how to calculate the expected incremental rate incorporating reservoir conditions. The variability in reservoir conditions and lack of available models can cause a wide range of unexpected results in field trials. Eakin et al. (1965) performed field tests of alcohol-surfactant treatments on 20 gas producing and storage wells. The highest improvement observed was 6.1 times increase in gas flow rate, and the worst cases reduced gas production rate by 50%.

Some of the most important properties of the reservoir are the forms of the relative permeability and capillary pressure curves. The curves are linked, and simultaneously affected by changes in pore scale wettability. There are no studies presented in the literature that take into account of this link when studying capillary end effects and water block.

Numerical models can be applied to account for all the combined effects at play, however they are computationally intensive and time consuming. On top of this

there is wide uncertainty in many of the reservoir characteristics. Time limitation can restrict the number of scenarios and sensitivities that can be analysed.

Due to these limitations, analytical models are preferred. Analytical models are faster, and the analysis is free from numerical errors. At the commencement of this research project, there were no analytical models that took into account of the effects of wettability, capillary forces, viscous forces, inertial forces, water cut and flow convergence around hydraulic fractures on the capillary end effect.

This research project aims to fulfil this research gap, by providing analytical models for the water block phenomenon. These models can be used for evaluating performance loss due to water-block and analyse the sensitivity of formation damage to the properties of the reservoir, the reservoir fluid, the well, the hydraulic fracture and the chemical treatment.

1.2. Research objectives

The main objective of this research is a systematic study of the effect of wettability, piecewise wettability alteration, water cut, capillary forces, viscous forces, inertial forces, compressibility and fracture half-length on the hydraulic resistance to hydrocarbon flow during the production of water and oil or water and gas. This is achieved by:

1. Deriving explicit formulae for two phase incompressible flow accounting for capillary end effects, water cut, capillary forces, viscous forces and piecewise wettability alteration.
2. Deriving explicit formulae for two phase compressible flow accounting for capillary end effects, water cut, capillary forces, viscous forces and piecewise wettability alteration.
3. Calculating the sensitivity of the productivity of a well to wettability, piecewise wettability alteration, compressibility, water cut, capillary forces and viscous forces.
4. Deriving explicit formulae for two phase compressible Darcy flow accounting for non-uniform flow convergence around a hydraulic fracture and capillary end effects.
5. Deriving formulae for two phase compressible non-Darcy flow accounting for non-uniform flow convergence around a hydraulic fracture and capillary end effects.
6. Calculating the sensitivity of the model for hydraulic fractures to capillary, viscous and inertial forces.
7. Developing a percolation model for the calculation of relative permeability and capillary pressure curves which accounts for average pore-network coordination number.
8. Practical application of the models derived for evaluation of water-block in a hydraulically fractured production well.

1.3. Thesis structure

This is a PhD thesis by publication. The thesis body is formed by seven chapters, four of which are made up of journal papers.

Chapter one provides the structure of the thesis and how each publication fulfils the objectives of the thesis.

Chapter two reviews the literature on the water block phenomenon, and the models developed so far for two phase flow in porous media and calculation of relative permeability and capillary pressure.

The third to sixth chapters are the novel parts of the thesis and are made up of five journal papers and two conference papers. Four papers have been published in peer reviewed journals. The final paper has been finished with the intention to submit to a journal at a later date. The PhD candidate is the first author in all abovementioned papers. The title of each paper, its corresponding chapter and its status is given in the following table:

Chapter	Title of paper	Status
3	Rate enhancement in unconventional gas reservoirs by wettability alteration	Published
	Effect of Wettability Alteration on Productivity Enhancement in Unconventional Gas Reservoirs: Application of Nanotechnology.	Published
4	Productivity index enhancement by wettability alteration in two-phase compressible flows	Published
	Well productivity enhancement by applying nanofluids for wettability alteration	Published
	Prevention of water-blocking formation damage in gas reservoirs wettability alteration, analytical modelling.	Published
5	Analytical modelling of the water block phenomenon in hydraulically fractured wells	Published
6	Application of Percolation theory, Critical Path Theory and Effective Medium Theory for calculation of two phase relative permeability	To be submitted

Chapter three includes the derivation, validation, and applications of the first analytical model. The first analytical model is for two-phase incompressible flow accounting for capillary end effects at the wellbore and core outlet. The model is

applied to calculate the sensitivity of well productivity index to the capillary-viscous ratio, macroscopic contact angle and for the proportion of piecewise altered wettability.

Chapter four includes the derivation, validation, and applications of the second analytical model. The second model is for two-phase compressible flow accounting for capillary end effects at the wellbore and core outlet. The model is applied for a comparison against the results of the first model, for calculation of sensitivity to water cut, for calculation of the impact of initial reservoir wettability on the impact of piecewise wettability alteration and for tuning of production data from two gas storage wells.

Chapter five includes the derivation, validation, and applications of the third and fourth analytical model. The third analytical model is for two-phase compressible Darcy flow accounting for capillary end effects and convergence of flow towards a hydraulic fracture face. The fourth analytical model includes non-Darcy flow effects. The sensitivity of the water block skin to parameters of the leveret J function and the capillary, viscous and inertial forces is investigated. The analytical model is applied for evaluation of water-block skin in a hydraulically fractured production well.

Chapter six includes the derivation, validation, and applications of the percolation model. The model is for two phase immiscible primary drainage. The pore network is modelled as a 3-D site-bond network. It is applied to calculate the capillary pressure curves during primary drainage. Effective medium theory and critical path theory are applied for calculation of the relative permeability curves, and their validity is tested via comparison against a numerical pore network simulator.

Chapter seven provides the summary of the results, the limitations of the thesis and the future outlook of research in this area.

Chapter eight provides the overall significance of the project, the novel contributions to the literature and conclusions of the thesis.

1.4. How the publications fulfil the aims of the thesis

The first paper, titled "Rate enhancement in unconventional gas reservoirs by wettability alteration" derives an analytical model for steady-state two-phase incompressible flow into a vertical well or through a core. The model accounts for wettability via a macroscopic contact angle and water block by including capillary end

effects at the core outlet and wellbore. The model is validated by tuning to core flooding data. The second paper, titled "Effect of Wettability Alteration on Productivity Enhancement in Unconventional Gas Reservoirs: Application of Nanotechnology" presents application of the model derived in the first paper. The derived model is applied in the first and second paper to calculate the effect of wettability alteration on the water-block phenomenon during two phase immiscible flow, and the effect of piecewise alteration of wettability under various ratios of capillary to viscous forces in the first and second paper. The first and second paper fulfil aim 1 and partly fulfil aim 3.

The third paper, titled "Productivity index enhancement by wettability alteration in two-phase compressible flows" derives a second analytical model which accounts for all the effects in the first model, but additionally accounts for compressibility. The model is validated by tuning to core flood data. The paper studies how gas compressibility affects the water block phenomenon, and is applied to tune production data from two gas storage wells. The third paper fulfils aim 2 and partly fulfils aim 3.

The fourth paper, titled "Well productivity enhancement by applying nano-fluids for wettability alteration" applies the model developed in the second paper to investigate the impact of water cut and initial wettability of the porous media.

The fifth paper, titled "Prevention of water-blocking formation damage in gas reservoirs wettability alteration" applies the model derived in the third paper for calculation of sensitivity of well productivity index to capillary viscous ratio and piecewise contact angle alteration. The first, second, third, fourth and fifth papers fulfil aim 3.

The sixth paper, titled "Analytical modelling of the water block phenomenon in hydraulically fractured wells" develops a model for Darcy and a model for non-Darcy flow, both accounting for capillary end effects and convergence of flow lines around a hydraulic fracture. Both models are validated by comparison to a numerical simulator. The paper provides a combined study of the inertial, capillary and viscous forces and determines the most important characteristics of the reservoir which impact water block. The non-Darcy model is applied for evaluation of water block in a hydraulically fractured well. The sixth paper fulfils aims 4 to 6 and 8.

The seventh paper, titled "Application of Percolation theory, Critical Path Theory and Effective Medium Theory for calculation of two phase relative permeability" develops a percolation model for calculation of capillary pressure and relative permeability curves, which are integral inputs for the models developed in the previous papers. The model is validated via comparison to a pore network simulator. The validity of effective medium and critical path theory in calculation of relative permeability are discussed. The seventh paper fulfils aim 7.

1.5. Scientific novelty

Four new analytical models have been developed. The first model is for two-phase incompressible immiscible flow and the second model is for two-phase immiscible flow, where one phase is compressible. The first and second models combine the effect of wettability alteration on relative permeability and capillary pressure and for the first time show the existence of an optimal contact angle for well productivity during two phase flow. The impacts of capillary forces, viscous forces, compressibility, water-cut and depth of wettability alteration on the optimal contact angle are presented in the first three papers.

The third and fourth models are the first analytical solutions for calculation of skin as a result of water block for hydraulically fractured gas and oil wells. The third model is for Darcy flow into a hydraulic fracture and the fourth is for non-Darcy flow. The solution for skin allows for screening of well candidates for chemical treatment opportunities.

The thesis also presents for the first time the method of applying mixed site-bond percolation coupled with effective medium theory for the calculation of capillary pressure and relative permeability during drainage. There have been a few publications on the application of effective medium theory for calculation of relative permeability with varying degrees of success. The comparison against the pore network simulator allows for a direct validation of the utility of effective medium theory and of critical path theory.

1.6. References for the contextual statement

Adibhatla, B., Mohanty, K.K., Berger, P. and Lee, C., 2006. Effect of surfactants on wettability of near-wellbore regions of gas reservoirs. Journal of petroleum science and engineering, 52(1-4), pp.227-236.

Al-Anazi, H.A., Xiao, J., Al-Eidan, A.A., Buhidma, I.M., Ahmed, M.S., Al-Faifi, M. and Assiri, W.J., 2007, January. Gas productivity enhancement by wettability alteration of gas-condensate reservoirs. In European Formation Damage Conference. Society of Petroleum Engineers.

Alvarez, J.O., Neog, A., Jais, A. and Schechter, D.S., 2014, April. Impact of surfactants for wettability alteration in stimulation fluids and the potential for surfactant EOR in unconventional liquid reservoirs. In SPE Unconventional Resources Conference. Society of Petroleum Engineers.

Bahrami, H., Rezaee, R. and Clennell, B., 2012. Water blocking damage in hydraulically fractured tight sand gas reservoirs: An example from Perth Basin, Western Australia. Journal of Petroleum Science and Engineering, 88, pp.100-106.

Bang, V.S.S., Pope, G.A., Sharma, M.M. and Baran Jr, J.R., 2009, January. Development of a successful chemical treatment for gas wells with liquid blocking. In SPE Annual Technical Conference and Exhibition. Society of Petroleum Engineers.

Bazin, B., Peysson, Y., Lamy, F., Martin, F., Aubry, E. and Chapuis, C., 2010. In situ water-blocking measurements and interpretation related to fracturing operations in tight gas reservoirs. SPE Production & Operations, 25(04), pp.431-437.

Bryant, E.M., Bowman, R.S. and Buckley, J.S., 2006. Wetting alteration of mica surfaces with polyethoxylated amine surfactants. Journal of Petroleum Science and Engineering, 52(1-4), pp.244-252.

Eakin, J.L., Miller, J.S. and Eckard, W.E., 1965, January. Removal of Water Blocks from Gas-producing Formations. In Drilling and Production Practice. American Petroleum Institute, pp.26-39.

Esmaeilzadeh, P., Sadeghi, M.T., Fakhroueian, Z., Bahramian, A. and Norouzbeigi, R., 2015. Wettability alteration of carbonate rocks from liquid-wetting to ultra gas-wetting using TiO2, SiO2 and CNT nanofluids containing fluorochemicals, for enhanced gas recovery. Journal of Natural Gas Science and Engineering, 26, pp.1294-1305.

Giraldo, J., Benjumea, P., Lopera, S., Cortés, F.B. and Ruiz, M.A., 2013. Wettability alteration of sandstone cores by alumina-based nanofluids. Energy & Fuels, 27(7), pp.3659-3665.

Huang, D.D. and Honarpour, M.M., 1998. Capillary end effects in coreflood calculations. Journal of Petroleum Science and Engineering, 19(1-2), pp.103-117.

Kamath, J., and Laroche, C., 2003. Laboratory-based evaluation of gas well deliverability loss caused by water blocking. SPE Journal, 8(01), pp.71-80.

Karimi, A., Fakhroueian, Z., Bahramian, A., Pour Khiabani, N., Darabad, J.B., Azin, R. and Arya, S., 2012. Wettability alteration in carbonates using zirconium oxide nanofluids: EOR implications. Energy & Fuels, 26(2), pp.1028-1036.

Kathel, P. and Mohanty, K.K., 2013. Wettability alteration in a tight oil reservoir. Energy & Fuels, 27(11), pp.6460-6468.

Kyte, J.R. and Rapoport, L.A., 1958. Linear waterflood behavior and end effects in water-wet porous media. Journal of Petroleum Technology, 10(10), pp.47-50.

Li, G., Ren, W., Meng, Y., Wang, C. and Wei, N., 2014. Micro-flow kinetics research on water invasion in tight sandstone reservoirs. Journal of Natural Gas Science and Engineering, 20, pp.184-191.

Li, K. and Firoozabadi, A., 2000. Experimental study of wettability alteration to preferential gas-wetting in porous media and its effects. SPE Reservoir Evaluation & Engineering, 3(02), pp.139-149.

Li, S. and Torsaeter, O., 2015, January. The impact of nanoparticles adsorption and transport on wettability alteration of intermediate wet berea sandstone. In SPE Middle East Unconventional Resources Conference and Exhibition. Society of Petroleum Engineers.

Mahadevan, J., Le, D.H. and Hoang, H.N., 2009, January. Impact of capillary suction on fracture face skin evolution in waterblocked wells. In SPE Hydraulic Fracturing Technology Conference. Society of Petroleum Engineers.

Paterniti, M.L., 2009, January. Microemulsion surfactant increases production in the codell formation of the DJ basin. In SPE Rocky Mountain Petroleum Technology Conference. Society of Petroleum Engineers.

Pini, R. and Benson, S.M., 2013. Simultaneous determination of capillary pressure and relative permeability curves from core ‐ flooding experiments with various fluid pairs. Water Resources Research, 49(6), pp.3516-3530.

Richardson, J.G., Kerver, J.K., Hafford, J.A. and Osoba, J.S., 1952. Laboratory determination of relative permeability. Journal of Petroleum Technology, 4(08), pp.187-196.

Roustaei, A., Moghadasi, J., Bagherzadeh, H. and Shahrabadi, A., 2012, January. An experimental investigation of polysilicon nanoparticles' recovery efficiencies through changes in interfacial tension and wettability alteration. In SPE international oilfield nanotechnology conference and exhibition. Society of Petroleum Engineers.

Virnovsky, G.A., Skjaeveland, S.M., Surdal, J. and Ingsoy, P., 1995, January. Steady-state relative permeability measurements corrected for capillary effects. In SPE Annual Technical Conference and Exhibition. Society of Petroleum Engineers.

Weiss, W.W. and Xie, X., 2009, January. Field test of wettability alteration to increase the flow rate from aquifer gas storage wells. In SPE Eastern Regional Meeting. Society of Petroleum Engineers.

Wu, S. and Firoozabadi, A., 2010. Permanent alteration of porous media wettability from liquid-wetting to intermediate gas-wetting. Transport in Porous Media, 85(1), pp.189-213.

Xie, X., Liu, Y., Sharma, M. and Weiss, W.W., 2009. Wettability alteration to increase deliverability of gas production wells. Journal of Natural Gas Science and Engineering, 1(1-2), pp.39-45.

2. Literature review

This thesis mainly focuses on the forces at play during flow from the reservoir into the wellbore. In particular it investigates how the flow rate is impacted by the presence of water which is trapped by capillary forces near to the wellbore. When this capillary-trapped water greatly reduces gas rate, it is referred to as "water-block".

This literature review will start with a review of the studies which cover the physical forces at play that cause the formation of water block and the remediation strategies published so far. Based on this we investigate the models which have been applied so far to take into account of water-block and their limitations. The literature review will then overview possible strategies published so far which can be applied to overcome these weaknesses.

What is discovered is that forms of the relative permeability and capillary pressure curves are of pivotal importance. Models used to calculate these curves in the literature, are also investigated. The drawbacks of the models and methods for improvement are discussed.

2.1. Formation of water block

This section covers the laboratory and numerical studies which show the formation of water block. This section also covers the explanation of the physical aspects which cause water block to occur.

2.1.1. Capillary end effects

During steady flow from the reservoir into the wellbore, there will be continuity in the pressure of the fluid between the reservoir and the wellbore. If there is steady flow of two phases, both phases will have pressure continuity. Therefore, capillary pressure will also have continuity between the reservoir and the wellbore. As the wellbore pipe has substantially higher diameter than the pore space of the reservoir, the capillary pressure in the wellbore is comparatively negligible. The continuity of capillary pressure causes the capillary pressure inside the reservoir pore space to be negligible at the location where the reservoir rock meets the wellbore. Far from the wellbore, the capillary pressure can be substantially higher. For this reason, there can be a decrease in capillary pressure in the reservoir pore space, as we approach the wellbore. This in turn will influence the water saturation.

This effect has been documented several times in laboratory core floods after steady state is reached. Richardson et al. (1952) determined the saturation profiles by weighing different segments of a core after steady state was reached. Graue (1994) applied nuclear imaging techniques to measure in situ-saturation profiles. Both authors observed increases in water saturation at the core outlet. The theoretical explanation given by Kyte and Rapoport, (1958) is as follows: During water-oil or water-gas core flooding of water wet porous media, the capillary pressure at the outlet is negligible. Water will build up at the core outlet until the water pressure is equal to the other phase pressure. When this occurs, water can flow through the outlet. This increase in water saturation at the outlet as a result of capillary pressure reduction is commonly called the "capillary end effect".

This effect can cause errors in core flood evaluation of relative permeability–saturation relationships if not accounted for. The increase in water saturation impedes gas flow and causes an increase in the pressure drop. Gupta and Maloney (2015) observed the extra pressure drop in laboratory corefloods and provide the mathematical technique to calculate relative permeability accounting for the extra pressure drop due to capillary end effects at low flow rates.

The water saturation at the outlet of a core is determined from the capillary forces. However, the saturation determined by viscous forces can be different from the outlet saturation. The competition between viscous and capillary forces determines the size of the capillary end effect. At high rates, when the viscous forces are significant, the capillary end effect can be negligible. Osoba et al. (1951) performed laboratory tests which showed that relative permeability curve measurements had errors caused by end-effects at low rates, but they are negligible at high rates. Rapoport and Leas (1953) showed in various laboratory tests that the remaining saturation in the core tended to a constant at high rates.

Holditch (1979) used a numerical simulator to show that if the pressure drop between the reservoir and the wellbore was not high enough to overcome the capillary end effect, the complete water block can occur. For this reason, depleted reservoirs are more susceptible to water block.

In porous media with low permeability, the difference in capillary pressure inside the porous media and at the outlet or wellbore can be substantial. Therefore,

low permeability gas reservoirs are more likely to be water blocked than high permeability reservoirs.

2.1.2. Drilling, completion and fracturing fluid loss

There are numerous sources for the water which makes up the capillary end effect or water block. On top of any water already present in the reservoir there can be fluid loss from the drilling, fracturing or completion operations. Bahrami et al. (2012) conduct a numerical simulation study that shows significant permeability can be lost due to leak-off water becoming trapped. They also conclude that even during gas production water can seep from the wellbore into the reservoir. During shut in, water produced from other formations can imbibe from the wellbore into the reservoir. Al-Anazi et al. (2005) measured the permeability reduction in cores before and after the injection of completion fluids. They observed that productivity of the core can reduce by more than 50% unless some chemical treatment is applied. For this reason control of any leak-off fluid is essential.

Yang et al. (2016) conducted a systematic experimental study on imbibition rates on sandstone, volcanic and shale cores. They observed that clay content in unconventional rocks also played an important role in the water imbibition process. The imbibition of water into these rocks will increase with the concentration of smectite/illite or smectite clays.

Of the water sources, hydraulic fracturing is a key concern. Particularly, because low permeability reservoirs are commonly hydraulically fractured. The typical hydraulic fracturing operation involves pumping fracturing fluid (primarily water) into the reservoir at a high enough pressure to fracture the rock. This high pressure combined with the capillary suction of the reservoir can cause substantial fracturing fluid to seep into the reservoir.

Li et al. (2014) used a numerical model to show that the invasion of fluid into the reservoir was greatly affected by the wettability. Control over wettability will not only benefit long term steady state production, but can also ensure prevention of the water block in the early stage.

2.2. Water block remediation

This section covers the strategies published in literature for the remediation of water block. It covers the techniques and technologies already applied in industry as well as technologies which are in development for future application.

It is undesirable for the introduced fluid to remain near the wellbore or fracture face, as it will cause water block. After the fracture operation is complete, there are two operations that can be done to aid in removal of the water from the near fracture face region. The operations are to flow the fracturing fluid back or to shut the well in. During the shut-in period the fracturing fluid can imbibe into the reservoir and spread away from the fracture.

Odumabo and Karpyn (2014) performed experimental tests to determine the impacts of extended shut-in time. They measured saturation distributions using X-ray CT imaging and permeability over a period of 48 hours after a pulse of water was injected into a core. They concluded that the benefit of extended shut-in periods were determined by formation properties such as the relative permeability curve. However, there may be some drawbacks to extended shut-in times. Ghanbari and Dehghanpour (2016) analysed field data for an 18 well pad and performed a simulation study. They reported that extending shut-in time before flow back increased early gas production, but significantly reduced fracturing fluid recovery. Sharma and Agrawal (2013) performed numerical simulations to show that the productivity recovery time increased with depth of fracturing fluid leak-off, and the peak productivity can be harmed by waiting too long for flow back and increasing fluid leak-off. Parekh and Sharma (2004) showed in their numerical simulations that shorter shut-in time can increase late time production, yield higher fracturing fluid and total gas recovery.

If the fracturing fluid is produced back, there will be two mechanisms at work which remove the water. Bazin et al. (2010) measured water saturation using X-ray scanning in cores during two phase flow. They observed that the first mechanism is viscous displacement and the second mechanism is evaporation. Kamath and Laroche (2003) came to the same conclusion by measuring liquid expelled, gas flow rate and change of weight in cores during two-phase core flooding. They observed that the displacement period can last a couple of weeks while the evaporation phase lasted for

several months. Bazin et al. (2010) showed in laboratory results that alcohol can enhance the evaporative effect.

The chemical remediation strategies for minimising water block can involve a combination of interfacial tension reduction, wettability alteration and application of alcohols, as shown in field case trials by Weiss and Xie (2009) and Penny et al. (1983). For the case where the reservoir is not dry or there is water seeping from the wellbore into the reservoir, wettability alteration can be the permanent solution. Anderson (1987a) performed a literature review on the impact of wettability on capillary pressure curves. His investigation into numerous laboratory measured capillary pressure curves showed that for intermediate wettability, the capillary pressure curve was closer to zero. This indicates there is potential that if the porous media is altered towards an intermediate wettability, the deviation in capillary pressure between the porous media and the wellbore is smaller, which will cause a smaller saturation deviation at the wellbore.

Altering wettability to more gas-wet will reduce the water block effect. However, there is a drawback. Anderson (1987b) performed a literature review on the impact of wettability on relative permeability. Over multiple laboratory cases they observed that altering wettability to the hydrocarbon phase reduced the relative permeability to the hydrocarbon phase. The two competitive effects imply that there may exist some optimal contact angle.

There are multiple ways to alter wettability, but the most commonly used is surfactants. The primary function of a surfactant is to reduce interfacial tension and/or alter wettability. Numerous types of surfactants have been tested for wettability alteration in the laboratory setting. Some includes fluoro-surfactants (Bang et al., 2009; Torres et al., 2010; Al-Anazi et al. 2007), fluorinated polymers (Wu and Firoozabadi, 2010), amine surfactants (Bryant et al., 2006), cationic surfactants (Li and Firoozabadi, 2000) and anionic surfactants (Kathel and Mohanty, 2013; Alvarez et al, 2014).

Nanoparticles ranging from Al_2O_3 (Giraldo et al., 2013), SiO_2 (Al-Anssari et al., 2016; Ju and Fan, 2009, 2013; Roustaei et al., 2012; Li and Torsaeter, 2015), TiO_2 (Esmaeilzadeh et al., 2015) and ZrO_2 (Karimi et al., 2012) have also been applied for wettability alteration in the laboratory setting. Many experimental studies have been

conducted to investigate the effectiveness of nanoparticles, but, to the best of our knowledge, field applications of nanoparticles have yet to be published.

Wettability alteration has been studied quite thoroughly in sandstone and carbonate reservoirs. There are a few laboratory studies on wettability alteration in unconventional reservoirs, such as shale (Morsy et al., 2014) and tight sandstone oil reservoirs (Kathel and Mohanty, 2013). However, it is not comprehensive and research on wettability alteration in unconventional rocks such as coals and shales is still very limited.

The chemical treatment can be designed for particular contact angles. Adibhatla et al. (2006) conducted experimental studies on the effectiveness of various types of amines, fluorinated surfactants, fluorosilanes, and fluorinated polymers in the alteration of the wettability of sandstone and carbonate rocks. Among the fluorosilanes, they observed that increasing number of fluoro groups reduces hydrophilicity.

Given the wide variety of options of chemicals and nanoparticles available for application of wettability alteration, there is capability for engineers in future to specify the contact-angle with which to alter the reservoir pore surface to. The optimization of contact-angle to maximize gas productivity has yet to be investigated or published in the literature.

2.3. Models for two phase flow in porous media

This section covers the models which have been developed and applied in the literature which are related to water-gas production in vertical and hydraulically fractured wells. It covers the models which have been applied for correcting core flood data for capillary end effects, models which can account for piecewise capillary pressure curves and models which account for flow convergence around hydraulic fractures.

2.3.1. Models accounting for capillary end effects in core floods

There are numerous analytical models for the capillary end effect for the correction of core flood calculations (Huang and Honarpour, 1998; Ramakrishnan and Cappiello, 1991; Virnovsky et al., 1995). In these cases capillary pressure either needs to be measured separately (Virnovsky et al., 1995) or in-situ saturation

measurements need to be made (Huang and Honarpour, 1998; Pini and Benson, 2013).

One of the earliest papers to introduce mathematical models for the capillary end effects was by Hadley and Handy (1956). They modelled one-dimensional Darcy flow of two immiscible incompressible fluids accounting for capillary pressure. They presented the calculation results for oil-wet systems. They concluded the impact of the ratio of capillary to viscous forces, the viscosity ratio of the two fluids and fractional flow curves.

Ramakrishnan and Cappiello, (1991) presented the technique of calculating the drainage capillary pressure curve and relative permeability for oil. The immobile water phase allows for the calculation of relative permeability and capillary pressure without requiring the additional measurement of capillary pressure or in-situ water saturation.

Virnovsky et al. (1995) presented the application of the model developed by Hadley and Handy (1956). The novelty in their publication is the application of the model to correct calculations of experimentally determined relative permeability, when both phases are flowing. In their method the capillary pressure curve has to be measured separately.

Huang and Hornapour (1998) presented another application of the same model as presented by Virnovsky et al. (1995). They acknowledged that in order to correct core flood results for capillary end effects, either the relationship between capillary pressure and relative permeability needs to be known or some additional measurement of either capillary pressure or in-situ saturation is required. They presented the method of determining capillary pressure and relative permeability simultaneously if in-situ saturation measurements were made. Pini and Benson (2013) revisited the same problem as Huang and Hornapour (1998). They provided better validation of the technique of using in-situ saturation by using three different fluid pairs and determined the same leveret-J function and relative permeability curves.

In principle, the idea is the same in both Huang and Hornapour (1998) and Virnovsky et al. (1995). They both showed that there was no method of determining the correct relative permeability curve without some additional measurement of either

in-situ saturation or capillary pressure. By extension, if we intend to predict additional pressure drop due to capillary end effects in gas wells, we need both the relative permeability curves and capillary pressure curves.

2.3.2. Models for porous media with piecewise capillary pressure curves

Capillary pressure curves are proportional to the root of permeability over porosity (Leverett, 1941). In heterogeneous formations when the permeability increases, the capillary pressure will decrease. Investigation into the effect that permeability and porosity heterogeneity has on two phase flow can give insight into what can happen after wettability alteration, as it incorporates the changes in capillary pressure curves.

Yortsos and Chang (1990) developed an analytical model for steady state two-phase incompressible immiscible flow in porous media with heterogeneity in permeability. They investigated porous media with a linear transition between two permeability values and various porous media with periodic oscillations in permeability. They observed when permeability increases linearly from low permeability to high permeability that the wetting fluid built up in the low permeability region. The degree to which the saturation increases depends on the slope of the linear transition. The saturation shock increases with slope, and reaches the maximum when the permeability follows a piecewise constant profile. From their conclusions we can gather that the piecewise reduction in capillary pressure curves that occurs at a core outlet, at a wellbore, at a fracture face, and even at the boundary of a wettability alteration treatment can cause a sharp increase in water saturation for water-wet media.

Chaouche et al. (1993) compared numerical simulation of two phase steady state flow to laboratory results. They modelled steady state flows with piecewise permeability. They observed that higher flow rate reduce the saturation deviation at the permeability heterogeneity. The also conclude that saturation variation can be used to map permeability profiles.

Van Duijn et al. (1995) developed a numerical model to study transient two-phase flows of incompressible liquids in porous media with discontinuous permeability or porosity. They derived two conditions at the interface of the

discontinuity, one of flux continuity and one of wetting phase pressure continuity. The pressure continuity condition can lead to discontinuous capillary pressure which results in the trapping of the non-wetting phase. In this instance the non-wetting phase is oil, and the amount which is trapped is dependent on water flow rate, interfacial tension and viscosity. The authors recommended interfacial reduction due to surfactant, water viscosity reduction through polymer or increase in flow rate in order to reduce the amount of trapped oil in high permeability regions.

Van Lingen et al. (1996) developed an analytical model to calculate oil trapped due to capillary forces in laminated cross bed sets, where permeability or wettability alternated between two sets of laminae. Using the simple analytical model, they study the impact of various parameters such as permeability, dimension of sets and flow velocity on residual oil saturation. However, they did not take into account the influence wettability alteration has on the relative permeability curves.

The modelling studies (Yortsos and Chang, 1990; Chaouche et al., 1993; Van Duijn et al., 1995, Van Lingen et al., 1996) all showed agreement with experiments made in lab with composite cores (Hinkley and Davis, 1986). In all studies the capillary number is seen to have important influence on the saturation profile.

2.3.3. Models for water-block in hydraulically fractured wells

Holditch (1979) presented a numerical study of the water block impact on hydraulically fractured wells. The used a finite-difference reservoir simulator to simulate the flow of water and gas into a fracture. The model for water block is a stepwise reduction in permeability for 1 and 5 inches next to the fracture face. While his extensive 2-year study provides conclusions on the importance of high drawdown and correct evaluation of the Leverett J function, it does not provide a simple method for reservoir engineers to evaluate water block across a variety of reservoir types. Furthermore, the model of stepwise decrease in permeability is not representative of the water block which is formed by the result of capillary forces.

Parekh and Sharma (2004) presented a numerical study of the water block clean up. They investigated the displacement of the fracture leak off water using the University of Texas Chemical Flooding Simulator. Their study was on the transient phase of the water block and how it was affected by viscous forces. Unlike in Holditch

(1979), they did not assume any permeability profile. The saturation profile was determined from combining effects of viscous forces, capillary forces, and relative permeability. They concluded that drawdown must be at least three times larger than the capillary pressure in order to overcome the water block effect. They also observed that altering wettability from strongly water-wet to intermediate-wet improved invaded water recovery, but hampered oil rate during flow back, suggesting that some optimization may be required.

Mahadevan et al. (2007) developed a numerical model for calculation of water block clean up. They were primarily interested in modelling the evaporative regime after a steady state profile is established. The inclusion of evaporation in their model is what differentiates their model from the works of Parekh and Sharma (2004). They concluded that evaporative clean-up is faster when the fluids are more volatile, the reservoir is hotter, the permeability is higher, and the drawdown is larger. While their conclusions are relevant, their model does not incorporate the impact of slip effects or wettability, and wettability alteration was not a part of their study. They also assumed a dry reservoir with no water cut. When there is some non-zero water cut, relying entirely on evaporation may not remove the water blocking effect.

Bahrami et al. (2012) investigated water block in a well producing from a tight gas sandstone using the CMG-IMEX black oil simulator. They primarily studied the impact of initial reservoir saturation in a sub-irreducible state, which was not considered in previous models. They showed that sub-irreducible water saturation made tight sandstones very sensitive to introduced water.

2.4. Limitations of the models in literature

This section covers the limitations of the models presented in the previous section, and how they do not fulfil the aims of the thesis. What was not considered in any of the analytical models (Virnovsky et al., 1995; Huang and Honarpour, 1998; Pini and Benson, 2013; Yortsos and Chang, 1990; Van Duijn et al., 1995; Van Lingen et al., 1996) was gas compressibility. While laboratory experiments can be engineered to minimize the effect of compressibility, production from gas fields cannot. Analytical models for gas production will need to account for compressibility, particularly when there are high pressure gradients. The thesis includes compressibility in 3 of the 4 analytical models.

The aforementioned analytical models also did not take into account of the impact of small pore throats in unconventional reservoirs on gas permeability. Conventional sandstone reservoirs generally have pore body sizes greater than 20 μm, and pore-throat sizes greater than 2 μm (Nelson, 2009). Unconventional reservoirs can be much lower. Nelson (2009) measured tight sandstones to have pore throat sizes in the range of 2 μm to 0.03 μm and shales to reach 0.005 μm. He concluded that the smallest detectable pore throat sizes in shales can be roughly ten times the diameter of water or methane molecules, and are comparable to asphaltene molecules. At this size the assumption of Darcy flow can break down.

Miguel and Serrenho (2007) perform experimental measurements of permeability in sand and woven fabric to air and helium. They conclude at small flow rates the interaction between the gas molecules and the pore walls will become non-negligible and will cause the relationship the pressure drawdown shares with flow rates to deviate from the Darcy model.

As the pore sizes decrease, the quantity of interactions the gas particles have with each other decreases and the quantity of interactions the gas particles have with the pore wall increases. There is a point at which the pore will be small enough such that the gas particles move independently from each other. This phenomenon is called Knudsen's diffusion.

The dimensionless number used for calculating when this diffusive flow occurs is called the Knudsen number. It is defined as the ratio of the molecular mean free path to the pore throat size. At Knudsen numbers less than 0.01, viscous flow dominates. This flow regime is referred to as continuum flow. At Knudsen numbers greater than 10 continuum fluid flow equations fully break down, and the flow is in the free molecular flow regime. The flow regimes for Knudsen numbers between 0.01 and 0.1 and 0.1 and 10 are referred to as slip flow and transition flow respectively. The Knudsen's correction factor as given by Beskok and Karniadakis (1999) can be used for these flow regimes.

However, the Klinkenberg slip correction equation as given by Klinkenberg (1941) is a much easier relationship and is more commonly used. The effects of compressibility and Klinkenberg slip effect can easily be incorporated into analytical models by replacement of the potential term in Darcy's law with a modified gas

pseudo pressure as shown in the review of gas well testing equations by Clarkson (2013). In the analytical models presented in the thesis this effect has been incorporated.

Rocks with piecewise permeability can have saturation shocks on the boundary of the permeability change (Van Duijn et al., 1995; Chaouche et al., 1993). Similarly, piecewise wettability alteration may also lead to saturation shocks at the boundary between the altered and unaltered zones. However, analytical solutions for two-phase linear flows have only been presented for uniform rock wettability (Chaouche et al., 1993; Van Lingen et al., 1996; Huang and Honarpour, 1998). To account for wettability change, the additional effect of the change in relative permeability also needs to be considered, and it has yet to be included in any analytical model.

There are models already available for calculation of relative permeability (Bradford et al., 1997) and capillary pressure (O'Carroll et al., 2005) accounting for macro-scale contact angle. Their application into analytical equations will allow for evaluation of the optimal contact angle, which was performed in this thesis.

Many modern wells are hydraulically fractured. Accounting for flow convergence around hydraulic fractures is pivotal for applicability of analytical models. There is a linear and radial transient flow regime during the early period of a hydraulically fractured well. The numerical model developed by Mahadevan et al. (2007) considered flow into a fracture as linear, which may not be true if the damage zone is large enough. However both the linear flow close to the fracture and radial flow far from the fracture can be better captured with an elliptic flow model, as presented by Hale and Evers (1981). If the pressure drop across the fracture is negligible compared to the pressure drop from the reservoir to the wellbore, the set of equations can be reduced down to one dimensional flow equations, as shown in Hale and Evers (1981) and Prats (1961). For this case, the assumption commonly used of linear flow close to the hydraulic fracture is no longer required. Despite numerous one dimensional flow models accounting for capillary end effects existing, they have yet to be applied for the case of a hydraulically fractured well for calculation of well skin. The models for water block which do take into account of flow convergence around a hydraulic fracture (Holditch, 1979; Bahrami et al., 2012; Parekh and Sharma, 2004)

are numerical only, which limits their speed and applicability. This thesis develops the analytical models for skin due to water blocking accounting for elliptic flow around a hydraulic fracture.

2.5. Relative permeability and capillary pressure models

This section covers the models developed for the calculation of capillary pressure and relative permeability curves. It also covers the strengths and weaknesses of the models developed.

The relative permeability and capillary pressure curves are one of the primary characteristics of the reservoir which determine the behaviour of fracturing fluid clean up. We have a good understanding of how these curves are affected qualitatively by wettability. The permeability to water will decrease and the permeability to oil will increase if the porous media becomes more water wet.

There have been several approaches to modelling mixed wet and fractionally wet porous media and they will be discussed below. The relative permeability and capillary pressure curves determined can be used in analytical models for analysing the sensitivity of the water block to wettability type, contact angle, and pore network topology.

2.5.1. Capillary bundle models

The capillary bundle model is one of the simplest models available for simultaneous calculation of relative permeability and capillary pressure. Bradford et al. (1997) modelled the impact of fractional wettability on relative permeability curves using the capillary bundle model. They introduced an empirical weighting function, which is the fraction of capillaries in the bundle model, either oil wet or gas wet, based on macroscopic contact angle. The curve is fitted to laboratory data presented by McCaffery and Bennion (1974), but also can be determined from the equation for composite surfaces presented by Cassie (1944).

O'Carroll et al. (2004) modelled capillary pressure-saturation relationships in fractionally wet systems, building on the equation for composite surfaces presented by Cassie (1944) and the capillary bundle model. In order to use their approach to model capillary pressure, a reference capillary pressure curve for a uniformly wet system with identical pore structure is required.

Zhou et al. (2014) used scanning electron microscope images of sandstones to construct cross sections for a capillary bundle model. This model was then used to simulate water flooding and calculate capillary pressure and relative permeability curves.

However, capillary bundle model may not be sufficient for modelling of capillary pressure for these intermediate wettabilities (Anderson, 1987a). The model cannot capture how the pore network topology will affect the connectivity of the invading phase, and consequently the pore throat size used in the model may not be representative of reality.

2.5.2. Percolation models

Percolation theory allows for taking into account the average coordination number of the network. Many percolation properties will follow a power law near to the percolation threshold. The exponents only depend on the dimensionality of the system (Sahimi, 2011), and this gives the theory wide versatility. Other applications of percolation theory were to calculate critical porosity to form a continuous void space (Larson, Scriven and Davis, 1981) and the calculation of capillary pressure profiles (Larson and Morrow, 1981).

There have been many publications applying this theory for the calculation of relative permeability and capillary pressure. The earliest applications of percolation theory for two phase flow in porous media were around the 1980s (Sahimi, 2011). Since it is contentious to claim which author came first, we will just take a look at some of the conclusions from papers published around this timeframe.

Larson et al. (1977) investigated the residual saturation of oil using percolation cluster size in Bethe lattices. The mobility of oil blobs in a network will depend on the capillary number and on the size of the blob. The authors relate the mobility of oil clusters in the network to the cluster size and calculate residual oil as the sum of all smaller clusters when the percolation threshold is reached. They can then qualitatively investigate the effects of network topology and capillary number on residual oil. The residual oil calculated by the percolation model successfully predicted the experimentally measured values by Abrams (1975) and Lefebvre du Prey (1973). Larson, Davis and Scriven (1981) reviewed the application of Bethe lattice percolation

models to several experimental results. In particular, the Bethe lattice coordination number is tuned to fit laboratory data by Pickell et al. (1966) and Keelan and Pugh (1975). A close fit to the laboratory data is achieved. They observed as capillary number decreases, residual oil rises and approaches an upper limit.

By assuming a simple bethe network, there can be simple analytical expressions for conductivity and ratio of bonds forming an infinitely connecting cluster. This allows for analytical expressions for relative permeability and capillary pressure, as shown in Heiba et al. (1983). However, a Bethe network may not be physically representative of a pore network in natural porous media.

Heiba et al. (1992) calculated relative permeability and capillary pressure using bond percolation. This procedure consisted entirely of bond percolation with cylindrical tubes as the bonds. Conductivity through each tube is defined using Poisuelle's law and conductivity through the media is defined using a modified effective medium approximation.

One of the issues with bond percolation is that modelling the bonds as if they are capillary tubes is not representative of real porous media. The pore bodies hold more of the volume and control saturation values, while the pore throats are the bottlenecks for conductance. Both Heiba et al. (1992) and Heiba et al. (1983) needed to introduce some empirical parameter in order to correct for this. Heiba et al. (1992) were able to find good agreement between their percolation model and the experimentally measure relative permeability presented by Talash (1976) after tuning the empirical parameter and the coordination number.

Bond correlated site percolation has been investigated by Diaz et al. (1987) for the calculation of capillary pressure. They had good agreement of the primary and secondary drainage capillary pressure curves modelled using percolation theory and the experimental results presented by Chatzis and Dullien (1977). They were less successful with imbibition and concluded that further research in this area was necessary.

Simple equations for network conductance using percolation exponents are available if the bonds have constant conductance. For networks with disordered

conductance a more complicated method for calculation network conductance is required.

2.5.3. Effective medium theory and critical path theory

The conductivity of a network with disordered bond conductance can be calculated using the effective medium approximation. Kirkpatrick (1973) presented the numerical validation of the effective medium theory and showed that it accurately describes the conductivity of the bond percolation problem, except close to the percolation threshold.

Levine and Cuthiell (1986) introduced calculating relative permeability using effective medium theory in a cubic lattice of cylindrical tubes. They concluded that close to threshold there is an inadequacy in effective medium theory in calculating relative permeability as it does not match the convex shape observed in experimental measure relative permeability curves.

Ghanbarian et al. (2016) used effective medium theory to calculate relative permeability. However, close to the percolation threshold they used a power law function. After comparison to 21 laboratory samples there was indication for good treatment with 14 samples but poor estimation of 7 samples. The authors suggested that factors such as wettability, viscous and capillary forces, pore geometry, accessibility and connectivity which causes difficulty in prediction of relative permeability.

Salimi et al. (2020) applied effective medium theory for the calculation of relative permeability during bond percolation. The novelty of their work is that they modelled bonds as if they were triangular capillaries. However, given the uncertainty in effective medium theory in predicting relative permeability, as shown by Ghanbarian et al. (2016), their technique need proper validation, which is not supplied in their work.

Hunt (2001) suggested that critical path theory was a possible solution for calculation of conductivity in highly heterogeneous porous media. The theory involves applying two concepts to simplify down the network. The first is that the conductance for a set of conductors in parallel is closer to the largest conductor. The second is that the conductance for a set of conductors in series is closer to the smallest

conductor. The theory presented by Ambegaoker et al. (1971) involves splitting the network into two sets of conductors based on conductivity. The smallest set of conductors is reduced down to the smallest conductor in it, which is zero. The large set of conductors is reduced down to the smallest conductor in its set; the critical conductance. While Hunt (2001) suggests that critical path theory shows promise in applicability, they also do write there is still some improvements required. They write that the weakest point in critical path theory is the uncertainty in the length of separation of paths contributing to the conduction.

2.5.4. Network simulation

The saturation, conductivity and capillary entry pressure are heavily affected by the geometry and shape of the bonds. It has become more popular now to use triangular shaped bonds. This allows for accounting for wetting phase residing in the corners of the bond. Patzek and Silin (2001) calculated the conductivity in and give analytical expressions for conductivity. They demonstrate that shape factor leads to simple expressions for hydraulic conductance in single phase flow in triangular, rectangular and elliptic capillaries.

Pore network simulators can account for non-uniform coordination number, correlations between pore body size, pore throat size and coordination number and on more realistic shapes for pore bodies and throats. Information on the microstructure of networks is generally determined from thin-section images of the porous media (Oren et al.,1997) or the pore throat sizes determined from mercury injection capillary pressure (MICP) tests (Valvatne and Blunt 2004). It can also be gathered from micro computerized tomography scanning (Dong and Blunt, 2009). After simplification of the pore topology or throat geometry, prediction of single phase or multiphase properties is possible via network simulation.

Wettability will also affect the displacement shape into the bond. Dixit et al. (2000) have developed a network model to derive capillary pressure curves from non-uniformly wetted systems. They observed in several different regimes the change in oil recovery has a dependency on the fraction of oil wet rocks and on the type of wettability.

Patzek (2000) developed a quasi-static pore network simulator of two-phase flow. The work has been validated by comparison to proprietary simulator of Statoil. It can predict primary secondary and higher order drainage and imbibition processes. The model takes into account of several filling types, such as piston like displacement, snap off and co-operative pore body filling. Valvatne and Blunt (2004) built on this work by including the effect of mixed wettability; where surface area of pore throats can have surface wettability partially altered. This changes the configuration of interfaces in the pore and consequently, the conductivity of both phases. They successfully predicted the flow properties of a sand pack and two reservoir sandstones.

One of the downsides of using a pore network simulator is that the process is numerical. Given the universality of the percolation exponents, a percolation model for capillary pressure can be analytical. The method for calculation of conductivity can be faster based on the algorithm used. However, in order for a percolation model to be as successful at predicting capillary pressure or relative permeability, it will need to have to account for the additional effects already employed in pore network models, such as the impact of size variation between bonds and sites and irregular shaped pore throats. These effects are incorporated in the bond-site percolation model developed in this thesis. Effective medium theory and critical path theory are both applied for calculation of relative permeability.

2.6. Conclusion of the literature review

The literature presents many analytical models for the case of one-dimensional linear flow accounting for capillary end effects (Virnovsky et al., 1995; Huang and Honarpour, 1998; Pini and Benson, 2013; Yortsos and Chang, 1990; Chaouche et al., 1993; Van Duijn et al., 1995; Van Lingen et al., 1996). The analytical models presented do not account for gas compressibility or slip effects which can be easily included by a change in the potential term in Darcy's law (Clarkson, 2013). The simultaneous impact of wettability alteration on capillary pressure and relative permeability has not been implemented in any of the analytical models in the literature and has been done in this thesis. The impact wettability alteration has on relative permeability and water block suggests that an optimal wettability may exist for productivity, but it has not been presented in the literature. The thesis finally presents the optimal contact angle and how it is impacted by wettability, piecewise wettability

alteration, water cut, capillary forces, viscous forces, inertial forces and compressibility.

There have been analytical models already published for elliptic flow into hydraulically fractured wells for incompressible (Prats, 1961) and compressible fluids (Hale and Evers, 1981). However, they are both for single phase flow only. All models presented in the literature for hydraulically fractured wells accounting for the water cut, hydraulic fracture length and the viscous, capillary and inertial forces are numerical. Given that analytical models for linear one-dimensional flow accounting for capillary end effects have been derived, there should exist a solution for elliptical flow accounting for capillary end effects. The analytical solution for elliptical flow accounting for capillary end effects is presented in this thesis.

The forms of relative permeability and capillary pressure are some of the most important characteristics of the reservoir which determine the skin due to water block. Models developed for calculating the effect of wettability alteration can be oversimplified or computationally expensive. Percolation models so far have involved only bond percolation and require some empirical parameters to take into account the relationship between pore bodies and pore throats (Heiba et al., 1983; Heiba et al., 1992). Effective medium theory has been applied with varying degrees of success (Ghanbarian et al., 2016). In this thesis a mixed bond-site percolation model coupled with effective medium theory and critical path theory is developed in order to take into account a more physically meaningful relationship between the pore throats and pore bodies as well as network coordination.

The critical literature review allows concluding that despite the vast quantity of literature on two phase flow in porous media, the main goals of this thesis have not been achieved. The objectives 1 to 8 have not been met in any of the reviewed publications.

2.7. References for the literature review

Abrams, A., 1975. The influence of fluid viscosity, interfacial tension, and flow velocity on residual oil saturation left by waterflood. Society of Petroleum Engineers Journal, 15(05), pp.437-447.

Adibhatla, B., Mohanty, K.K., Berger, P. and Lee, C., 2006. Effect of surfactants on wettability of near-wellbore regions of gas reservoirs. Journal of petroleum science and engineering, 52(1-4), pp.227-236.

Al-Anazi, H.A., Okasha, T.M., Haas, M.D., Ginest, N.H. and Al-Faifi, M., 2005, January. Impact of Completion Fluids on Productivity in Gas/Condensate Reservoirs. In SPE Production Operations Symposium. Society of Petroleum Engineers.

Al-Anazi, H.A., Xiao, J., Al-Eidan, A.A., Buhidma, I.M., Ahmed, M.S., Al-Faifi, M. and Assiri, W.J., 2007, January. Gas productivity enhancement by wettability alteration of gas-condensate reservoirs. In European Formation Damage Conference. Society of Petroleum Engineers.

Al-Anssari, S., Barifcani, A., Wang, S., Maxim, L. and Iglauer, S., 2016. Wettability alteration of oil-wet carbonate by silica nanofluid. Journal of colloid and interface science, 461, pp.435-442.

Alvarez, J.O., Neog, A., Jais, A. and Schechter, D.S., 2014, April. Impact of surfactants for wettability alteration in stimulation fluids and the potential for surfactant EOR in unconventional liquid reservoirs. In SPE Unconventional Resources Conference. Society of Petroleum Engineers.

Ambegaokar, V., Halperin, B.I. and Langer, J.S., 1971. Hopping conductivity in disordered systems. Physical review B, 4(8), p.2612.

Anderson, W. G., 1987a. Wettability literature survey-part 4: Effects of wettability on capillary pressure. Journal of Petroleum Technology, 39(10), 1-283.

Anderson, W. G., 1987b. Wettability literature survey part 5: the effects of wettability on relative permeability. Journal of Petroleum Technology, 39(11), 1-453.

Bahrami, H., Rezaee, R. and Clennell, B., 2012. Water blocking damage in hydraulically fractured tight sand gas reservoirs: An example from Perth Basin, Western Australia. Journal of Petroleum Science and Engineering, 88, pp.100-106.

Bang, V.S.S., Pope, G.A., Sharma, M.M. and Baran Jr, J.R., 2009, January. Development of a successful chemical treatment for gas wells with liquid blocking. In SPE Annual Technical Conference and Exhibition. Society of Petroleum Engineers.

Bazin, B., Peysson, Y., Lamy, F., Martin, F., Aubry, E. and Chapuis, C., 2010. In-situ water-blocking measurements and interpretation related to fracturing operations in tight gas reservoirs. SPE Production & Operations, 25(04), pp.431-437.

Beskok, A. and Karniadakis, G.E., 1999. Report: a model for flows in channels, pipes, and ducts at micro and nano scales. Microscale Thermophysical Engineering, 3(1), pp.43-77.

Bradford, S.A., Abriola, L.M. and Leij, F.J., 1997. Wettability effects on two-and three-fluid relative permeabilities. Journal of contaminant hydrology, 28(1-2), pp.171-191.

Bryant, E.M., Bowman, R.S. and Buckley, J.S., 2006. Wetting alteration of mica surfaces with polyethoxylated amine surfactants. Journal of Petroleum Science and Engineering, 52(1-4), pp.244-252.

Cassie, A.B.D. and Baxter, S., 1944. Wettability of porous surfaces. Transactions of the Faraday society, 40, pp.546-551.

Chaouche, M., Rakotomalala, N., Salin, D. and Yortsos, Y.C., 1993. Capillary effects in immiscible flows in heterogeneous porous media. EPL (Europhysics Letters), 21(1), p.19.

Chatzis, I. and Dullien, F.A., 1977. Modelling pore structure by 2-d and 3-d networks with application to sandstones. Journal of Canadian Petroleum Technology, 16(01), pp.97-108.

Clarkson, C.R., 2013. Production data analysis of unconventional gas wells: Review of theory and best practices. International Journal of Coal Geology, 109, pp.101-146.

Diaz, C.E., Chatzis, I. and Dullien, F.A.L., 1987. Simulation of capillary pressure curves using bond correlated site percolation on a simple cubic network. Transport in Porous media, 2(3), pp.215-240.

Dixit, A.B., Buckley, J.S., McDougall, S.R. and Sorbie, K.S., 2000. Empirical measures of wettability in porous media and the relationship between them derived from pore-scale modelling. Transport in porous media, 40(1), pp.27-54.

Dong, H. and Blunt, M.J., 2009. Pore-network extraction from micro-computerized-tomography images. Physical review E, 80(3), p.036307.

Esmaeilzadeh, P., Sadeghi, M.T., Fakhroueian, Z., Bahramian, A. and Norouzbeigi, R., 2015. Wettability alteration of carbonate rocks from liquid-wetting to ultra gas-wetting using TiO2, SiO2 and CNT nanofluids containing fluorochemicals, for enhanced gas recovery. Journal of Natural Gas Science and Engineering, 26, pp.1294-1305.

Ghanbarian, B., Sahimi, M. and Daigle, H., 2016. Modeling relative permeability of water in soil: Application of effective - medium approximation and percolation theory. Water Resources Research, 52(7), pp.5025-5040.

Ghanbari, E. and Dehghanpour, H., 2016. The fate of fracturing water: A field and simulation study. Fuel, 163, pp.282-294.

Giraldo, J., Benjumea, P., Lopera, S., Cortés, F.B. and Ruiz, M.A., 2013. Wettability alteration of sandstone cores by alumina-based nanofluids. Energy & Fuels, 27(7), pp.3659-3665.

Graue, A., 1994. Imaging the effects of capillary heterogeneities on local saturation development in long corefloods. SPE Drilling & Completion, 9(01), pp.57-64.

Gupta, R. and Maloney, D., 2015, August. Applications of the intercept method to correct steady state relative permeability for capillary-end effects. In International Symposium of the Society of Core Analysts held in St. John's Newfoundland and Labrador Canada (pp. 16-21).

Hadley, G.F. and Handy, L.L., 1956, January. A theoretical and experimental study of the steady state capillary end effect. In Fall Meeting of the Petroleum Branch of AIME. Society of Petroleum Engineers.

Hale, B.W. and Evers, J.F., 1981. Elliptical flow equations for vertically fractured gas wells. Journal of Petroleum Technology, 33(12), pp.2-489.

Heiba, A.A., Davis, H.T. and Scriven, L.E., 1983, January. Effect of wettability on two-phase relative permeabilities and capillary pressures. In SPE annual technical conference and exhibition. Society of Petroleum Engineers.

Heiba, A.A., Sahimi, M., Scriven, L.E. and Davis, H.T., 1992. Percolation theory of two-phase relative permeability. SPE Reservoir Engineering, 7(01), pp.123-132.

Hinkley, R.E. and Davis, L.A., 1986, January. Capillary pressure discontinuities and end effects in homogeneous composite cores: effect of flow rate and wettability. In SPE Annual Technical Conference and Exhibition. Society of Petroleum Engineers.

Holditch, S.A., 1979. Factors affecting water blocking and gas flow from hydraulically fractured gas wells. Journal of Petroleum Technology, 31(12), pp.1-515.

Huang, D.D. and Honarpour, M.M., 1998. Capillary end effects in coreflood calculations. Journal of Petroleum Science and Engineering, 19(1-2), pp.103-117.

Hunt, A.G., 2001. Applications of percolation theory to porous media with distributed local conductances. Advances in Water Resources, 24(3-4), pp.279-307.

Ju, B. and Fan, T., 2009. Experimental study and mathematical model of nanoparticle transport in porous media. Powder Technology, 192(2), pp.195-202.

Ju, B. and Fan, T., 2013. Experimental study on nanoparticles transport and its effects on two-phase flow behavior in porous networks. Particulate Science and Technology, 31(2), pp.114-118.

Kamath, J., and Laroche, C., 2003. Laboratory-based evaluation of gas well deliverability loss caused by water blocking. SPE Journal, 8(01), pp.71-80.

Karimi, A., Fakhroueian, Z., Bahramian, A., Pour Khiabani, N., Darabad, J.B., Azin, R. and Arya, S., 2012. Wettability alteration in carbonates using zirconium oxide nanofluids: EOR implications. Energy & Fuels, 26(2), pp.1028-1036.

Kathel, P. and Mohanty, K.K., 2013. Wettability alteration in a tight oil reservoir. Energy & Fuels, 27(11), pp.6460-6468.

Keelan, D.K. and Pugh, V.J., 1975. Trapped-gas saturations in carbonate formations. Society of Petroleum Engineers Journal, 15(02), pp.149-160.

Kirkpatrick, S., 1973. Percolation and conduction. Reviews of modern physics, 45(4), p.574.

Klinkenberg, L.J., 1941, January. The permeability of porous media to liquids and gases. In Drilling and production practice. American Petroleum Institute.

Kyte, J.R. and Rapoport, L.A., 1958. Linear waterflood behavior and end effects in water-wet porous media. Journal of Petroleum Technology, 10(10), pp.47-50.

Larson, R.G., Davis, H.T. and Scriven, L.E., 1981. Displacement of residual nonwetting fluid from porous media. Chemical Engineering Science, 36(1), pp.75-85.

Larson, R. G., and Morrow, N. R., 1981. Effects of sample size on capillary pressures in porous media. Powder technology, 30(2), 123-138.

Larson, R. G., Scriven, L. E., and Davis, H. T., 1977. Percolation theory of residual phases in porous media. Nature, 268(5619), 409-413.

Larson, R. G., Scriven, L. E., and Davis, H. T., 1981. Percolation theory of two phase flow in porous media. Chemical Engineering Science, 36(1), 57-73.

Lefebvre du Prey, E.J., 1973. Factors affecting liquid-liquid relative permeabilities of a consolidated porous medium. Society of Petroleum Engineers Journal, 13(01), pp.39-47.

Leverett, M., 1941. Capillary behavior in porous solids. Transactions of the AIME, 142(01), pp.152-169.

Levine, S. and Cuthiell, D.L., 1986. Relative Permeabilities In Two-Phase Flow Through Porous Media: An Application Of Effective Medium Theory. Journal of Canadian Petroleum Technology, 25(05), pp.74-84.

Li, G., Ren, W., Meng, Y., Wang, C. and Wei, N., 2014. Micro-flow kinetics research on water invasion in tight sandstone reservoirs. Journal of Natural Gas Science and Engineering, 20, pp.184-191.

Li, K. and Firoozabadi, A., 2000. Experimental study of wettability alteration to preferential gas-wetting in porous media and its effects. SPE Reservoir Evaluation & Engineering, 3(02), pp.139-149.

Li, S. and Torsaeter, O., 2015, January. The impact of nanoparticles adsorption and transport on wettability alteration of intermediate wet berea sandstone. In SPE Middle East Unconventional Resources Conference and Exhibition. Society of Petroleum Engineers.

Mahadevan, J., Le, D.H. and Hoang, H.N., 2009, January. Impact of capillary suction on fracture face skin evolution in waterblocked wells. In SPE Hydraulic Fracturing Technology Conference. Society of Petroleum Engineers.

Mahadevan, J., Sharma, M.M., Yortsos, Y.C., 2007. Capillary wicking in gas wells. SPEJ. 12 (4), pp.429-437.

McCaffery, F.G. and Bennion, D.W., 1974. The Effect of Wettability on Two-Phase Relative Permeabilities. Journal of Canadian Petroleum Technology, 13(04).

Miguel, A.F. and Serrenho, A., 2007. On the experimental evaluation of permeability in porous media using a gas flow method. Journal of Physics D: Applied Physics, 40(21), pp.6824.

Morsy, S., Gomaa, A. and Sheng, J.J., 2014, April. Improvement of mancos shale oil recovery by wettability alteration and mineral dissolution. In SPE Improved Oil Recovery Symposium. Society of Petroleum Engineers.

Nelson, P.H., 2009. Pore-throat sizes in sandstones, tight sandstones, and shales. AAPG bulletin, 93(3), pp.329-340.

O'Carroll, D.M., Abriola, L.M., Polityka, C.A., Bradford, S.A. and Demond, A.H., 2005. Prediction of two-phase capillary pressure–saturation relationships in fractional wettability systems. Journal of contaminant hydrology, 77(4), pp.247-270.

Odumabo, S.M. and Karpyn, Z.T., 2014. Investigation of gas flow hindrance due to fracturing fluid leakoff in low permeability sandstones. Journal of Natural Gas Science and Engineering, 17, pp.1-12.

Oren, P.E., Bakke, S. and Arntzen, O.J., 1997, January. Extending predictive capabilities to network models. In SPE Annual Technical Conference and Exhibition. Society of Petroleum Engineers.

Osoba, J.S., Richardson, J.G., Kerver, J.K., Hafford, J.A. and Blair, P.M., 1951. Laboratory measurements of relative permeability. Journal of Petroleum Technology, 3(02), pp.47-56.

Parekh, B. and Sharma, M.M., 2004, January. Cleanup of water blocks in depleted low-permeability reservoirs. In SPE Annual Technical Conference and Exhibition. Society of Petroleum Engineers.

Patzek, T.W., 2000, January. Verification of a complete pore network simulator of drainage and imbibition. In SPE/DOE Improved Oil Recovery Symposium. Society of Petroleum Engineers.

Patzek, T.W. and Silin, D.B., 2001. Shape factor and hydraulic conductance in noncircular capillaries: I. One-phase creeping flow. Journal of colloid and interface science, 236(2), pp.295-304.

Penny, G.S., Conway, M.W. and Briscoe, J.E., 1983, January. Enhanced load water-recovery technique improves stimulation results. In SPE Annual Technical Conference and Exhibition. Society of Petroleum Engineers.

Pickell, J.J., Swanson, B.F. and Hickman, W.B., 1966. Application of air-mercury and oil-air capillary pressure data in the study of pore structure and fluid distribution. Society of Petroleum Engineers Journal, 6(01), pp.55-61.

Pini, R. and Benson, S.M., 2013. Simultaneous determination of capillary pressure and relative permeability curves from core-flooding experiments with various fluid pairs. Water Resources Research, 49(6), pp.3516-3530.

Prats, M., 1961. Effect of vertical fractures on reservoir behavior-incompressible fluid case. Society of Petroleum Engineers Journal, 1(02), pp.105-118.

Ramakrishnan, T.S. and Cappiello, A., 1991. A new technique to measure static and dynamic properties of a partially saturated porous medium. Chemical engineering science, 46(4), pp.1157-1163.

Rapoport, L.A. and Leas, W.J., 1953. Properties of linear waterfloods. Journal of Petroleum Technology, 5(05), pp.139-148.

Richardson, J.G., Kerver, J.K., Hafford, J.A. and Osoba, J.S., 1952. Laboratory determination of relative permeability. Journal of Petroleum Technology, 4(08), pp.187-196.

Roustaei, A., Moghadasi, J., Bagherzadeh, H. and Shahrabadi, A., 2012, January. An experimental investigation of polysilicon nanoparticles' recovery efficiencies through changes in interfacial tension and wettability alteration. In SPE international oilfield nanotechnology conference and exhibition. Society of Petroleum Engineers.

Sahimi, M., 2011. Flow and transport in porous media and fractured rock: from classical methods to modern approaches. John Wiley & Sons.

Salimi, H., Bruining, J. and Joekar-Niasar, V., 2020. Comparison of modified effective-medium approximation to pore-network theory for relative permeabilities. Journal of Petroleum Science and Engineering, 184, p.106594.

Sharma, M. and Agrawal, S., 2013, February. Impact of liquid loading in hydraulic fractures on well productivity. In SPE hydraulic fracturing technology conference. Society of Petroleum Engineers.

Talash, A.W., 1976, January. Experimental and calculated relative permeability data for systems containing tension additives. In SPE improved oil recovery symposium. Society of Petroleum Engineers.

Torres, D.E., Sharma, M.M., Pope, G.A., Ahmadi, M., McCulley, C.A., Linnemeyer, H. and Gilani, S.F., 2010, January. A Novel Chemical Treatment to Enhance Productivity of Volatile Oil Wells. In Canadian Unconventional Resources and International Petroleum Conference. Society of Petroleum Engineers.

Valvatne, P.H. and Blunt, M.J., 2004. Predictive pore-scale modeling of two-phase flow in mixed wet media. Water resources research, 40(7).

Van Duijn, C.J., Molenaar, J. and De Neef, M.J., 1995. The effect of capillary forces on immiscible two-phase flow in heterogeneous porous media. Transport in porous media, 21(1), pp.71-93.

Van Lingen, P.P., Bruining, J. and Van Kruijsdijk, C.P.J.W., 1996. Capillary entrapment caused by small-scale wettability heterogeneities. SPE Reservoir Engineering, 11(02), pp.93-100.

Virnovsky, G.A., Skjaeveland, S.M., Surdal, J. and Ingsoy, P., 1995, January. Steady-state relative permeability measurements corrected for capillary effects. In SPE Annual Technical Conference and Exhibition. Society of Petroleum Engineers.

Weiss, W.W. and Xie, X., 2009, January. Field test of wettability alteration to increase the flow rate from aquifer gas storage wells. In *SPE Eastern Regional Meeting*. Society of Petroleum Engineers.

Wu, S. and Firoozabadi, A., 2010. Permanent alteration of porous media wettability from liquid-wetting to intermediate gas-wetting. Transport in Porous Media, 85(1), pp.189-213.

Yang, L., Ge, H., Shi, X., Cheng, Y., Zhang, K., Chen, H., Shen, Y., Zhang, J. and Qu, X., 2016. The effect of microstructure and rock mineralogy on water imbibition characteristics in tight reservoirs. Journal of Natural Gas Science and Engineering, 34, pp.1461-1471.

Yortsos, Y.C. and Chang, J., 1990. Capillary effects in steady-state flow in heterogeneous cores. Transport in Porous Media, 5(4), pp.399-420.

Zhou, Y., Helland, J. and Hatzignatiou, D.G., 2014. Pore-scale modeling of waterflooding in mixed-wet-rock images: Effects of initial saturation and wettability. SPE Journal, 19(01), pp.88-100.

3. Rate enhancement in unconventional gas reservoirs by wettability alteration

Statement of Authorship

Title of Paper	Rate enhancement in unconventional gas reservoirs by wettability alteration
Publication Status	☑ Published ☐ Accepted for Publication ☐ Submitted for Publication ☐ Unpublished and Unsubmitted work written in manuscript style
Publication Details	Naik, S., You, Z. and Bedrikovetsky, P., 2015. Rate enhancement in unconventional gas reservoirs by wettability alteration. Journal of Natural Gas Science and Engineering, 26, pp.1573-1584.

Principal Author

Name of Principal Author (Candidate)	Saurabh Naik
Contribution to the Paper	Literature review, development of mathematical model, implementation of mathematical solution in Mat-lab, creating figures, analysis of results, writing the manuscript
Overall percentage (%)	85%
Certification:	This paper reports on original research I conducted during the period of my Higher Degree by Research candidature and is not subject to any obligations or contractual agreements with a third party that would constrain its inclusion in this thesis. I am the primary author of this paper.
Signature	Date 03/08/2019

Co-Author Contributions

By signing the Statement of Authorship, each author certifies that:

i. the candidate's stated contribution to the publication is accurate (as detailed above);

ii. permission is granted for the candidate in include the publication in the thesis; and

iii. the sum of all co-author contributions is equal to 100% less the candidate's stated contribution.

Name of Co-Author	Zhenjiang You
Contribution to the Paper	Support on implementation in Matlab, reviewing manuscript
Signature	Date 29/7/19

Name of Co-Author	Pavel Bedrikovetsky
Contribution to the Paper	problem formulation, reviewing manuscript
Signature	Date 30/07/2019

Please cut and paste additional co-author panels here as required.

Journal of Natural Gas Science and Engineering 26 (2015) 1573–1584

Contents lists available at ScienceDirect

Journal of Natural Gas Science and Engineering

journal homepage: www.elsevier.com/locate/jngse

Rate enhancement in unconventional gas reservoirs by wettability alteration

Saurabh Naik, Zhenjiang You*, Pavel Bedrikovetsky

Australian School of Petroleum, The University of Adelaide, Adelaide, SA 5005, Australia

ARTICLE INFO

Article history:
Received 4 February 2015
Received in revised form
21 May 2015
Accepted 9 June 2015
Available online 25 June 2015

Keywords:
Wettability alteration
Production rate
Unconventional gas reservoirs
Capillary end effect
Two phase flow
Contact angle

ABSTRACT

In unconventional water-wet gas reservoirs with extremely low permeability, water blockage due to the capillary end effect near the fracture face and in the wellbore vicinity is a severe obstacle to gas production. Wettability alteration of rock surface is discussed as an effective way to reduce water blockage and enhance gas production. It can also be applied to accelerating dewatering and preventing drilling and fracturing fluid leak-off. The current paper develops analytical models for steady-state two-phase linear and radial flows, accounting for the contact-angle-dependent capillary pressure and relative permeability. The model has been validated by comparison with laboratory test. Applications of the proposed model to porous media with constant and piecewise-constant contact angles are presented. The modelling shows that the competition between the viscous and capillary effects on productivity results in an optimal contact angle for the maximum well productivity indexes for water and gas. The productivity index increases with the capillary-viscous ratio and the altered zone length.

1. Introduction

Natural gas from the unconventional reservoirs is one of the key energy resources that can meet the current world's energy and environmental objectives (Economides and Wood, 2009). However, the unconventional reservoirs have extremely low well productivity. Therefore, hydraulic fracturing is commonly used to stimulate wells in coal seam, shale and tight gas reservoirs (Wang et al., 2012). For reservoirs with very low permeability, fracturing and drilling fluid leak-off along with capillary end effect leads to an increase of water saturation in the near wellbore or fracture-wall regions (Xie et al., 2009; Bahrami et al., 2011; Odumabo et al., 2014). Fluid invasion into the reservoir is greatly affected by the contact angle (Li et al., 2014).

The increased water saturation in the fracture or wellbore neighbourhood throttles gas flow from reservoir to the well. This water entrapment is referred to as water blockage. A few studies have been conducted on water block clean-up (Mahadevan et al., 2007, 2009) and the long-term effects on production (Bahrami et al., 2011). One of the most effective methods to reduce water retention is wettability alteration (Barenblatt et al., 1990). Wettability modification of rock surface towards less water-wet results in decrease of capillary pressure and mitigation of the water-blockage effect.

Altering wettability to more water-wet increases the relative permeability for gas (Anderson, 1987), which is a positive factor for gas production. However, it is accompanied by the increase of water blocking effect which restricts gas flow from reservoir matrix towards well or fractures (Xie et al., 2009). These two competitive factors suggest the existence of the optimal contact angle (wettability), corresponding to the maximum flow rate during gas production. Yet, the existence of the optimal contact angle for gas production has not been reported in the literature.

Two competitive factors also suggest the existence of the contact angle that maximises water rate with gas-water production. Fast dewatering in coal seams or shale gas reservoirs is required at the beginning of the reservoir exploitation, in order to facilitate rapid decrease of the reservoir pressure which intensifies gas desorption from the matrix. Numerous experimental studies on wettability alteration have been performed. The contact angle of rock surfaces can be altered artificially through injection of surfactants (Adibhatla et al., 2006; Bryant et al., 2006; Kumar et al., 2008; Chen and Mohanty, 2014), high temperature steam

* Corresponding author.
E-mail address: zyou@asp.adelaide.edu.au (Z. You).

http://dx.doi.org/10.1016/j.jngse.2015.06.016
1875-5100/

(Bruining and Van Duijn, 2006), brine with various salinities (Nasralla et al., 2013) and water with different pH (Morsy et al., 2014). Significant change of contact angle in sandstones and carbonates with variations of salinity and pH has been reported with regards to low salinity waterflooding (Fogden et al., 2011; Morrow and Buckley, 2011). Presently, intensive research is ongoing for wettability alteration using nanoparticles (Roustaei et al., 2012; Arab and Pourafshary, 2013; Hendraningrat et al., 2013; Assef et al., 2014). To some extent, surface contact angle can be controlled by varying concentrations and compositions of injected agents. It inspires the investigation of contact angle as a continuous parameter, controllable by surface treatment. Although wettability alteration has been extensively studied in sandstone and carbonate reservoirs, research on unconventional rocks such as coals and shales is still very limited. There are a few studies on shale (Morsy et al., 2014) and tight sandstone (Kathel and Mohanty, 2013) oil reservoirs. However, comprehensive research on wettability alteration in unconventional gas reservoirs is unavailable in the literature.

Rate enhancement by wettability alteration has been discussed by Kathel and Mohanty (2013). Piecewise wettability alteration may lead to saturation shock on the boundary of altered and unaltered zones similarly to those on the boundary of rocks with piecewise permeability (Barenblatt et al., 1990; Bedrikovetsky, 1993; Van Duijn et al., 1995). The saturation shock may highly affect well productivity index. However, steady-state solutions for two-phase linear flows have been presented for uniform rock wettability only (Barenblatt et al., 1990; Chaouche et al., 1993; Van Lingen et al., 1996; Huang and Honarpour, 1998). Analytical models accounting for wettability variation along the core or near to fracture face and wellbore are not available in the literature.

In the current study, the effects of contact angle alteration on well productivity for both water and gas are investigated using the analytical model. The formulae for steady-state saturation distribution in heterogeneous rocks with piecewise-constant contact angle and for well index are derived. It is found that there does exist an optimal contact angle to maximise the water production rate; another value of the contact angle maximises the production rate for gas. Calculations using the analytical model show that the wettability alterations cause increase in productivity index 2.0–4.7 times for gas and around 2.0 times for water.

The structure of the paper is as follows: Section 2 presents the contact-angle-dependent models for capillary pressure and two-phase relative permeabilities, which are then applied in Section 3 for derivation of analytical model for steady-state two-phase flows in rocks with piecewise-constant contact angle. Laboratory data of two coreflood tests obtained from literature are analysed for the model validation in Section 4. Analysis of the results from developed analytical model is then conducted in both linear and radial flows (Section 5). Section 6 presents application of nanotechnology to rock surface treatment for enhanced dewatering and gas production from unconventional reservoirs. Discussions of the model validity and conclusions on optimal contact angle finalise the paper (Sections 7 and 8).

2. Contact-angle-dependent model for capillary pressure and relative permeability

This section presents the models for water-saturation- and contact-angle-dependent capillary pressure and relative permeability. To introduce the capillary pressure model, let us define the normalised water saturation S as:

$$S(s) = \frac{s - s_{wc}}{1 - s_{wc} - s_{gr}} \tag{1}$$

where s is the water saturation, and s_{wc} and s_{gr} are the connate water and irreducible gas saturations, respectively.

The contact angle at rock surface θ is measured between the water–gas interface and the water–solid interface. The rock is water-wet (hydrophilic) if $\theta < \pi/2$ and is hydrophobic if $\theta > \pi/2$. Therefore, saturation of the wetting phase S_w can be expressed as:

$$S_w(S,\theta) = \begin{cases} S(s), & \theta < \dfrac{\pi}{2} \\ 1 - S(s), & \theta > \dfrac{\pi}{2} \end{cases} \tag{2}$$

Unconventional reservoirs exhibit a variety of mineralogy and surface types such as organic matter (e.g. kerogen), aluminosilicate clays and silica sands; each mineral has its own wettability. This leads to the necessity of using fractional wettability to describe the rock surface.

In the present work, the Leverett–Cassie equation (O'Carroll et al., 2005) is applied to describe a porous medium which has three fractions of surface area (f_1, f_2, f_3) with different contact angles. The major fraction f_1 has the contact angle which is considered alterable from 0 to π by some wettability altering agent. A small fraction f_2 is considered permanent water wet with contact angle 0 and another small fraction f_3 is permanently hydrocarbon wet with contact angle π. The overall capillary pressure of porous medium with fractional wettability is:

$$P_c(s,\theta) = \frac{2\sigma}{\sqrt{\dfrac{k}{\phi}}} J(s,\theta),$$

$$J(s,\theta) = f_1 \cos(\theta) C S_w(s,\theta)^{-\frac{1}{\alpha}} + f_2 C S(s)^{-\frac{1}{\alpha}} + f_3 C (1 - S(s))^{-\frac{1}{\alpha}} \tag{3}$$

where σ is the interfacial tension, k is the rock permeability, ϕ is the porosity, f_1, f_2, f_3 are the major fraction and two minor fractions of rock surface respectively, $f_1 + f_2 + f_3 = 1$; C and α are empirical model parameters.

The relative permeabilities of water (k_{rw}) and gas (k_{rg}) are expressed as functions of water saturation as (Chen et al., 2013):

$$k_{rw}(s) = (S(s))^{\eta} \frac{\int_0^S w^2(s)ds}{\int_0^1 w^2(s)ds} \tag{4}$$

$$k_{rg}(s) = (1 - S(s))^{\eta} \frac{\int_S^1 w^2(s)ds}{\int_0^1 w^2(s)ds} \tag{5}$$

where η is the tortuosity index and $w(S)$ is the cleat height or capillary radius, expressed as $w(S) = \sqrt{k/\phi}/CS^{-1/\alpha}$ according to Young–Laplace model (Barenblatt et al., 1990; Bedrikovetsky, 1993).

In this model, the rock is assumed to be water-wet and water occupies smaller cleats or pores. As water saturation increases, the cleats or pores are filled by water in order of increase of their aperture (radius). Conversely, if the rock is hydrophobic, the water filling sequence occurs from the largest to the smallest cleats and pores. While this model is applicable to uniformly-wet media, it

cannot explain the behaviour of intermediately-wet natural rocks where the fractional or mixed wettability is more likely due to surface roughness, mineral heterogeneity and different adsorbed compounds (Bradford et al., 1997).

In order to describe the relation between relative permeability and contact angle, we apply the model that accounts for wettability heterogeneity of natural cores at the pore scale, which results in a difference in pore filling sequence for intermediate wettability (McCaffery and Bennion (1974); see also Bradford et al. (1997) for experimental validation of the model). An empirical weighting function $g(\theta)$ represents the portion of pores exhibiting hydrophobic surfaces:

$$g(\theta) = (1 - \cos\theta)/2 \tag{6}$$

As it follows from Eqs (4) and (5), the contact-angle-dependent relative permeabilities for water and gas become:

$$k_{rw}(s,\theta) = (S(s))^{\eta}\frac{[1-g(\theta)]\int_0^S w^2(s)ds + g(\theta)\int_{1-S}^1 w^2(s)ds}{\int_0^1 w^2(s)ds} \tag{7}$$

$$k_{rg}(s,\theta) = (1-S(s))^{\eta}\frac{g(\theta)\int_0^{1-S} w^2(s)ds + [1-g(\theta)]\int_S^1 w^2(s)ds}{\int_0^1 w^2(s)ds} \tag{8}$$

Particularly, for gas flow in tight formation, especially in nanoporous media, molecular scale interactions can have significant impact on gas flow (Shapiro and Wesselingh, 2008). Gas velocity is non-zero at the distance from the pore wall less than the mean free path of gas (Wu and Pruess, 1998). At this scale, the collision frequency between gas molecules and the pore walls increases if compared with gas molecular–molecular collisions, yielding higher gas flux than that calculated from no-slip condition at the pore wall. This effect is referred to as the Klinkenberg (gas slip) effect. It is evaluated by multiplying the Klinkenberg term $(1 + b/\overline{P_g})$ to the gas permeability (8) as:

$$k_{rg}(s,\theta) = \left(1+\frac{b}{\overline{P_g}}\right)(1-S(s))^{\eta}\frac{g(\theta)\int_0^{1-S} w^2(s)ds + [1-g(\theta)]\int_S^1 w^2(s)ds}{\int_0^1 w^2(s)ds} \tag{9}$$

where $\overline{P_g}$ is the average gas pressure along the distance, and b is the Klinkenberg factor. For tight gas reservoirs with permeability below 1 md, formula for Klinkenberg factor is given by Jones and Owen (1980) as:

$$b = 0.86k_{\infty}^{-0.33} \tag{10}$$

where k_{∞} is the gas permeability at infinite pressure.

Contact-angle-dependent models for capillary pressure and relative permeability presented in this section will be applied to the governing system of two-phase flow in the next section.

3. Analytical model for steady-state two-phase flow

In this section, analytical solution to the system of immiscible steady-state two-phase flow is derived, accounting for the effects of contact angle on capillary pressure and relative permeability. The analytical model will be applied to the treatment of laboratory coreflood data (Section 4) and sensitivity study on gas-water productivity (Section 5).

3.1. Analytical model

Darcy's law applies to the flow of each phase (Barenblatt et al., 1990; Cinar and Riaz, 2014):

$$u_w = -\frac{kk_{rw}(s,\theta)}{\mu_w}\nabla P_w,\ u_g = -\frac{kk_{rg}(s,\theta)}{\mu_g}\nabla P_g,\ \ U = u_w + u_g \tag{11}$$

where u_w and u_g stand for flow velocities of water and gas, respectively; U is the total velocity; k_{rw} and k_{rg} are relative permeabilities of water and gas, respectively; μ_w and μ_g are viscosities of water and gas, respectively; P_w and P_g are phase pressures.

Capillary pressure P_c is defined as the difference between the gas and water pressures:

$$P_c = P_g - P_w \tag{12}$$

Substituting Darcy equation for water in (11) and capillary pressure equation (12) into Darcy equation for gas in (11), we obtain:

$$k\frac{k_{rg}(s,\theta)}{\mu_g}\nabla P_c = u_w\left(1+\frac{k_{rg}(s,\theta)\mu_w}{k_{rw}(s,\theta)\mu_g}\right) - U \tag{13}$$

Fractional flow function f is calculated as the ratio of water mobility k_{rw}/μ_w to the total mobility λ:

$$f(s,\theta) = \frac{k_{rw}(s,\theta)/\mu_w}{\lambda(s,\theta)},\quad \lambda(s,\theta) = \frac{k_{rw}(s,\theta)}{\mu_w} + \frac{k_{rg}(s,\theta)}{\mu_g} \tag{14}$$

Substituting Eqs. (14) and (3) into (13) results in:

$$\varepsilon_c\int_{s_0}^{s}\frac{f(s,\theta)k_{rg}(s,\theta)J'(s,\theta)}{f(s,\theta)-f^0}ds = \int_{y_0}^{y}x^a dx \tag{15}$$

where ε_c is the capillary-viscous ratio, defined as $\varepsilon_c = \sigma\sqrt{k\phi}/\mu_g|U|L$ in linear flow and $\varepsilon_c = 2\pi\sigma\sqrt{k\phi}/\mu_g|q|$ in radial flow. Water flux ratio $f^0 = u_w/U$. For linear flow, distance $y = X$, $y_0 = 0$, $a = 0$, and s_0 is water saturation at the core outlet or fracture face. For radial flow, $y = R$, $y_0 = R_w$, $a = -1$, and s_0 is water saturation at wellbore. Eq. (15)

defines the analytical solution for saturation profile in both linear and radial flows.

The flow direction is inverse to increasing distance y, from $y = 1$ to y_0. At the flow exit point $y = y_0$, capillary pressure is $P_c = 0$. As capillary pressure is a monotonic function of saturation, the exit point saturation s_0 can be determined from $P_c(s_0, \theta) = 0$ for various contact angles. The saturation also tends to a certain value s^0 at the distance far away from the exit, i.e., as $y \to \infty$, $s \to s^0$. Inlet point saturation s^0 can be determined from $f^0 = f(s^0, \theta)$ for various contact angles.

The productivity index (PI) for each phase is calculated as the flow rate divided by the phase pressure drawdown:

$$\mathrm{PI}_i = q_i / \Delta P_i \tag{16}$$

in which i stands for either w (for water) or g (for gas). ΔP is the pressure drop calculated from Darcy equation (11) by integration over the distance from inlet to outlet:

$$\Delta P_i = \frac{u_i \mu_i}{k} \int_{y_0}^{1} \frac{x^a}{k_{ri}(s(x), \theta)} dx \tag{17}$$

3.2. Solution procedure

For uniform wettability with known contact angle, the solution procedure is as follows. First, water saturation at flow outlet s_0 is determined from capillary pressure function $P_c(s_0, \theta) = 0$. Second, saturation profile is calculated from (15) for given ε_c and f^0. Third, pressure drops of water and gas are calculated from (17). Finally, productivity indexes for both phases are obtained from (16).

Let us consider piecewise-constant wettability in which the contact angle alteration is applied up to a fraction of the full length. The region $y_0 \le y < \beta$ is considered the altered zone, where β is the altered zone length. The contact angle in this zone is $\theta = \theta_a$ (Fig. 1).

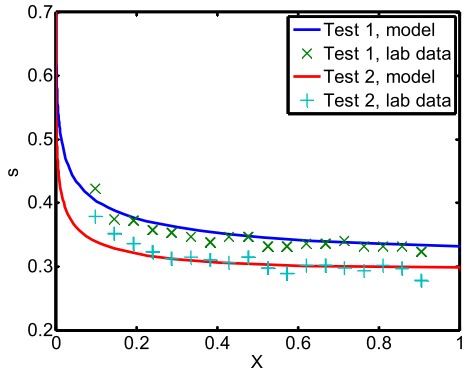

Fig. 2. Matching of the measured saturation profiles by the analytical model.

The region where $y \ge \beta$ is considered the unaltered zone and the contact angle is set as the initial contact angle; $\theta = \theta^0$ (Fig. 1). The solution procedure for piecewise-constant wettability case is similar to that for uniform wettability. Water saturation at flow outlet s_0 is obtained from $P_c(s_0) = 0$. Then the saturation profile is calculated from y_0 up to β for given ε_c and f^0. Capillary pressure and pressures for both phases are continuous across the boundary $y = \beta$. The saturation on the outer side of the boundary s^+, is calculated from the value on the inner side of the boundary s^- as: $P_c(s^+, \theta^0) = P_c(s^-, \theta_a)$. Afterwards, the saturation profile is calculated in the unaltered zone from $y = \beta$ to the inlet $y = 1$. Pressure drops of water and gas are calculated from (17). Finally, productivity indexes for both phases are obtained from (16).

4. Treatment of laboratory coreflood data

In this section, the laboratory coreflooding carried out by Bazin et al. (2010) under two flow rates are analysed in order to validate the model proposed in Sections 2 and 3.

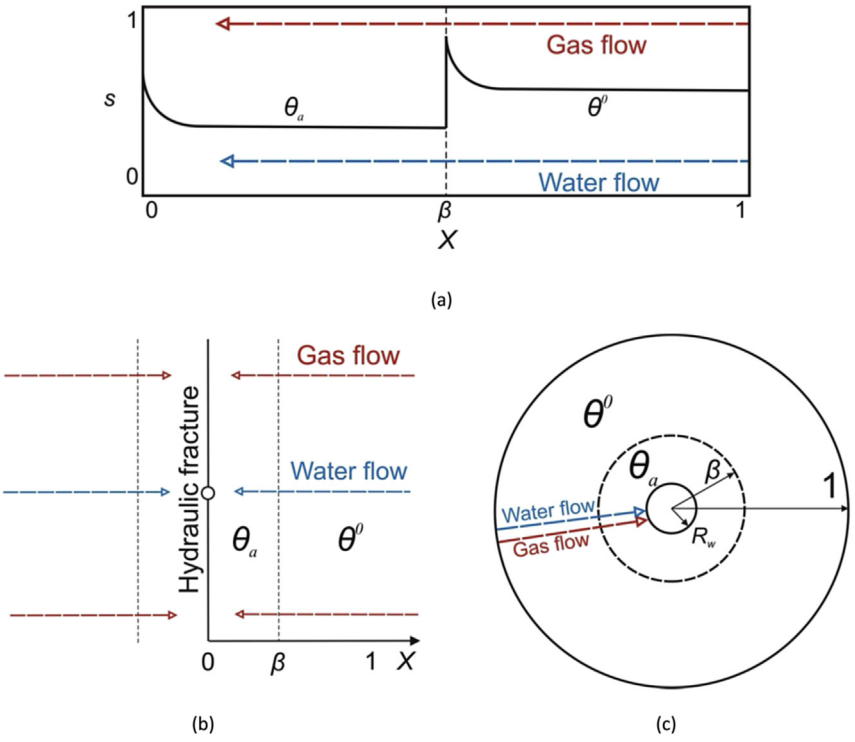

Fig. 1. Schematic of piecewise-constant wettability inflow cases: (a) linear flow in coreflooding; (b) linear flow towards fracture face; (c) radial flow towards wellbore.

Cylindrical Môlière sandstone core from tight gas reservoir with diameter of 3.8 cm and length of 7 cm is used. The initial core permeability is extremely low (0.01 md) and is typical for unconventional reservoirs; the porosity is 0.144. The tortuosity for tight sandstone is taken as $\eta = 2.0$ (Barenblatt et al., 1990). The laboratory procedure is as follows: first, the core was fully saturated with water under vacuum. Second, nitrogen was injected into the core until irreducible water saturation was reached. Third, water was injected into the core with constant pressure until breakthrough. Fourth, nitrogen backflow was performed with constant pressure drawdown 10 bars in Test 1 and 15 bars in Test 2, respectively. The measured saturation profiles are shown in Fig. 2. Measured irreducible saturation for water was $s_{wc} = 0.22$ and for gas was $s_{gr} = 0.2$.

The mathematical model presented in Sections 2 and 3 is applied to the calculation of saturation profile under the laboratory conditions. s^0 values are approximated from the saturation profiles of each test; 0.320 and 0.295 for test 1 and test 2, respectively. The values of tuned parameters as obtained by least-square method (Chalk et al., 2012; You et al., 2013) are: capillary pressure model parameters $C = 10^{-4}$, $\alpha = 0.4$ and contact angle $\theta = 57.3^{\circ}$. The obtained saturation profiles for the two tests (blue and red curves (in the web version) in Fig. 2) are in good agreement with measured profiles (green and cyan points in Fig. 2).

5. Analysis of the results

In this section, the analytical model developed in Section 3 is applied to investigating the effect of contact angle on the productivity behaviour of both phases in linear and radial flows. The linear case applies to flow towards a fracture or coreflood in the laboratory; while the radial case applies to flow towards wellbore in the field. Sensitivities of productivity for gas and water to the capillary-viscous ratio and altered zone length are analysed.

The values of rock and fluid properties used in this study to portray unconventional reservoirs with low permeability are listed in Table 1. The well radius is: $r_w = 0.15$ m.

The contact angle affects boundary saturation and relative permeability curves. Sensitivity of the contact angle to fractional flow function and boundary saturations s^0 and s_0 is analysed. Fractional flow function $f(s)$ calculated from (14) is presented in Fig. 3a. The fractional flow decreases with contact angle for any given saturation in the range $s_{wc} < s < 1 - s_{gr}$.

Fig. 3b shows the contact angle dependences of s_0 calculated from $P_c(s_0,\theta) = 0$ and s^0 calculated from $f(s^0,\theta) = f^0$. Both saturations s^0 and s_0 decrease with contact angle; s^0 and s_0 are equal at an intermediate contact angle (Fig. 3b), which results in a constant saturation profile at this contact angle.

Alteration of contact angle introduces two competitive effects on the productivity for water and gas. One effect is the reduction of saturation profile with contact angle (capillary effect), which decreases water production and increases gas production; the other is increase in fractional flow function with contact angle (viscous effect), which increases water production and decreases gas production.

Table 1
Values of rock and fluid properties.

Parameter	Value
k (md)	1
ϕ	0.05
η	0.75
σ (N/m)	0.08
C	0.5
α	0.9
μ_g(Pa s)	1.5×10^{-5}
μ_w (Pa s)	1×10^{-3}

The dimensionless total mobility is defined as the product of total mobility and water viscosity: $\Lambda = \lambda\mu_w$. Fig. 3c presents dimensionless total mobility versus water saturation s at different contact angles. At small contact angle θ, increase of saturation leads to increase of relative permeability for water k_{rw} and decrease of relative permeability for gas k_{rg}. The dominance of gas permeability due to large water–gas viscous ratio causes reduction of dimensionless total mobility Λ with saturation.

At large contact angle θ, k_{rw} is high and k_{rg} is low at large water saturation. The effect of k_{rw} increase dominates over that of k_{rg} decrease, which yields increase of Λ at large water saturation.

Fig. 4 presents the saturation profiles $s(X)$ for different contact angles with small (Fig. 4a) and large (Fig. 4b) capillary-viscous ratios in linear flow. The curves start at $X = 0$ from saturation value S_0. For $X \to \infty$, the profiles tend to s^0. The curves are monotonic. The conditions at $X = 0$ and $X \to \infty$, as determined by the rock wettability and by the rates of both phases, are independent. At a certain contact angle, $s_0 > s^0$ yields decreasing saturation profiles (blue, green and red curves) and $s_0 < s^0$ yields increasing saturation profiles (grey and cyan curves). The slope of $s(X)$ increases with θ, from low negative value at $\theta = 0$ (blue curves) to high positive value at $\theta = \pi$ (cyan curves). The capillary-viscous ratio ε_c determines the significance of capillary end effect. The magnitude of slope of $s(X)$ curve decreases with ε_c (Fig. 4). The same behaviour occurs in radial flow.

The productivity index (Eq. (16)) can be used to evaluate the total effect of contact angle on productivity for each phase. The full range of contact angle from 0 to π is examined (Fig. 5). PI values for gas and water at contact angle of $\pi/2$ are used as scales to obtain dimensionless PIs. The saturation profile is constant for all ε_c values at this contact angle, which corresponds to the condition $s_0 = s^0$ (intersection between blue and green curves in Fig. 3b). Therefore, relative permeabilities (7, 8) are independent of ε_c. PIs for both gas and water at $\theta = \pi/2$ are independent of ε_c (Fig. 5).

For large values of ε_c, the effect of saturation decrease with contact angle (capillary effect) dominates over the effect of fractional flow increase (viscous effect) on PI. Increase of contact angle leads to the increase of PI for gas (blue and green (in the web version) curves in Fig. 5a) and decrease of PI for water (blue and green curves in Fig. 5b). As ε_c decreases, the capillary and viscous effects become comparable. The two competitive effects lead to an optimal PI at an intermediate contact angle (red and cyan curves in Fig. 5a and b). The optimal contact angle increases with ε_c for gas and decreases with ε_c for water. Larger value of ε_c yields higher increase in PI for both gas and water (Fig. 5).

Let us investigate the effect of altering the contact angle of a fraction of the production zone on the PI-contact angle profile. We consider an example where the rock surface is partially treated by a wettability alteration agent from the flow exit y_0 up to a certain distance y_1. The zone from y_1 to the inlet y_2 remains unaltered. Without losing generality, the rock surface is assumed water wet before treatment and the initial contact angle is zero. After the treatment, the contact angle of the altered zone θ_a is shifted to a chosen value ranging from 0 to π.

Fig. 6 shows the saturation profile at different altered contact angles θ_a for low (Fig. 6a) and high (Fig. 6b) capillary-viscous ratios. Saturation decreases with contact angle in the wettability alteration zone ($0 < X < \beta$). Capillary pressure continuity is satisfied across the boundary between wettability altered and unaltered zones ($X = \beta$), which yields discontinuous saturation at this boundary (Fig. 6). Increase of contact angle in the zone near to core outlet or fracture face ($0 < X < \beta$) of water-wet rocks results in

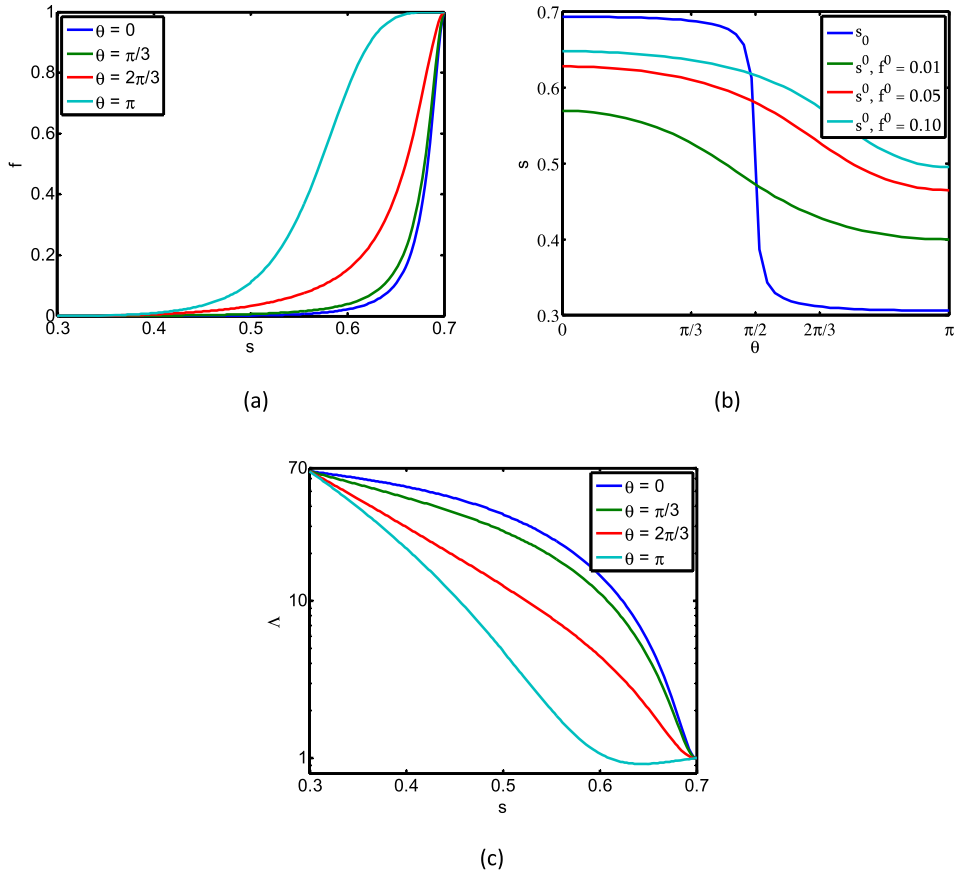

Fig. 3. Effects of contact angle on steady-state two-phase flow: (a) fractional flow curve for water at different contact angles; (b) boundary saturations versus contact angle at different fractional flow for water f^0; (c) dimensionless total mobility versus saturation at different contact angles.

decrease of saturation near the exit, but the capillary end effect still occurs in the unaltered zone ($X > \beta$).

Restriction of gas flow due to capillary end effect occurs at the exit ($X = 0$) for low θ_a and at the boundary between wettability altered and unaltered zones ($X = \beta$) for high θ_a (Fig. 6). Despite the intention of reducing the end effect by wettability alteration in the zone near to wellbore or fracture face, end effect at the altered zone boundary can still occur. Higher capillary-viscous ratio results in larger end effect. It reduces the productivity for gas at both high and low contact angles (Fig. 7a). Contact angle alteration affects saturation in the altered zone significantly (Fig. 6). In this zone the competing capillary and viscous effects yield an intermediate optimal contact angle for the maximum gas productivity (Fig. 7a). The optimal contact angle is around $\pi/2$.

However, the water flow is only restricted at high contact angles. As capillary-viscous ratio increases, the end effect increases. It reduces the water productivity at high contact angles (Fig. 7b). Water production from water-wet reservoirs can be maximised by altering the contact angle in wettability alteration zone ($0 < X < \beta$) towards the optimal value $\theta_a < \pi/2$, and can be minimised by altering the contact angle towards $\theta_a = \pi$ (Fig. 7b).

The sensitivity of productivity index to the altered zone length β is investigated. PI for gas versus contact angle in the case of piecewise-constant contact angle in linear flow is shown in Fig. 8a.

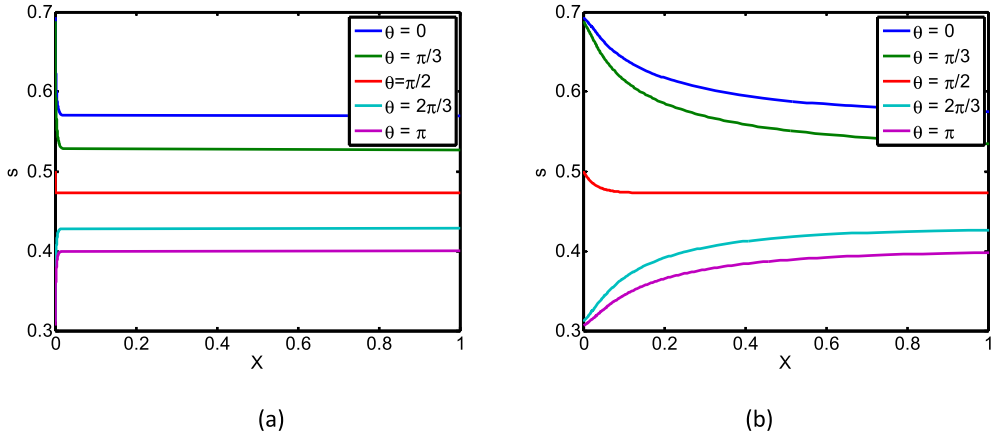

Fig. 4. Saturation profiles for different contact angles in linear flow ($f^0 = 0.01$): (a) $\varepsilon_c = 0.1$; (b) $\varepsilon_c = 10$.

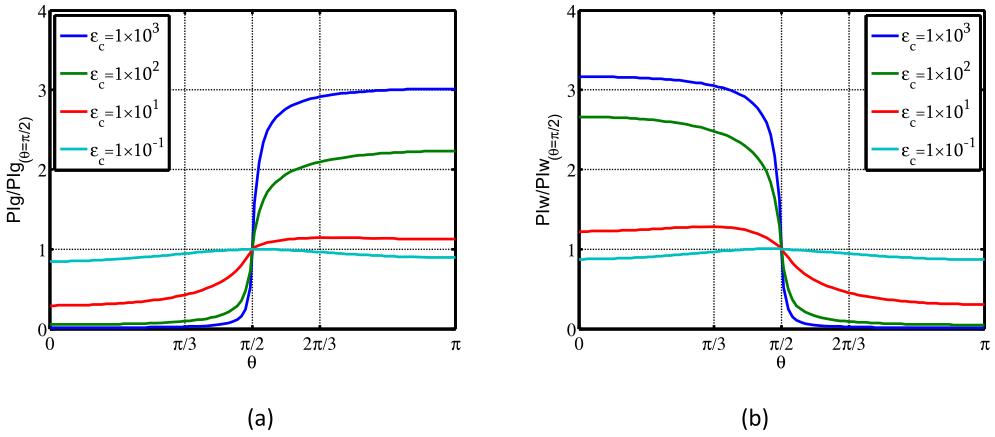

Fig. 5. Productivity index versus contact angle at different capillary-viscous ratios ε_c in linear flow ($f^0 = 0.01$): (a) gas; (b) water.

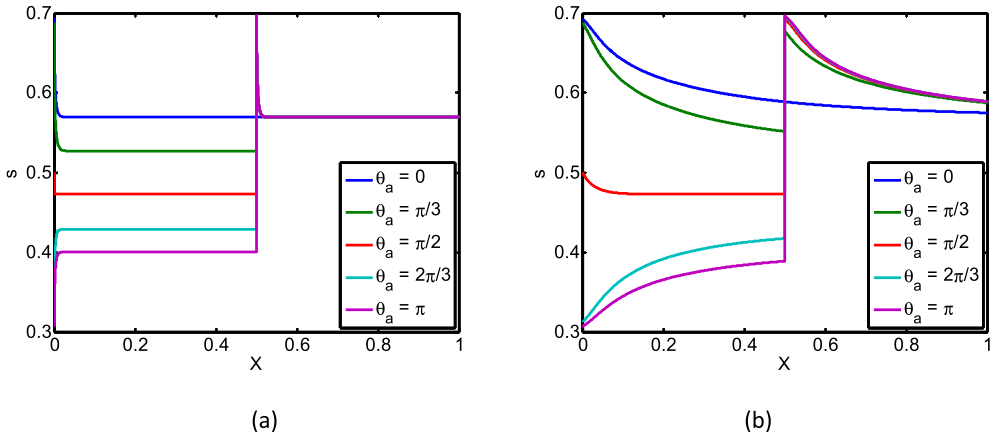

Fig. 6. Saturation profile at different altered contact angle θ_a in linear flow with piecewise alteration of contact angle ($f^0 = 0.01$, $\beta = 0.5$): (a) $\varepsilon_c = 0.1$; (b) $\varepsilon_c = 10$.

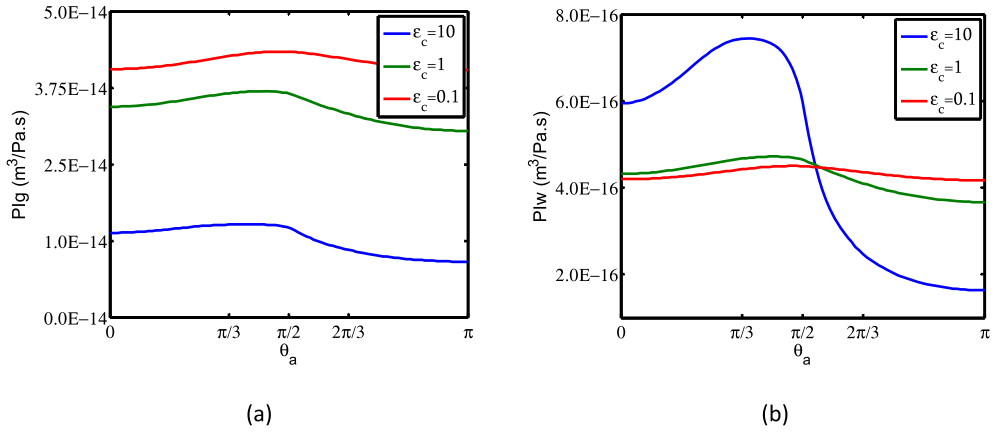

Fig. 7. Productivity index versus piecewise alteration of contact angle in water-wet rock at different ε_c in linear flow ($f^0 = 0.01$, $\beta = 0.5$): (a) gas; (b) water.

The maximum value of PI for gas increases with β, since the variation of saturation and relative permeability in altered zone occurs over a larger distance with β. The increase of β from 0.005 to 0.5 results in the increase of productivity index for gas from 0.1% to 7% at $\theta_a = \pi/2$ (green curve in Fig. 8b).

Saturation profiles in radial flow towards well at different θ_a for low (Fig. 9a) and high (Fig. 9b) ε_c are presented in the case of piecewise alteration of contact angle. Saturation decreases with contact angle θ_a in the wettability alteration zone ($0 < R < \beta$). Increase of contact angle in the zone near to wellbore ($0 < R < \beta$) of water-wet rocks results in decrease of saturation near the exit, but the capillary end effect still occurs in the unaltered zone ($R > \beta$) (Fig. 9). The pressure drop across the altered zone near the wellbore is much higher compared to that in linear case, causing the altered zone properties to be more influential over the total flow in radial than in linear case. Therefore, PI profile is more sensitive to β in radial case than that in linear case (Fig. 10a). Higher β leads to higher productivity index; the increase of β from 5×10^{-4} to 0.05

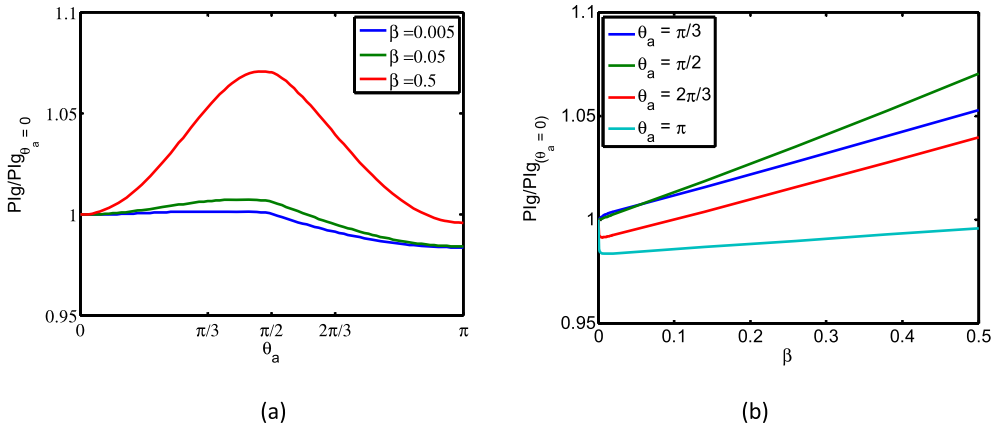

Fig. 8. Productivity index for gas in the case of piecewise-contact angle in linear flow ($f^0 = 0.01$, $\varepsilon_c = 0.1$): (a) PI_g versus θ_a; (b) PI_g versus β.

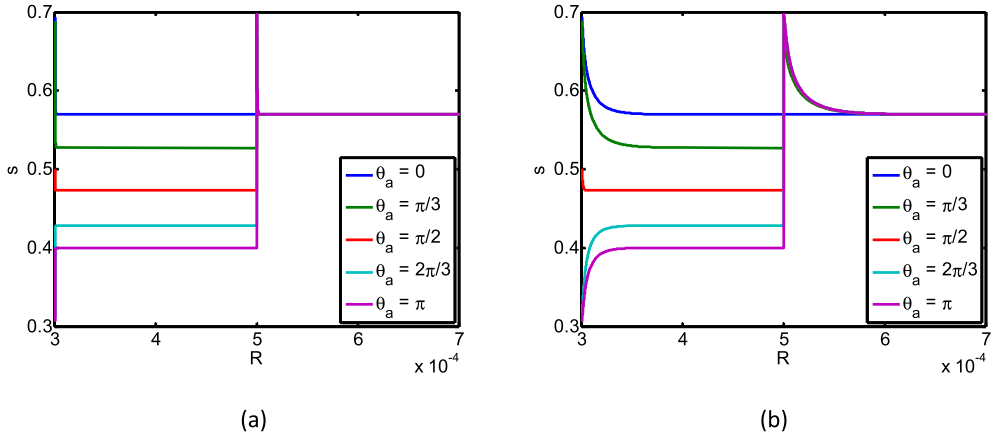

Fig. 9. Saturation profiles at different altered contact angle θ_a in radial flow with piecewise alteration of contact angle ($f^0 = 0.01$, $\beta = 5.0 \times 10^{-4}$): (a) $\varepsilon_c = 0.01$; (b) $\varepsilon_c = 0.5$.

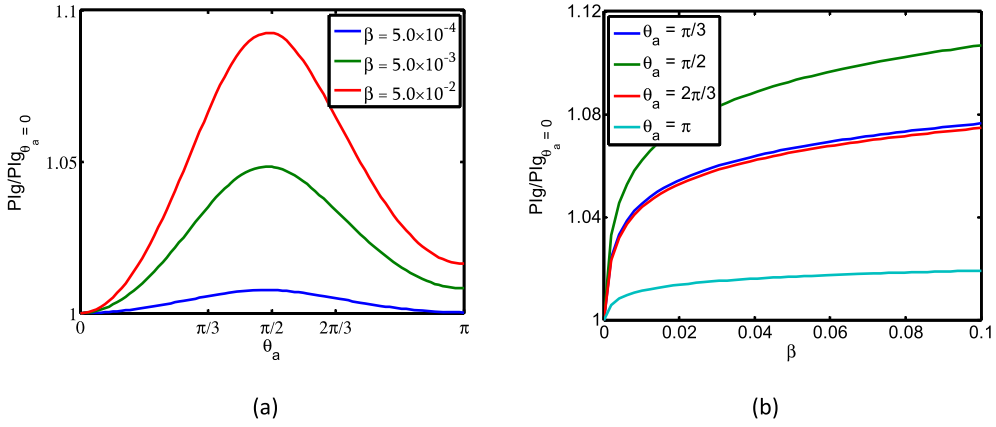

Fig. 10. Productivity index for gas in the case of piecewise contact angle in radial flow ($f^0 = 0.01$, $\varepsilon_c = 0.01$): (a) PI_g versus θ_a; (b) PI_g versus β.

results in the increase of productivity index for gas from 1% to 9% at $\theta_a = \pi/2$ (green curve in Fig. 10b).

6. Nanoparticle injection for wettability alteration in unconventional rocks

Presently, nanoparticles (NPs) are extensively applied to wettability alteration of reservoir rocks for waterflooding (Maghzi et al., 2012; Giraldo et al., 2013; Ju and Fan, 2013; Hendraningrat and Torsaeter, 2014). The adsorption of nanoparticles onto rock surface is dependent on DLVO forces exerting on NPs (Li and Torsaeter, 2015), which indicates that different types of NPs and surface materials exhibit different interactions. The wettability alteration of rock surface is affected by the types of NPs and the underlying mineralogy, leading to different resultant contact angles based on their combinations.

The main minerals present in unconventional coal seam and shale reservoirs are sand, clays and organic matter. Karimi et al.

(2012) applied zirconium dioxide (ZrO_2) NPs to decrease carbonate contact angle from 90° to 0°. Li and Torsaeter (2015) used hydrophilic silica NPs to decrease contact angle of sandstone rock surface from 54° to 22°. Hendraningrat and Torsaeter (2014) investigated three metal oxides NPs: aluminium (Al_2O_3), titanium (TiO_2) and silicon (SiO_2). Nano fluids used in the experiment with the concentration 0.05 wt% result in the contact angles measured in brine (NaCl 3 wt%) lowered from 53.68° to 28.6°, 21.64° and 38.82° for Al_2O_3, TiO_2 and SiO_2, respectively. To increase the contact angle, lipophilic polysilicon NPs with surface modification can be used (Ju and Fan, 2009). Hydrophobic and neutral wet polysilicon nano fluids with concentration 4 g/L successfully altered sandstone contact angle from 50° to 84.56° and 98.12°, respectively (Roustaei et al., 2012). Cupric oxide (CuO) NPs increased water contact angles from less than 5° up to 130° and 150° with amine- and thiol-modified surfaces, respectively (Basu et al., 2011).

Lebedeva and Fogden (2011) investigated the wettability alteration of kaolinite clay surface, due to the deposition of asphaltene nanoparticles. The clay surface was altered from hydrophilic to hydrophobic with contact angle 140°.

To the best of our knowledge, application of NPs to the wettability alteration of organic matter has not been reported in the contemporary literature.

Let us estimate the effects of contact angle alteration by applying different NPs using the analytical model (Section 3) for the above-mentioned cases. Productivity index values versus contact angle are shown in Figs. 5 and 7 for $f^0 = 0.01$. For low water fractional flow $f^0 = 0.01$ and the contact angle altered from 50° to 90° (Roustaei et al., 2012), $\varepsilon_c = 5$ and 0.05 result in PI_g increase by 2.0 and 1.08 times, respectively. For high water fractional flow $f^0 = 0.95$ and the contact angle altered from 0° to 130° (Basu et al., 2011), gas productivity index PI_g can be increased by 4.7 and 1.25 times for high ($\varepsilon_c = 5$) and low ($\varepsilon_c = 0.05$) capillary-viscous ratios, respectively. Given $f^0 = 0.01$ with contact angle alteration from 0° to 50° (Vafaei et al., 2006), water productivity index PI_w is increased by 2.1 and 1.96 times for $\varepsilon_c = 5$ and 0.05, respectively.

Different types of NPs affect wettability of shale- or coal-minerals differently; hence, a mixture (cocktail) of NPs must be developed for multi-mineral rocks. The corresponding technology includes adding nanoparticles that increase the resulting contact angle, into a drilling or fracturing fluid. The contact angle increase yields the pore-scale deviation of water into larger pores, increasing water rate during dewatering, and decreasing water saturation to facilitate the gas flow in the future. Injection of nanoparticles, making the rock more water-wet, after the dewatering, leads to water displacement into smaller pores with the consequent gas rate increase. The fast pore pressure decrease in both scenarios results in more intensive gas desorption. To summarise, the well treatment described above includes adding NPs into drilling or fracturing fluids with the consequent increase of the contact angle (first stage); at the second stage, hydrophilic NPs are injected into the reservoir in order to decrease the contact angle after dewatering during gas production. Therefore, two different cocktails must be developed for two stages. The delivery of nanoparticles is performed by the injection together with fast deteriorating gas-based foam (Farajzadeh et al., 2011).

The analytical model for steady-state gas-water flow in rocks with piecewise-constant contact angle can be used for design of the treatment technology, including defining volumes of injected fluids and their compositions. The analytical model can also be applied to the upscaling of laboratory data for well index prediction.

7. Discussions

The analytical model for steady-state flow is based on equality of the pressure and capillary-pressure gradients. The exact solution for steady-state flow with piecewise-constant contact angle is expressed by implicit analytical formulae, allowing for explicit expressions for the well productivity index.

The saturation profile for steady-state flow in the rock with constant contact angle starts at the boundary value s_0, which corresponds to zero capillary pressure, and tends to constant s^0 as X tends to infinity, where the constant saturation is determined by fractional flow. Size of the end effect zone, where the significant fraction of variation $s_0 - s^0$ occurs, is equal to $\varepsilon_c L$. Therefore, at low capillary-viscous ratio, the saturation profile is almost uniform, while the saturation varies along the distance at high capillary-viscous ratio. In the rocks with piecewise-constant contact angle, the above profiles are valid in constant-contact-angle intervals; the profiles in different intervals are matched by the continuity condition for capillary pressure yielding the saturation jumps.

A plane-parallel-flow analytical model is applied to the treatment of coreflood data, and also to flow and saturation prediction near to the fractured well. The axi-symmetric model is applied for vertical and horizontal wells.

Let us discuss the limitations of the analytical model (15). It assumes gas is incompressible. Since the gas density is a function of pressure, the incompressibility assumption is valid if the pressure drawdown is much less than the reservoir pressure:

$$\frac{\Delta P}{P} \ll 1 \tag{18}$$

For linear flow during coreflooding, substitution of Darcy's law $U = k/\mu(\Delta P/L)$ into the condition (18) yields:

$$\frac{\Delta P}{P} = \frac{U\mu L}{kP} \ll 1 \tag{19}$$

or

$$U \ll \frac{kp}{\mu L} \tag{20}$$

For core length $L = 0.1$ m, permeability k varying from 0.01 to 10 md, gas viscosity μ varying from 10^{-5} to 4×10^{-5} Pa s, and pressure P varying from 5×10^5 to 10^7 Pa, the maximum velocity where the incompressibility assumption is valid varies from 1.2×10^{-5} to 1 m/s. The typical flow velocities in cores have the order of magnitude 10^{-6}–10^{-5} m/s (Barenblatt et al., 1990; Bazin et al., 2010). Therefore, gas compressibility is negligible under the conditions of these laboratory studies by Bazin et al. (2010), so the incompressibility assumption is valid.

For fractured wells, velocity at the fracture face is calculated using Eq. (20). For permeability variation $k = 0.01$–10 md, $\mu = 10^{-5}$–4×10^{-5} Pa s, reservoir pressure $P = 5 \times 10^6$–10^8 Pa, and length of linear flow region towards the fracture $L = 10$–250 m, the maximum velocity where the incompressibility assumption is valid varies from 5×10^{-8} to 0.1 m/s. Typical velocities at fracture faces in gas reservoirs have the order of 10^{-5}–10^{-4} m/s (see Shaoul et al., 2012). Therefore, there are some unconventional field cases where the incompressibility assumption is valid, and where it is not. Inequality (20) defines the conditions where the analytical model (15) is valid.

For radial flow towards well, the rate of incompressible fluid per unit height of reservoir (Q) is calculated as:

$$Q = \frac{2\pi k \Delta P}{\mu \ln(r_e/r_w)} \tag{21}$$

Substitution of rate expression in vertical well into the condition (18) yields:

$$Q \ll \frac{2\pi kp}{\mu \ln(r_e/r_w)} \tag{22}$$

For $k = 0.01$–10 md, $\mu = 10^{-5}$–4×10^{-5} Pa s, $P = 10^7$–10^8 Pa, ratio between drainage and well radii $r_e/r_w = 10^3$–10^4, the maximum rate per unit height, where the incompressibility assumption is valid varies from 1.7×10^{-5} to 0.9 m^2/s. Some typical rates for tight gas reservoirs vary in the range 10^{-3}–0.1 m^2/s (see McGowen et al., 2007). Thus, the gas compressibility can be ignored in some cases, and cannot be ignored in other cases.

For the linear flow case in this paper, $k = 1$ md, $\mu = 2 \times 10^{-5}$ Pa s and length of linear flow region is 10^3 m. For pressure varying from 5×10^6 to 10^8 Pa, the maximum velocity where the incompressibility assumption is valid varies from 2.5×10^{-6} to 5×10^{-5} m/s. The velocities in the synthetic case (Section 5) are in the order of 10^{-7} m/s, therefore the incompressibility assumption is valid. For the radial flow regime, we use the same permeability, viscosity and pressure range. For $r_e/r_w = 6.67 \times 10^3$, the maximum rate per unit height where the incompressibility assumption is valid varies from 2×10^{-3} to 3.5×10^{-2} m^2/s. The rates in the synthetic case have the order of 10^{-4} m^2/s, therefore the incompressibility assumption is valid.

In the case that the gas compressibility cannot be neglected, such as for high rates or high pressure drawdowns, equation of state for gas $\rho_g(P_g)$ is included in gas rate equation (10). The final expression for steady-state solution is a system of two ordinary differential equations with respect to pressure and saturation.

The gas slip effect can be significant in porous media with low pressure or low permeability (Wu and Pruess, 1998; Civan et al., 2011). According to gas permeability Equation (9), the slip effect is negligible if gas pressure is much larger than the Klinkenberg factor b. For typical permeability $k = 0.001$ and 1 md, the value of b is 3.3×10^5 and 2.8×10^5 Pa, respectively. A typical reservoir pressures in coal seams are 10^6–10^7 Pa (Gaurav et al., 2012). The corresponding error in calculated relative permeability for gas using (9) is 2–6%, if gas slip effect is ignored. In shallow gas reservoirs, pressure can be even lower, which leads to higher effect of gas slip. For shallow reservoirs or reservoirs with ultra-low permeability, the gas slip effect can cause rate miscalculation around 10% if it is ignored. It can be especially prevalent in core-flooding tests, where low pressures are commonly used.

Knudsen diffusion occurs where the gas with low enough density flows in small enough capillaries, such that the gas particles collide more frequently with the solid walls than with other particles (Bhatia et al., 2011). Knudsen diffusion can be evaluated by the Knudsen number K_n, defined as the ratio between the mean free path of gas molecule and the pore size:

$$K_n = \frac{\lambda}{d_p}, \quad \lambda = \frac{k_B T}{\sqrt{2} P \pi d_g^2} \tag{23}$$

where λ is mean free path of gas, d_p is pore diameter, k_B is Boltzmann constant (1.38×10^{-23} J/K), T is gas temperature, d_g is diameter of gas molecule. Knudsen diffusion is negligible if $K_n \ll 0.1$ (He et al., 2014). We consider methane molecule diameter 4.14×10^{-10} m and typical reservoir temperature 373 K. Pore sizes in coal seam reservoirs can range from a few angstroms to over a micron. For pressure varying from 5×10^6 to 10^8 Pa, K_n in coal seams can vary from 7×10^{-5} to 3. Pore sizes in shales range from 0.005 to 0.1 μm (Nelson, 2009). For pressure varying from 5×10^6 to 10^8 Pa, K_n in shale reservoirs can vary from 7×10^{-4} to 0.3. Therefore, Knudsen diffusion effect can be significant in tight formation; however, it is not always the case.

For rocks with permeability 1 md (corresponding $d_p = 0.1$ μm), the calculated $K_n = 0.1$ for gas pressure $P = 6.8 \times 10^5$ Pa. For rocks with low permeability 0.01 md ($d_p = 0.01$ μm), the calculated $K_n = 0.1$ for $P = 6.8 \times 10^6$ Pa. From this we conclude that the model neglecting Knudsen diffusion is applicable only for reservoirs at high reservoir pressures ($P > 6.8 \times 10^5$ Pa for 1 md, $P > 6.8 \times 10^6$ Pa for 0.01 md).

The Young–Laplace model for capillary pressure is valid if the disjoining pressure is negligible and surface tension is constant. It is inappropriate for pore/channel sizes in the range of nanometres. In this scale, applying the augmented Young–Laplace equation, the capillary pressure can be calculated as the sum of the traditional Young–Laplace term and the disjoining pressure in the thin water film which can wet the surface. The disjoining pressure effects have been used to describe the wetting film behaviour of a meniscus in regions around 0.1 μm (Kelly, 2013). If pore sizes are above this size, the Young–Laplace equation can be used to calculate capillary pressure. For the synthetic case study in Section 4, the average pore radius estimated from Kozeny–Carman model is 0.3 μm. Therefore, the capillary pressure calculated from Young–Laplace model is valid.

Good agreement between two saturation profiles as obtained from corefloods with different rates, and the prediction by the analytical model (15) with three tuning parameters C, α and θ has been observed (Fig. 2). The two measured saturation profiles can be approximated by exponential functions with three degrees of freedom each: $s(X) = A + Be^{CX}$, giving the two curves six degrees of freedom totally. Good match by tuning only three parameters validates the analytical model.

A simplified model for relative permeability and capillary pressure (Section 2) has been applied in this paper. The model corresponds to pore-space geometry as a bundle of parallel capillary with different wettability. In reality, natural rocks consist of numerous minerals with different wettability and grid-like pore-space geometry. One way around is the percolation-effective media model for the rocks with spotted micro heterogeneity in both capillary pressure and relative permeability (Barenblatt et al., 1990; Bedrikovetsky, 1993).

The obtained steady-state solutions provide the long-term asymptotics for non-steady state problems of immiscible Newtonian and Now-Newtonian displacements, which is important information for the transient analysis (Bedrikovetsky, 1993; Morrow and Buckley, 2011; Fogden et al., 2011). Since the long-term asymptotic states are in thermodymanic equilibrium, the solutions are applicable for partly-miscible flows also (Farajzadeh et al., 2011; Cinar and Riaz, 2014).

Two scenarios are investigated for water–gas flow with well treatment by NPs. One scenario involves increasing contact angle under high water saturation which corresponds to the processes of dewatering and the fracturing-fluid flow-back. The other scenario involves decreasing contact angle under low water saturation, which occurs during gas production.

Based on the analytical model developed, the strategy of gas productivity enhancement is as follows: For rocks with uniform wettability, alter contact angle of rock surface towards $\pi/2$ for low capillary-viscous ratio and π for high capillary-viscous ratio. For piecewise wettability alteration of water-wet rocks, optimal contact angle is $\pi/2$ for both low and high capillary-viscous ratios. The strategy targeting maximum water productivity is contact angle alteration towards $\pi/2$ for low capillary-viscous ratio and zero for high capillary-viscous ratio.

8. Conclusions

Analytical modelling and its application to enhancing the well productivity for gas and water by wettability alteration allow drawing the following conclusions:

- Competition between the viscous and capillary effects on gas productivity results in non-monotonic contact-angle-dependency of gas productivity index, suggesting the existence of optimal contact angle for enhanced gas production.
- For dewatering and fracturing fluid flow-back, competition between the viscous and capillary effects on water productivity yields the optimal contact angle which maximises the productivity index for water.
- In the case of wettability alteration over the full length, the higher the capillary-viscous ratio ε_c, the higher the capillary end effect, the larger the end effect zone and the higher the maximum productivity indexes for gas and water.
- In the case of wettability alteration on a fraction of water-wet rock, increase of the capillary-viscous ratio ε_c leads to the increase of the maximum productivity index for water and decrease for gas. This is because the capillary end effect at the boundary between wettability altered and unaltered zones reduces gas flow more severely with higher ε_c.
- The larger the altered zone length β, the higher the contact angle effect on gas and water productivity index. This is due to alteration of saturation profile and relative permeability over a larger distance.
- Productivity index is sensitive to small value of β in radial flow towards well, indicating that wettability alteration in small neighbourhood of wellbore can effectively improve productivity indexes for gas and water.
- Wettability alteration in the range achieved by nanoparticles, leads to 2.0–4.7 times increase of well productivity for gas and twice increase for water.
- The maximum productivity index for water should be applied during dewatering and slick water removal. The maximum productivity index for gas must be used during gas production stage.

Acknowledgements

Financial support from the Australian Research Council (ARC) Discovery and Linkage Projects is gratefully acknowledged. Authors thank the Editor and three anonymous reviewers for their comments that greatly improved the manuscript.

Nomenclature

b	Klinkenberg factor, Pa
C	capillary model parameter
d_g	diameter of gas molecule, m
d_p	pore diameter, m
f	fractional flow function
k	permeability, m^2
k_B	Boltzmann constant, J/K
k_r	relative permeability
P	pressure, Pa
P_c	capillary pressure, Pa
R	dimensionless radius
r	radius, m
S	normalised water saturation
s	water saturation
s_{gr}	irreducible gas saturation
s_{wc}	connate water saturation
U	total velocity, m/s
u	flow velocity of water or gas, m/s
x	distance, m
T	gas temperature, K
y_0	flow exit distance, m
y_1	treated distance, m
y_2	flow entrance distance, m

Greek letters

α	capillary model parameter
β	Altered zone length
ε_c	capillary-viscous ratio
η	tortuosity index
θ	surface contact angle
Λ	dimensionless total mobility
λ	mean free path of gas, m; total mobility, 1/Pa s
μ	viscosity, Pa s
ρ	density, kg/m^3
σ	interfacial tension, N/m
ϕ	porosity

Abbreviations

DLVO	Derjaguin–Landau–Verwey–Overbeek
NP	nanoparticle
PI	productivity index

Subscripts

a	altered
e	drainage radius
g	gas
w	water (for productivity index and relative permeability), wetting (for saturation), well (radius)
0	exit

Superscripts

0	inlet

References

Adibhatla, B., Mohanty, K., Berger, P., Lee, C., 2006. Effect of surfactants on wettability of near-wellbore regions of gas reservoirs. J. Pet. Sci. Eng. 52 (1), 227–236.
Anderson, W.G., 1987. Wettability literature survey part 5: the effects of wettability on relative permeability. J. Pet. Technol. 39 (11), 1453–1468.
Arab, D., Pourafshary, P., 2013. Nanoparticles-assisted surface charge modification of the porous medium to treat colloidal particles migration induced by low salinity water flooding. Colloids Surf. A Physicochem. Eng. Asp. 436, 803–814.
Assef, Y., Arab, D., Pourafshary, P., 2014. Application of nanofluid to control fines migration to improve the performance of low salinity water flooding and alkaline flooding. J. Pet. Sci. Eng. 124, 331–340.
Bahrami, H., et al., 2011. Effect of water blocking damage on flow efficiency and productivity in tight gas reservoirs. In: SPE-142283. SPE Production and Operations Symposium. Oklahoma, USA. 27–29 March.
Barenblatt, G.I., Entov, V.M., Ryzhik, V.M., 1990. Theory of Fluid Flows through Natural Rocks. Kluwer Academic Publishers, Dordrecht.
Basu, M., Sinha, A.K., Pradhan, M., Sarkar, S., Negishi, Y., Pal, T., 2011. Fabrication and functionalization of CuO for tuning superhydrophobic thin film and cotton wool. J. Phys. Chem. C 115, 20953–20963.
Bazin, B., et al., 2010. In-situ water-blocking measurements and interpretation related to fracturing operations in tight gas reservoirs. SPE Prod. Oper. 25 (4), 431–437.
Bedrikovetsky, P.G., 1993. Mathematical Theory of Oil & Gas Recovery (With Applications to Ex-USSR Oil & Gas Condensate Fields). Kluwer Academic Publishers, London-Boston-Dordrecht.
Bhatia, S.K., Bonilla, M.R., Nicholson, D., 2011. Molecular transport in nanopores: a theoretical perspective. Phys. Chem. Chem. Phys. 13 (34), 15350–15383.
Bradford, S.A., Abriola, L.M., Leij, F.J., 1997. Wettability effects on two- and three-fluid relative permeabilities. J. Contam. Hydrol. 28 (1–2), 171–191.
Bruining, J., Van Duijn, C.J., 2006. Traveling waves in a finite condensation rate model for steam injection. Comput. Geosci. 10 (4), 373–387.
Bryant, E., Bowman, R., Buckley, J., 2006. Wetting alteration of mica surfaces with polyethoxylated amine surfactants. J. Pet. Sci. Eng. 52 (1), 244–252.
Chalk, P., Gooding, N., Hutten, S., You, Z., Bedrikovetsky, P., 2012. Pore size distribution from challenge coreflood testing by colloidal flow. Chem. Eng. Res. Des. 90, 63–77.
Chaouche, M., Rakotomalala, N., Salin, D., Yortsos, Y., 1993. Capillary effects in immiscible flows in heterogeneous porous media. EPL Europhys. Lett. 21 (1), 19.
Chen, D., Pan, Z., Liu, J., Connell, L.D., 2013. An improved relative permeability model for coal reservoirs. Int. J. Coal Geol. 109, 45–57.
Chen, P., Mohanty, K.K., 2014. Wettability alteration in high temperature carbonate reservoirs. In: SPE-169125. SPE Improved Oil Recovery Symposium, Tulsa, Oklahoma, USA, 12–16 April.
Cinar, Y., Riaz, A., 2014. Carbon dioxide sequestration in saline formations: part 2-review of multiphase flow modeling. J. Pet. Sci. Eng. 124, 381–398.

Civan, F., Rai, C.S., Sondergeld, C.H., 2011. Shale-gas permeability and diffusivity inferred by improved formulation of relevant retention and transport mechanisms. Transp. Porous Media 86 (3), 925–944.
Economides, M.J., Wood, D.A., 2009. The state of natural gas. J. Nat. Gas Sci. Eng. 1 (1), 1–13.
Farajzadeh, R., Muruganathan, R.M., Rossen, W.R., Krastev, R., 2011. Effect of gas type on foam film permeability and its implications for foam flow in porous media. Adv. Colloid Interface Sci. 168 (1–2), 71–78.
Fogden, A., Kumar, M., Morrow, N.R., Buckley, J.S., 2011. Mobilization of fine particles during flooding of sandstones and possible relations to enhanced oil recovery. Energy Fuels 25 (4), 1605–1616.
Gaurav, K., Akbar, A., Saada, T.H., Kumar, S., 2012. Performance analysis in coal seam gas. In: SPE-157696. SPETT 2012 Energy Conference and Exhibition, Port-of-Spain, Trinidad. 11–13 June.
Giraldo, J., Benjumea, P., Lopera, S., Cortes, F.B., Ruiz, M.A., 2013. Wettability alteration of sandstone cores by alumina-based nanofluids. Energy Fuels 27 (7), 3659–3665.
He, W., Lv, W., Dickerson, J.H., 2014. Gas diffusion mechanisms and models. In: Gas Transport in Solid Oxide Fuel Cells. Springer, pp. 9–17.
Hendraningrat, L., Li, S., Torsæter, O., 2013. A coreflood investigation of nanofluid enhanced oil recovery. J. Pet. Sci. Eng. 111, 128–138.
Hendraningrat, L., Torsaeter, O., 2014. Unlocking the potential of metal oxides nanoparticles to enhance the oil recovery. In: OTC-24696, Offshore Technology Conference Asia, Kuala Lumpur, Malaysia, 25–28 March.
Huang, D.D., Honarpour, M.M., 1998. Capillary end effects in coreflood calculations. J. Pet. Sci. Eng. 19 (1), 103–117.
Jones, F.O., Owens, W.W., 1980. A laboratory study of low-permeability gas sands. J. Pet. Technol. 32 (9), 1631–1640.
Ju, B., Fan, T., 2009. Experimental study and mathematical model of nanoparticle transport in porous media. Powder Technol. 192, 195–202.
Ju, B., Fan, T., 2013. Experimental study on nanoparticles transport and its effects on two-phase flow behavior in porous networks. Part. Sci. Technol. 31 (2), 114–118.
Karimi, A., Fakhroueian, Z., Bahramian, A., Pour Khiabani, N., Darabad, J.B., Azin, R., Arya, S., 2012. Wettability alteration in carbonates using zirconium oxide nanofluids: EOR implications. Energy Fuels 26 (2), 1028–1036.
Kathel, P., Mohanty, K.K., 2013. Wettability alteration in a tight oil reservoir. Energy Fuels 27 (11), 6460–6468.
Kelly, S., 2013. Experimental investigation of the influence of molecular surface interactions on imbibition in shale nano-pore proxies. In: SPE-167635. SPE Annual Technical Conference and Exhibition, New Orleans, Louisiana, USA, 30 September-2 October.
Kumar, K., Dao, E.K., Mohanty, K.K., 2008. Atomic force microscopy study of wettability alteration by surfactants. SPE J. 13 (2), 137–145.
Lebedeva, E.V., Fogden, A., 2011. Wettability alteration of kaolinite exposed to crude oil in salt solutions. Colloids Surf. A Physicochem. Eng. Asp. 377 (1), 115–122.
Li, G., Ren, W., Meng, Y., Wang, C., Wei, N., 2014. Micro-flow kinetics research on water invasion in tight sandstone reservoirs. J. Nat. Gas Sci. Eng. 20, 184–191.
Li, S., Torsaeter, O., 2015. The impact of nanoparticles adsorption and transport on wettability alteration of intermediate wet berea sandstone. In: SPE-172943, SPE Middle East Unconventional Resources Conference and Exhibition, Muscat, Oman, 26–28 January.
Maghzi, A., Mohammadi, S., Ghazanfari, M.H., Kharrat, R., Masihi, M., 2012. Monitoring wettability alteration by silica nanoparticles during water flooding to heavy oils in five-spot systems: a pore-level investigation. Exp. Therm. Fluid Sci. 40, 168–176.
Mahadevan, J., Le, D., Hoang, H., 2009. Impact of capillary suction on fracture face skin evolution in waterblocked wells. In: SPE-119585. SPE Hydraulic Fracturing Technology Conference. The Woodlands, Texas, USA, 19–21 January.
Mahadevan, J., Sharma, M.M., Yortsos, Y.C., 2007. Capillary wicking in gas wells. SPE J. 12 (4), 429–437.
McCaffery, F., Bennion, D., 1974. The effect of wettability on two-phase relative permeabilities. J. Can. Pet. Technol. 13 (4), 42–53.
McGowen, J.M., Gilbert, J.V., Samari, E., 2007. Hydraulic fracturing down under. In: SPE-106051. SPE Hydraulic Fracturing Technology Conference. College Station, Texas, USA, 29–31 January.
Morrow, N., Buckley, J., 2011. Improved oil recovery by low-salinity waterflooding. J. Pet. Technol. 63 (5), 106–113.
Morsy, S., Gomaa, A., Sheng, J., 2014. Improvement of Mancos shale oil recovery by wettability alteration and mineral dissolution. In: SPE-169033. SPE Improved Oil Recovery Symposium, Society of Petroleum Engineers, Tulsa, Oklahoma, USA, 12–16 April.
Nasralla, R.A., Bataweel, M.A., Nasr-El-Din, H.A., 2013. Investigation of wettability alteration and oil-recovery improvement by low-salinity water in sandstone rock. J. Can. Pet. Technol. 52 (2), 144–154.
Nelson, P.H., 2009. Pore-throat sizes in sandstones, tight sandstones, and shales. AAPG Bull. 93 (3), 329–340.
O'Carroll, D.M., Abriola, L.M., Polityka, C.A., Bradford, S.A., Demond, A.H., 2005. Prediction of two-phase capillary pressure–saturation relationships in fractional wettability systems. J. Contam. Hydrol. 77 (4), 247–270.
Odumabo, S.M., Karpyn, Z., Ayala, H.,L., 2014. Investigation of gas flow hindrance due to fracturing fluid leakoff in low permeability sandstones. J. Nat. Gas Sci. Eng. 17, 1–12.
Roustaei, A., Moghadasi, J., Bagherzadeh, H., Shahrabadi, A., 2012. An experimental investigation of polysilicon nanoparticles' recovery efficiencies through changes in interfacial tension and wettability alteration. In: SPE-156976. SPE International Oilfield Nanotechnology Conference, Noordwijk, The Netherlands, 12–14 June 2012.
Shaoul, J.R., Spitzer, W., Dahan, M., 2012. Case study of unconventional gas-well fracturing in Hungary. SPE Prod. Oper. 27 (2), 145–157.
Shapiro, A.A., Wesselingh, J.A., 2008. Gas transport in tight porous media: gas kinetic approach. Chem. Eng. J. 142 (1), 14–22.
Vafaei, S., Borca-Tasciuc, T., Podowski, M.Z., Purkayastha, A., Ramanath, G., Ajayan, P.M., 2006. Effect of nanoparticles on sessile droplet contact angle. Nanotechnology 17 (10), 2523–2527.
Van Duijn, C.J., Molenaar, J., De Neef, M.J., 1995. The effect of capillary forces on immiscible two-phase flow in heterogeneous porous media. Transp. Porous Media 21 (1), 71–93.
Van Lingen, P.P., Bruining, J., Van Kruijsdijk, C.P.J.W., 1996. Capillary entrapment caused by small-scale wettability heterogeneities. SPE Reserv. Eng. 11 (2), 93–99.
Wang, J.Y., Holditch, S.A., McVay, D.A., 2012. Effect of gel damage on fracture fluid cleanup and long-term recovery in tight gas reservoirs. J. Nat. Gas Sci. Eng. 9, 108–118.
Wu, Y.-S., Pruess, K., 1998. Gas flow in porous media with Klinkenberg effects. Transp. Porous Media 32 (1), 117–137.
Xie, X., Liu, Y., Sharma, M., Weiss, W.W., 2009. Wettability alteration to increase deliverability of gas production wells. J. Nat. Gas Sci. Eng. 1 (1), 39–45.
You, Z., Badalyan, A., Bedrikovetsky, P., 2013. Size-exclusion colloidal transport in porous media – stochastic modeling and experimental study. SPE J. 18, 620–633.

Statement of Authorship

Title of Paper	Effect of Wettability Alteration on Productivity Enhancement in Unconventional Gas Reservoirs: Application of Nanotechnology.
Publication Status	☑ Published ☐ Accepted for Publication ☐ Submitted for Publication ☐ Unpublished and Unsubmitted work written in manuscript style
Publication Details	Naik, S., You, Z. and Bedrikovetsky, P., 2015, November. Effect of Wettability Alteration on Productivity Enhancement in Unconventional Gas Reservoirs: Application of Nanotechnology. In SPE Asia Pacific Unconventional Resources Conference and Exhibition. Society of Petroleum Engineers.

Principal Author

Name of Principal Author (Candidate)	Saurabh Naik
Contribution to the Paper	creating figures, analysis of results, writing the manuscript
Overall percentage (%)	85%
Certification:	This paper reports on original research I conducted during the period of my Higher Degree by Research candidature and is not subject to any obligations or contractual agreements with a third party that would constrain its inclusion in this thesis. I am the primary author of this paper.
Signature	Date 05/08/2019

Co-Author Contributions

By signing the Statement of Authorship, each author certifies that:

i. the candidate's stated contribution to the publication is accurate (as detailed above);

ii. permission is granted for the candidate in include the publication in the thesis; and

iii. the sum of all co-author contributions is equal to 100% less the candidate's stated contribution.

Name of Co-Author	Zhenjiang You
Contribution to the Paper	reviewing manuscript
Signature	Date 5/8/19

Name of Co-Author	Pavel Bedrikovetsky
Contribution to the Paper	reviewing manuscript
Signature	Date 5/8/19

Please cut and paste additional co-author panels here as required.

SPE-177021-MS

Effect of Wettability Alteration on Productivity Enhancement in Unconventional Gas Reservoirs: Application of Nanotechnology

Saurabh Naik, Zhenjiang You, and Pavel Bedrikovetsky, University of Adelaide, Australia

This paper was prepared for presentation at the SPE Asia Pacific Unconventional Resources Conference and Exhibition held in Brisbane, Australia, 9–11 November 2015.

Abstract

In unconventional water-wet gas reservoirs with very low permeability, water entrapment or blockage can occur near the wellbore due to the capillary end effect, resulting in low gas production. A reduction in capillary forces through wettability alteration of reservoir rock surface is proposed as an effective approach to reduce water blockage and enhance gas production. The method can be applied to accelerating dewatering and preventing drilling and fracturing fluid leak-off as well. Analytical models for steady-state water-gas linear and radial flows are developed in the current paper. The effects of contact angle on capillary pressure and relative permeabilities have been included. The new model is validated using experimental data. Applications to fully and partially treated regimes show the competition between viscous and capillary effects on productivity of gas and water, which leads to an optimal contact angle for the maximum productivity index for each phase. This study shows the potential for optimising unconventional gas productivity through wettability control. Application of nanotechnology to rock wettability alteration is proposed.

Introduction

Unconventional gas reservoir provides one of the key energy resources that can meet the current world's energy objectives. However, in such reservoirs with naturally low permeability, the capillary effect is significant if compared to the viscous effect. The capillary end effect as well as loss of fracturing and drilling fluids will lead to an increase of water saturation near the wellbore or fracture faces (Xie et al., 2009; Bahrami et al., 2011; Odumabo et al., 2014). Fluid invasion and water saturation in wellbore vicinity are sensitive to the contact angle of rock surface (Li et al., 2014).

The increased water saturation in the fracture or wellbore neighbourhood restricts gas flow from reservoir to the well. It is referred to as water blockage. Some research has been performed on water block clean-up (Mahadevan et al., 2007) and the long-term effect on production (Bahrami et al., 2011). One of the most effective methods to reduce water retention is wettability alteration (Anderson, 1987; Ford et al., 1988). Wettability modification of grain surface towards more hydrophobic by increasing contact angle results in decrease of capillary pressure and reduction of water blockage.

Many experimental works on wettability alteration have been reported in the literature. The contact angle of rock surface can be modified by surfactants (Kumar et al., 2008; Chen and Mohanty, 2014), nanoparticle (Maghzi et al., 2011; Alomair et al., 2015), high temperature steam (Bruining and Van Duijn, 2006), brine with various salinities (Lin et al., 2010; Nasralla et al., 2013) and water with different pH (Hoeiland et al., 2001; Morsy et al., 2014). Alteration of contact angle in sandstones and carbonates with variations of salinity and pH has been reported on low salinity waterflooding (Fogden et al., 2011; Morrow and Buckley, 2011). However, comprehensive research on wettability alteration in unconventional gas reservoirs is not available yet.

This paper presents the effects of contact angle alteration on well productivity for both water and gas, resulting from analytical models. The equations for steady-state saturation distribution and well index in heterogeneous rocks with piecewise-constant contact angle are derived. It is found that there exists an optimal contact angle to maximise the water production rate; another value of the contact angle maximises the production rate for gas. Calculations using the analytical model show that the wettability alterations cause increase in productivity index 2–4.7 times for gas and around two times for water.

Contact angle dependence on capillary pressure and relative permeability

The capillary pressure model starts from definition of the normalised water saturation S:

$$S(s) = \frac{s - s_{wc}}{1 - s_{wc} - s_{gr}} \tag{1}$$

where s is water saturation, s_{wc} and s_{gr} are connate water and irreducible gas saturations, respectively.

The contact angle at rock surface θ is measured between the water-gas interface and the water-solid interface. The rock is hydrophilic if $\theta<\pi/2$ and is hydrophobic if $\theta>\pi/2$. Hence, the wetting phase saturation S_w has two possible cases:

$$S_w(S,\theta) = \begin{cases} S(s), & \theta < \frac{\pi}{2} \\ 1 - S(s), & \theta > \frac{\pi}{2} \end{cases} \tag{2}$$

Unconventional reservoirs exhibit a variety of mineralogy and surface types such as organic matter (e.g. kerogen), aluminosilicate clays and silica sands; each mineral has its own wettability. This leads to the necessity of using fractional wettability to describe the rock surface.

In the present work, the Leverett-Cassie equation (O'Carroll et al., 2005) is applied to describe a porous medium which has three fractions of surface area with different contact angles. The major fraction f_1 has the contact angle which is considered alterable by wettability altering agents. A small fraction f_2 is permanently water wet with contact angle 0 and another small fraction f_3 is permanently hydrocarbon wet with contact angle π. Therefore, the overall capillary pressure of porous medium can be expressed as:

$$P_c(s,\theta) = \frac{2\sigma}{\sqrt{\frac{k}{\phi}}} J(s,\theta), \quad J(s,\theta) = f_1 \cos(\theta) C S_w(s,\theta)^{-\frac{1}{\alpha}} + f_2 C S(s)^{-\frac{1}{\alpha}} + f_3 C\big(1 - S(s)\big)^{-\frac{1}{\alpha}} \tag{3}$$

where f_1, f_2, f_3 are the major fraction and two minor fractions of rock surface respectively, $f_1 + f_2 + f_3 = 1$; C and α are empirical model parameters; σ is the interfacial tension, k is the rock permeability, and ϕ is the porosity.

The relative permeabilities of water and gas can be expressed as functions of water saturation (Chen et al., 2013):

$$k_{rw}(s) = \big(S(s)\big)^{\eta} \frac{\int_0^S w^2(s)ds}{\int_0^1 w^2(s)ds} \tag{4}$$

$$k_{rg}(s) = \left(1 - S(s)\right)^{\eta} \frac{\int_S^1 w^2(s)ds}{\int_0^1 w^2(s)ds} \tag{5}$$

where η is the tortuosity index and $w(S) = \sqrt{\frac{k}{\phi}}/CS^{-\frac{1}{\alpha}}$ is the capillary radius or cleat height.

To express the relative permeability as a function of rock contact angle, we apply the model accounting for wettability heterogeneity of natural cores in microscale (McCaffery and Bennion, 1974); Bradford et al., 1997). Introduce a weighting function $g(\theta)$ describing the fraction of total pores with hydrophobic surfaces:

$$g(\theta) = (1 - \cos\theta)/2 \tag{6}$$

Thus, the contact-angle-dependent relative permeabilities for water and gas become:

$$k_{rw}(s,\theta) = \left(S(s)\right)^{\eta} \frac{[1-g(\theta)]\int_0^S w^2(s)ds + g(\theta)\int_{1-S}^1 w^2(s)ds}{\int_0^1 w^2(s)ds} \tag{7}$$

$$k_{rg}(s,\theta) = \left(1 - S(s)\right)^{\eta} \frac{g(\theta)\int_0^{1-S} w^2(s)ds + [1-g(\theta)]\int_S^1 w^2(s)ds}{\int_0^1 w^2(s)ds} \tag{8}$$

Particularly, for gas flow in tight formation, especially in nano-porous media, Klinkenberg (gas slip) effect can have significant impact on gas flow. Eq. (8) for gas relative permeability is modified to take into account of the Klinkenberg effect:

$$k_{rg}(s,\theta) = \left(1 + \frac{b}{\overline{P_g}}\right)\left(1 - S(s)\right)^{\eta} \frac{g(\theta)\int_0^{1-S} w^2(s)ds + [1-g(\theta)]\int_S^1 w^2(s)ds}{\int_0^1 w^2(s)ds} \tag{9}$$

in which $\overline{P_g}$ is the average gas pressure along the distance, and b is the Klinkenberg factor. For tight gas reservoirs with permeability lower than 1 md, Klinkenberg factor is calculated as: $b = 0.86{k_\infty}^{-0.33}$ (Jones and Owen, 1980), where k_∞ is the gas permeability at infinite pressure.

Analytical model for steady-state two-phase flow

Darcy's law for water and gas flow can be expressed as (Cinar and Riaz, 2014):

$$u_w = -\frac{kk_{rw}(s,\theta)}{\mu_w}\nabla P_w, u_g = -\frac{kk_{rg}(s,\theta)}{\mu_g}\nabla P_g,\ U = u_w + u_g \tag{10}$$

where u_w and u_g stand for flow velocities of water and gas, respectively; U is the total velocity; k_{rw} and k_{rg} are relative permeabilities of water and gas, respectively; μ_w and μ_g are viscosities of water and gas, respectively; P_w and P_g are phase pressures.

Capillary pressure P_c is the difference between the gas and water pressures:

$$P_c = P_g - P_w \tag{11}$$

Fractional flow function f is calculated as the ratio of water mobility k_{rw}/μ_w to the total mobility λ:

$$f(s,\theta) = \frac{k_{rw}(s,\theta)/\mu_w}{\lambda(s,\theta)},\quad \lambda(s,\theta) = \frac{k_{rw}(s,\theta)}{\mu_w} + \frac{k_{rg}(s,\theta)}{\mu_g} \tag{12}$$

From Eqs (3, 10–12), we obtain the equation for saturation profile as:

$$\varepsilon_c \int_{s_0}^{s} \frac{f(s,\theta)k_{rg}(s,\theta)J'(s,\theta)}{f^0 - f(s,\theta)}ds = \int_{y_0}^{y} x^a dx \tag{13}$$

where ε_c is the capillary-viscous ratio, $f^0 = u_w/U$ is the fration of water flux. In linear flow, $\varepsilon_c = \frac{\sigma\sqrt{k\phi}}{\mu_g UL}$, distance $y = X$, $y_0 = 0$, a=0, s_0 is water saturation at the core outlet or fracture face. In radial flow,

$\varepsilon_c = \frac{2\pi\sigma\sqrt{k\phi}}{\mu_g q}$, $y = R$, $y_0 = R_w$, $a = -1$, s_0 is water saturation at wellbore. Eq. (13) defines the analytical solution for saturation profile in both linear and radial flows.

Note that the flow direction is from $y = 1$ to y_0. At the flow exit $y = y_0$, capillary pressure is $P_c = 0$. As capillary pressure is a monotonic function of saturation, the exit point saturation s_0 can be determined from $P_c(s_0, \theta) = 0$ for various contact angles. The saturation also tends to a certain value s^0 at the distance far away from the exit, i.e., as $y \to \infty$, $s \to s^0$. Inlet point saturation s^0 can be determined from $f^0 = f(s^0, \theta)$ for various contact angles.

The productivity index (PI) for each phase is calculated as the ratio of flow rate to the pressure drop in each phase:

$$\mathrm{PI}_i = q_i/\Delta P_i \tag{14}$$

where i represents either w (for water) or g (for gas). ΔP is the pressure drop calculated from (11) by integration over the distance from inlet to exit as:

$$\Delta P_i = \frac{u_i \mu_i}{k} \int_{y_0}^{1} \frac{x^a}{k_{ri}(s(x),\theta)} dx \tag{15}$$

The solution procedure for uniform wettability is: First, water saturation at the exit s_0 is calculated from capillary pressure condition $P_c(s_0, \theta) = 0$. Second, saturation profile is obtained from (13) for given ε_c and f^0. Third, pressure drops of water and gas are calculated from (15). Finally, productivity indexes for both phases are obtained from (14).

For piecewise-constant wettability, the region $y_0 \le y < \beta$ is considered the altered zone, where β is the altered zone length. The contact angle in this zone is $\theta = \theta_a$ (Fig. 1). the contact angle in the unaltered zone ($y \ge \beta$) is fixed as $\theta = \theta^0$ (Fig. 1). Capillary pressure and pressures for both phases are continuous across the boundary $y = \beta$. The saturation on the outer side of the boundary S^+, is calculated from the value on the inner side of the boundary s^- as: $P_c(s^+, \theta^0) = P_c(s^-, \theta_a)$. Then the saturation profile is calculated in the unaltered zone from $y = \beta$ to the inlet $y = 1$. Productivity indexes for gas and water are obtained from (14).

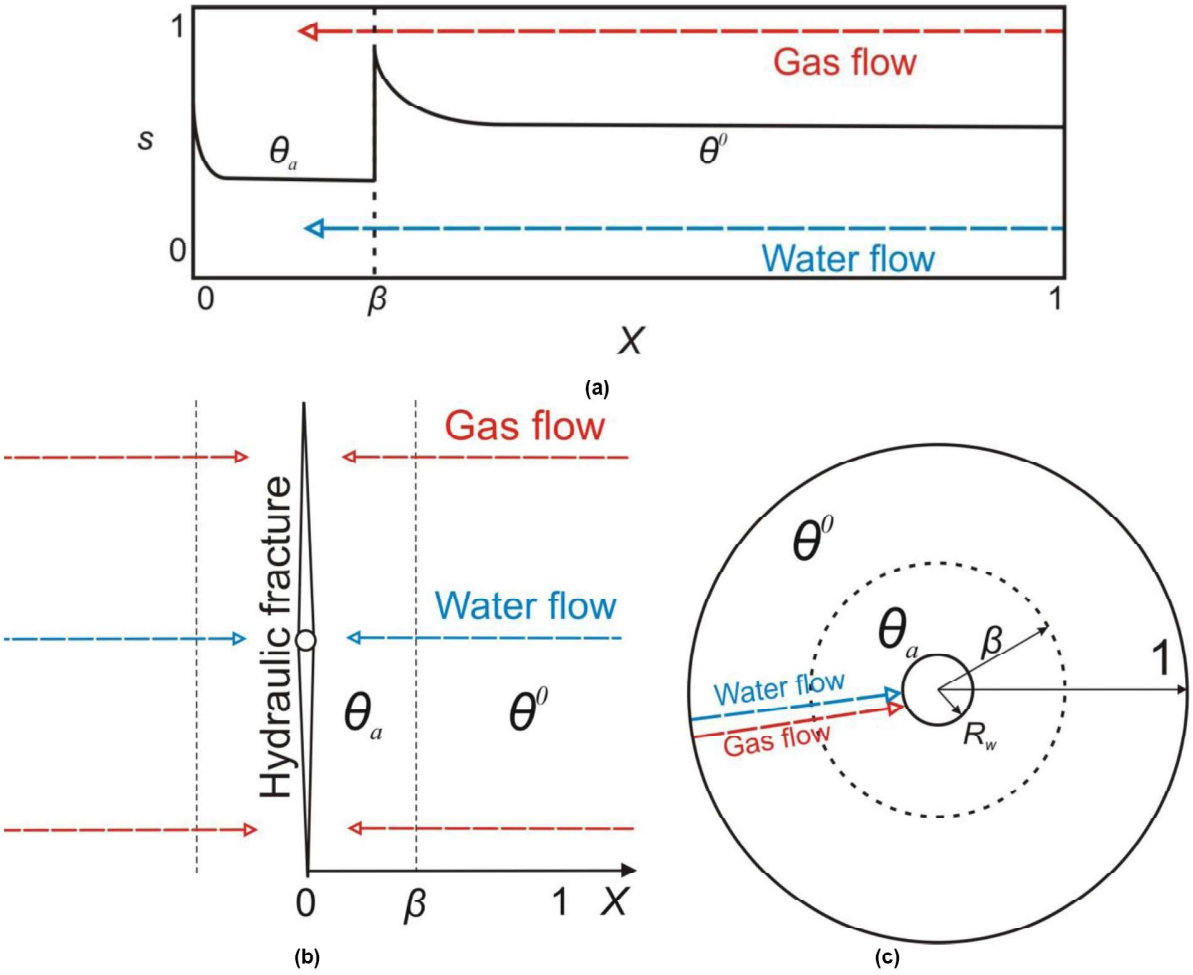

Figure 1—Schematic of partially treated inflow cases: (a) linear flow in coreflooding; (b) linear flow towards fracture face; (c) radial flow towards wellbore

Laboratory coreflood data analysis

Laboratory coreflooding tests with two flow rates (Bazin et al., 2010) are analysed to validate the model developed in Section 3.

Cylindrical Môlière sandstone core from tight gas reservoir with diameter 3.8 cm and length 7 cm is used in the test. The porosity ϕ=0.144, the initial core permeability is extremely low (0.01 md) and is typical for unconventional reservoirs, the tortuosity η = 2.0. The experimental procedure is: first, the core was fully saturated with water under vacuum. Second, nitrogen was injected into the core until irreducible water saturation was reached. Third, water was injected into the core with constant pressure until breakthrough. Fourth, nitrogen backflow was performed with constant pressure drawdown 10 bars in Test 1 and 15 bars in Test 2, respectively. The measured saturation profiles are shown in Fig. 2.

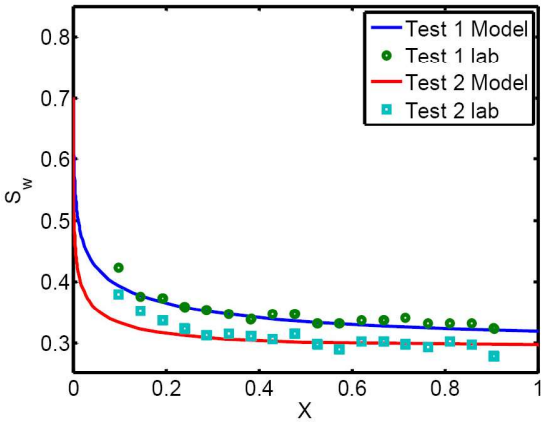

Figure 2—Saturation profiles from modelling compared with coreflood data

The analytical model in Section 3 is applied to the calculation of saturation profile under the laboratory conditions. Least-square optimisation, which has been well developed and widely used for data fitting (Forst and Hoffmann, 2010; Chalk et al., 2012; You et al., 2014, 2015), is applied here to optimising the values of tuning parameters as: capillary pressure model parameters $C = 10^{-4}$, $\alpha = 0.4$ and contact angle $\theta = 57.3°$. The obtained saturation profiles for the two tests match well with the measured profiles (Fig. 2), which validate the derived model.

Results analysis

The analytical model developed in Section 3 is applied to investigating the effect of contact angle on the productivity behaviour of both phases in linear and radial flows. The linear case applies to flow towards a fracture or coreflood in the laboratory; while the radial case applies to flow towards wellbore in the field.

The values of rock and fluid properties used in the case study are listed in Table 1. The well radius r_w=0.15 m.

Table 1—Rock and fluid properties in case study

Parameter	Value
k (md)	1
ϕ	0.05
η	0.75
C	0.5
α	0.9
σ (N/m)	0.08
μ_g(Pa.s)	1.5×10^{-5}
μ_w (Pa.s)	1.0×10^{-3}

The contact angle affects boundary saturation and relative permeability curves. Sensitivity of the contact angle to fractional flow function and boundary saturations s^0 and s_0 is analysed. Fig. 3(a) shows the fractional flow decreases with θ for any given saturation in the range $s_{wc} < s < 1\text{-}s_{gr}$. Fig. 3(b) shows the dependences of s_0 on θ calculated from $P_c(S_0,\theta) = 0$ and s^0 calculated from $f(s^0,\theta) = f^0$. Both saturations s^0 and s_0 decrease with θ; s^0 and s_0 are equal at an intermediate θ (Fig. 3(b)), which results in a constant saturation profile at this contact angle.

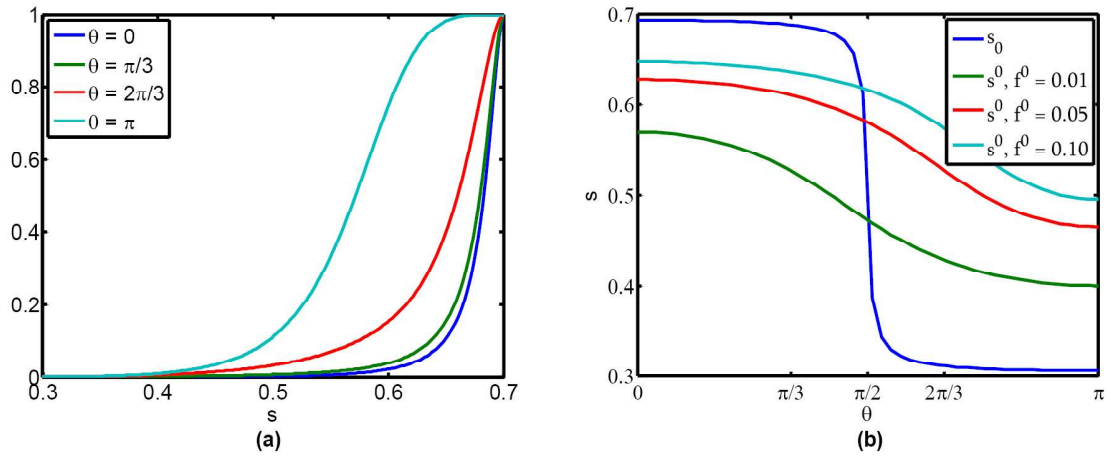

Figure 3—Effects of contact angle on steady-state two-phase flow: (a) fractional flow curve at different contact angles; (b) boundary saturations versus contact angle at different fractional flow for water f^0

Alteration of contact angle introduces two competitive effects on the productivity for water and gas. One effect is the reduction of saturation profile with contact angle. This is caused by capillarity, which decreases water production while increasing gas production. The other effect is the increase in fractional water flux with contact angle (viscous effect), which increases water production while decreasing gas production.

Fig. 4 presents the saturation profiles $s(X)$ for different θ with small and large capillary-viscous ratios in linear flow. The monotonic curves start at $X = 0$ from saturation value S_0, and tend to s^0 if $X \to \infty$. The conditions at $X = 0$ and $X \to \infty$ determined by the rock wettability and rates of both phases, are independent. Saturation decreases if $s_0 > s^0$ (blue, green and red curves) and increases if $s_0 < s^0$ (grey and cyan curves). The slope of $s(X)$ increases with θ, from low negative value at $\theta = 0$ (blue curves) to high positive value at $\theta = \pi$ (cyan curves). The capillary-viscous ratio ε_c determines the significance of capillary end effect. The magnitude of slope of $s(X)$ curve decreases with ε_c (Fig. 4). The same behaviour occurs in radial flow.

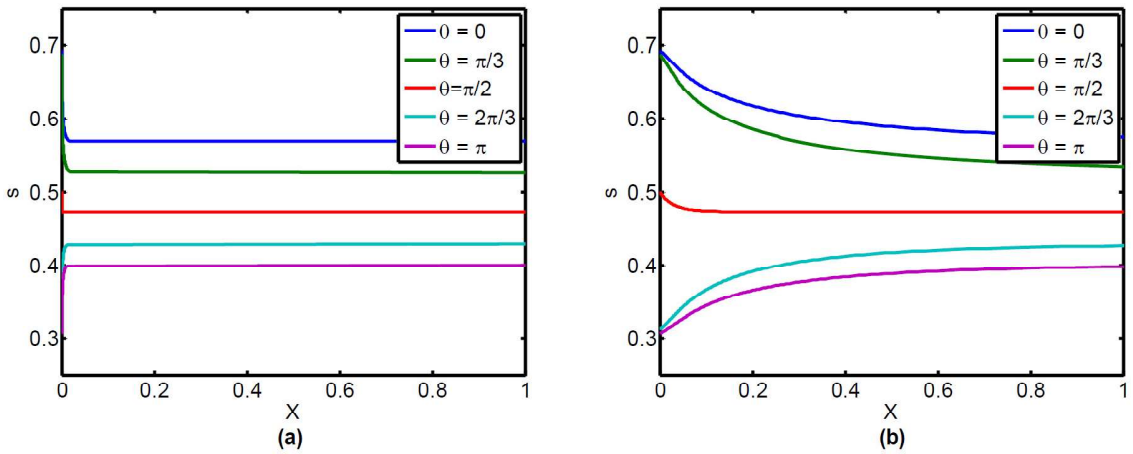

Figure 4—Saturation profiles for different contact angles in linear flow (f^0=0.01): (a) ε_c = 0.1; (b) ε_c = 10

The productivity index (Eq. (14)) can be used to evaluate the total effect of contact angle on productivity for each phase. The full range of θ from 0 to π is investigated (Fig. 5). PI values for gas and water at $\theta = \pi/2$ are used as scales to obtain dimensionless PIs. The saturation profile is constant for all

ε_c values at this contact angle, which corresponds to the condition $s_0 = s^0$ (intersection between blue and green curves in Fig. 3b). Therefore, relative permeabilities (7, 8) are independent of ε_c. PIs for both gas and water at $\theta = \pi/2$ are independent of ε_c (Fig. 5).

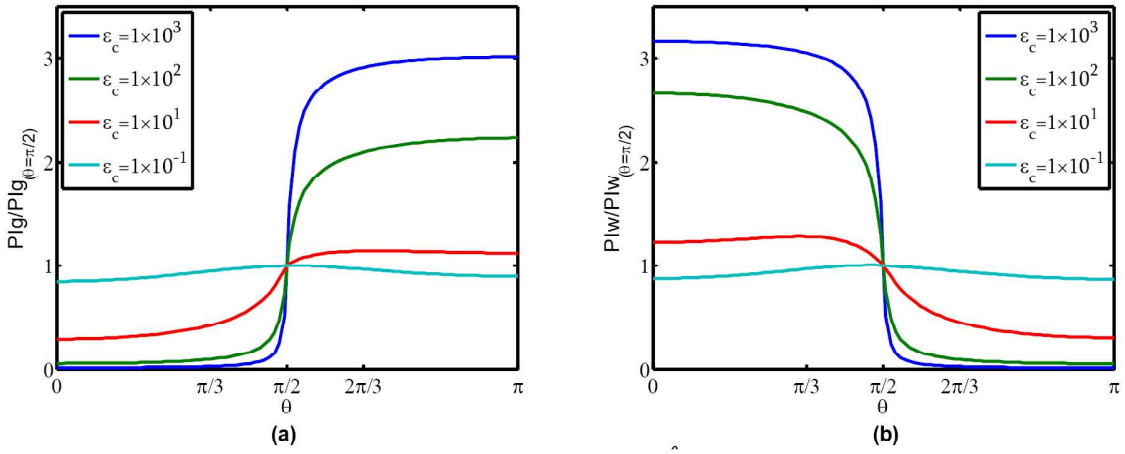

Figure 5—Productivity index versus contact angle at different ε_c in linear flow (f^0=0.01): (a) gas; (b) water

For large ε_c, the effect of saturation decrease with contact angle (capillary effect) dominates over the effect of fractional flow increase (viscous effect) on PI. Increase of contact angle leads to the increase of PI for gas (blue and green curves in Fig. 5a) and decrease of PI for water (blue and green curves in Fig. 5b). As ε_c decreases, the capillary and viscous effects become comparable. The two competitive effects lead to an optimal PI at an intermediate contact angle (red and cyan curves in Figs. 5a and 5b). The optimal contact angle increases with ε_c for gas and decreases with ε_c for water. Larger value of ε_c yields higher increase in PI for both gas and water (Fig. 5).

Consider the scenario where the rock surface is partially treated by a wettability alteration agent from the flow exit y_0 up to a certain distance y_1. The zone from y_1 to the inlet y_2 remains unaltered. The rock surface is assumed water wet before treatment and the initial contact angle is zero. After the treatment, the contact angle of the altered zone θ_a is shifted to a chosen value ranging from 0 to π.

Fig. 6 shows the saturation profile at different altered contact angles θ_a for low and high capillary-viscous ratios. Saturation decreases with contact angle in the wettability alteration zone ($0 < X < \beta$). Capillary pressure continuity is satisfied across the boundary between wettability altered and unaltered zones ($X = \beta$), which yields discontinuous saturation at this boundary (Fig. 6). Increase of contact angle in the zone near to core outlet or fracture face ($0 < X < \beta$) of water-wet rocks results in decrease of saturation near the exit, but the capillary end effect still occurs in the unaltered zone ($X > \beta$).

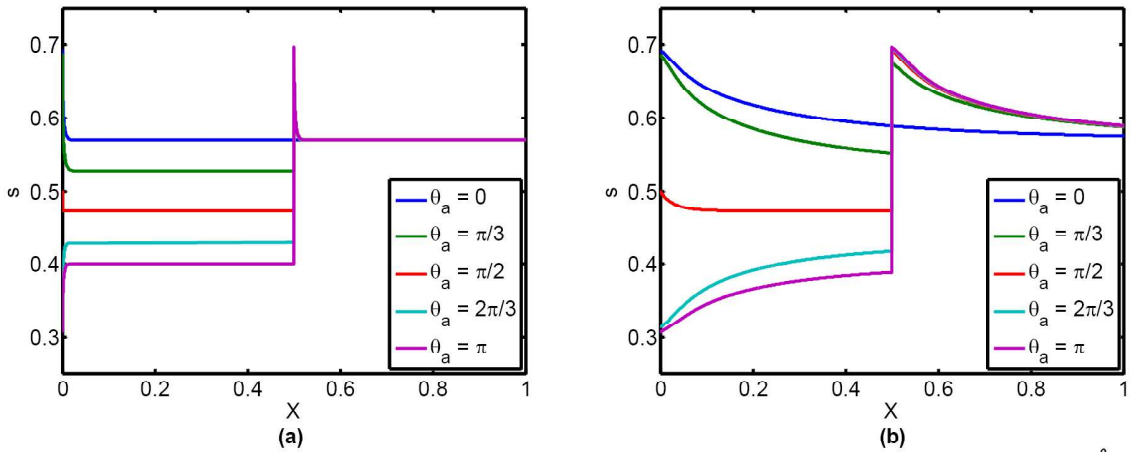

Figure 6—Saturation profile at different altered contact angle θ_a in linear flow with piecewise alteration of contact angle (f^0=0.01, β=0.5): (a) ε_c = 0.1; (b) ε_c = 10

Restriction of gas flow due to capillary end effect occurs at the exit ($X = 0$) for low θ_a and at the boundary between wettability altered and unaltered zones ($X = \beta$) for high θ_a (Fig. 6). Despite the reduction of the end effect by wettability alteration in the zone near to wellbore or fracture face, the end effect at the altered zone boundary is increased. Higher capillary-viscous ratio results in larger end effect. It reduces the productivity for gas at both high and low contact angles (Fig. 7a). Contact angle alteration affects saturation in the altered zone significantly (Fig. 6). In this zone the competing capillary and viscous effects yield an intermediate optimal contact angle for the maximum gas productivity (Fig. 7a). The optimal contact angle is around $\pi/2$.

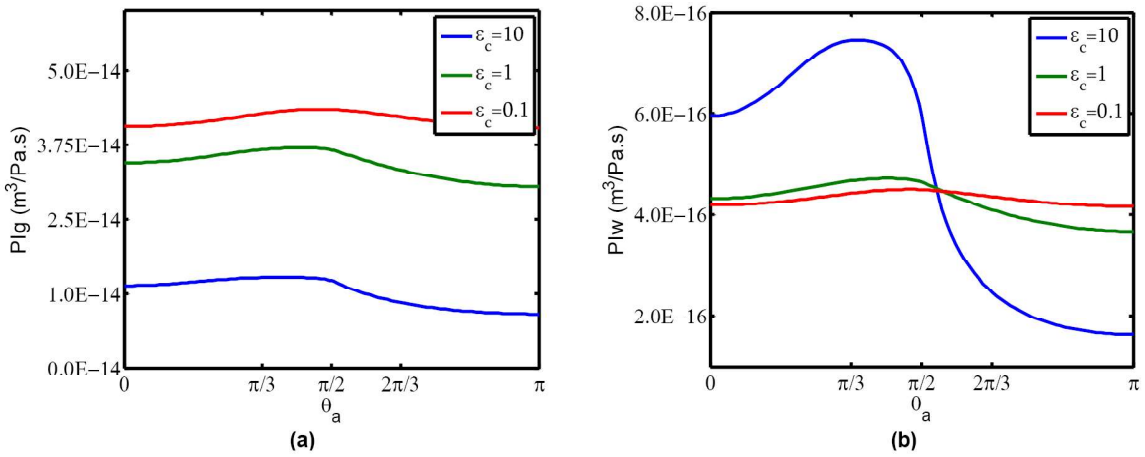

Figure 7—Productivity index versus piecewise alteration of contact angle in water-wet rock at different ε_c in linear flow (f^0=0.01, β=0.5): (a) gas; (b) water

However, the water flow is only restricted at high contact angles. As capillary-viscous ratio increases, the end effect increases. It reduces the water productivity at high contact angles (Fig. 7b). Water production from water-wet reservoirs can be maximised by altering the contact angle in wettability alteration zone ($0 < X < \beta$) towards the optimal value $\theta_a < \pi/2$, and can be minimised by altering the contact angle towards $\theta_a = \pi$ (Fig. 7b).

The sensitivity of productivity index to the altered zone length β is investigated. PI for gas versus contact angle in the case of piecewise-constant contact angle in linear flow is shown in Fig. 8. The

maximum value of PI for gas increases with β, since the variation of saturation and relative permeability in altered zone occurs over a larger distance with β.

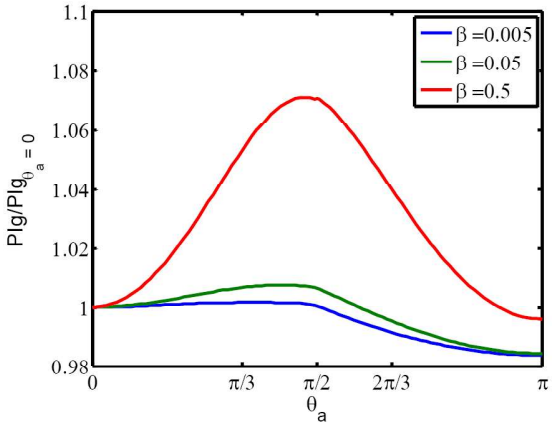

Figure 8—Productivity index for gas in the case of piecewise-contact angle in linear flow (f^0=0.01, ε_c = 0.1): PI_g versus θ_a

Saturation profiles in radial flow towards well at different θ_a for low (Fig. 9a) and high (Fig. 9b) ε_c are presented in the case of piecewise alteration of contact angle. Saturation decreases with contact angle θ_a in the wettability alteration zone ($0 < R < \beta$). Increase of contact angle in the zone near to wellbore ($0 < R < \beta$) of water-wet rocks results in decrease of saturation near the exit, but the capillary end effect still occurs in the unaltered zone ($R > \beta$) (Fig. 9). The pressure drop across the altered zone near the wellbore is much higher compared to that in linear case, causing the altered zone properties to be more influential over the total flow in radial than in linear case. Therefore, PI profile is more sensitive to β in radial case than that in linear case (Fig. 10).

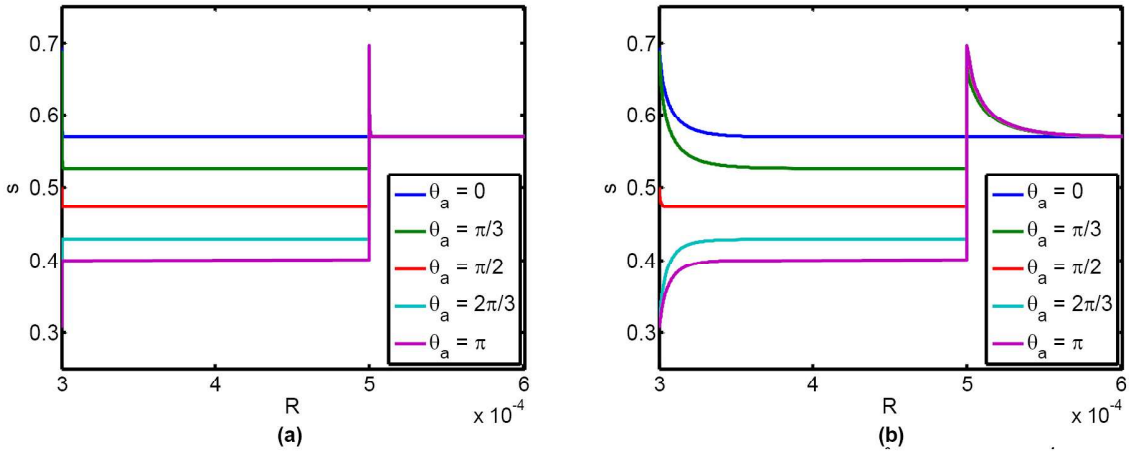

Figure 9—Saturation profiles at different θ_a in radial flow with piecewise alteration of contact angle (f^0=0.01, β=5.0×10^{-4}): (a) ε_c = 0.01; (b) ε_c = 0.5

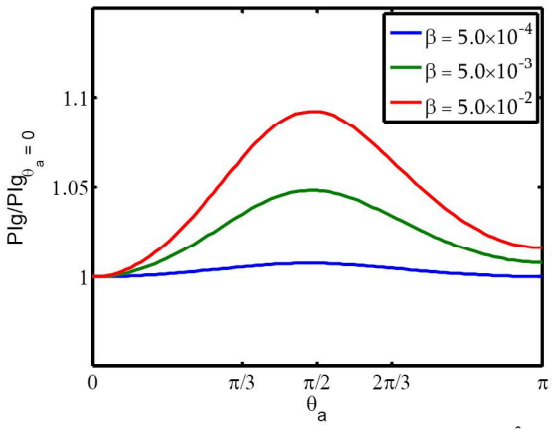

Figure 10—Productivity index for gas in the case of piecewise contact angle in radial flow (f^o=0.01, ε_c=0.01): PI_g versus θ_a

Application of nanoparticles to wettability alteration in unconventional reservoir

Nanoparticles (NPs) have been extensively used for wettability alteration of reservoir rocks for water-flooding (Maghzi et al., 2011; Giraldo et al., 2013; Hendraningrat et al., 2013; Alomair et al., 2015). The wettability alteration of rock surface is affected by the types of NPs and the underlying mineralogy, leading to different resultant contact angles based on their combinations.

The main minerals present in unconventional coal seam and shale reservoirs are sand, clays and organic matter. Karimi et al. (2012) applied zirconium dioxide (ZrO_2) NPs to decrease carbonate contact angle from 90° to 0°. Li and Torsaeter (2015) used hydrophilic silica NPs to decrease contact angle of sandstone rock surface from 54° to 22°. Hendraningrat and Torsaeter (2014) investigated three metal oxides NPs: aluminium (Al_2O_3), titanium (TiO_2) and silicon (SiO_2). Nano fluids used in the experiment with the concentration 0.05 wt% result in the contact angles measured in brine (NaCl 3 wt%) lowered from 53.68° to 28.6°, 21.64° and 38.82° for Al_2O_3, TiO_2 and SiO_2, respectively. To increase the contact angle, lipophilic polysilicon NPs with surface modification can be used (Ju and Fan, 2009). Hydrophobic and neutral wet polysilicon nano fluids with concentration 4 g/L successfully altered sandstone contact angle from 50° to 84.56° and 98.12°, respectively (Roustaei et al., 2012). Cupric oxide (CuO) NPs increased water contact angles from less than 5° up to 130° and 150° with amine- and thiol-modified surfaces, respectively (Basu et al., 2011).

Lebedeva and Fogden (2011) investigated the wettability alteration of kaolinite clay surface, due to the deposition of asphaltene nanoparticles. The clay surface was altered from hydrophilic to hydrophobic with contact angle 140°.

To the best of our knowledge, application of NPs to the wettability alteration of organic matter is not available in the literature.

It is worthwhile to evaluate the effects of contact angle alteration by applying different NPs using the analytical model (Section 3). PI values versus contact angle are shown in Figs. 5 and 7 for f^o = 0.01. For low water fractional flow f^o = 0.01 and the contact angle altered from 50° to 90° (Roustaei et al., 2012), ε_c= 5 and 0.05 result in PI_g increase by 2 and 1.08 times, respectively. For high water fractional flow f^o = 0.95 and the contact angle altered from 0° to 130° (Basu et al., 2011), gas productivity index PI_g can be increased by 4.7 and 1.25 times for high (ε_c= 5) and low (ε_c = 0.05) capillary-viscous ratios, respectively. Given f^o = 0.01 with contact angle alteration from 0° to 50° (Vafaei et. al., 2006), water productivity index PI_w is increased by 2.1 and 1.96 times for ε_c= 5 and 0.05, respectively.

Different types of NPs affect wettability of shale- or coal-minerals differently; hence, a mixture of NPs must be developed for multi-mineral rocks. The well treatment includes adding NPs into drilling or

fracturing fluids with the consequent increase of the contact angle to reduce water retention (first stage); depending on the capillary-viscous ratio, rock surface is altered to neutral or gas wet by NPs during gas production (second stage).

The analytical model for steady-state gas-water flow in rocks with piecewise-constant contact angle can be used for design of the treatment technology, including defining volumes of injected fluids and their compositions. The analytical model can also be applied to the upscaling of laboratory data for well index prediction.

Discussions

Let us discuss the limitations of the analytical model (13). Since the gas density is a function of pressure, the incompressibility assumption is valid if the pressure drawdown is much less than the reservoir pressure:

$$\frac{\Delta P}{P} \ll 1 \tag{16}$$

For linear flow during coreflooding, substitution of Darcy's law $U = \frac{k}{\mu}\frac{\Delta P}{L}$ into the condition (16) yields:

$$\frac{\Delta P}{P} = \frac{U\mu L}{kP} \ll 1 \tag{17}$$

or

$$U \ll \frac{kp}{\mu L} \tag{18}$$

With core length L=0.1 m, permeability k varying from 0.01 to 10 md, gas viscosity μ varying from 10^{-5} to 4×10^{-5} Pa.s, and pressure P varying from 5×10^{5} to 10^{7} Pa, the maximum velocity where the incompressibility assumption is valid varies from 1.2×10^{-5} to 1 m/s. The typical flow velocities in cores have the order of magnitude 10^{-6}–10^{-5} m/s (Barenblatt et al., 1990; Bazin et al., 2010). Therefore, gas compressibility is negligible under the conditions of these laboratory studies by Bazin et al. (2010), so the incompressibility assumption is valid.

For fractured wells, velocity at the fracture face is calculated using Eq. (18). For permeability variation k = 0.01–10.0 md, μ = 10^{-5}–4×10^{-5} Pa.s, reservoir pressure P = 5×10^{6}–10^{8} Pa, and length of linear flow region towards the fracture L=10–250 m, the maximum velocity where the incompressibility assumption is valid varies from 5×10^{-8} to 0.1 m/s. Typical velocities at fracture faces in gas reservoirs have the order of 10^{-5}–10^{-4} m/s (see Shaoul et al., 2012). Therefore, there are some unconventional field cases where the incompressibility assumption is valid, and where it is not. Inequality (18) defines the conditions where the analytical model (13) is valid.

For radial flow towards well, the rate of incompressible fluid per unit height of reservoir is calculated as:

$$Q = \frac{2\pi k\Delta P}{\mu \ln(r_e/r_w)} \tag{19}$$

Substitution of rate expression in vertical well into the condition (16) yields:

$$Q \ll \frac{2\pi kp}{\mu \ln(r_e/r_w)} \tag{20}$$

For k = 0.01–10 md, μ = 10^{-5}–4×10^{-5} Pa.s, P = 10^{7}–10^{8} Pa, the ratio between drainage and well radii r_e/r_w=10^{3}–10^{4}, the maximum rate per unit height, where the incompressibility assumption is valid varies from 1.7×10^{-5} to 0.9 m^2/s. Some typical rates for tight gas reservoirs vary in the range 10^{-3}–0.1 m^2/s (see McGowen et al., 2007). Thus, the gas compressibility can be ignored in some cases, and cannot be ignored in other cases.

For the linear flow case in the current work, $k=1$ md, $\mu=2\times10^{-5}$ Pa.s and length of linear flow region is 10^3 m. For pressure varying from 5×10^6 to 10^8 Pa, the maximum velocity where the incompressibility assumption is valid varies from 2.5×10^{-6} to 5×10^{-5} m/s. The velocities in the synthetic case (Section 5) are in the order of 10^{-7} m/s, therefore the incompressibility assumption is valid. For the radial flow regime, we use the same permeability, viscosity and pressure range. For $r_e/r_w=6.67\times10^3$, the maximum rate per unit height where the incompressibility assumption is valid varies from 2×10^{-3} to 3.5×10^{-2} m^2/s. The rates in the synthetic case have the order of 10^{-4} m^2/s, which verifies the incompressibility assumption is valid.

The gas slip effect can be significant in porous media with low pressure or low permeability (Wu and Pruess, 1998; Civan et al., 2011). According to gas permeability equation (9), the slip effect is negligible if gas pressure is much larger than the Klinkenberg factor b. For typical permeability $k=0.001$ and 1 md, the value of b is 3.3×10^5 and 2.8×10^5 Pa, respectively. A typical reservoir pressures in coal seams are 10^6–10^7 Pa (Gaurav et al., 2012). The corresponding error in calculated relative permeability for gas using (9) is 2–6%, if gas slip effect is ignored. In shallow gas reservoirs, pressure can be even lower, which leads to higher effect of gas slip. For shallow reservoirs or reservoirs with ultra-low permeability, the gas slip effect can cause rate miscalculation around 10% if it is ignored. It can be especially prevalent in coreflooding tests, where low pressures are commonly used.

Two scenarios are investigated for water-gas flow with well treatment by NPs. One scenario involves increasing contact angle under high water saturation which corresponds to the processes of dewatering and the fracturing-fluid flow-back. The other scenario involves decreasing contact angle under low water saturation, which occurs during gas production. Based on the analytical model developed, the strategy of gas productivity enhancement is as follows: For rocks with uniform wettability, alter contact angle of rock surface towards $\pi/2$ for low capillary-viscous ratio and π for high capillary-viscous ratio. For piecewise wettability alteration of water-wet rocks, optimal contact angle is $\pi/2$ for both low and high capillary-viscous ratios. The strategy targeting maximum water productivity is contact angle alteration towards $\pi/2$ for low capillary-viscous ratio and zero for high capillary-viscous ratio.

Conclusions

Mathematical modelling and its application to enhancing the well productivity for gas and water by wettability alteration lead to the following conclusions:

- Competition between the viscous and capillary effects on gas productivity results in non-monotonic function of gas productivity index versus contact angle, suggesting the existence of optimal contact angle for enhanced gas production.
- For dewatering and fracturing fluid flow-back processes, competition between the viscous and capillary effects on water productivity yields the optimal contact angle for maximum water production.
- In the case of wettability alteration over the full length, the higher capillary-viscous ratio ε_c leads to the higher capillary end effect and the higher maximum productivity indexes for gas and water.
- In the case of wettability alteration on a fraction of water-wet rock, increase of ε_c yields the increase of the maximum productivity index for water and decrease for gas. This is because the capillary end effect at the boundary between altered and unaltered zones reduces gas flow more significantly with higher ε_c.
- The larger is the treated zone fraction β, the greater is the contact angle effect on gas and water productivity index. This is due to a higher proportion of surface being altered.
- Productivity index is sensitive to small value of β in radial flow towards well, indicating that wettability alteration in small neighbourhood of wellbore can effectively improve productivity indexes for gas and water.

- The maximum productivity index for water should be applied during dewatering and slick water removal. The maximum productivity index for gas must be used during gas production stage.

Nomenclature

b	*Klinkenberg factor, Pa*
C	*Capillary model parameter*
d_g	*Diameter of gas molecule, m*
d_p	*Pore diameter, m*
f	*Fractional flow function*
k	*Permeability, m^2*
k_B	*Boltzmann constant, J/K*
k_r	*Relative permeability*
P	*Pressure, Pa*
P_c	*Capillary pressure, Pa*
R	*Dimensionless radius*
r	*Radius, m*
S	*Normalised water saturation*
s	*Water saturation*
s_{gr}	*Irreducible gas saturation*
s_{wc}	*Connate water saturation*
U	*total velocity, m/s*
u	*flow velocity of water or gas, m/s*
x	*Distance, m*
T	*Gas temperature, K*
y_0	*Flow exit distance, m*
y_1	*Treated distance, m*
y_2	*Flow entrance distance, m*

Greek letters

α	*Capillary model parameter*
β	*Altered zone length*
ε_c	*Capillary-viscous ratio*
η	*Tortuosity index*
θ	*Surface contact angle*
Λ	*Dimensionless total mobility*
λ	*Mean free path of gas, m; total mobility, 1/Pa·s*
μ	*Viscosity, Pa·s*
ρ	*Density, kg/m^3*
σ	*Interfacial tension, N/m*
ϕ	*Porosity*

Abbreviations

DLVO	*Derjaguin-Landau-Verwey-Overbeek*
NP	*Nanoparticle*
PI	*Productivity index*

Subscripts

a	*altered*
e	*drainage radius*
g	*gas*
w	*water (productivity index and relative permeability), wetting (saturation), well (radius)*
0	*exit*

Superscripts

0	*inlet*

Acknowledgments

Financial support from the Australian Research Council (ARC) Linkage Project and Santos Ltd. is gratefully acknowledged.

References

Alomair, O.A., Matar, K.M. and Alsaeed, Y.H. 2015. experimental study of enhanced-heavy-oil recovery in Berea sandstone cores by use of nanofluids applications. *SPE Reservoir Evaluation & Engineering,* **18**: 387–399.

Anderson, W.G., 1987. Wettability literature survey part 5: the effects of wettability on relative permeability. *Journal of Petroleum Technology,* **39**(11): 1453–1468.

Bahrami, H. et al., 2011. Effect of water blocking damage on flow efficiency and productivity in tight gas reservoirs. SPE-142283. SPE Production and Operations Symposium. Oklahoma, USA. 27–29 March.

Barenblatt, G.I., Entov, V.M. and Ryzhik, V.M., 1990. *Theory of fluid flows through natural rocks,* Kluwer Academic Publishers, Dordrecht.

Basu, M., Sinha, A.K., Pradhan, M., Sarkar, S., Negishi, Y. and Pal, T., 2011. Fabrication and functionalization of CuO for tuning superhydrophobic thin film and cotton wool. *Journal of Physical Chemistry C,* **115**: 20953–20963.

Bazin, B. et al., 2010. In-situ water-blocking measurements and interpretation related to fracturing operations in tight gas reservoirs. *SPE Production & Operations,* **25**(4): 431–437.

Bedrikovetsky P.G., 1993, *Mathematical Theory of Oil & Gas Recovery (With applications to ex-USSR oil & gas condensate fields),* Kluwer Academic Publishers, London-Boston-Dordrecht, 600 p.

Bradford, S.A., Abriola, L.M. and Leij, F.J., 1997. Wettability effects on two- and three-fluid relative permeabilities. *Journal of contaminant hydrology,* **28**(1–2): 171–191.

Bruining, J. and Van Duijn, C.J., 2006. Traveling waves in a finite condensation rate model for steam injection. *Computational Geosciences,* **10**(4): 373–387.

Chalk, P., Gooding, N., Hutten, S., You, Z. and Bedrikovetsky, P., 2012. Pore size distribution from challenge coreflood testing by colloidal flow. *Chemical Engineering Research and Design,* **90**: 63–77.

Chen, D., Pan, Z., Liu, J. and Connell, L.D., 2013. An improved relative permeability model for coal reservoirs. *International Journal of Coal Geology,* **109**: 45–57.

Chen, P. and Mohanty, K.K., 2014. Wettability alteration in high temperature carbonate reservoirs. SPE-169125. SPE Improved Oil Recovery Symposium. Tulsa, Oklahoma, USA. 12–16 April.

Cinar, Y. and Riaz, A., 2014. Carbon dioxide sequestration in saline formations: Part 2-Review of multiphase flow modeling. *Journal of Petroleum Science and Engineering,* **124**: 381–398.

Civan, F., Rai, C.S. and Sondergeld, C.H., 2011. Shale-gas permeability and diffusivity inferred by improved formulation of relevant retention and transport mechanisms. *Transport in Porous Media,* **86**(3): 925–944.

Fogden, A., Kumar, M., Morrow, N.R. and Buckley, J.S., 2011. Mobilization of fine particles during flooding of sandstones and possible relations to enhanced oil recovery. *Energy & Fuels,* **25**(4): 1605–1616.

Forst, W. and Hoffmann, D., 2010. *Optimization—Theory and Practice,* Springer, New York.

Ford, W.G.F., Penny, G.S. and Briscoe, J.E., 1988. Enhanced water recovery improves stimulation results. *SPE production engineering,* **3**(4): 515–521.

Gaurav, K., Akbar, A., Saada, T.H. and Kumar, S., Performance analysis in coal seam gas. SPE-157696, SPETT 2012 Energy Conference and Exhibition, Port-of-Spain, Trinidad. 11–13 June.

Giraldo, J., Benjumea, P., Lopera, S., Cortés, F.B. and Ruiz, M.A., 2013. Wettability alteration of sandstone cores by alumina-based nanofluids. *Energy & Fuels,* **27**(7): 3659–3665.

Hendraningrat, L., Li, S. and Torsæter, O., 2013. A coreflood investigation of nanofluid enhanced oil recovery. *Journal of Petroleum Science and Engineering,* **111**: 128–138.

Hendraningrat, L. and Torsaeter, O., 2014. Unlocking the potential of metal oxides nanoparticles to enhance the oil recovery, OTC-24696, Offshore Technology Conference Asia, Kuala Lumpur, Malaysia, 25–28 March.

Hoeiland, S., Barth, T., Blokhus, A. and Skauge, A., 2001. The effect of crude oil acid fractions on wettability as studied by interfacial tension and contact angles. *Journal of Petroleum Science and Engineering,* **30**(2): 91–103.

Jones, F.O. and Owens, W.W., 1999. A laboratory study of low-permeability gas sands. *SPE Reprint Series,* **52**: 13–22.

Ju, B. and Fan, T., 2009. Experimental study and mathematical model of nanoparticle transport in porous media. *Powder Technology,* **192**: 195–202.

Karimi, A., Fakhroueian, Z., Bahramian, A., Pour Khiabani, N., Darabad, J. B., Azin, R. and Arya, S., 2012. Wettability alteration in carbonates using zirconium oxide nanofluids: EOR implications. *Energy & Fuels,* **26**(2): 1028–1036.

Kumar, K., Dao, E.K. and Mohanty, K.K., 2008. Atomic force microscopy study of wettability alteration by surfactants. *SPE Journal,* **13**(2): 137–145.

Lebedeva, E.V. and Fogden, A., 2011. Wettability alteration of kaolinite exposed to crude oil in salt solutions. *Colloids and Surfaces A: Physicochemical and Engineering Aspects,* **377**(1): 115–122.

Li, G., Ren, W., Meng, Y., Wang, C. and Wei, N., 2014. Micro-flow kinetics research on water invasion in tight sandstone reservoirs. *Journal of Natural Gas Science and Engineering,* **20**: 184–191.

Li, S., Torsaeter, O., 2015. The impact of nanoparticles adsorption and transport on wettability alteration of intermediate wet berea sandstone. SPE-172943, SPE Middle East Unconventional Resources Conference and Exhibition, Muscat, Oman, 26–28 January.

Lin, D., Tian, X., Wu, F. and Xing, B., 2010. Fate and transport of engineered nanomaterials in the environment. *Journal of Environmental Quality,* **39**(6): 1896–1908.

Maghzi, A., Mohebbi, A., Kharrat, R. and Ghazanfari, M.H., 2011. Pore-scale monitoring of wettability alteration by silica nanoparticles during polymer flooding to heavy oil in a five-spot glass micromodel. *Transport in Porous Media,* **87**(3): 653–664.

Mahadevan, J., Sharma, M.M. and Yortsos, Y.C., 2007. Capillary wicking in gas wells. *SPE Journal,* **12**(4): 429–437.

McCaffery, F. and Bennion, D., 1974. The effect of wettability on two-phase relative permeabilities. *Journal of Canadian Petroleum Technology,* **13**(4): 42–53.

McGowen, J.M., Gilbert, J.V. and Samari, E., 2007. Hydraulic Fracturing Down Under. SPE-106051. SPE Hydraulic Fracturing Technology Conference. College Station, Texas. 29–31 January.

Morrow, N. and Buckley, J., 2011. Improved oil recovery by low-salinity waterflooding. *Journal of Petroleum Technology,* **63**(5): 106–113.

Morsy, S., Gomaa, A. and Sheng, J., 2014. Improvement of Mancos Shale Oil Recovery by Wettability Alteration and Mineral Dissolution. SPE-169033. SPE Improved Oil Recovery Symposium. Society of Petroleum Engineers. Tulsa, Oklahoma. 12–16 April.

Nasralla, R.A., Bataweel, M.A. and Nasr-El-Din, H.A., 2013. Investigation of wettability alteration and oil-recovery improvement by low-salinity water in sandstone rock. *Journal of Canadian Petroleum Technology,* **52**(2): 144–154.

O'Carroll, D.M., Abriola, L.M., Polityka, C.A., Bradford, S.A. and Demond, A.H., 2005. Prediction of two-phase capillary pressure–saturation relationships in fractional wettability systems. *Journal of Contaminant Hydrology,* **77**(4): 247–270.

Odumabo, S.M., Karpyn, Z. and Ayala H, L., 2014. Investigation of gas flow hindrance due to fracturing fluid leakoff in low permeability sandstones. *Journal of Natural Gas Science and Engineering,* **17**: 1–12.

Roustaei, A., Moghadasi, J., Bagherzadeh, H. and Shahrabadi, A., 2012. An experimental investigation of polysilicon nanoparticles' recovery efficiencies through changes in interfacial tension and wettability alteration. SPE-156976. SPE International Oilfield Nanotechnology Conference. Noordwijk, The Netherlands. 12–14 June 2012.

Shaoul, J.R., Spitzer, W. and Dahan, M., 2012. Case study of unconventional gas-well fracturing in Hungary. *SPE Production & Operations,* **27**(2): 145–157.

Shapiro, A.A. and Wesselingh, J.A., 2008. Gas transport in tight porous media: Gas kinetic approach. *Chemical Engineering Journal,* **142**(1): 14–22.

Vafaei, S., Borca-Tasciuc, T., Podowski, M.Z., Purkayastha, A., Ramanath, G. and Ajayan, P.M., 2006. Effect of nanoparticles on sessile droplet contact angle. *Nanotechnology,* **17**(10): 2523–2527.

Wu, Y.-S., and Pruess, K., 1998. Gas flow in porous media with Klinkenberg effects. *Transport in porous media,* **32**(1): 117–137.

Xie, X., Liu, Y., Sharma, M. and Weiss, W.W., 2009. Wettability alteration to increase deliverability of gas production wells. *Journal of Natural Gas Science and Engineering,* **1**(1): 39–45.

You, Z., Bedrikovetsky, P., Badalyan, A. and Hand, M., 2015. Particle mobilization in porous media: temperature effects on competing electrostatic and drag forces. *Geophysical Research Letters,* **42**: 2852–2860.

You, Z., Osipov, Y., Bedrikovetsky, P. and Kuzmina, L., 2014. Asymptotic model for deep bed filtration. *Chemical Engineering Journal,* **258**: 374–385.

4. Productivity index enhancement by wettability alteration in two-phase compressible flows

Statement of Authorship

Title of Paper	Productivity index enhancement by wettability alteration in two-phase compressible flows.
Publication Status	☑ Published ☐ Accepted for Publication ☐ Submitted for Publication ☐ Unpublished and Unsubmitted work written in manuscript style
Publication Details	Naik, S., You, Z. and Bedrikovetsky, P., 2018. Productivity index enhancement by wettability alteration in two-phase compressible flows. Journal of Natural Gas Science and Engineering, 50, pp.101-114.

Principal Author

Name of Principal Author (Candidate)	Saurabh Naik
Contribution to the Paper	Literature review, development of mathematical model, Implementation of mathematical solution in Mat-lab, creating figures, analysis of results, writing the manuscript
Overall percentage (%)	85%
Certification:	This paper reports on original research I conducted during the period of my Higher Degree by Research candidature and is not subject to any obligations or contractual agreements with a third party that would constrain its inclusion in this thesis. I am the primary author of this paper.
Signature	Date 03/08/2019

Co-Author Contributions

By signing the Statement of Authorship, each author certifies that:

i. the candidate's stated contribution to the publication is accurate (as detailed above);

ii. permission is granted for the candidate in include the publication in the thesis; and

iii. the sum of all co-author contributions is equal to 100% less the candidate's stated contribution.

Name of Co-Author	Zhenjiang You
Contribution to the Paper	Support on implementation in Matlab, reviewing manuscript
Signature	Date 29/7/19

Name of Co-Author	Pavel Bedrikovetsky
Contribution to the Paper	problem formulation, reviewing manuscript
Signature	Date 30/7/2019

Please cut and paste additional co-author panels here as required.

Journal of Natural Gas Science and Engineering 50 (2018) 101–114

Contents lists available at ScienceDirect

Journal of Natural Gas Science and Engineering

journal homepage: www.elsevier.com/locate/jngse

Productivity index enhancement by wettability alteration in two-phase compressible flows

Saurabh Naik, Zhenjiang You*, Pavel Bedrikovetsky

Australian School of Petroleum, The University of Adelaide, Adelaide, SA 5005, Australia

ARTICLE INFO

Keywords:
Wettability alteration
Productivity index
Compressible flow
Capillary end effect
Two phase flow
Contact angle

ABSTRACT

Water blocking due to the capillary end effect near the wellbore vicinity creates significant formation damage and decreases well productivity for oil and gas. The alteration of the rock wettability by a chemical well treatment is an effective way to reduce water blockage and enhance oil and gas production. Presently, several surfactants and nanofluids are used in the industry for contact angle alteration. After the treatment, the porous medium in the well vicinity (or along the core) has stepwise contact angle. The previous paper (Naik et al., 2015) develops analytical models for incompressible steady-state two-phase linear and axi-symmetric flows, accounting for the piecewise constant contact angle and contact-angle-dependent capillary pressure and relative permeability. The current paper adds the effect of compressibility, which is particularly important for high rate gas wells and wells in unconventional and tight-sand reservoirs. The obtained semi-analytical model has been validated by comparison with a set of laboratory coreflood tests. The modelling reveals a complex interplay between the competing effects of compressibility, viscous and capillary forces, yielding non-monotonic dependencies of well productivity on the wettability and the optimal contact angle. The model closely matches the productivity index data for two production wells from a field case before and after wettability treatment using surfactant.

1. Introduction

The reservoir rock wettability determines the phase distribution near the wellbore during commingled gas-water and oil-water production. Particularly, the capillary end effect in water-wet rocks creates water film/layer near the wellbore with residual saturation of gas or oil. This layer enhances the hydraulic resistance for gas or oil flow and is called water-blocking (Barenblatt et al., 1990; Bedrikovetsky, 1993). Water blocking in gas and oil wells is a widespread source of formation damage, resulting in low productivity index (Mahadevan and Sharma, 2005). The effect is loudly pronounced in low-permeability fields, especially in tight-sand and unconventional reservoirs (Bazin et al., 2010; Bahrami et al., 2011; Morsy et al., 2014).

In hydrophobic rocks, the effluent water saturation is equal to the connate water saturation, and water blocking does not occur. Therefore, alteration of wettability from hydrophilic to hydrophobic may increase the well productivity index. Significant efforts have been made to develop the technologies to alter wettability near the wellbore (Parekh and Sharma, 2004; Kumar et al., 2008; Sheydaeemehr et al., 2014). Treatment of wells by surfactants and nanoparticles that change the rock wettability near the wellbore remove the wetting water barrier and increase well productivity (Weiss et al., 2006; Li and Liu, 2008; Butler et al., 2009; Al-Yami et al., 2013). Numerous types of surfactants have been applied to wettability alteration (Adibhatla et al., 2006), which includes fluoro-surfactants (Bang et al., 2009; Torres et al., 2010), amine surfactants (Bryant et al., 2006), and anionic surfactants (Kathel and Mohanty, 2013). Nanoparticles ranging from Al_2O_3 (Giraldo et al., 2013), SiO_2 (Ju and Fan, 2009, 2013; Roustaei et al., 2012; Li and Torsaeter, 2015), TiO_2 (Esmaeilzadeh et al., 2015) and ZrO_2 (Karimi et al., 2012) have also been applied for wettability alteration. Polymers and amine salts have also been tested for this purpose (Restrepo et al., 2012; Liu et al., 2015). Presently, chemical wettability-altering well-stimulation methods are widely spread in gas and oil production.

Fig. 1a shows the schematic of gas and water flow towards the fractured well; here β is the dimensionless treatment depth. It is assumed that the reservoir is fully water-wet. Fig. 1b presents saturation profiles near to the fracture face. The upper curve corresponds to the case where the altered contact angle, θ_1, is lower than 90°, and the altered contact angle for the lower curve exceeds 90°. Contact angle alteration yields a decrease in the water saturation near to the fracture face and an increase in the gas relative permeability. The same effects

* Corresponding author.
E-mail address: zyou@asp.adelaide.edu.au (Z. You).

https://doi.org/10.1016/j.jngse.2017.11.007
Received 31 December 2016; Received in revised form 29 August 2017; Accepted 10 November 2017
Available online 16 November 2017

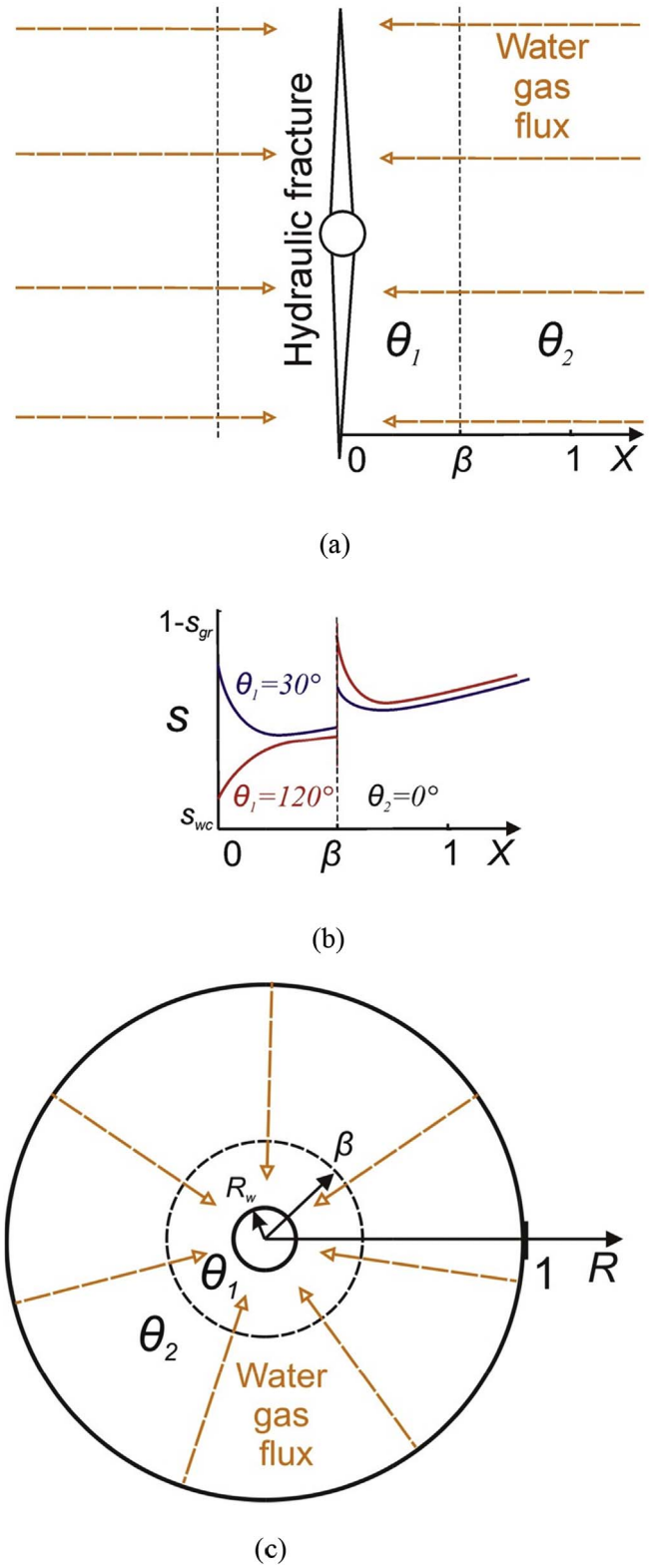

Fig. 1. Schematic figure for commingled gas-water production in the reservoir with piecewise-constant contact angle: a) water-gas flow towards fracture; b) saturation profiles near the fracture face; c) inflow of gas and water towards well.

occur near the vertical and horizontal wellbores (Fig. 1c).

Decision-making on a chemical well treatment and its planning and design rely on the results of laboratory-based mathematical modelling. Particularly, the choice of chemicals and injected volume will depend on the initial and altered contact angles, relative permeability, capillary pressure and rock heterogeneity, which are reflected in the mathematical models. Analytical models for inflow performance with laboratory-based empirical functions provide a reliable tool for planning and design of various well stimulation techniques (Economides and Nolte, 2000).

Mathematical models for chemical treatment contain piecewise-constant contact-angle as a function of the spatial coordinate. Chaouche et al. (1993) investigated steady-state two-phase incompressible flow in rocks with piecewise constant permeability. The condition at the permeability discontinuity is the continuity of capillary pressure. It allows matching steady-state flow in rocks with constant permeability into solutions for the overall core with piecewise constant permeability. Yortsos and Chang (1990) studied steady state two-phase incompressible immiscible flow for the case of multiple abrupt permeability changes along the flow path and observed that saturation response is sensitive to parameters such as rate and heterogeneity length scale. The particular case of two-phase incompressible flow with immobile oil phase has been investigated by Van Lingen et al. (1996) in order to estimate trapped oil in heterogeneous rocks, i.e. for upscaling the residual oil saturation.

Van Duijn et al. (1995) studied transient two-phase flows of incompressible liquids in porous media with discontinuous permeability. Matching the unsteady-state solutions in rock segments with piecewise constant permeability was also performed by the capillary-pressure continuity condition on the permeability discontinuity.

Two competitive factors define the well behaviour during chemical treatment. On the one hand, the contact angle increase will yield the decrease, or even removal, of the wetting water barrier, resulting in the increase of well productivity. On the other hand, increase in the contact angle displaces oil or gas into smaller pores, causing a decrease in the oil or gas production (Berman and Mirotchnik, 2005). This yields a non-monotonic well-productivity dependence on contact angle and capillary pressure. These effects are obtained from steady-state solutions for two-phase incompressible flow with piecewise-constant wettability (Naik et al., 2015).

However, gas-compressibility effects are significant in inflow-performance modelling and well productivity estimation (Economides et al., 2012). Compressibility along with the effects of wetting film removal and gas displacement in small pores would result in more complex gas well behaviour due to chemical treatment. Yet, analytical solutions for compressible flow in rocks with discontinuous wettability are not available in the literature.

In the current paper, the previous work is extended by accounting for fluid compressibility during commingled water-gas production. Steady-state profiles for compressible flow in rocks with piecewise-constant wettability have been investigated for linear and axi-symmetric flows. Asymptotic value for inlet saturation in long cores is defined by a relationship derived and is determined graphically. A non-monotonic dependency of gas-well index on the contact angle has been discovered, indicating the existence of an optimal contact angle for the maximum well productivity.

The structure of this paper is as follows. Section 2 derives the solution for steady-state compressible flow in linear and axi-symmetric geometry. Section 3 validates the model by comparison with laboratory coreflood data. Section 4 analyses the interplay between compressibility and wettability-alteration effects and presents typical dependency of well index of the well-treatment parameters. Section 5 interprets two field cases of well treatment using the analytical model. Discussion in Section 6 and conclusions in Section 7 finalise the paper.

2. Mathematical modelling of steady-state two-phase immiscible flows

In this section, we describe the steady-state two-phase immiscible flow of water and gas accounting for gas compressibility. Linear and axi-symmetric flows are considered. The porous media with piecewise-

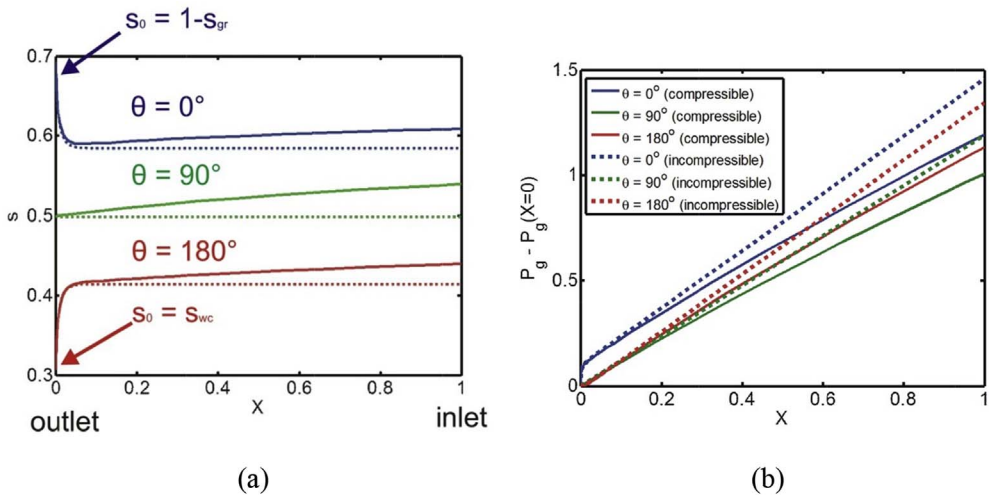

Fig. 2. Schematic for steady state flow profiles along the rock sample at different contact angles for the cases of compressible (solid curves) and incompressible gas (dotted curve): a) saturation profiles; b) gas pressure profiles.

constant wettability corresponds to the formation after well treatment by surfactant or nanofluid, which changes the contact angle.

2.1. Linear and axi-symmetric steady-state gas-water flows in homogeneous porous media

Consider one-dimensional steady-state flow of gas and water (Fig. 2). Mass fluxes for water q_w and gas q_g accounting for two-phase Darcy's flow are

$$q_w = k\frac{k_{rw}(s,\theta)}{\mu_w}\rho_w\frac{dp_w}{dx} \tag{1}$$

$$q_g = kk_{kg}(p_g)\frac{k_{rg}(s,\theta)}{\mu_g}\rho_g(p_g)\frac{dp_g}{dx} \tag{2}$$

where subscripts w and g correspond to water and gas, respectively; k is the permeability, s is the water saturation, θ is the contact angle, k_{kg} is the Klinkenberg correction coefficient, k_r is the relative permeability, μ is the viscosity, ρ is the density, and p is the pressure. Real gas equation is used for gas density:

$$\rho_g = \frac{p_g M}{z(p_g)R_c T} \tag{3}$$

where M is the molar mass, R_c is the universal gas constant, T is the temperature, and z is compressibility factor.

The capillary pressure p_c is the difference between the phase pressures and is expressed via the dimensionless J-function:

$$p_c = p_g - p_w = \frac{\sigma}{\sqrt{k/\phi}}J(s,\theta) \tag{4}$$

Here σ is the interfacial tension, and ϕ is the porosity of the rock.

The mass fluxes for both water and gas are constant under steady-state flow. Introduce the fraction of water and gas fluxes in the total flux as:

$$Q_w = \frac{q_w}{q_g + q_w}, \quad 1 - Q_w = \frac{q_g}{q_g + q_w} \tag{5}$$

Let us introduce the following dimensionless variables and parameters:

$$P_i = \frac{k\rho_w}{(q_g+q_w)\mu_w L}p_i, \quad i = w, g,$$
$$\varepsilon_x = \frac{\sigma\rho_w\sqrt{k\phi}}{(q_g+q_w)\mu_w L},$$
$$D(p_g) = \frac{\rho_g(p_g)\mu_w}{\rho_w\mu_g} \tag{6}$$

Here P is the dimensionless pressure, X is dimensionless distance, and D is the density-viscosity ratio. The capillary-viscous ratio ε_x is the dimensionless ratio between the reference capillary pressure and pressure drop across the core with linear single-phase water flow (the modified capillary number).

Substituting the dimensionless parameters (5, 6) into Eqs. (1), (2) and (4) yields

$$Q_w = k_{rw}(s,\theta)\frac{dP_w}{dX} \tag{7}$$

$$1 - Q_w = k_{kg}(P_g)k_{rg}(s,\theta)D(P_g)\frac{dP_g}{dX} \tag{8}$$

$$P_g - P_w = \varepsilon_x J(s,\theta) \tag{9}$$

The pressure gradient in gas can be expressed from Eq. (8) as

$$\frac{dP_g}{dX} = \frac{1 - Q_w}{k_{kg}(P_g)k_{rg}(s,\theta)D(P_g)} \tag{10}$$

Expressing pressure gradient in water from Eq. (7), subtracting the result from Eq. (10) and accounting for Eq. (4) yield:

$$\varepsilon_x\frac{dJ(s,\theta)}{dX} = \frac{1 - Q_w}{k_{kg}(P_g)k_{rg}(s,\theta)D(P_g)} - \frac{Q_w}{k_{rw}(s,\theta)} \tag{11}$$

We assume that the capillary pressure equals zero at the core outlet, and that the pressure is set at the core outlet:

$$X = 0: \quad s = s_0, \quad J(s_0) = 0, \quad P_g = P_0 \tag{12}$$

The system of two ordinary differential equations (10) and (11) subject to the Cauchy conditions (12) determines the steady state profiles $s(X)$ and $P_g(X)$ for one-dimensional steady state water-gas flow.

System (10, 11) subject to boundary conditions (12) is solved numerically using Gear's method, based on numerical differentiation formulas with quasi-constant step size (Klopfenstein, 1971) implemented in Matlab. The step size is automatically adjusted and ranges from $\Delta X = 10^{-9}$ to 10^{-2}, depending on s- and P- gradients. The forms of relative permeability and capillary pressure are presented in Appendix A. Qualitative analysis of solution is presented in Appendix B.

Fig. 2 shows the saturation and pressure drop profiles for water-wet rock ($s_0 = 1 - s_{gr}$), oil-wet rock ($s_0 = s_{wc}$) and intermediate-wet rock ($s_{wc} < s_0 < 1 - s_{gr}$), where s_{gr} and s_{wc} are irreducible gas saturation and connate water saturation, respectively.

Solutions for $s(X)$ and $P_g(X)$ allow calculating the dimensionless productivity indexes for water and gas

$$PI_w = \frac{Q_w}{\Delta P_w}, \quad PI_g = \frac{1 - Q_w}{\Delta P_g} \tag{13}$$

for the cases of linear (core or fracture) and axi-symmetric (well) flows.

The detailed derivations of axi-symmetric two-phase compressible flow in presented in Appendix C. Change of variables $X = \ln(R)$ maps the system (C-6, C-7) into system (10, 11). The boundary condition (C-8) is set at $X_w = \ln(r_e/r_w)$, and the inlet corresponds to $X = 0$. Therefore, the saturation and pressure profiles for axi-symmetric flow is obtained from the linear flow profiles by expansion of coordinate ($-X_w$) times.

Saturation profiles versus natural logarithm of radius during well inflow performance have the same forms as those shown in Fig. 2.

2.2. Steady state gas-water flow in rock with piecewise constant contact angle

Consider the linear flow case where the initial contact angle θ_2 has been changed toθ_1 in the fraction β of the core adjacent to the outlet by some chemical treatment:

$$\theta = \begin{cases} \theta_1, & 0 < X < \beta \\ \theta_2, & \beta < X < 1 \end{cases} \tag{14}$$

Continuity of pressure for both phases is assumed at the interface $X = \beta$:

$$X = \beta: P_g^- = P_g^+, P_w^- = P_w^+ \tag{15}$$

where "-" and "+" correspond to downstream and upstream of the interface $X = \beta$, respectively. Therefore, the capillary pressure is also continuous across the interface $X = \beta$.

For radial flow, consider the case of water-gas inflow from a reservoir with wettability alternated in the wellbore vicinity. The contact angle is changed due to surfactant treatment near to well from θ_2 to θ_1 in the fraction β of the reservoir adjacent to the wellbore, see Eq. (14). The boundary condition at $R = \beta$ corresponds to continuity of pressures in both phases and consequently, to the continuity of capillary pressure, as in Eq. (15).

3. Model validation

In this section, the laboratory coreflooding carried out by Pini and Benson (2013) under seven flow rates are analysed, for validation of the mathematical model for compressible water-gas flow represented by Eqs. (9) and (10).

A cylindrical core of Berea sandstone with a diameter of 0.05 m and length of 0.085 m was used. The core has an average porosity of 18.8% and an initial permeability of 329 mD.

The laboratory procedure is as follows: the core is prepared by injection of CO_2, followed by the circulation of fresh water to dissolve the remnants of CO_2. Then, the permeability is measured during water flowing through the core. The coreflooding experiment starts by injecting gas (nitrogen) at constant flow rate until steady state is reached. After 10 pore volumes have been injected, the flow rate is increased. Seven different flow rates ranging from 8.3×10^{-9} to 1.0×10^{-6} m^3/s are used. Pressure drop is measured during the injection. The saturation profile is simultaneously measured by X-Ray CT scanning system. The measured saturation profiles are shown as black dotted lines in Fig. 4a and b. The measured pressure drop is shown as cross points in Fig. 4c. The numbers 1 to 7 correspond to the tests with flow rates of 1.0×10^{-6}, 4.2×10^{-7}, 2.3×10^{-7}, 1.3×10^{-7}, 6.7×10^{-8}, 3.3×10^{-8} and 8.3×10^{-9} m^3/s, respectively.

The mathematical model given by Eqs. (10) and (11) and presented in Section 2 is applied to calculating saturation profiles and pressure drops along the core under laboratory conditions for three flow rates (curves 1–3 in Fig. 4a). The optimisation of the following 8 parameters is performed by maximising the coefficient of determination R^2: J-function coefficient C and exponent α, contact angle θ, tortuosity η, wettability alteration fraction φ_1, permanently water wet fraction φ_2,

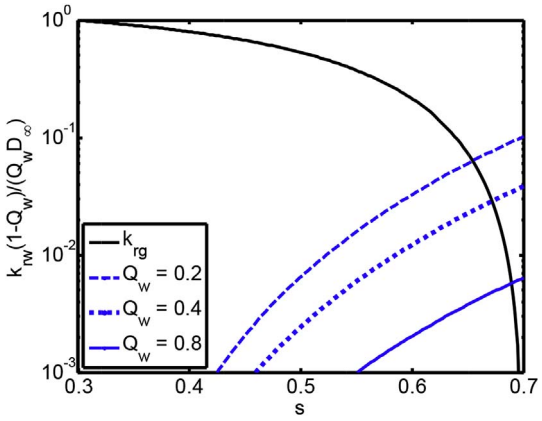

Fig. 3. Graphical solution for inlet saturation value where core length (drainage radius) tends to infinity.

residual gas saturation s_{gr}, and water connate saturation s_{wc}.

Now let us calculate the number of degrees of freedom for seven sets of the experimental data. Each saturation-profile curve in Fig. 4a has 3 degrees of freedom; outlet saturation for the water-wet rock is equal to 1- s_{gr}, where s_{gr} is the same for all flow cases; so, the total degree of freedom for seven saturation profiles is $2 \times 7 + 1 = 15$. The curve of pressure drop along the core versus gas rate (Fig. 4b) has 3 degrees of freedom. The capillary pressure curve also has 3 degrees of freedom. Therefore, the laboratory data set on saturation profiles, pressure drop across the core and capillary pressure has 21 degrees of freedom. We treat this 21-parametric set of the experimental data to tune 8 parameters by minimising the least square deviation between the experimental and modelling data. Non-linear least square method (improved Levenberg-Marquardt procedure) is applied (Coleman and Li, 1996).

The obtained parameter values by the tuning are: capillary J-function coefficient $C = 0.1$, J-function exponent $\alpha = 3.05$, contact angle $\theta = 18.3^\circ$, tortuosity $\eta = 1.15$, wettability alteration fraction $\varphi_1 = 0.98$, permanently water wet fraction $\varphi_2 = 0.014$, residual gas saturation $s_{gr} = 0$, and irreducible water saturation $s_{wc} = 0.38$. The matched saturation profiles are presented in Fig. 4a; Fig. 4b shows the matched pressure drops, Fig. 4c shows the matched capillary pressure and Fig. 4d exhibits gas relative permeability matching.

The results from modelling closely agree with those from experimental measurement: R^2 is 0.81 for saturation profiles, 0.92 for capillary pressure and 0.99 for pressure drops. The saturation data show significant scattering around the monotone profiles, which is typical for CT data (Mays and Hunt, 2005, 2007). Relatively low coefficient of determination for saturation profiles is explained by their extensive scattering. Usually, the length-resolution of computational tomography is higher than the length scale of rock micro heterogeneity. The scattering is explained by the rock micro-heterogeneity. Therefore, CT-determined saturation profiles are usually highly scattered (Shi et al., 2011; Alemu et al., 2011).

Also, usually high deviations between the measured and modelled profiles are observed near to core ends (Al-Abduwani et al., 2005a, 2005b). The interaction between X-rays and aluminium flanges (end-caps) used in the tests, affects CT measurements and explains the deviation near to core inlet and outlet. Therefore, the saturation profiles were accounted for only outside the end-effect zones.

Pressure drop across the core is an integral of pressure gradient; micro-heterogeneous deviations of saturation profiles annihilate during integration. Therefore, the coefficient of determination for pressure drop is significantly higher than that for saturation profiles. Fig. 4b shows uncertainty in pressure drop measurements, calculated by the method proposed by Badalyan et al. (2012, 2014). The modelling curve matches the laboratory points in the range of uncertainties.

Besides the above-mentioned artefacts, the quality of matching of

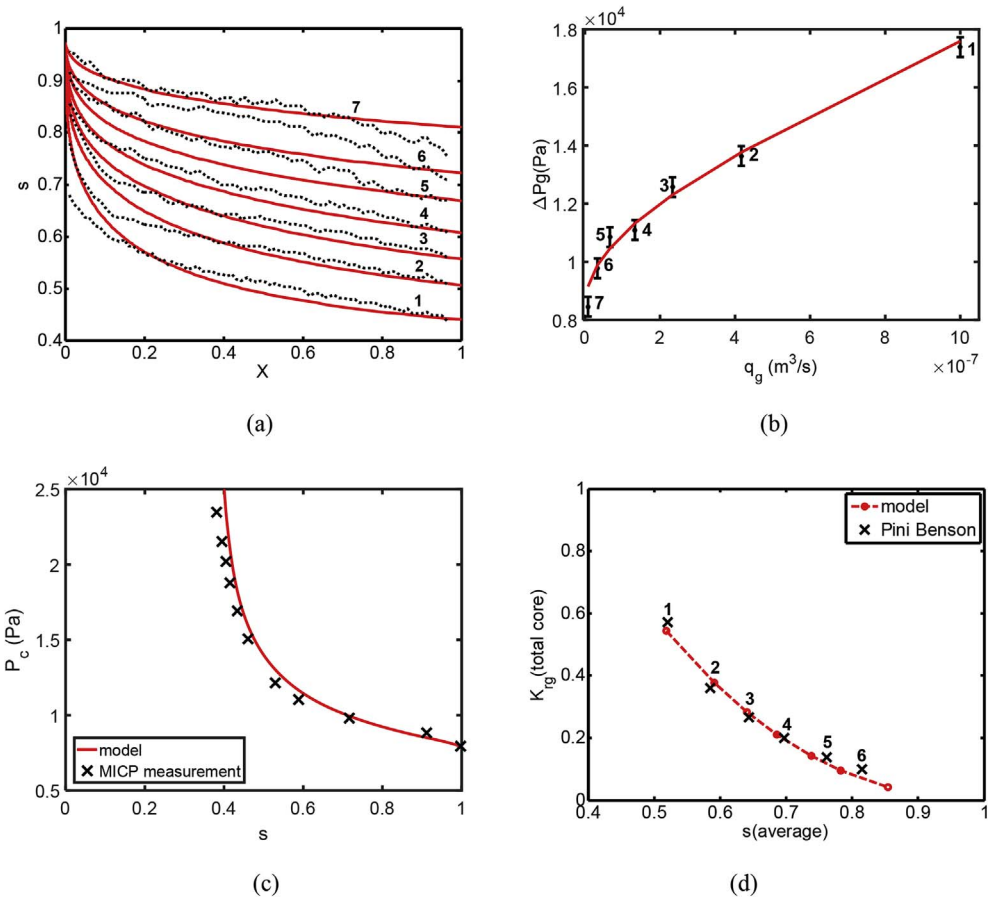

Fig. 4. Laboratory coreflood data treatment using the analytical model: a) matched saturation profiles for all tests with different rates; b) pressure drop measured in all seven tests compared with modelling results. c) matching the MICP-measured capillary pressure by the analytical model; d) matching of gas relative permeability measurements by the model.

the data from seven tests is high.

The model parameters obtained by tuning vary in common intervals: α is in the range of 0–7 (Brooks and Corey, 1964); C is in the range of 0.09–0.6 (Desbarats, 1995; Thungsuntonkhun and Engler, 2004); η can be in the range of 0.5–2 (Mualem, 1976; Bradford et al., 1997; Chen et al., 2014).

Pini and Benson (2013) also performed an independent measurement of the capillary pressure curve for the rock, used in the coreflooding, by Mercury Injection Capillary Pressure (MICP) apparatus. Fig. 4c presents high agreement between the measurements and the values obtained from the tuning of the coreflood data.

The above experimental data treatment validates the mathematical model for compressible two-phase steady-state flow in porous media.

4. Analysis of results

In the present section, we predict well productivity and its dependency on the contact angle and flow rate using typical parameter values.

4.1. Homogeneous core/reservoir

The effects of contact angle on saturation profile in 1d linear flow are shown in Fig. 2. The following typical values for the model parameters have been used in the model (10, 11) for calculating water-gas flow presented in Figs. 2, 3 and 5-8: $C = 0.4$, $\alpha = 0.99$, $\eta = 0.75$, $\varphi_1 = 0.98$, $\varphi_2 = 0.01$, $s_{gr} = 0.3$, $s_{wc} = 0.3$, $k = 1$md, and $\phi = 0.1$. Those constants are typical for water-gas flows (Brooks and Corey, 1964; Desbarats, 1995; Chen et al., 2014). Additionally, in Fig. 2, we applied $Q_w = 0.35$ and $\varepsilon_x = 0.2$.

The blue curve in Fig. 2 corresponds to water-wet, green to neutral-wet and red to gas-wet rocks (contact angles 0°, 90° and 180°, respectively). The solid curves correspond to compressible gas; while the dashed curves correspond to incompressible flows. Mass fluxes of gas and water are constant in steady-state flows. Pressure decreases along the flow direction. The higher is the pressure, the higher is the gas density and, consequently, the lower is the volume filled by gas. Therefore, gas saturation increases along the flow. Consequently, water saturation decreases along the flow, as shown in Fig. 2a (solid curves).

Approaching the outlet, capillary pressure approaches zero. This leads to the decrease of the saturation profile $s(X)$ in hydrophobic media, reaching the saturation value $s = s_{wc}$ at the outlet. In water-wet media, the saturation profile reaches the minimum and increases until reaching the outlet with $s = 1\text{-}s_{gr}$. The influence of capillary pressure explains why there can be non-monotonic saturation profiles.

Because pressure variation near the outlet is small, the solid and dashed curves converge. The difference between the curves decreases along the flow direction due to pressure decreasing.

Fig. 2b shows gas pressure profiles for different rock wettability. In water-wet media, the pressure steeply increases near the outlet (wellbore) due to the hydraulic resistance to gas flow created by water barrier. The pressure profiles for hydrophobic and mixed-wet rocks are significantly lower than those for the water-wet case, i.e. water-wet case is more formation-damaging.

An observation from Fig. 2b is that pressure for compressible flow is lower than that for incompressible flow. In compressible flow, saturation increases towards the inlet if compared with incompressible flow. So, phase permeability for water also increases. Therefore, pressure gradient in water decreases. Far away from the outlet, pressure gradients in water and gas are equal.

The effect of capillary-viscous ratio on saturation profiles is shown in Fig. 5. The constants applied are $Q_w = 0.6$, $\theta = 0°$. The saturation profiles for compressible and incompressible cases almost coincide for high capillary-viscous ratio $\varepsilon_x = 10$, exhibit small deviation for

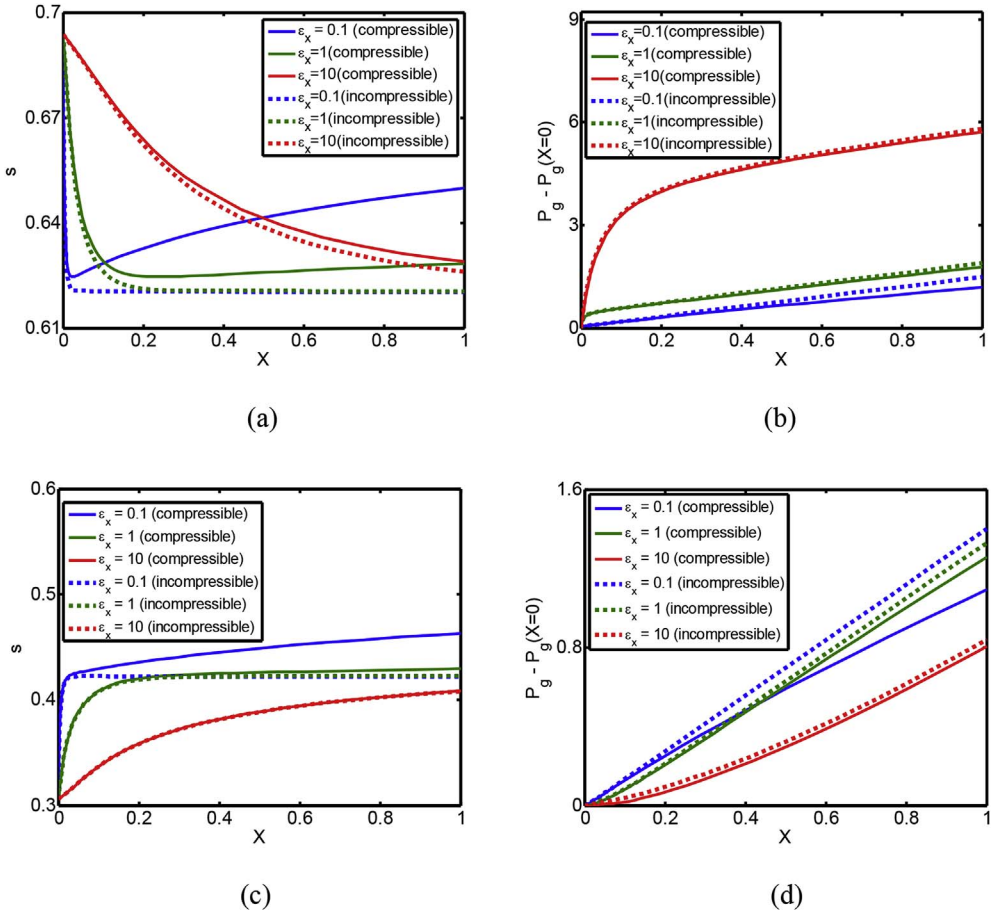

Fig. 5. a) Saturation profiles at different capillary-viscous ratios in linear flow: (a) for water wet case ($\theta = 0$); b) pressure profiles for linear flow for water wet case ($\theta = 0$); c) Saturation profiles at different capillary-viscous ratios in linear flow for hydrophobic rock ($\theta = \pi$); d) pressure profiles for linear flow for hydrophobic rock ($\theta = \pi$).

intermediate capillary-viscous ratio $\varepsilon_x = 1$ and significantly deviate for small $\varepsilon_x = 0.1$. Large ε_x corresponds to small rates and, consequently, small pressure drops, so the compressibility effect is negligible. The same corresponds to deviation of compressible pressure profiles from those for incompressible case (Fig. 5b). The deviation increases as the capillary-viscous ratio decreases.

Low ε_x –values correspond to high rates and, consequently, high pressure profiles along the core. Gas density decreases significantly along the flow, resulting in increasing of gas volumetric flux, i.e. gas saturation increases. The continuous blue curve in Fig. 5a lies above the continuous green curves, while the order for dotted profiles is opposite.

Increase in ε_x results in the expansion of the end-effect zone (Fig. 5a). As a result, the minimum in the saturation profile can be located outside the investigated region. Therefore, the saturation profile is monotonic in the region X∈ [0, 1] for large capillary-viscous ratio ε_x (red curves in Fig. 5a).

In hydrophobic rocks, saturation decreases along the flow trajectory due to gas compressibility, outside the end effect zone. It also decreases up to s_{wc} at the outlet, so all saturation profiles in Fig. 5c are monotonic. Large capillary-viscous ratios correspond to slow flows, caused by low pressure gradient (Fig. 5d).

Fig. 6 shows the effect of contact angle on gas and water productivity indexes for linear flows. The constant used is $Q_w = 0.6$. The non-monotonic dependencies are explained by the competing factors of compressibility, capillary pressure and viscous forces. Contact angle increase leads to decrease of water saturation along the overall core, resulting in increase of relative permeability for gas. Yet, the corresponding wettability altering yields displacement of gas into small

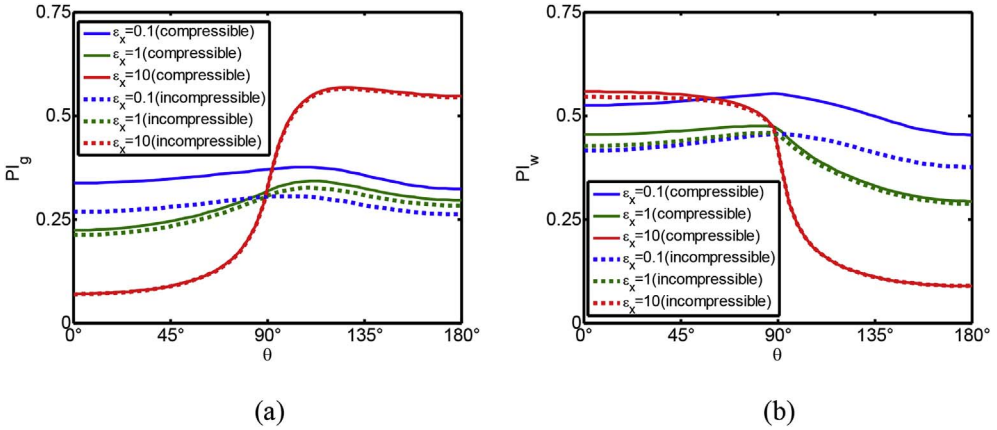

Fig. 6. Productivity index versus contact angle at different capillary-viscous ratios ε_x under linear flow with boundary condition $Q_w = 0.6$ for: a) gas and b) water.

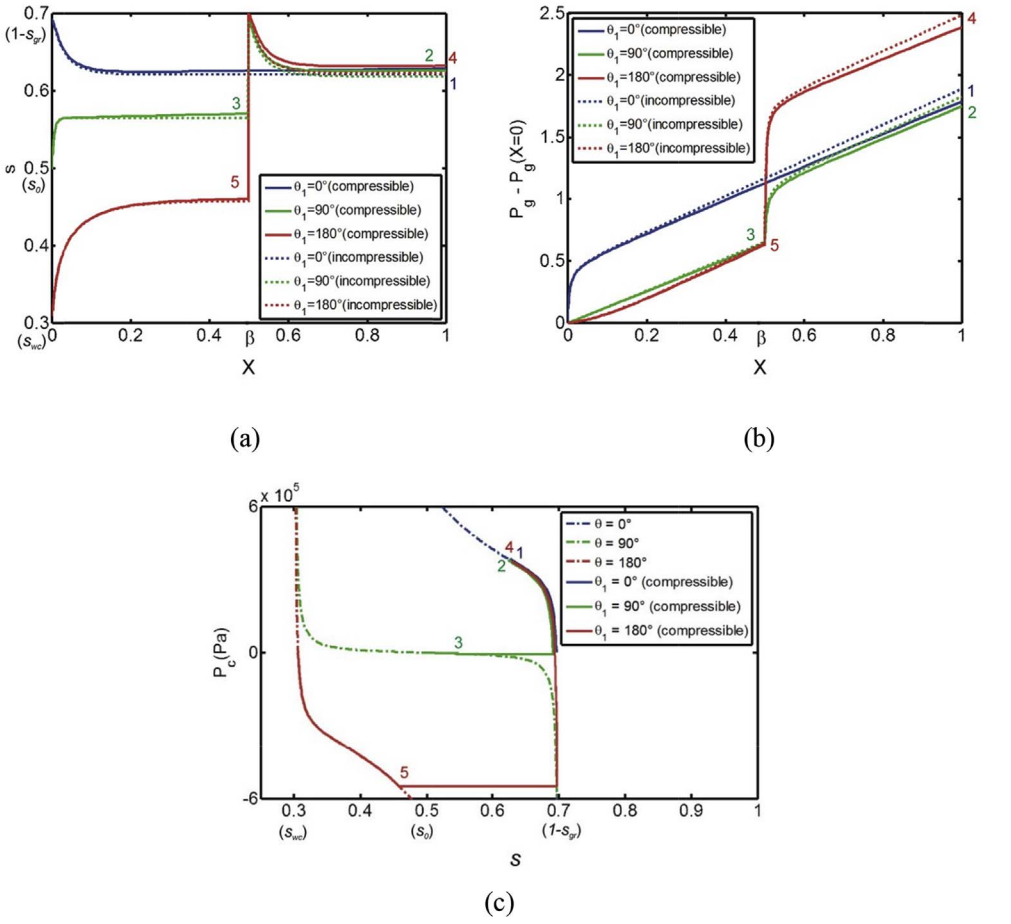

Fig. 7. Saturation and pressure profiles with corresponding paths on capillary pressure curves at different altered contact angle θ_1 in linear flow with piecewise alteration of contact angle: a) saturation profile; b) gas pressure profiles; c) capillary pressure curves.

pores, causing the decrease in gas relative permeability. The above factors result in non-monotonic curves for gas and water productivity indexes versus contact angle.

At high capillary-viscous ratios, the saturation is controlled predominantly by outlet capillary pressure. When the contact angle is increased, the decrease of water saturation has much larger effect on the PIs for gas and water, than the reduction of gas relative permeability has on the PIs. Therefore, gas PI is much higher at large contact angles (red curves in Fig. 6a) and water PI is much lower at large contact angles (red curves in Fig. 6b).

The productivity index for compressible case is higher than that for in compressible case, as shown in Fig. 6. This is due to the reduction in pressure gradient previously observed in Figs. 2b and 4b.

Fig. 6a shows that for each capillary-viscous ratio, there does exist an optimal contact angle, causing the highest productivity index for gas. This conclusion is important for planning and design of gas well treatment with wettability alteration.

4.2. Core/reservoir with piecewise constant contact angle

Fig. 7 presents saturation and pressure profiles with contact angle altering from 0° to 90° (green curve) and to 180° (red curve). The constants used are $Q_w = 0.6$, $\beta = 0.5$, $\varepsilon_x = 1$ and $\theta_2 = 0°$. The blue curve corresponds to gas-water flow without wettability change. Point $X = \beta$ corresponds to the depth of chemical treatment, where saturation shock with continuous capillary pressure occurs; see Eqs.(14) and (15). Water saturation at $\theta_1 = 0°$ increases along the flow path from point 1 at the inlet up to the value 1 - s_{gr} at the outlet (sand-face of the well).

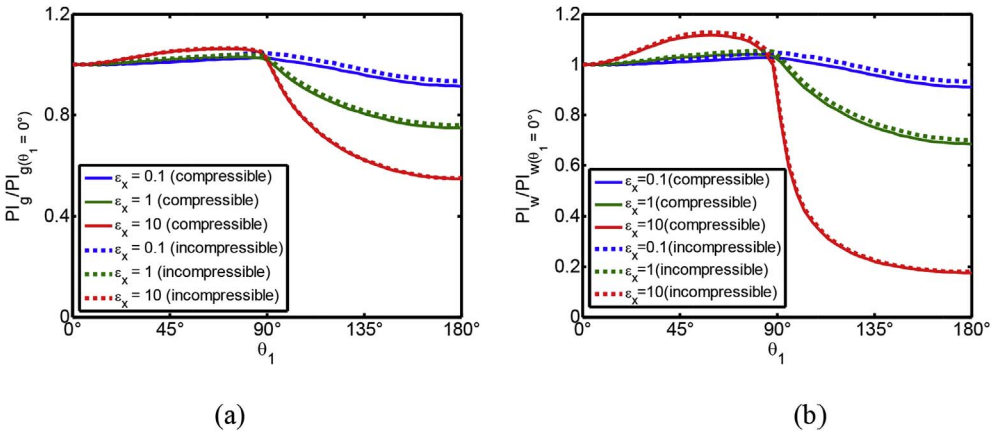

Fig. 8. Productivity index versus altered contact angle θ_1 at different capillary-viscous ratios ε_x in linear flow with piecewise alteration of contact angle for a) gas and b) water.

The green curve corresponds to the altered contact angle $\theta_1 = 90^\circ$. The saturation increases from point 2 at the inlet up to the value 1 - s_{gr} upstream the treatment boundary, where it drops down to point 3 with further decrease up to s_0 at the outlet. The red curve corresponds to complete wettability alternation: $\theta_1 = 180^\circ$. It increases from point 4 at the inlet to 1 - s_{gr} at the boundary, then it drops to point 5 across the boundary; then it decreases up to point s_{wc}.

The corresponding pressure drop profiles are shown in Fig. 7b. The above-mentioned profiles are also presented in the capillary pressure curves for three values of contact angles (Fig. 7c). The saturation jumps across the treatment boundary corresponds to horizontal lines of continuous capillary pressure.

When θ_1 is increased in the altered zone, capillary pressure is decreased. Due to the capillary pressure decrease and the capillary continuity condition at $X = \beta$, saturation will rise outside the treatment boundary. The saturation will approach 1 - s_{gr}, as the altered contact angle θ_1 approaches 90°. This leads to a pressure gradient increase with contact angle at the treatment boundary (Fig. 7b).

Fig. 8 presents the productivity index versus contact angle at different capillary-viscous ratios ε_x under linear flow after the chemical treatment for gas and water. The constants used are: $Q_w = 0.6, \beta = 0.5$ and $\theta_2 = 0^\circ$. When θ_1 is increased, the water barrier at $X = 0$ decreases. However, the water barrier at $X = \beta$ increases. The pressure gradient increase at the treatment boundary introduces another hindrance to gas production with the increase of contact angle. The optimal contact angle is therefore lower if compared with the fully altered case (Fig. 6).

5. Well behaviour prediction

In this section, we analyse the productivity behaviour of two gas wells producing from gas storage in aquifer, before and after wettability alteration near the wellbore, by using the mathematical model given by Eqs. (C-6, C-7).

Natural gas is injected into an St. Peter's aquifer (Illinois, US) during summer for storage purposes, and is withdrawn during winter. The details of the gas storage operations at different reservoir pressures and rock properties are presented in the works by Buschbach and Bond (1973), Weiss and Xie (2009) and Xie et al. (2009). The gas withdrawal in this reservoir is affected by water capillary barrier in the near-wellbore region. The surfactant Tomadory N-4 is injected into the near-wellbore region of a few selected wells to alter wettability, remove the capillary water barrier and enhance gas deliverability.

Fig. 9a and b shows gas rates q_p versus accumulated volume of produced gas Q_p for Stenemeyer and Thomas wells, respectively. Blue crosses correspond to gas production before well stimulation, and red crosses reflect gas productivity after the stimulation. Fig. 10a shows the productivity index before (blue crosses) and after (red crosses) wettability alteration treatment for the Stenemeyer well. The analogous data for the Thomas well are presented in Fig. 10b.

The following data are taken from the above-mentioned papers for well-behaviour modelling: initial contact angle 0°, altered contact angle 70°, permeability 1.22×10^{-12} m^2, well drainage area 4.05×10^4 m^2, temperature 300 K, connate water saturation 0.3, wellbore diameter 0.1397 m, for both wells. The data that are different for two wells are presented in Table 1.

Five model parameters are tuned to match PI data, before and after the treatment in each well: J-function coefficient C, J-function exponent α, tortuosity η, wellbore pressure $P_1(R_w)$ at the beginning of pressure depletion for maximum value of P_{res} for $Q_p = 0$, and wellbore pressure $P_2(R_w)$ at the end of pressure depletion for minimum value of P_{res}. Reservoir pressures shown in Fig. 10a and b by crosses, are estimated in source papers from the observation well data. In modelling, we fix $P_{res} = P(r_e)$. Table 1 shows similar values of the reservoir parameters for both wells. To minimise the number of tuned parameters, rock properties C, α, and η are assumed to be equal for both wells. Therefore, the field data from both wells are treated simultaneously.

The tuning is performed by minimising the least square deviation between the well and modelling data. Non-linear least square method (improved Levenberg-Marquardt procedure) is applied (Coleman and Li, 1996). The values of tuned parameters for Stenemeyer and Thomas wells are listed in Table 2. The results of modelling by numerical solution of two ordinary differential equations (C-6, C-7) are shown in Fig. 10a and b for Stenemeyer and Thomas wells, respectively (solid curves).

The PI curves obtained from modelling (solid curves in Fig. 10a and b) deviate from the field data (cross points in Fig. 10a and b) in the early stage of well operation, which corresponds to $P_{res} > 5 \times 10^6$ Pa. Field data scattering presented in both wells are explained by Weiss and Xie (2009). There are complications in the field operation which are not accounted for in the current model. Post-treatment gas injection was limited due to the loss of a disposal well and pipeline repairs and replacements. The loss of the disposal well after treatment prevented dewatering of the storage zone. The loss of the well and pipeline repairs resulted in reduction of the total volume of gas injected into the reservoir and altered the distribution of saturation in the reservoir (Weiss and Xie, 2009). The resulted non-uniform gas distribution and transient effects at the beginning of gas withdrawal lead to data scattering in post-treatment PI curve withdrawal cycles (red crosses in Fig. 10a and b). There are also several other reasons for field data scattering: not all data points represent steady states; several data were taken during transition period where the steady states had not been reached. Also, the reservoir rock is assumed to be incompressible in the model (C-6, C-7). Reservoir heterogeneity is not accounted for in the model. Therefore, only qualitative match between the field and modelling data is expected.

Despite the above-mentioned effects of field operations, rock compressibility and reservoir heterogeneity are neglected in Eqs. (C-6, C-7), the model qualitatively matches the trend of PI data of the withdrawal

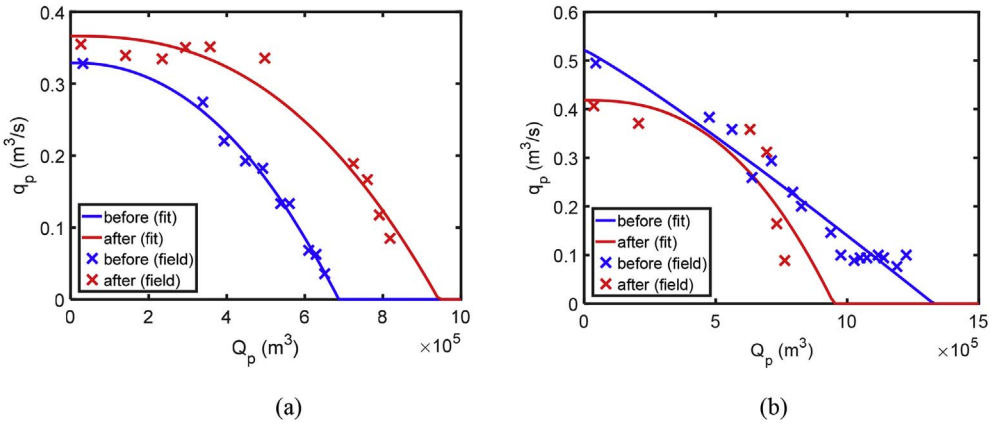

Fig. 9. Gas rates q_p versus accumulated volume of produced gas Q_p before and after well treatment (marked by blue and red crosses), respectively: (a) Stenemeyer well; (b) Thomas well. (For interpretation of the references to colour in this figure legend, the reader is referred to the web version of this article.)

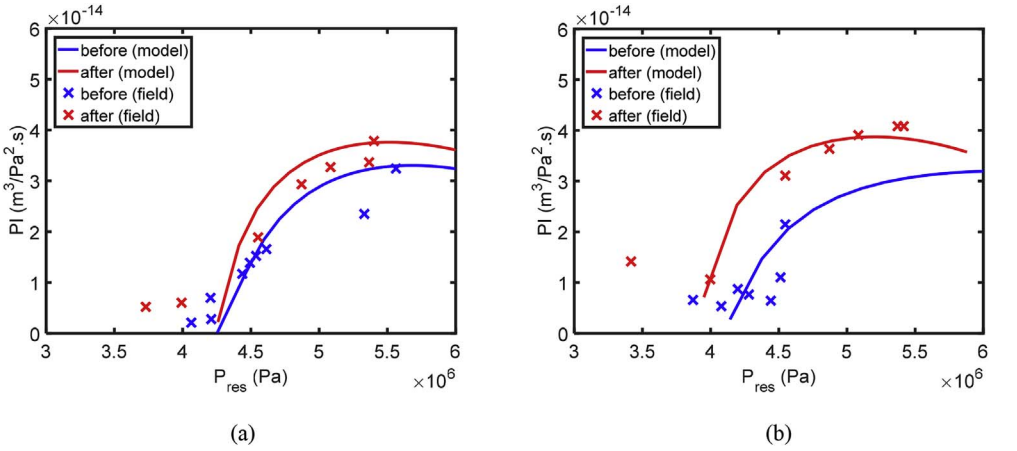

Fig. 10. Field case study of wettability-alteration effects on well productivity index – field and modelling data before and after well stimulation: a) Stenemeyer well; b) Thomas well.

Table 1
Field parameters in the areas of Stenemeyer and Thomas wells.

Parameter	Stenemeyer	Thomas
Reservoir thickness	8.23 m	7.01 m
Treatment radius	5.97 m	6.43 m
Porosity	0.20	0.18
Reservoir depth	359 m	356 m

Table 2
The parameter tuning results for Stenemeyer and Thomas wells.

Parameter	Stenemeyer	Thomas
C	2.34	2.34
α	0.76	0.76
η	1.04	1.04
P_1 (before)	5.33 × 10^6 Pa	5.34 × 10^6 Pa
P_2 (before)	4.11 × 10^6 Pa	3.95 × 10^6 Pa
P_1 (after)	5.30 × 10^6 Pa	4.78 × 10^6 Pa
P_2 (after)	4.08 × 10^6 Pa	3.73 × 10^6 Pa

cycle. The coefficient of determination is $R^2 = 0.85$ for the Stenemeyer well (Fig. 10a), and $R^2 = 0.68$ for the Tomas well (Fig. 10b). However, the field and modelling data exhibit close agreement at the late stage of pressure depletion for $P_{res} < 5 \times 10^6$ Pa.

6. Discussion

Saturation and pressure profiles for axi-symmetric flow are obtained from the linear-flow profiles by the substitution $X = \ln(R)$ and transformation of the abscissa from the interval [0, 1] to [ln(R_w), 0]. It allows re-calculating coreflood data on two-phase flow after the chemical treatment, into the well inflow performance and behaviour prediction.

Near to and far away from the inlet, the model for steady-state two-phase compressible flow can be asymptotically simplified. Inside the capillary end-effect zone close to the core outlet, fracture face or wellbore, gas compressibility can be neglected. Far away from the end-effect zone, i.e., a long distance from the outlet or wellbore, capillary pressure gradient is negligible. In both cases, pressure and saturation profiles are given by implicit formulae.

With the core length or drainage radius tending to infinity, capillary pressure gradient at the inlet or drainage radius tends to zero. The ratio of gas and water rates becomes equal to the ratio of gas and water mobilities. It allows determining inlet saturation, either graphically or by solving transcendental equation.

Outside the end-effect zone, water saturation decreases along the flow path due to gas compressibility. Saturation continues decreasing within the end-effect zone of gas-wet rock down to the value of s_{wc}. For water-wet rock, saturation increases in the end-effect zone up to 1-s_{gr}, yielding non-monotonic saturation profile.

Section 3 validates the model for compressible gas-water flow, given by Eqs. (10) and (11) and used in the present work to study the compressibility effects on well productivity during wettability alterations. The model uses relative permeability and capillary pressure curves, presented in Appendix A. Those formulae of relative permeability and capillary pressure include the dependency of contact angle as an independent variable, reflecting possible wettability alterations, described in Section 2.2. The formulae have been proposed by Bradford et al. (1997) and O'Carroll et al. (2005), based on numerous laboratory tests with changing wettability, and used by Naik et al. (2015) to study incompressible two-phase flux during wettability alterations.

Matching of seven coreflood tests by the semi-analytical model represented by Eqs. (10) and (11) yields the coefficient of determination $R^2 = 0.99$ for pressure drops across the core and 0.82 for saturation profiles. Relatively low R^2 value for saturation profiles is explained by high data scattering, which is typical for CT data. Comparison between the capillary pressure function tuned from the coreflood tests, and that measured independently exhibits $R^2 = 0.92$. The above validates the model proposed. In particular, it validates the usage of formulae (A-3, A-4) for relative permeability and capillary pressure for compressible-flow modelling.

The semi-analytical modelling shows that the effect of compressibility on the inflow performance with commingled gas-water production could be quite significant. The difference between pressure drawdowns for compressible and incompressible cases reaches 19% (green curves for contact angle $\theta = \pi/2$ in Fig. 2b) and 40% (blue curves for capillary-viscous ratio $\varepsilon_x = 0.1$ in Fig. 5d); the difference in saturations can be up to 10% (blue curves for capillary-viscous ratio $\varepsilon_x = 0.1$ in Fig. 5c); the difference in productivity index is up to 25% (blue curves for capillary-viscous ratio $\varepsilon_x = 0.1$ in Fig. 6a).

For the above case where $\theta = \pi/2$ and $\varepsilon_x = 0.1$, doubling rate and decreasing the outlet pressure at $x = 0$ from 5 × 10^6 Pa to 3 × 10^6 Pa yields an increase in the difference between compressible and incompressible cases: the difference is 66% for pressure drawdown, is 58% for PI, and is 10% for saturation.

The Brooks-Corey forms for relative permeability and capillary pressure, which are more habitual in petroleum industry, can be also used in the semi-analytical model given by Eqs. (10) and (11).

The semi-analytical model for linear flow can be applied not only for coreflood tests, but also for fractured wells. The proposed model can be used to describe two-phase water-gas flow from formation towards fracture face.

The semi-analytical model can be applied for design of the chemical well treatment to maximise gas production and minimise produced water volumes. Matching the data of steady-state commingled gas-water flow through the reservoir cores before and after treatment by

wettability-alternating chemicals (surfactants or nano-fluids) using the linear-geometry analytical model allows tuning the model parameters as functions of concentration of the applied chemical. The obtained plots for productivity index permit determining an optimal contact angle, yielding possible choice of the wettability-alternating chemical. The axi-symmetric model re-calculates flow for well conditions, applying the laboratory-based model parameters. The calculated dependencies of well productivity of concentration and volumes of the applied chemicals allow determining the optimal values for given reservoir conditions.

The above-mentioned approach can be used for design of well treatment decreasing water-blocking in gas producers in conventional, coal-bed and shale-gas reservoirs.

The proposed 1d model (C-6, C-7) assumes uniform rock homogeneity. Multi-layer model with areal heterogeneity can yield better match of the well data before and after the surfactant treatment (Fig. 10). Another limitation of the model is the Darcy's law for two-phase flows. Well behaviour deviates from the modelling data at high drawdowns and rates. Additional productivity index enhancement can be attributed to removal of water drops from small pores by high-velocity gas (Barenblatt et al., 1990). Reduction in pore-blocking explains permeability enhancement at high rates. The above effects can be captured by the modified Darcy's law with initial pressure gradient, where the value of the initial pressure gradient increases as permeability decreases. The effect of the water-droplet mobilisation can be particularly important in low-permeable unconventional gas and oil fields.

The model (C-6, C-7) also assumes rock incompressibility, i.e. the permeability is independent of the reservoir pressure. However, the reservoir-pressure decrease yields stress increase, resulting in permeability decline (Barenblatt et al., 1990). The effect can be captured by using $k = k(p)$ in Eqs. (C-6, C-7). Using exponential permeability dependency of pressure adds an extra tuning parameter, yielding better matching of the field data by the modelling curves.

Water block on the matrix-fracture boundaries is a serious obstacle for gas production from fractured-porous reservoirs (Van Golf-Racht, 1996). The effect of well neighbourhood treatment by wettability-changing surfactants or nanofluids must be investigated. The mathematical model for gas flow towards well in fractured-porous formation is unsteady-state (Barenblatt et al., 1990), while the present paper derives steady-state solution for inflow performance in homogeneous reservoir as a special case.

The mathematical model developed reveals non-monotonic productivity-index dependency of the contact angle. It is attributed to two competitive factors: the higher is the contact angle, the lower is the capillary water barrier yielding higher PI for gas; on the contrary, the higher is the contact angle, the lower is the radius of the gas-filled pores and the lower is the relative permeability for gas. Therefore, there does exist an optimal contact angle, which must be achieved during well treatment.

7. Conclusions

The semi-analytical modelling of steady-state gas-water flow in the rock with constant and piecewise-constant contact angles accounting for gas compressibility allows making the following conclusions:

For high capillary-viscous ratio and water-wet rock, gas pressure significantly rises in the end-effect zone, creating a hydraulic resistance for gas inflow.

Increase of contact angle or decrease in capillary-viscous ratio near to well removes the capillary barrier and increases well productivity for gas.

For high capillary-viscous ratio, the end effect zone covers the overall region, and saturation increases monotonically along the flow path from inlet to the outlet for water-wet rocks.

Pressure drop across the core is higher for lower capillary-viscous ratios. For small ε values, the effect of compressibility is higher, and the difference between profiles for compressible and incompressible gas is larger.

For inflow of water and gas, the interplay between the physical phenomena of capillary pressure, pressure in gas phase and compressibility leads to a non-monotonic dependency of the productivity indexes for gas and water versus contact angle.

For the porous media with piecewise altered contact angle, increase in altered contact angle forms a second water barrier outside the altered zone. This additional end effect reduces the optimal contact angle if compared to the fully altered case.

Acknowledgements

The authors are grateful to Dr. Kirill Gerke (CSIRO) and Eng. Matthew Wooley (Santos Ltd) for fruitful discussions.

Many thanks are due to David H. Levin (Murphy, NC, USA) who provided professional English-language editing of this article.

Nomenclature

b	Klinkenberg factor, Pa
C	J-function coefficient
D	density-viscosity ratio
g	gas-wet capillary fraction
J	J-function
k	permeability, m^2
k_{kg}	Klinkenberg correction coefficient
k_r	relative permeability
L	length scale, m
M	molar mass, kg/mol
p_c	capillary pressure, Pa
p	pressure, Pa
P	dimensionless pressure
P_1	wellbore pressure at the beginning of depletion, Pa
P_2	wellbore pressure at the end of depletion, Pa
P_{res}	reservoir pressure, Pa
PI	dimensionless productivity index
q	mass rate (per unit area for linear flow, $kg/m^2 \cdot s$)(per unit height for radial flow, $kg/m \cdot s$)
q_p	gas volumetric flow rate, m^3/s
Q_w	water cut by mass
Q_p	accumulated volume of produced gas, m^3

R	radius, m
r_e	drainage radius, m
R	dimensionless radius
R_c	universal gas constant, 8.3144621 J/Mol·K
S	water saturation
s_{gr}	irreducible gas saturation
s_{wc}	connate water saturation
S	normalised saturation
T	temperature, K
W	capillary size, m
x	distance, m
X	dimensionless distance
Z	compressibility factor

Greek letters

α	J-function exponent
β	fraction of wettability altered zone
ε	capillary-viscous ratio
η	tortuosity index
ϕ	porosity
φ	fraction of pore surface
μ	viscosity, Pa·s
ρ	density, kg/m^3
σ	interfacial tension, N/m
θ	contact angle
θ_1	altered contact angle
θ_2	initial contact angle

Subscripts

g	gas
w	water (for density, pressure, productivity index, relative permeability and viscosity)wetting phase (for normalised saturation), well (for radius)
x	linear
r	radial
0	outlet
∞	inlet

Appendix A. Relative permeability and capillary pressure functions

Following papers by Bradford et al. (1997) and O'Carroll et al. (2005), we introduce the model for relative permeability and capillary pressure for the capillary bundle model. Introduce normalised water saturation as follows:

$$S(s) = \frac{s - s_{wc}}{1 - s_{gr} - s_{wc}} \tag{A-1}$$

where s is the water saturation, s_{wc} is the connate water saturation, s_{gr} is the residual gas saturation. The rock is hydrophobic for contact angle exceeding 90°. The normalised wetting phase saturation is

$$S_w(s) = \begin{cases} S(s), \theta < 90° \\ 1 - S(s), \theta > 90° \end{cases} \tag{A-2}$$

The capillary pressure is a function of normalised wetting phase saturation and contact angle. A fractionally wet rock is assumed, which is split into three fractions. The first fraction φ_1 has the contact angle θ. The fractions φ_2 and φ_3 are the fractions of surfaces which are fully hydrophilic and hydrophobic, respectively. Fractions φ_2 and φ_3 vary in the intervals 0–0.03. The sum of φ_1, φ_2 and φ_3 is one. The capillary pressure is expressed using Leverett's J-function as:

$$P_c(s, \theta) = \frac{\sigma}{\sqrt{k/\phi}} J(s, \theta),$$
$$J(s, \theta) = \varphi_1 \cos(\theta) C S_w(s, \theta)^{-\frac{1}{\alpha}} + \varphi_2 C S(s)^{-\frac{1}{\alpha}} - \varphi_3 C\left(1 - S(s)^{-\frac{1}{\alpha}}\right) \tag{A-3}$$

Relative phase permeabilities for water and gas are expressed by the following formulae, respectively

$$k_{rw}(s, \theta) = (S(s))^{\eta} \frac{[1 - g(\theta)] \int_0^S w^2(S) dS + g(\theta) \int_{1-S}^1 w^2(S) dS}{\int_0^1 w^2(S) dS}$$
$$k_{rg}(s, \theta) = (1 - S(s))^{\eta} \frac{g(\theta) \int_0^{1-S} w^2(S) dS + [1 - g(\theta)] \int_S^1 w^2(S) dS}{\int_0^1 w^2(S) dS} \tag{A-4}$$

where

$$g(\theta) = \frac{1}{2}[1 - \cos(\theta)], \quad w(S) = \frac{S^{\frac{1}{\alpha}}}{C}\sqrt{k/\phi} \tag{A-5}$$

Particularly, in the case where permeability or pressure is low, such as in laboratory conditions with rock permeability less than 1 md, the slip effect can affect gas permeability. The slip effect can be accounted for by multiplying gas permeability with a Klinkenberg correction coefficient k_{kg} (Jones and Owens, 1980) as

$$k_{kg}(p_g) = \left(1 + \frac{b}{p_g}\right), \quad b = 0.86k^{-0.33} \tag{A-6}$$

The functions of capillary pressure (A-3) and relative permeability (A-5) contain 9 constants: J-function coefficients C and exponent α, contact angle θ, tortuosity η, wettability alteration fraction φ_1, permanently water wet fraction φ_2, residual gas saturation s_{gr}, irreducible water saturation s_{wi}, and the ratio of permeability k over porosity ϕ.

The above functions for relative permeability and capillary pressure are used in the derivation of analytical models in Section 2.

Appendix B. Qualitative analysis of solution

Consider how compressible flow tends to incompressible flow in important asymptotical cases. In the case where the pressure drop across the core is significantly lower than the outlet pressure P_0, gas is considered incompressible. In this case, Eq. (11) separates from Eq. (10) and allows for an implicit solution (Barenblatt et al., 1990):

$$X = \varepsilon_x \int_{s_0(\theta)}^{s} \frac{dJ(s,\theta)}{ds} \times \left[\frac{1 - Q_w}{k_{kg}(P_0)k_{rg}(s,\theta)D(P_0)} - \frac{Q_w}{k_{rw}(s,\theta)}\right]^{-1} ds \tag{B-1}$$

The solution to Eq. (B-1) is an asymptotic one to (11) near the core outlet, where $X \to 0$.

Another special case corresponds to negligible capillary pressure gradient, which provides the asymptotic solution far away from the end effect zone. Assuming $\varepsilon_x = 0$ in Eq. (11) yields

$$\frac{Q_w}{1 - Q_w} = \frac{k_{rw}(s,\theta)}{k_{rg}(s,\theta)k_{kg}(P_g)D(P_g)} \tag{B-2}$$

Eq. (B-2) allows expressing saturation via pressure as an implicit function: $s = s(P_g)$. Its substitution into Eq. (10) and separation of variables yield the solution $s(X)$:

$$X = \frac{1}{1 - Q_w}\int_{P_0}^{P} k_{kg}(P_g)k_{rg}(s(P_g),\theta)D(P_g)dP_g \tag{B-3}$$

Consider pressure and saturation profiles in long cores and the structure of the solution as X tends to infinity. For the incompressible case, as X tends to infinity, the saturation tends to the limit s_∞, and the left side of Eq. (11) tends to zero, which corresponds to the condition where the mobility ratio equals the rate ratio

$$\frac{Q_w}{1 - Q_w} = \frac{k_{rw}(s_\infty,\theta)}{k_{kg0}k_{rg}(s_\infty,\theta)}\frac{1}{D(P_0)} \tag{B-4}$$

and pressure tends to infinity (Naik et al., 2015).

For the compressible case, we assume that at X tending to infinity with pressure tending to infinity, gas density tends to a limit ρ_∞. The saturation limit s_∞ corresponds to the left-hand side of Eq. (11) equalling zero, and satisfies the condition

$$k_{rg}(s_\infty,\theta) = k_{rw}(s_\infty,\theta)\frac{1 - Q_w}{Q_w D_\infty}, \quad D_\infty = \frac{\rho_\infty \mu_w}{\rho_w \mu_g} \tag{B-5}$$

Graphical solution of Eq. (B-5) defining saturation at infinity s_∞ is presented in Fig. 3 in semi-log plot. Left-hand side of Eq. (B-5) is relative permeability for gas; right-hand side depends on water rate. The graphical solution shows that an increase in the water injection rate Q_w leads to an increase in the water saturation at infinity.

Let us show that s_∞ for compressible case is higher than s_∞ for incompressible case. Outlet pressure is less than the inlet pressure, so the outlet gas density is smaller than gas density at the inlet. Therefore, $D(P_0) < D_\infty$. Right-hand side of Eq. (B-5) increases as D decreases. Fig. 3 shows that s_∞ for compressible case is higher than that for incompressible case.

Appendix C. Axi-symmetric steady-state gas-water flow

We discuss steady state axi-symmetric flow towards the well. The expressions for water and gas phases follow from modified Darcy's law

$$q_w = 2\pi r \frac{k k_{rw}(s,\theta)}{\mu_w}\rho_w \frac{dp_w}{dr} \tag{C-1}$$

$$q_g = 2\pi r \frac{k k_{kg}(p_g) k_{rg}(s,\theta)}{\mu_g} \rho_g(p_g) \frac{dp_g}{dr} \tag{C-2}$$

Let us introduce the following dimensionless variables and parameters:

$$P_i = \frac{2\pi k \rho_w}{(q_w+q_g)\mu_w} p_i,\ i = w, g,$$
$$R = \frac{r}{r_e},$$
$$\varepsilon_r = \frac{2\pi\sigma\rho_w\sqrt{k\phi}}{(q_w+q_g)\mu_w} \tag{C-3}$$

where r_e is the drainage radius, and R is the dimensionless radius. The capillary-viscous ratio ε_r is the dimensionless ratio between the reference capillary pressure and pressure drop across the core with axi-symmetric single-phase water flow.

Substitution of dimensionless parameters (C-3) into Eqs. (C-1, C-2) yields

$$Q_w = R k_{rw}(s,\theta) \frac{dP_w}{dR} \tag{C-4}$$

$$1 - Q_w = RD(p_g) k_{kg}(p_g) k_{rg}(s,\theta) \frac{dP_g}{dR} \tag{C-5}$$

The equation for gas flux (C-5) allows the gas pressure gradient to be expressed as

$$\frac{dP_g}{dR} = \frac{1 - Q_w}{RD(P_g) k_{kg}(P_g) k_{rg}(s,\theta)} \tag{C-6}$$

Expressing the pressure gradient in water from Eq. (C-4), subtracting it from Eq. (C-6) and accounting for capillary pressure (9) will yield

$$\varepsilon_r R \frac{dJ(s)}{dR} = \left[\frac{1 - Q_w}{D(P_g) k_{kg}(P_g) k_{rg}(s,\theta)} - \frac{Q_w}{k_{rw}(s,\theta)} \right] \tag{C-7}$$

The capillary pressure equals zero at the wellbore; the constant pressure is set at the wellbore:

$$R = R_w: \quad s = s_0, \quad J(s_0) = 0, \quad P_g = P_0 \tag{C-8}$$

System of two ordinary differential equations (C-6, C-7) subject to Cauchy conditions (C-8) determines the steady-state profiles *s(R)* and $P_g(R)$ for axi-symmetric steady state gas-water flow

Like for the linear flow presented in Appendix B, in the case where pressure drop across the reservoir is significantly lower than the outlet pressure P_o, gas is considered incompressible. The functions k_{kg} and D become constant. Eq. (C-7) separates from Eq. (C-6). Solving ordinary differential equation (C-7) by separation of variables and accounting for Cauchy conditions (C-8) yields:

$$R = R_w \exp\left(\varepsilon_r \int_{s_0(\theta)}^{s} \frac{dJ(s)}{ds}^{-1} \times \left[\frac{1 - Q_w}{D(P_0) k_{kg}(P_0) k_{rg}(s,\theta)} - \frac{Q_w}{k_{rw}(s,\theta)} \right] ds \right) \tag{C-9}$$

This solution is asymptotic in the near-wellbore zone $R - R_w << R_w$

Far away from the well, saturation derivative tends to zero. As it follows from Eq. (C-7), Eq. (B-2) holds. It allows determining $s = s(P_g)$, similar as in Eqs. (B-2, B-3). Substituting it into Eq. (C-7) and separating variables yield pressure distribution far away from the well:

$$R = R_w \exp\left[\frac{1}{1 - Q_w} \times \int_{P_0}^{P} k_{kg}(P_g) k_{rg}(s(P_g),\theta) D(P_g) dP_g \right] \tag{C-10}$$

As in the linear case, Eq. (B-5) determines saturation far away from the well.

References

Adibhatla, B., Mohanty, K., Berger, P., Lee, C., 2006. Effect of surfactants on wettability of near-wellbore regions of gas reservoirs. J. Petrol. Sci. Eng. 52 (1), 227–236.

Al-Abduwani, F.A.H., Bedrikovetsky, P., Farajzadeh, R., Van Den Broek, W., Currie, P.K., 2005a. External Filter Cake Erosion: Mathematical Model and Experimental Study. Paper SPE-94635, Presented at the SPE European Formation Damage Conference. Sheveningen, The Netherlands, 25–27 May. .

Al-Abduwani, F.A., Hime, G., Alvarez, A., Farajzadeh, R., 2005b. New Experimental and Modelling Approach for the Quantification of Internal Filtration. Paper SPE-94634, Presented at the SPE European Formation Damage Conference. The Netherlands, 25–27 May. .

Al-Yami, A.M., Gomez, F.A., AlHamed, K.I., Al-Buali, M.H., 2013. A Successful Field Application of a New Chemical Treatment in a Fluid Blocked Well in Saudi Arabia. SPE-168086, presented at the SPE Saudi Arabia Section Technical Symposium and Exhibition, Al-Khobar, Saudi Arabia, 19–22 May. .

Alemu, B.L., Aker, E., Soldal, M., Johnsen, Ø., Aagaard, P., 2011. Influence of CO_2 on rock physics properties in typical reservoir rock: a CO_2 flooding experiment of brine saturated sandstone in a CT-scanner. Energy Procedia 4, 4379–4386.

Badalyan, A., Carageorgos, T., Bedrikovetsky, P., You, Z., Zeinijahromi, A., Aji, K., 2012. Critical analysis of uncertainties during particle filtration. Rev. Sci. Instrum. 83, 095106.

Badalyan, A., You, Z., Aji, K., Bedrikovetsky, P., Carageorgos, T., Zeinijahromi, A., 2014. Size exclusion deep bed filtration: experimental and modelling uncertainties. Rev. Sci. Instrum. 85, 015111.

Bahrami, H., Rezaee, M.R., Nazhat, D.H., Ostojic, J., Clennell, M.B., Jamili, A., 2011. Effect of Water Blocking Damage on Flow Efficiency and Productivity in Tight Gas Reservoirs. Paper SPE-142283, presented at the SPE Production and Operations Symposium, Oklahoma, USA. 27–29 March. .

Bang, V.S.S., Pope, G.A., Sharma, M.M., Baran Jr., J.R., 2009. Development of a Successful Chemical Treatment for Gas Wells with Liquid Blocking. Paper SPE-

124977, SPE Annual Technical Conference and Exhibition, New Orleans, Louisiana, 4–7 October. .
Barenblatt, G.I., Entov, V.M., Ryzhik, V.M., 1990. Theory of Fluid Flows through Natural Rocks. Kluwer Academic Publishers, Dordrecht.
Bazin, B., Peysson, Y., Lamy, F., Martin, F., Aubry, E., Chapuis, C., 2010. In-situ water-blocking measurements and interpretation related to fracturing operations in tight gas reservoirs. SPE Prod. Oper. 25 (4), 431–437.
Bedrikovetsky, P.G., 1993. Mathematical Theory of Oil & Gas Recovery (With Applications to Ex-USSR Oil & Gas Condensate Fields). Kluwer Academic Publishers, London.
Berman, L., Mirotchnik, K., 2005. Enhancement of productivity in oil and gas-condensate wells by the artificial alteration of wettability. J. Can. Petrol. Technol. 44 (11), 15–19.
Bradford, S.A., Abriola, L.M., Leij, F.J., 1997. Wettability effects on two-and three-fluid relative permeabilities. J. Contam. Hydrol. 28 (1), 171–191.
Brooks, R.H., Corey, A.T., 1964. Hydraulic Properties of Porous Media. Hydrology Papers No. 3. Colorado State University, Fort Collins.
Bryant, E., Bowman, R., Buckley, J., 2006. Wetting alteration of mica surfaces with polyethoxylated amine surfactants. J. Petrol. Sci. Eng. 52 (1), 244–252.
Buschbach, T.C., Bond, D.C., 1973. Underground storage of natural gas in Illinois. Ill. petrol. 101.
Butler, M., Trueblood, J.B., Pope, G.A., Sharma, M.M., Baran Jr., J.R., Johnson, D., 2009. A Field Demonstration of a New Chemical Stimulation Treatment for Fluid-blocked Gas Wells. Paper SPE-125077, Presented at the SPE Annual Technical Conference and Exhibition. New Orleans, Louisiana, 4–7 October. .
Chaouche, M., Rakotomalala, N., Salin, D., Yortsos, Y., 1993. Capillary effects in immiscible flows in heterogeneous porous media. Europhys. Lett. 21 (1), 19–24.
Chen, D., Shi, J.Q., Durucan, S., Korre, A., 2014. Gas and water relative permeability in different coals: model match and new insights. Int. J. Coal Geol. 122, 37–49.
Coleman, T.F., Li, Y., 1996. An interior, trust region approach for nonlinear minimization subject to bounds. SIAM J. Optim. 6, 418–445.
Desbarats, A.J., 1995. Upscaling capillary pressure-saturation curves in heterogeneous porous media. Water Resour. Res. 31 (2), 281–288.
Economides, M.J., Nolte, K.G., 2000. Reservoir Stimulation, third ed. John Wiley & Sons, West Sussex, England.
Economides, M.J., Hill, A.D., Ehlig-Economides, C., Zhu, D., 2012. Petroleum Production Systems. Pearson Education, Upper Saddle River, NJ.
Esmaeilzadeh, P., Sadeghi, M.T., Fakhroueian, Z., Bahramian, A., Norouzbeigi, R., 2015. Wettability alteration of carbonate rocks from liquid-wetting to ultra gas-wetting using TiO_2, SiO_2 and CNT nanofluids containing fluorochemicals, for enhanced gas recovery. J. Nat. Gas Sci. Eng. 26, 1294–1305.
Giraldo, J., Benjumea, P., Lopera, S., Cortés, F.B., Ruiz, M.A., 2013. Wettability alteration of sandstone cores by alumina-based nanofluids. Energy & Fuels 27 (7), 3659–3665.
Jones, F.O., Owens, W.W., 1980. A laboratory study of low-permeability gas sands. J. Petrol. Technol. 32 (9), 1631–1640.
Ju, B., Fan, T., 2009. Experimental study and mathematical model of nanoparticle transport in porous media. Powder Technol. 192 (2), 195–202.
Ju, B., Fan, T., 2013. Experimental study on nanoparticles transport and its effects on two-phase flow behavior in porous networks. Part. Sci. Technol. 31 (2), 114–118.
Karimi, A., Fakhroueian, Z., Bahramian, A., Pour Khiabani, N., Darabad, J.B., Azin, R., Arya, S., 2012. Wettability alteration in carbonates using zirconium oxide nanofluids: EOR implications. Energy & Fuels 26 (2), 1028–1036.
Kathel, P., Mohanty, K.K., 2013. Wettability alteration in a tight oil reservoir. Energy & Fuels 27 (11), 6460–6468.
Klopfenstein, R.W., 1971. Numerical differentiation formulas for stiff systems of ordinary differential equations. RCA (Radio Corp. Am. Rev. 32 (3), 447–462.
Kumar, K., Dao, E.K., Mohanty, K.K., 2008. Atomic force microscopy study of wettability alteration by surfactants. SPE J. 13 (2), 137–145.
Li, K., Liu, Y., 2008. Production Enhancement in Gas-condensate Reservoirs by Altering Wettability to Gas Wetness: Field Application. Paper SPE-112750, Presented at the SPE Symposium on Improved Oil Recovery. Tulsa, Oklahoma, USA, 20–23 April. .
Li, S., Torsaeter, O., 2015. The Impact of Nanoparticles Adsorption and Transport on Wettability Alteration of Intermediate Wet Berea Sandstone. Paper SPE-172943, Presented at the SPE Middle East Unconventional Resources Conference and Exhibition, Muscat, Oman, 26–28 January. .
Liu, X., Luo, P., Kang, Y., You, L., 2015. Mechanisms of wetting modification by fluoride to mitigate phase trapping. J. Nat. Gas Sci. Eng. 26, 494–501.
Mahadevan, J., Sharma, M.M., 2005. Factors affecting clean-up of water-blocks: a laboratory investigation. SPE J. 10 (3), 238–246.
Mays, D.C., Hunt, J.R., 2005. Hydrodynamic aspects of particle clogging in porous media. Environ. Sci. Technol. 39 (2), 577–584.
Mays, D.C., Hunt, J.R., 2007. Hydrodynamic and chemical factors in clogging by montmorillonite in porous media. Environ. Sci. Technol. 41 (16), 5666–5671.
Morsy, S., Gomaa, A., Sheng, J., 2014. Improvement of Mancos Shale Oil Recovery by Wettability Alteration and Mineral Dissolution. Paper SPE-169033, Presented at the SPE Improved Oil Recovery Symposium, Tulsa, Oklahoma, 12–16 April. .
Mualem, Y., 1976. A new model for predicting the hydraulic conductivity of unsaturated porous media. Water Resour. Res. 12 (3), 513–522.
Naik, S., You, Z., Bedrikovetsky, P., 2015. Rate enhancement in unconventional gas reservoirs by wettability alteration. J. Nat. Gas Sci. Eng. 26, 1573–1584.
O'Carroll, D.M., Abriola, L.M., Polityka, C.A., Bradford, S.A., Demond, A.H., 2005. Prediction of two-phase capillary pressure–saturation relationships in fractional wettability systems. J. Contam. Hydrol. 77 (4), 247–270.
Parekh, B., Sharma, M.M., 2004. Cleanup of Water Blocks in Depleted Low-permeability Reservoirs. Paper SPE-89837, Presented at the SPE Annual Technical Conference and Exhibition, Houston, Texas, 26–29 September. .
Pini, R., Benson, S.M., 2013. Simultaneous determination of capillary pressure and relative permeability curves from core-flooding experiments with various fluid pairs. Water Resour. Res. 49 (6), 3516–3530.
Restrepo, A., Ocampo, A., Rendon, N., Arenas, M., Osorio, R., Reyes, D., 2012. Wettability Modifier Field Trial in a Sandstone Condensate System: Facts and Gaps of a Promising Technology. Paper SPE-152310, Presented at the SPE Latin America and Caribbean Petroleum Engineering Conference, Mexico City, Mexico, 16–18 April. .
Roustaei, A., Moghadasi, J., Bagherzadeh, H., Shahrabadi, A., 2012. An Experimental Investigation of Polysilicon Nanoparticles' Recovery Efficiencies through Changes in Interfacial Tension and Wettability Alteration. Paper SPE-156976, presented at the SPE International Oilfield Nanotechnology Conference, Noordwijk, The Netherlands, 12–14 June 2012. .
Sheydaeemehr, M., Sedaeesola, B., Vatani, A., 2014. Gas-condensate production improvement using wettability alteration: a giant gas condensate field case study. J. Nat. Gas Sci. Eng. 21, 201–208.
Shi, J.Q., Xue, Z., Durucan, S., 2011. Supercritical CO_2 core flooding and imbibition in Tako sandstone-Influence of sub-core scale heterogeneity. Int. J. Greenh. Gas Control 5 (1), 75–87.
Thungsuntonkhun, W., Engler, T.W., 2004. Applying NMR-hydraulic Flow Unit Technique to Estimate J-function and Capillary Pressure. Paper SPWLA-2004-EE, Presented at the SPWLA 45th Annual Logging Symposium, Noordwijk, Netherlands, 6–9 June. .
Torres, D.E., Sharma, M.M., Pope, G.A., Ahmadi, M., McCulley, C.A., Linnemeyer, H., Gilani, S.F., 2010. A Novel Chemical Treatment to Enhance Productivity of Volatile Oil Wells. Paper SPE-138124, Presented at the Canadian Unconventional Resources and International Petroleum Conference, Calgary, Alberta, Canada, 19–21 October. .
Van Duijn, C.J., Molenaar, J., De Neef, M.J., 1995. The effect of capillary forces on immiscible two-phase flow in heterogeneous porous media. Transp. Porous Media 21 (1), 71–93.
Van Golf-Racht, T.D., 1996. Naturally-fractured carbonate reservoirs. Dev. Petrol. Sci. 44, 683–771.
Van Lingen, P.P., Bruining, J., Van Kruijsdijk, C.P.J.W., 1996. Capillary entrapment caused by small-scale wettability heterogeneities. SPE Reserv. Eng. 11 (2), 93–100.
Weiss, W.W., Xie, X., 2009. Field Test of Wettability Alteration to Increase the Flow Rate from Aquifer Gas Storage Wells. Paper SPE-125867, Presented at the SPE Eastern Regional Meeting, Charleston, West Virginia, USA, 23–25 September. .
Weiss, W.W., Xie, X., Weiss, J., Subramanian, V., Taylor, A.R., Edens, F.J., 2006. Artificial intelligence used to evaluate 23 single-well surfactant-soak treatments. SPE Reserv. Eval. Eng. 9 (3), 209–216.
Xie, X., Liu, Y., Sharma, M., Weiss, W.W., 2009. Wettability alteration to increase deliverability of gas production wells. J. Nat. Gas Sci. Eng. 1 (1), 39–45.
Yortsos, Y.C., Chang, J., 1990. Capillary effects in steady-state flow in heterogeneous cores. Transp. Porous Media 5 (4), 399–420.

Statement of Authorship

Title of Paper	Well productivity enhancement by applying nanofluids for wettability alteration.
Publication Status	☑ Published ☐ Accepted for Publication ☐ Submitted for Publication ☐ Unpublished and Unsubmitted work written in manuscript style
Publication Details	Naik, S., Malgaresi, G., You, Z. and Bedrikovetsky, P., 2018. Well productivity enhancement by applying nanofluids for wettability alteration. The APPEA Journal, 58(1), pp.121-129.

Principal Author

Name of Principal Author (Candidate)	Saurabh Naik		
Contribution to the Paper	Problem formulation, literature review, development of mathematical model, Implementation of mathematical solution in Mat-lab, creating figures, analysis of results, writing the manuscript		
Overall percentage (%)	90%		
Certification:	This paper reports on original research I conducted during the period of my Higher Degree by Research candidature and is not subject to any obligations or contractual agreements with a third party that would constrain its inclusion in this thesis. I am the primary author of this paper.		
Signature		Date	05/08/2019

Co-Author Contributions

By signing the Statement of Authorship, each author certifies that:

i. the candidate's stated contribution to the publication is accurate (as detailed above);

ii. permission is granted for the candidate in include the publication in the thesis; and

iii. the sum of all co-author contributions is equal to 100% less the candidate's stated contribution.

Name of Co-Author	Gabriel Malgaresi		
Contribution to the Paper	Support on literature review		
Signature		Date	30/07/19.

Name of Co-Author	Zhenjiang You		
Contribution to the Paper	Reviewing manuscript		
Signature		Date	29/7/19

Name of Co-Author	Pavel Bedrikovetsky
Contribution to the Paper	Reviewing manuscript
Signature	

Date	30/07/2019

Please cut and paste additional co-author panels here.

The APPEA Journal 2018, **58**, 121–129
https://doi.org/10.1071/AJ17149

Peer reviewed paper

Well productivity enhancement by applying nanofluids for wettability alteration

Saurabh Naik[A,B], *Gabriel Malgaresi*[A], *Zhenjiang You*[A] *and Pavel Bedrikovetsky*[A]

[A]Australian School of Petroleum, The University of Adelaide, Adelaide, SA 5005, Australia.
[B]Corresponding author. Email: Saurabh.Naik@adelaide.edu.au

Abstract. Water blocking is a frequent cause for gas productivity decline in unconventional and conventional fields. It is a result of the capillary end effect near the wellbore vicinity. It creates significant formation damage and decreases gas well productivity. The alteration of the rock wettability by nanofluids is an effective way to reduce water blockage and enhance gas production. Presently, several types of surfactants and nanofluids are used in the industry for contact angle alteration. In this study, we developed an analytical model and analysed the sensitivity to several parameters.

After the treatment, the porous medium in the well vicinity (or along the core) will have a stepwise constant contact angle profile. We derive analytical models for compressible steady-state two-phase linear and axi-symmetric flows, accounting for the piecewise-constant contact angle and contact-angle-dependent capillary pressure and relative permeability. The modelling reveals a complex interplay between the competing effects of compressibility, viscous and capillary forces, which influence the optimal contact angle for treatment.

The optimal contact angle for treatment will depend on the initial wettability of the formation, the water cut and the capillary-viscous ratio.

Keywords: contact angle, gas production, Nanofluids, Nanoparticles, Productivity Index, two-phase flow, wettability.

Received 17 December 2017, accepted 19 January 2018, published online 28 May 2018

Introduction

Two-phase steady flow in porous media is an important process that occurs during production of many petroleum reservoirs. During two-phase immiscible flow, capillary pressure affects the fluid distribution among the pore throats. The capillary pressure approaches very low values where the reservoir rock meets the wellbore or fracture face. This effect is known as the capillary end effect (CEE), and is frequently observed during core flood tests (Huang and Honarpour 1998). In low permeable reservoirs, the CEE is more dramatic and can cause water saturation to rise dramatically, severely reducing gas production (Naik *et al.* 2015, 2018). To avoid these issues in common to low permeability reservoirs, technology has been developed to alter wettability, which is one of the most effective ways to modify capillary forces and reduce capillary blocking (Penny *et al.* 1983).

A new method for wettability alteration is the application of nanotechnology. This new technology uses particles, or any materials of nanoscale, characterised by their large surface area with different structures, composition, functional groups on the surface, charges and other singular characteristics (Mohanraj and Chen 2006).

The effect of nanofluid on enhanced oil recovery (EOR) is explained by numerous authors as wettability alteration (Kong and Ohadi 2010; Mcelfresh *et al.* 2012; Torsater *et al.* 2012; Skauge *et al.* 2010). However, wettability alteration is explained by different mechanisms in the literature. One of the mechanisms proposed is the reduction in interfacial tension (IFT), where the nanoparticles adsorb on the oil/water interface, changing the energy between the two fluids and consequently altering the wettability (Hendraningrat and Torsæter 2014; Nwidee *et al.* 2016; Al-Anssari *et al.* 2016). Another mechanism proposed is the wedge effect, where the nanoparticles spread around the three-phase contact (solid/water/oil) and changes the contact angle of the surface (Chengara *et al.* 2004; Nikolov and Wasan 2014; Zhang *et al.* 2014).

Our work is motivated by situations in which gas is being produced with water from a porous medium with constant or piecewise-constant contact angle. This situation could arise during production from gas reservoir with nanoparticle

application near the wellbore or fracture face. The effect of piecewise-constant contact angle can have similar effects on capillary pressure as piecewise-constant permeability.

Yortsos and Chang (1990) investigated steady-state two-phase flows with sharp and smooth permeability change in porous media, where the capillary pressure is inversely proportional to permeability. The saturation fluctuation becomes larger with the sharper change in permeability. Van Duijn *et al*. (1995) and Van Lingen *et al.* (1996) observed that the viscosity, flow rate and interfacial parameters were essential for determining the saturation profile in rocks with piecewise permeability and porosity.

While piecewise permeability helps explain the effect of altering the capillary pressure curve in the near wellbore region, it does not allow us to fully explore what occurs under piecewise wettability. Contact angle alteration will also affect relative permeability relationship and this may be very consequential to productivity.

Mathematical models, including governing equations, boundary conditions and steady-state solutions, are presented. Sensitivity of piecewise-constant macroscopic contact angle to capillary-viscous ratio and altered fraction are investigated in *Results and analysis*. Limitations of the model are discussed, and finally, conclusions are drawn.

Mathematical model

Linear flow

The mass fluxes for water q_w and gas q_g during two-phase water-gas flow are described by Darcy's law as:

$$q_w = k\frac{k_{rw}(s,\theta)}{\mu_w}\rho_w\frac{dp_w}{dx} \tag{1}$$

$$q_g = kk_{kg}(p_g)\frac{k_{rg}(s,\theta)}{\mu_g}\rho_g(p_g)\frac{dp_g}{dx} \tag{2}$$

where the subscripts w and g refer to water and gas, respectively; k is permeability, s is water saturation, θ is the contact angle, k_{kg} is the Klinkenberg coefficient, k_r is the relative permeability, μ is the viscosity, ρ is the density p is pressure and x is distance from fracture face. The real gas equation is used to calculate gas density:

$$\rho_g = \frac{p_g M}{z(p_g)R_c T} \tag{3}$$

where M is the molar mass, R_c is the universal gas constant, T is the temperature and z is the compressibility factor.

The capillary pressure p_c is the difference between the gas pressure and the water pressure. It is also expressed via the dimensionless J-function as:

$$p_c = p_g - p_w = \frac{\sigma}{\sqrt{k/\phi}}J(s,\theta) \tag{4}$$

where σ refers to the IFT and ϕ to the rock porosity. The forms of relative permeability and capillary pressure are presented in Appendix 1.

If we consider steady-state flow, we can introduce a constant for the ratio of total mass flux that water contributes to:

$$Q_w = \frac{q_w}{q_g + q_w}, 1 - Q_w = \frac{q_g}{q_g + q_w} \tag{5}$$

Let us also introduce the following dimensionless variables for pressure, length, capillarity and viscosity:

$$\begin{aligned} P_g &= \frac{k\rho_w}{(q_g + q_w)\mu_w L}p_g, P_w = \frac{k\rho_w}{(q_g + q_w)\mu_w L}p_w, \\ X &= \frac{x}{L}, D(p_g) = \frac{\rho_g(p_g)\mu_w}{\rho_w\mu_g}, \varepsilon = \frac{\sigma\rho_w\sqrt{k\phi}}{(q_g + q_w)\mu_w L} \end{aligned} \tag{6}$$

where P refers to the dimensionless pressure, X to the dimensionless length and D to the density-viscosity ratio. The constant ε is the dimensionless ratio between the reference capillary pressure and pressure drop and is called the capillary-viscous ratio. L is the length scale over which the solution is investigated.

Substituting the dimensionless variables from Eqns 5 and 6 into Eqns 1, 2 and 4 gives us:

$$Q_w = k_{rw}(s,\theta)\frac{dP_w}{dX} \tag{7}$$

$$1 - Q_w = k_{kg}(P_g)k_{rg}(s,\theta)D(P_g)\frac{dP_g}{dX} \tag{8}$$

$$P_g - P_w = \varepsilon J(s,\theta) \tag{9}$$

The pressure gradient for gas is expressed as:

$$\frac{dP_g}{dX} = \frac{1 - Q_w}{k_{kg}(P_g)k_{rg}(s,\theta)D(P_g)} \tag{10}$$

Expressing pressure gradient in water from Eqn 7, subtracting the result from Eqn 10 and accounting for Eqn 9 will give us:

$$\frac{ds}{dX} = \left(\frac{1 - Q_w}{k_{kg}(P_g)k_{rg}(s,\theta)D(P_g)} - \frac{Q_w}{k_{rw}(s,\theta)}\right)\left(\varepsilon\frac{dJ(s,\theta)}{ds}\right)^{-1} \tag{11}$$

We assume that the capillary pressure equals zero at $X=0$, which can represent the hydraulic fracture face or the core outlet:

$$X = 0: \; s = s_0, \; J(s_0) = 0, \; P_g = P_0 \tag{12}$$

The steady-state profiles for s and P_g for one-dimensional steady-state water-gas flow are determined by the system of two ordinary differential Eqns (10, 11) subject to the Cauchy conditions (Eqn 12).

The system is solved numerically using implicit numerical differentiation formulae with quasi-constant step size implemented in Matlab (Shampine and Reichelt 1997).

To estimate the effects of nanofluid treatment, we consider a piecewise-constant contact angle profile, where the initial contact angle θ_2 has been changed to θ_1 in the neighbourhood close to the hydraulic fracture:

$$\theta = \begin{cases} \theta_1, & 0 < X < \beta \\ \theta_2, & \beta < X < 1 \end{cases} \tag{13}$$

where β is the depth of treatment over L. Fig. 1 shows the schematic for this case. At this discontinuity in contact angle, there must be continuity of both water and gas pressures:

$$X = \beta : P_g^- = P_g^+, P_w^- = P_w^+ \tag{14}$$

where the negative '–' and positive '+' signs correspond to downstream and upstream of the discontinuity at $X=\beta$, respectively.

The solution for P_g allows calculation of the dimensionless productivity indexes (PIs) for water and gas as:

$$PI_w = \frac{Q_w}{\Delta P_w}, PI_g = \frac{1 - Q_w}{\Delta P_g} \tag{15}$$

Radial flow

The system of Eqns 10 and 11 can be easily converted from linear to axi-symmetric radial flow, which can describe radial flow to a wellbore. To do this, the coordinate X is replaced with $\ln(R)$, where R is the distance from wellbore r, over the drainage area r_e:

$$R = \frac{r}{r_e} \tag{16}$$

The pressure gradient for gas is then expressed as:

$$\frac{dP_{gr}}{d\ln R} = \frac{1 - Q_w}{k_{kg}(P_{gr}) k_{rg}(s,\theta) D(P_{gr})} \tag{17}$$

The saturation gradient is expressed as:

$$\frac{ds}{d\ln R} = \left(\frac{1 - Q_w}{k_{kg}(P_{gr}) k_{rg}(s,\theta) D(P_{gr})} - \frac{Q_w}{k_{rw}(s,\theta)} \right) \left(\varepsilon_r \frac{dJ(s,\theta)}{ds} \right)^{-1} \tag{18}$$

The dimensionless constants for radial case are:

$$P_{gr} = \frac{2\pi k \rho_w}{(q_w + q_g)\mu_w} p_g, \; P_{wr} = \frac{2\pi k \rho_w}{(q_w + q_g)\mu_w} p_w, \quad \varepsilon_r = \frac{2\pi\sigma\rho_w\sqrt{k\phi}}{(q_w + q_g)\mu_w} \tag{19}$$

The boundary conditions are set at the wellbore instead:

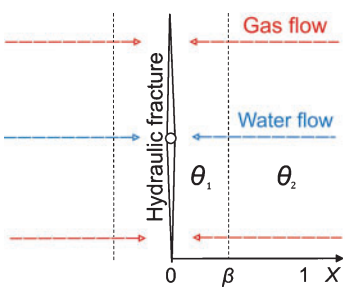

Fig. 1. Schematic figure of flow into hydraulic fracture. The rock has contact angle θ_2, which is altered in the near fracture face zone (from $\times = 0$ to $\times = \beta$) to θ_1.

$$R = \frac{r_w}{r_e}: \; s = s_0, \; J(s_0) = 0, \; P_{gr} = P_0 \tag{20}$$

The saturation and pressure profiles versus natural logarithm of radius during well inflow have the same forms as those for linear flow case.

Field case

The PI for the field case can be estimated by:

$$PI = \frac{q_g}{\rho_g(p_{sc}) 2\pi k h} \frac{1}{\int_{p_{rw}}^{p_{re}} \frac{\rho_g(p_g)}{\mu_g(p_g)} dp_g} \tag{21}$$

where the subscript *sc* stands for surface conditions, *rw* stands for wellbore *re* stands for the drainage area and *h* stands for height of reservoir. For the model dimensionless PI for a well is calculated by:

$$PI = \frac{1}{S_a + S_{wb}} \tag{22}$$

where S_a is a constant and S_{wb} is a skin due to a water block. The constant S_a accounts for drainage area and other skins, which are assumed to be constant. The water block skin is calculated from assuming linear flow in the near fracture face region. The skin results from the relative permeability reduction due to water build up:

$$S_{wb} = \frac{\pi}{2x_f} \left[\int_0^1 \frac{1}{k_{rg}(s_d(X),\theta)} - \frac{1}{k_{rg}(s_{ud}(X),\theta)} dX \right] \tag{23}$$

where x_f stands for fracture half-length, the subscript *d* stands for damaged case (case accounting for CEE) and subscript *ud* stands for undamaged case (case not accounting for CEE).

Results and analysis

The adjustment of wettability has two effects on productivity of the fluid. For example, with hydrophilic rocks, increase in contact angle will reduce the saturation near the fracture face dues to end effects, positively impacting gas productivity. However, as gas will begin to imbibe into smaller pores, it will also reduce the relative permeability function to gas. This negatively impacts gas productivity. The result of these two competitive effects is that contact angle needs to be optimised to maximise the PI.

For the analysis required, we investigated a case where $\varepsilon = 1$, $k = 1$ mD, $\phi = 0.1$, $Q_w = 0.05$ and $\beta = 0.3$. The *J*-function coefficient $C = 0.1$, *J*-function exponent $\alpha = 0.6$, and the relative permeability tortuosity index $\eta = 2$. Flow is presented from right to left with $X = 0$ representing the fracture face and $X = 1$ the boundary for investigation.

Fig. 2*a* shows the steady-state saturation profiles for a hydrophilic rock with contact angle altered in the near fracture face region. The blue curve indicates the case for no contact angle alteration. Very close to the fracture face ($X = 0$), saturation quickly rises because of the CEE. The capillary pressures in the fracture are zero, and the continuity in capillary pressure causes the capillary pressure in the near fracture face region to be close to or equal to zero. When this

happens, the pressure of the gas phase is not large enough to overcome the capillary forces, which favour the water phase, and the water saturation rises.

The red curve indicates when the contact angle has increased to 90°. The water saturation at $X=0$ is determined by the capillary pressure curve, and the water saturation further from the fracture face is determined by the mobilities and the ratio of gas and water fluxes. As the capillary pressure in the near fracture face region is reduced close to zero, the boundary at $X=\beta$ will behave similar to the fracture face when there was no contact angle alteration. Capillary pressure continuity causes a discontinuity in the saturation profile. For this case there is a small jump in saturation.

The yellow curve indicates when the contact angle is completely altered to 180°. At this contact angle, the capillary forces favour the gas phase, so at the fracture face, the gas phase saturation will rise. However, capillary pressure continuity must exist at the boundary between the unaltered and the altered zone. In this instance the capillary pressure is a negative value, and the effect on saturation profile is even stronger than that when the contact angle was altered to 90°. The jump in saturation is much larger.

Fig. 2*b* shows the dimensionless pressure drop. The blue curve shows the highest gradient at $X=0$. The water saturation at this point is close to $1-s_{gr}$, so the gas relative permeability is close to zero. This causes a very large pressure gradient at the point $X=0$. Further from the fracture face, the pressure gradient decreases as the saturation reduces.

When the contact angle is increased, the gradient at $X=0$ decreases as the saturation decreases. When the contact angle is increased to 180° the pressure gradient at $X=0$ is the lowest.

Away from the fracture face, the dimensionless pressure gradient is determined by the mobilities and the ratio of phase fluxes. For the case with complete alteration, the effect of the second water barrier is seen by a sharp rise in dimension less pressure at $X=\beta$. Despite the reduction of pressure gradient in the near wellbore zone, the second boundary effect can negate the pressure gradient decrease. This can make the treatment strategy suboptimal.

For this case, the dimensionless pressure drop for the neutral contact angle of 90° is the lowest, meaning it is the optimal contact angle.

Fig. 3*a* shows saturation profiles for hydrophobic rocks with contact angle altered in the near wellbore region. The yellow curve indicates the case for no contact angle alteration. When contact angle is reduced, capillary pressure in the altered region increases. At the boundary $X=\beta$, the capillary pressure continuity causes the saturation to drop in the hydrophobic section of the rock.

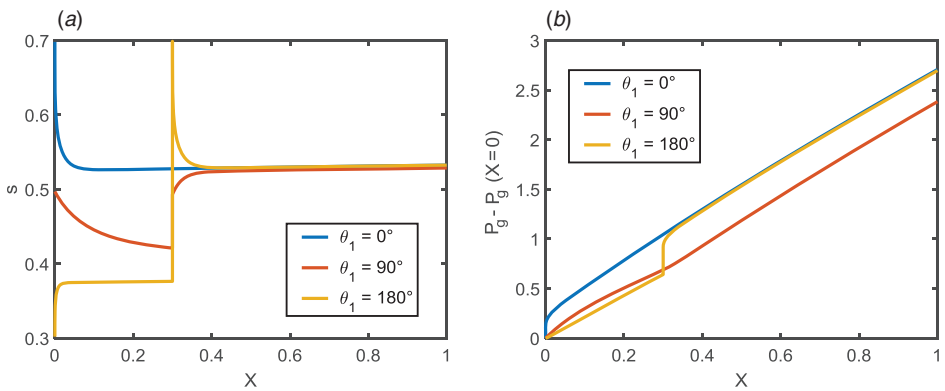

Fig. 2. (*a*) Saturation and (*b*) pressure versus depth for a hydrophilic rock with piecewise alteration. The blue curve indicates that the near fracture zone contact angle has been altered to 0°, the red curve indicates it has been altered to 90° and the yellow curve that it has been altered to 180°.

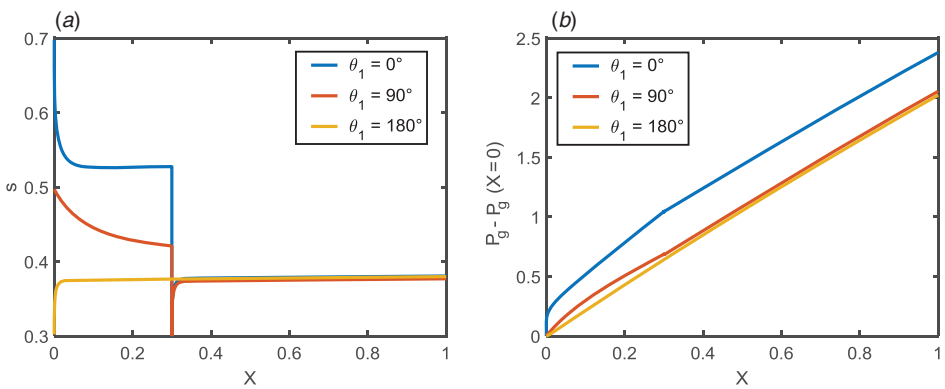

Fig. 3. (*a*) Saturation and (*b*) pressure versus depth for a hydrophobic rock with piecewise alteration. The blue curve indicates that the near fracture zone contact angle has been altered to 0°, the red curve indicates it has been altered to 90° and the yellow curve that it has been altered to 180°.

Fig. 3*b* shows the dimensionless pressures for this case. When the contact angle is reduced, the pressure gradient increases at $X=0$ due to the CEE. However, the second end effect does not induce a sharp increase in the pressure gradient like in the hydrophilic reservoir. This is due to the saturation decreasing rather than increasing at the boundary. The yellow curve for the hydrophobic rock has the lowest pressure drop, indicating that contact angle alteration may not improve recovery.

The effect on dimensionless PI is shown in Fig. 4 and Fig. 5. Fig. 4*a* shows PI for hydrophilic rock with contact angle altered near to the fracture face. For gas productivity the optimal contact angle is shown to be close to 90°.

Low capillary-viscous ratios correspond to lower IFT, higher viscosities or higher fluid velocities. In this regime, the impact the end effects have on production is lower, so the altering contact angle shows less improvement in PI.

Higher capillary-viscous ratios correspond to higher IFT, lower viscosities and lower fluid velocities. In this regime, the CEEs have more impact on PI. The negative impact of completely altering the contact angle is much higher and the positive impact of altering contact angle to the optimal is higher.

Fig. 4*b* shows the PI for hydrophobic rocks. The blue curve indicates the case for low capillary-viscous ratios. The optimal contact angle exists at low capillary-viscous ratios; here it is close to 90°.

The yellow curve indicates the case for high capillary-viscous ratios. At high capillary-viscous ratios, the optimal contact angle is closer to 180°. The end effects are larger at high capillary-viscous ratios, and in this instance, the CEE increases the water saturation at $X=0$. This ultimately causes contact angle reduction to increase dimensionless pressure drop.

As the saturation and pressure gradients further away from the fracture face will be determined by the water gas flux ratios, it is reasonable to assume that the water cut will impact the PI and the optimal contact angle.

Fig. 5*a* shows PI for hydrophilic rocks with sensitivity to water cut by mass Q_w. The blue curve indicates the case for when half the mass produced is water. When water production is this high, the water saturation in the reservoir is also very high. At contact angle of 90° the PI is at its highest.

At lower water cuts, such as the case for the red and yellow curves, the optimal contact angle shifts closer to 180°. When water cut approaches zero, the saturation determined away from the fracture face approaches zero, so the pressure gradient away from the end effect region is the lowest. The gas phase relative permeability will be at its highest. When this happens, reducing saturation due to end effects will improve PI. This is done by increasing the contact angle past 90° towards 180°. However, the second end effect at $X=\beta$ will cause the optimal contact angle to be slightly less than 180°.

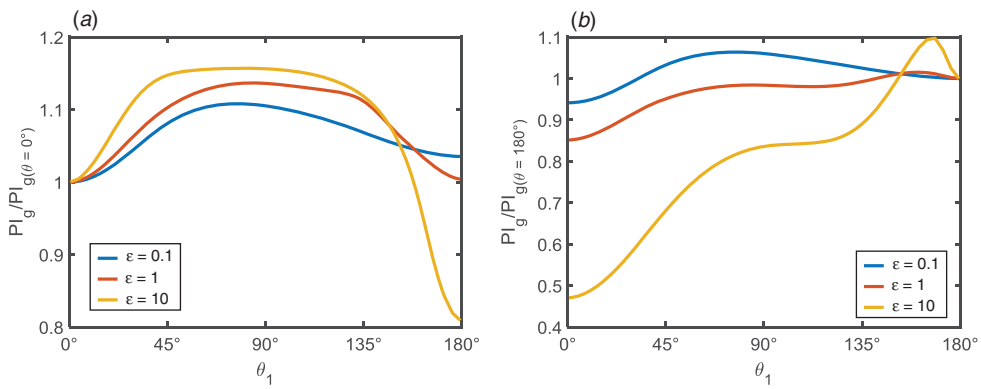

Fig. 4. Productivity index (PI) over initial PI plotted against altered contact angle θ_1 for (*a*) water wet and (*b*) gas wet rocks. The blue curve indicates capillary-viscous ratios ε of 0.1, the red curve an ε of 1 and yellow curve an ε of 10.

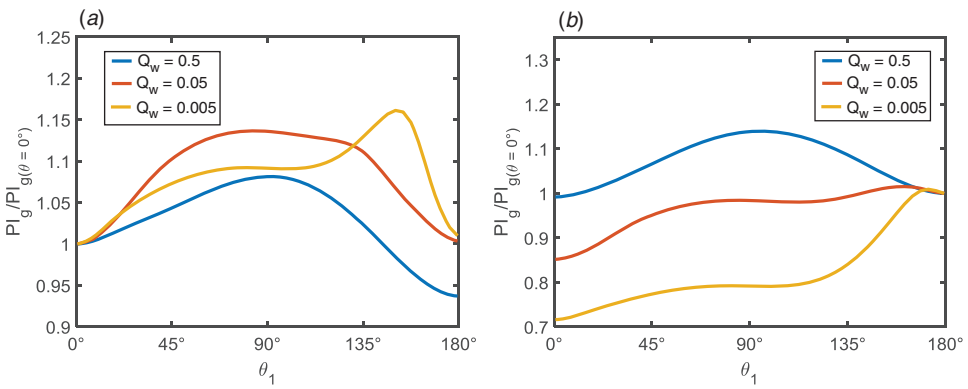

Fig. 5. Productivity index (PI) over initial PI plotted against altered contact angle θ_1 for (*a*) water wet and (*b*) gas wet rocks. The blue curve indicates water cut by mass Q_w of 0.5, the red curve a Q_w of 0.05 and the yellow curve a Q_w of 0.005.

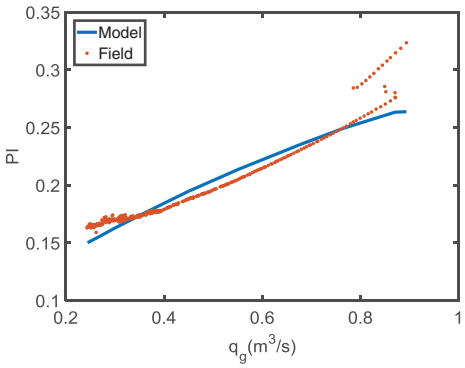

Fig. 6. Productivity index plotted against production rate q_g for a field case.

Fig. 5*b* shows the sensitivity for water for the hydrophobic rock. A similar observation can be made: at high water cuts, the optimal contact angles is near 90° and at lower water cuts the optimal contact angle tends to 180°.

Discussion

The mathematical model presented in this work has been applied to a field case study. Field 'A' (Australia) is a tight gas reservoir. During many years of exploitation, the linear model has been applied for a fractured well in this field. Because the formation damage during leak-off is localised close to the well, the flow in the fractured well vicinity is linear and the flux is directed perpendicular to the plane of fracture.

The reservoir pressure decline is estimated from shut-in periods of the well as wellhead rate and pressure are recorded during the production of the well. The parameters k and h are estimated from the logs. The gas pressure, volume and temperature properties are analysed in the laboratory. The PI for the well can then be calculated using Eqn 21 throughout the well life. The PI decreases as the rate decreases, and this could possibly be explained by water saturation build up. The model was applied to match the data using Eqn 22.

By adjusting parameters S_a, J-function coefficient C, J-function exponent α, relative permeability constant η and contact angle θ can fit this data. The results are $S_a = 1.66$, $C = 0.1$, $\alpha = 0.16$ $\eta = 1.85$ and contact angle $\theta = 0.05°$. Fig. 6 shows the productivity index plotted against the flow rate. During the start of production there is a jump in PI due to non-steady effects, and the model does not account for it.

One of the negative aspects observed in this paper is that a second capillary barrier builds up after the alteration of contact angle. The piecewise-constant contact angle can have similar effects to piecewise-constant permeability. Yortsos and Chang (1990), observed a reduced saturation peak when the sharpness of the heterogeneity is decreased. It is possible that having a gradual change in contact angle as opposed to a sharp discontinuity would reduce the negative aspect of this discontinuity; this, however, was not investigated in this paper.

It has been documented in literature that reducing IFT will reduce the residual saturations of both phases and increase the relative permeability for both phases (Chatzis and Morrow 1984); however, this was also not accounted for in this paper. It is likely that the PI improvement for neutral contact angles is underestimated for this reason.

Conclusions

The semi-analytical modelling of steady-state gas-water flow in the rock with piecewise-constant contact angles allows the following conclusions:

- The optimal contact angle for contact angle adjustment in the near fracture face region depends on the wettability of the formation, the water cut and the ratio of capillary and viscous forces.
- For hydrophilic rocks, the optimal contact angle reduces if flow rate is reduced.
- For hydrophobic rocks, the optimal contact angle increases if flow rate is reduced.
- At high flow rates, the optimal contact angle is close to 90° for both hydrophilic and hydrophobic rocks.
- The optimal contact angle reduces with water cut for both hydrophilic and hydrophobic rocks.

Conflicts of interest

No conflicts of interest exist.

Nomenclature

b Klinkenberg factor, Pa
C J-function coefficient
D density-viscosity ratio
g gas-wet fraction of pores
h height of reservoir, m
J J-function
k permeability, m^2
k_{kg} Klinkenberg correction coefficient
k_r relative permeability
L length scale, m
M molar mass, kg/mol
p_c capillary pressure, Pa
p pressure, Pa
P dimensionless pressure
PI dimensionless productivity index
q mass rate (per unit area for linear flow, $kg/m^2 \cdot s$)
(per unit height for radial flow, kg/m·s)
Q_w water cut by mass
r radius, m
r_e drainage radius, m
R dimensionless radius
R_c universal gas constant, 8.3144621 J/Mol K
s water saturation
s_{gr} irreducible gas saturation
s_{wc} connate water saturation
S normalised saturation
T temperature, K
w capillary size, m
x distance from fracture face, m
x_f fracture half-length, m
X dimensionless distance
z compressibility factor

Greek Letters

α *J*-function exponent
β fraction of wettability altered zone
ε capillary-viscous ratio
η tortuosity index
ϕ porosity
φ fraction of pore surface
μ viscosity, Pa s
ρ density, kg/m^3
σ interfacial tension, N/m
θ contact angle
θ_1 altered contact angle
θ_2 initial contact angle

Subscripts

d damaged case
g gas
w water (for density, pressure, productivity index, relative permeability and viscosity) wetting phase (for normalised saturation), well (for radius)
x linear
r radial
re drainage radius
rw wellbore radius
ud undamaged case
0 outlet
∞ inlet

Acknowledgements

Financial support from the Australian Research Council (ARC) Linkage Project (LP150100626) is gratefully acknowledged.

References

Al-Anssari, S., Barifcani, A., Wang, S., and Iglauer, S. (2016). Wettability alteration of oil-wet carbonate by silica nanofluid. *Journal of Colloid and Interface Science* **461**, 435–442. doi:10.1016/j.jcis.2015.09.051

Bradford, S. A., Abriola, L. M., and Leij, F. J. (1997). Wettability effects on two-and three-fluid relative permeabilities. *Journal of Contaminant Hydrology* **28**(1–2), 171–191. doi:10.1016/S0169-7722(97)00024-7

Chatzis, I., and Morrow, N. R. (1984). Correlation of capillary number relationships for sandstone. *Society of Petroleum Engineers Journal* **24**(5), 555–562. doi:10.2118/10114-PA

Chengara, A., Nikolov, A. D., Wasan, D. T., Trokhymchuk, A., and Henderson, D. (2004). Spreading of nanofluids driven by the structural disjoining pressure gradient. *Journal of Colloid and Interface Science* **280**(1), 192–201. doi:10.1016/j.jcis.2004.07.005

Hendraningrat, L., and Torsæter, O. (2014). Effects of the initial rock wettability on silica-based nanofluid-enhanced oil recovery processes at reservoir temperatures. *Energy & Fuels* **28**(10), 6228–6241. doi:10.1021/ef5014049

Huang, D. D., and Honarpour, M. M. (1998). Capillary end effects in coreflood calculations. *Journal of Petroleum Science Engineering* **19**(1–2), 103–117. doi:10.1016/S0920-4105(97)00040-5

Jones, F. O., and Owens, W. W. (1980). A laboratory study of low-permeability gas sands. *Journal of Petroleum Technology* **32**(9), 1631–1640. doi:10.2118/7551-PA

Kong, X., and Ohadi, M. (2010). Applications of micro and nano technologies in the oil and gas industry-overview of the recent progress. In 'Abu Dhabi international petroleum exhibition and conference, Abu Dhabi, UAE, 1–4 November 2010'. (Society of Petroleum Engineers).

McElfresh, P. M., Holcomb, D. L., and Ector, D. (2012). Application of nanofluid technology to improve recovery in oil and gas wells. In 'SPE International Oilfield Nanotechnology Conference and Exhibitionn, Noordwijk, The Netherlands, 12–14 June 2012'. (Society of Petroleum Engineers).

Mohanraj, V. J., and Chen, Y. (2006). Nanoparticles-a review. *Tropical Journal of Pharmaceutical Research* **5**(1), 561–573.

Naik, S., You, Z., and Bedrikovetsky, P. (2015). Rate enhancement in unconventional gas reservoirs by wettability alteration. *Journal of Natural Gas Science and Engineering* **26**, 1573–1584. doi:10.1016/j.jngse.2015.06.016

Naik, S., You, Z., and Bedrikovetsky, P. (2018). Productivity index enhancement by wettability alteration in two-phase compressible flows. *Journal of Natural Gas Science and Engineering* **50**, 101–114. doi:10.1016/j.jngse.2017.11.007

Nikolov, A., and Wasan, D. (2014). Wetting–dewetting films: The role of structural forces. *Advances in Colloid and Interface Science* **206**, 207–221. doi:10.1016/j.cis.2013.08.005

Nwidee, L., Al-Anssari, S., Barifcani, A., Sarmadivaleh, M., and Iglauer, S. (2016). Nanofluids for enhanced oil recovery processes: wettability alteration using zirconium oxide. In 'Offshore Technology Conference Asia, Kuala Lumpur, Malaysia, 22–25 March 2016'. (Offshore Technology Conference.)

O'Carroll, D. M., Abriola, L. M., Polityka, C. A., Bradford, S. A., and Demond, A. H. (2005). Prediction of two-phase capillary pressure–saturation relationships in fractional wettability systems. *Journal of Contaminant Hydrology* **77**(4), 247–270. doi:10.1016/j.jconhyd.2005.01.004

Penny, G. S., Thomas, B. D., and Soliman, M. Y. (1983). Enhanced Load Water Recovery Technique Improves Stimulation Results in the Appalachian Area. In SPE Eastern Regional Meeting, Champion, Pennsylvania, 9–11 November 1983. Society of Petroleum Engineers.

Shampine, L. F., and Reichelt, M. W. (1997). The matlab ode suite. *SIAM Journal on Scientific Computing* **18**(1), 1–22. doi:10.1137/S1064827594276424

Skauge, T., Spildo, K., and Skauge, A. (2010). Nano-sized particles for EOR. In 'SPE improved oil recovery symposium, Tulsa, Oklahoma, USA, 24–28 April, 2010'. (Society of Petroleum Engineers).

Torsater, O., Engeset, B., Hendraningrat, L., and Suwarno, S. (2012). Improved oil recovery by nanofluids flooding: an experimental study. In 'SPE Kuwait international petroleum conference and exhibition, Kuwait City, Kuwait, 10–12 December 2012'. (Society of Petroleum Engineers).

Van Duijn, C. J., Molenaar, J., and De Neef, M. J. (1995). The effect of capillary forces on immiscible two-phase flow in heterogeneous porous media. *Transport in Porous Media* **21**(1), 71–93. doi:10.1007/BF00615335

Van Lingen, P. P., Bruining, J., and Van Kruijsdijk, C. P. J. W. (1996). Capillary entrapment caused by small-scale wettability heterogeneities. *SPE Reservoir Engineering* **11**(2), 93–100. doi:10.2118/30782-PA

Yortsos, Y. C., and Chang, J. (1990). Capillary effects in steady-state flow in heterogeneous cores. *Transport in Porous Media* **5**(4), 399–420. doi:10.1007/BF01141993

Zhang, H., Nikolov, A., and Wasan, D. (2014). Dewetting film dynamics inside a capillary using a micellar nanofluid. *Langmuir* **30**(31), 9430–9435. doi:10.1021/la502387j

Appendix 1

Following papers by Bradford *et al.* (1997) and O'Carroll *et al.* (2005), we introduce the model for relative permeability and capillary pressure for the capillary bundle model. The normalised water saturation is:

$$S(s) = \frac{s - s_{wc}}{1 - s_{gr} - s_{wc}} \tag{A-1}$$

The capillary pressure is expressed using Leverett's J-function as:

$$P_c(s,\theta) = \frac{\sigma}{\sqrt{k/\phi}} J(s,\theta),\ J(s,\theta) = g(\theta) C S(s)^{-\frac{1}{\alpha}} - g(\theta) C (1 - S(s)^{-\frac{1}{\alpha}}) \tag{A-2}$$

where g is the ratio of hydrophobic to hydrophilic pores and is defined as:

$$g(\theta) = \frac{1}{2}[1 - \cos(\theta)] \tag{A-3}$$

The relative phase permeabilities for water and gas are expressed by the following formulae, respectively:

$$\begin{aligned} k_{rw}(s,\theta) &= (S(s))^{\eta} \frac{[1 - g(\theta)] \int_0^S w^2(S)dS + g(\theta) \int_{1-S}^1 w^2(S)dS}{\int_0^1 w^2(S)dS} \\ k_{rg}(s,\theta) &= (1 - S(s))^{\eta} \frac{g(\theta) \int_0^{1-S} w^2(S)dS + [1 - g(\theta)] \int_S^1 w^2(S)dS}{\int_0^1 w^2(S)dS} \end{aligned} \tag{A-4}$$

where:

$$w(S) = \frac{S^{\frac{1}{\alpha}}}{C} \sqrt{k/\phi} \tag{A-5}$$

The slip effect can affect gas permeability, particularly in the case where permeability or pressure is low, such as in laboratory conditions with rock permeability less than 1 md. The slip effect can be accounted for by multiplying gas permeability with a Klinkenberg correction coefficient k_{kg} (Jones and Owens 1980) as:

$$k_{kg}(p_g) = \left(1 + \frac{b}{p_g}\right),\ b = 0.86 k^{-0.33} \tag{A-6}$$

The functions of capillary pressure (Eqn A-3) and relative permeability (Eqn A-5) contain 7 constants: J-function coefficients C and exponent α, contact angle θ, tortuosity η, residual gas saturation s_{gr}, irreducible water saturation s_{wi} and the ratio of permeability k over porosity ϕ.

The authors

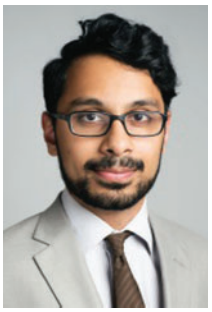

Saurabh Naik is a PhD candidate at the Australian School of Petroleum at the University of Adelaide, Australia. His research interests include wettability alteration in porous media, percolation theory and application of nanoparticles in oil/gas/geothermal reservoirs. Saurabh received his BEng degree in petroleum engineering from the University of Adelaide. Email: Saurabh.Naik@adelaide.edu.au

Gabriel Malgaresi is a PhD candidate at the Australian School of Petroleum at the University of Adelaide, Australia. His research interests include core flooding and nanoparticles application. Gabriel received his BEng degree in chemical engineering from the Federal University of Sergipe and his MSc in petroleum and reservoir engineering from North Fluminense State University. Email: Gabriel.deveigacabralmalgaresi@adelaide.edu.au

Zhenjiang You is a Senior Researcher in the Australian School of Petroleum at the University of Adelaide, Australia. His research interests include suspension/colloid/nanoparticle transport in porous media, fines migration induced formation damage in oil/gas/geothermal reservoirs, EOR from low-salinity waterflooding and flow distribution within gas and oil wells. Dr You received his BEng degree in engineering mechanics and PhD degree in fluid mechanics, both from Zhejiang University. He is the author of three book chapters and over 100 papers in international journals and conferences. Email: zhenjiang.you@adelaide.edu.au

Pavel Bedrikovetsky is a Professor in the Australian School of Petroleum at the University of Adelaide. He is also a Senior Staff consultant to Petrobras in the areas of formation damage, waterflooding and improved oil recovery. During 1991–1994, Bedrikovetsky was a visiting Professor at Delft University of Technology and the Imperial College of Science and Technology. His main research interests include formation damage, suspension/colloid transport in porous media, mathematical modelling of well stimulation and exploitation of unconventional energy resources. Bedrikovetsky is the author of two books on reservoir engineering and 150 technical papers published in international and SPE journals. He holds BEng and MSc degrees in applied mathematics, a PhD degree in fluid mechanics and a DSc degree in reservoir engineering, all from Moscow Gubkin Petroleum University. Bedrikovetsky served as section chairperson, short-course instructor, key speaker and steering committee member at several SPE conferences, and he was the 2008–2009 and 2016–2017 SPE Distinguished Lecturer. Email: Pavel.bedrikovetski@adelaide.edu.au

Statement of Authorship

Title of Paper	Prevention of water-blocking formation damage in gas reservoirs wettability alteration, analytical modelling.
Publication Status	☑ Published ☐ Accepted for Publication ☐ Submitted for Publication ☐ Unpublished and Unsubmitted work written in manuscript style
Publication Details	Naik, S., You, Z. and Bedrikovetsky, P., 2016, October. Prevention of water-blocking formation damage in gas reservoirs wettability alteration, analytical modelling. In SPE Asia Pacific Oil & Gas Conference and Exhibition. Society of Petroleum Engineers.

Principal Author

Name of Principal Author (Candidate)	Saurabh Naik
Contribution to the Paper	creating figures, analysis of results, writing the manuscript
Overall percentage (%)	85%
Certification:	This paper reports on original research I conducted during the period of my Higher Degree by Research candidature and is not subject to any obligations or contractual agreements with a third party that would constrain its inclusion in this thesis. I am the primary author of this paper.
Signature	Date 05/08/2019

Co-Author Contributions

By signing the Statement of Authorship, each author certifies that:

i. the candidate's stated contribution to the publication is accurate (as detailed above);

ii. permission is granted for the candidate in include the publication in the thesis; and

iii. the sum of all co-author contributions is equal to 100% less the candidate's stated contribution.

Name of Co-Author	Zhenjiang You
Contribution to the Paper	reviewing manuscript
Signature	Date 5/8/19

Name of Co-Author	Pavel Bedrikovetsky
Contribution to the Paper	reviewing manuscript
Signature	Date 5/8/19

Please cut and paste additional co-author panels here as required.

SPE-182283-MS

Prevention of Water-Blocking Formation Damage in Gas Reservoirs Wettability Alteration, Analytical Modelling

Saurabh Naik, Zhenjiang You, and Pavel Bedrikovetsky, Australian School of Petroleum, The University of Adelaide

This paper was prepared for presentation at the SPE Asia Pacific Oil & Gas Conference and Exhibition held in Perth, Australia, 25-27 October 2016.

Abstract

Water blocking is a widespread formation damage mechanism in oil and gas reservoirs. The end effect on the well sand-face or fracture results in the creation of a water film which significantly reduces gas permeability. The removal of the water film by changing wettability near to the wellbore or hydraulic fracture is the traditional method of well stimulation. We describe inflow performance by two-phase steady-state flow towards well. The wettability affects the relative permeability and the capillary pressure. Treatment of the well neighbourhood by nanoparticles or surfactants results in a reservoir with non-uniform wettability. We present a steady-state solution for inflow performance and show how the alteration of the contact angle and the treatment depth affects the well productivity index. The model is verified by comparison with coreflood data. The developed analytical model can be used for the prediction of gas well productivity, and for the planning and design of wettability-alteration well-stimulation. The main result of the paper is the existence of the optimal contact angle.

Introduction

The phase distributions near the wellbore during commingled gas-water or oil-water production are determined by the reservoir rock wettability. In particular, for water-wet rocks, the capillary end effect creates a water film in the wellbore neighbourhood, which reduces the gas or oil saturation towards its residual value. This water film enhances the hydraulic resistance to the flow of gas or oil and is called water blocking. For hydrophobic rocks, the water saturation at the wellbore is equal to the irreducible water saturation, thus, water blocking does not occur. The well skin factor is the total of skin created from drilling, completion, fracturing fluid loss, and by the steady state two-phase inflow profiles established during commingled production. Each of these components is affected by the rock wettability.

Significant efforts have been made to develop technologies for wettability alteration near the wellbore, in order to increase well production or enhance oil and gas recovery. Well stimulation methods include wellbore vicinity treatment by surfactants (Xie et al., 2009), nanofluids (Mousavi et al., 2013) and salinity (Morrow and Buckley, 2011; Nasralla et al., 2013). The optimal choice of chemicals and injected volume can be determined from mathematical modelling. The proper mathematical model consists of governing

equations for two-phase steady-state flow in the reservoir with piecewise constant contact angle, which allows for the forecast of the wettability treatment efficiency.

Barenblatt (1990) and Van Duijn et al. (1995) investigated incompressible two-phase flow in rocks with piecewise constant permeability. The condition at shock in permeability or wettability is the continuity of capillary pressure.

The particular case with immobile oil phase has been investigated by Van Lingen et al. (1996), to estimate residual oil in rocks with heterogeneous wettability and permeability. In our previous work, Naik et al. (2015) derived analytical solution for incompressible two-phase flow and applied it to the evaluation of well productivity index with wettability alteration.

The current paper extends previous work by accounting for compressibility of the gas phase during gas production. Steady-state profiles for linear and axisymmetric compressible flows in rocks with piecewise constant wettability have been investigated. Non-monotonic dependency of gas productivity index on rock wettability has been discovered, indicating the existence of an optimal contact angle for the maximum well productivity.

Mathematical model of steady-state two-phase immiscible flows

In this section, we describe the steady-state two-phase immiscible flows of incompressible water and gas obeying the equation of state for real gases. Linear and axisymmetric flows are considered. The porous media with piecewise constant wettability corresponds to well with treatment of surfactants which change the contact angle.

The derivations of governing equations are presented in Appendixes. Appendix A contains the governing system for linear steady-state gas-water flow in homogeneous porous media, which corresponds to coreflooding. The system of two ordinary differential equations (9) and (10), determine the steady-state distributions of saturation and pressure during two-phase gas-water flow in cores. Fig. 1 shows the schematic for saturation profiles for water-wet rock ($s_0 = 1\text{-}s_{or}$) and oil-wet rock ($s_0 = s_{wi}$).

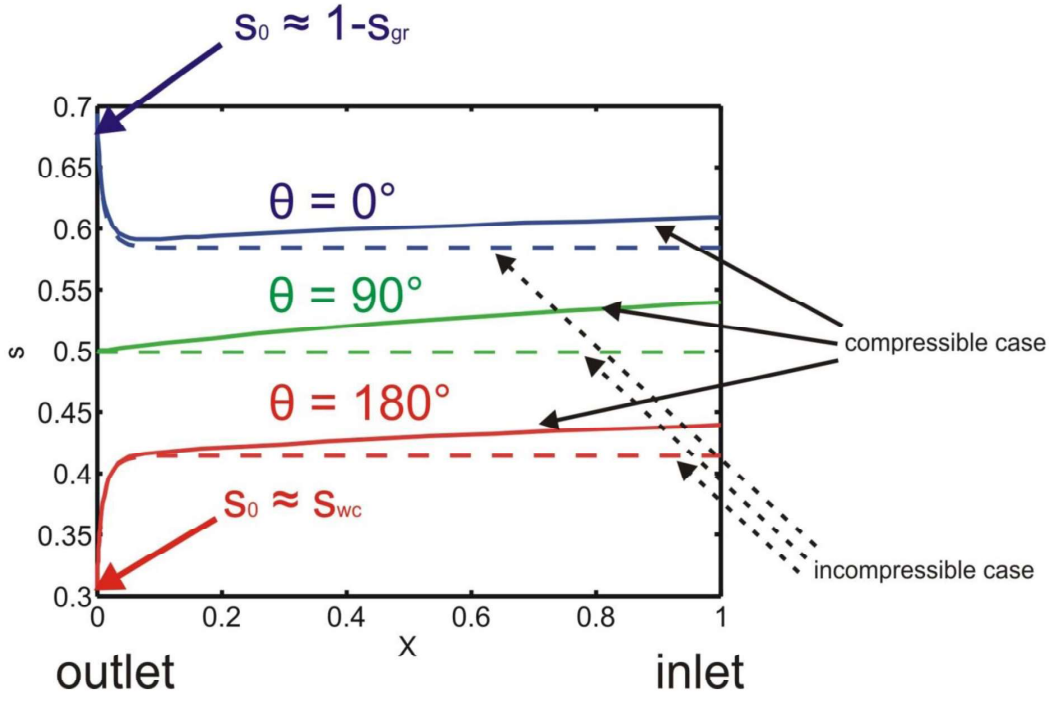

Figure 1—Schematic for saturation profile under steady state flow along the rock sample at different contact angles

Appendix B provides the contact angle profile and the pressure continuity condition at the contact angle discontinuity point (21-22).

Appendix C presents the governing system for axisymmetric steady-state gas-water flux towards well. The system of two ordinary differential equations (28) and (29) determine the steady-state distributions of saturation and pressure during the two-phase gas-water inflow. The solution is used for well index calculations for gas and for water during the inflow performance.

Water-gas inflow into a reservoir with wettability alternated in the wellbore vicinity uses the equations (28) and (29), where the wettability is altered in the wellbore vicinity The contact angle is changed due to surfactant treatment near to well from θ_2 to θ_1 in the fraction β of the reservoir adjacent to the wellbore (Eq. (21)). The boundary condition at $R = \beta$ corresponds to continuity of pressures in both phases and, consequently, to capillary pressure continuity. It is analogous to Eq. (22) for linear flow.

Governing equations for linear and radial flows (12, 23) are solved using Gear's method, based on numerical differentiation formulas with quasi-constant step size (Klopfenstein, 1971). The step size ranges from $\Delta X = 10^{-9}$ to 10^{-2} for linear case and $\Delta R = 10^{-12}$ to 10^{-3} for radial case.

Model validation

In this section, the laboratory core-flooding carried out by Pini and Benson (2013) under seven flow rates are analyzed in order to validate the model proposed in the previous section.

A cylindrical core of Berea sandstone with a diameter of 5 cm and length of 8.5 cm was used. The core has an average porosity of 18.8% and an initial permeability of 329 mD.

The laboratory procedure is as follows: the core is prepared by injection of CO_2, followed by the circulation of fresh water to dissolve the remnants of CO_2. After this, the permeability is measured while injecting water through the core. The core-flooding experiment starts by injecting the gas phase at constant flow rate until steady state is reached. After 10 PV injected, flow rate is increased. 7 different flow rates ranging from 0.5 to 60 mL/min are used. Pressure drop is measured during injection. The saturation profile is simultaneously measured by X-Ray CT scanning system. The measured saturation profiles are shown as black dotted lines in Figs. 2a and b. The measured pressure drop is shown as cross points in Fig. 2c. The numbers 1 to 7 correspond to the tests with flow rates of 60, 25, 14, 8, 4, 2 and 0.5 mL/min, respectively.

The mathematical model presented in the previous section is applied to calculate the saturation profiles and the pressure drops along the core under laboratory conditions for three flow rates (curves 1-3 in Fig. 2a). The optimization of 8 parameters is performed by maximizing R^2 value. The least-square optimization method is applied (Forst and Hoffmann, 2010; Yang et al., 2016; You et al., 2015, 2016). The values of optimized parameters are: Leveret J-function parameters C = 0.09, $\alpha = 3.95$, contact angle $\theta = 4°$, tortuosity $\eta = 0.61$, wettability alteration fraction $\varphi_1 = 0.99$, permanently water wet fraction φ_2=0.09, residual gas saturation $s_{gr} = 0.046$, irreducible water saturation $s_{wi} = 0.42$. Each curve in Fig. 2a has 3 degrees of freedom, so the total number of degrees of freedom for saturation profiles is $2 \times 3 + 1 = 7$. Pressure drops measured in the first three tests (points 1-3 in Fig. 2c) has 3 degrees of freedom. So, a set of 10-parametric experimental data was treated in order to determine 8 parameters. The results from modeling agree well with those from experimental measurement; $R^2 = 0.73$ for saturation profiles and 0.89 for pressure drops. The saturation data show significant scattering around the monotone profiles, which is typical for CT data. Also, usually the profiles are disturbed near to inlet (Al-Abduwani, 2005). Besides those artifacts, the quality of matching is high. The agreement between the laboratory and modelling data is good.

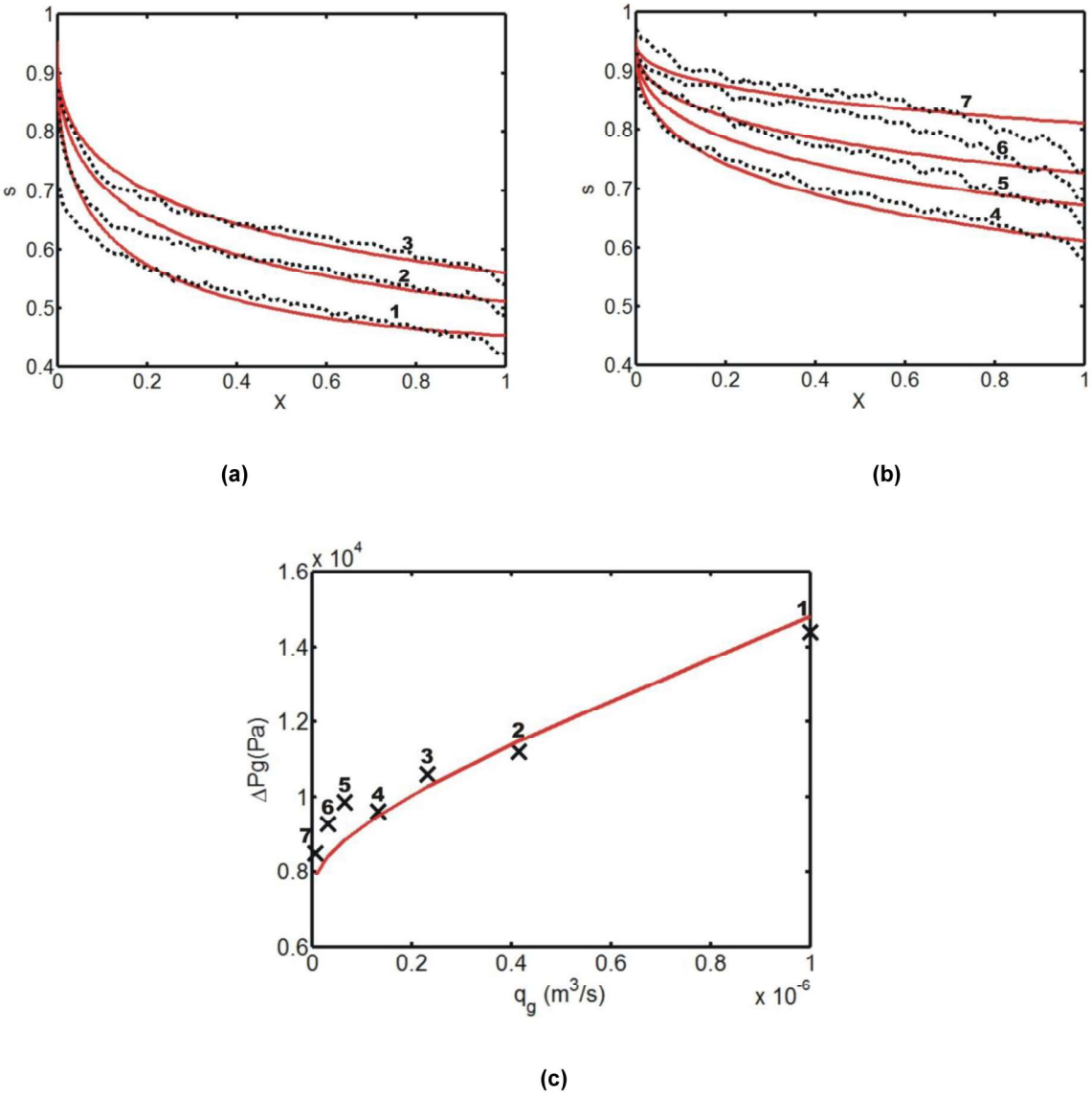

Figure 2—Laboratory coreflood data treatment using the analytical model: (a) matched saturation profiles for three tests with different rates; (b) predicted saturation profiles for four tests with different rates; (c) pressure drop for each test versus the modelling results

Model prediction using these tuned parameters is applied to the remaining 4 tests (curves 4-7 in Fig. 2b). The obtained saturation profiles are in good agreement with measured profiles; $R^2 = 0.81$ for predicted profiles (Fig. 2b). The pressure drop versus rate obtained from the model is also in good agreement with measured values, with $R^2 = 0.89$ (Fig. 2c).

The model parameters obtained by tuning vary in common intervals: α is in the range of 0~7 (Brooks and Corey, 1964); C is in the range of 0.09~0.25 (Thungsuntonkhun and Engler, 2004); $\eta \approx 0.5$ (Mualem, 1976).

The above validates the mathematical model for two-phase compressible two-phase steady-state flow in porous media.

Results analysis

Linear flow in porous media with constant contact angle

The saturation profile for incompressible flows is determined by the rates of the two phases, q_w and q_g and by the saturation at the outlet. The outlet saturation can be found from where the capillary pressure curve is equal to zero. There is no boundary condition at the core inlet (X = L), and a unique saturation profile can be obtained between the interval [0,∞).

However, the saturation and pressure equations (9, 10, 28, 29) are coupled for compressible flow. The solution of the system of two ordinary differential equations can be determined, when the rates q_w and q_g and pressure P_0 at the outlet are given. The pressure at the inlet tends to infinity as the core length tends to infinity. Saturation at infinity can then be determined from Eq. (19) for the incompressible and Eq. (20) for the compressible cases. The graphical solution to the transcendental equation (20) is shown in Fig. 3 for multiple values of water cuts. It is important to note that gas density approaches a limited value when the pressure tends to infinity, which allows the left hand side of (20) to be determined.

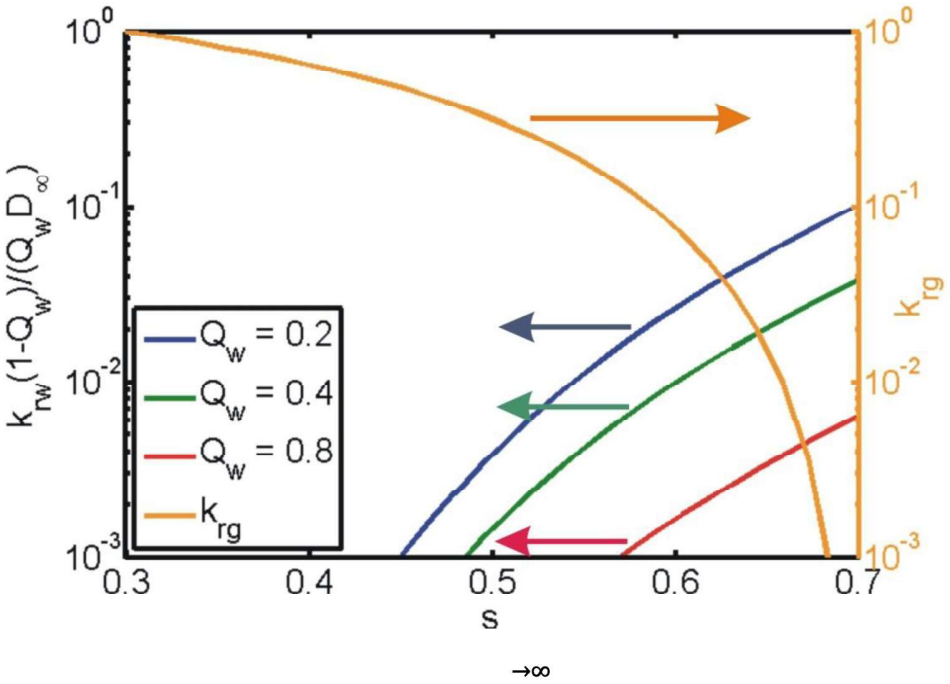

Figure 3—Graphical solution of the condition of equality of pressure gradients in water and gas, which defines saturation value at X→∞

The effect of compressibility on saturation profiles is shown in Fig. 4a. The "compressible" saturation profiles are always located above the "incompressible" saturation profiles. This is due to gas density decrease along the flux (from right to left), resulting in gas expansion and decreasing water saturation from right to left. For the high capillary-viscous ratio (ε = 50), the saturation profiles for compressible and incompressible cases almost coincide. The saturation profiles have a small deviation for the intermediate capillary-viscous ratio (ε = 5), and significant difference when the capillary-viscous ratio is small (ε = 0.5). As the large ε values correspond to small rates, they also consequently correspond to small pressure drops. This makes the compressibility effect negligible when ε is large.

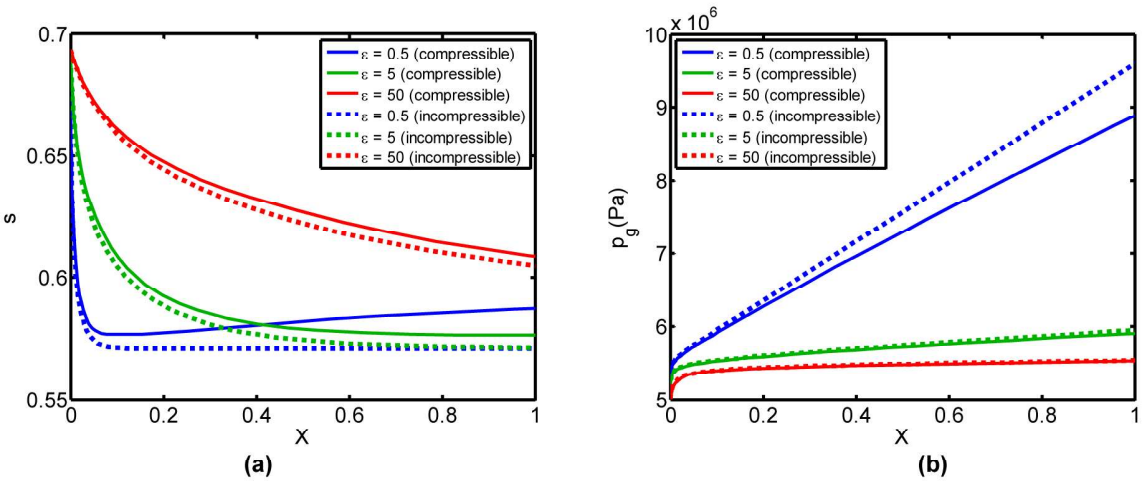

Figure 4—(a) Saturation profiles at different capillary-viscous ratios in linear flow; (b) pressure profiles for linear flow (Q_w = 0.4, θ=0°)

The effect of capillary-viscous ratio on gas pressure profile is shown in Fig. 4b. As the capillary-viscous ratio is inversely proportional to flow rate, its decrease will result in the increase of pressure gradient. Far from the outlet, the capillary pressure gradient is negligible and Eq. (13) is satisfied. The total mobility will increase as gas density increases. This decreases the pressure gradient (Eq. (14)), and causes the "incompressible" pressure profile to be higher than the "compressible" profile.

The effect of contact angle on saturation profile is shown in Fig. 5a. Increase in contact angle reduces capillary effects, but also affects relative permeability functions and boundary saturation values. During incompressible steady-state two-phase flow, the saturation far away from the core outlet stabilizes as X → ∞. The limit saturation value s_∞ satisfies the condition Eq. (19). The saturation profile is monotonic; saturation changes from 1 - s_{gr} at X = 0 to s_∞ at X → ∞.

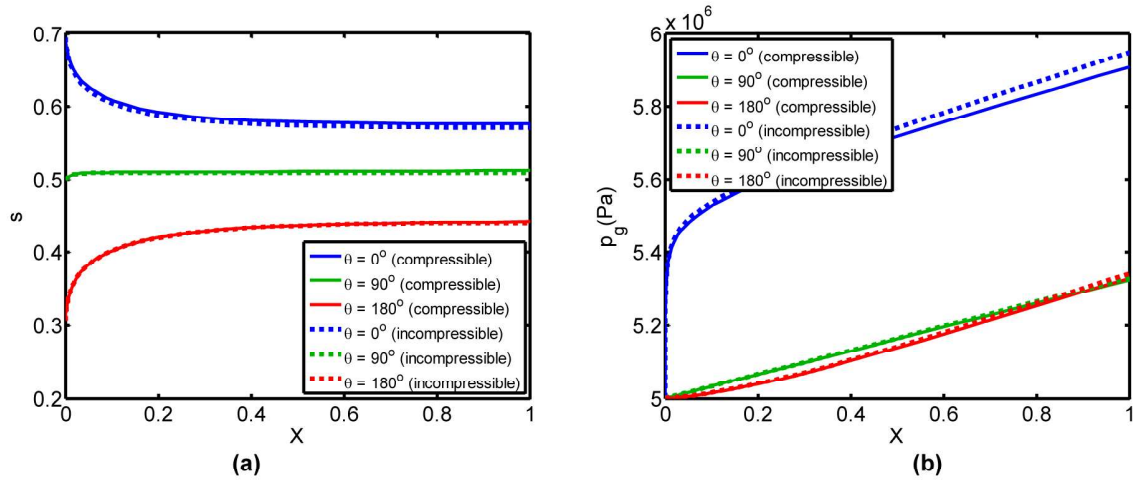

Figure 5—(a) Saturation profiles at different contact angles in linear flow; (b) Pressure profiles for gas in linear flow (Q_w = 0.4, ε = 5)

For compressible flow in hydrophobic media, saturation also monotonically increases from s_{wi} at X = 0 to s_∞ at X → ∞. However, in water-wet rock, the saturation profile is non-monotonic. Saturation tends from 1-s_{gr} at X = 0 to s_∞ at X → ∞, where s_∞ is determined from gas density with pressure tending to infinity.

The effect of contact angle on gas pressure profile is shown in Fig. 5b. For $\theta = 0$, the relative permeability of gas approaches zero at X = 0. As the flow rate is constant, the pressure gradient approaches infinity at

X = 0 (Eq. (9)). For higher contact angles, the relative permeability for gas does not approach zero, so the relative permeability approaches a constant value.

The effect of contact angle on productivity index (PI) for gas and water are shown in Fig. 6. At high capillary viscous ratios, the capillary end effect is large, so the saturation of the wetting phase is high. The high wetting phase saturation reduces the PI of the non-wetting phase. Therefore, at high capillary viscous ratios, the PI for gas monotonically increases with contact angle (red curve in Fig. 6a). The PI for water monotonically decreases with the increase of the contact angle (red curve in Fig. 6b).

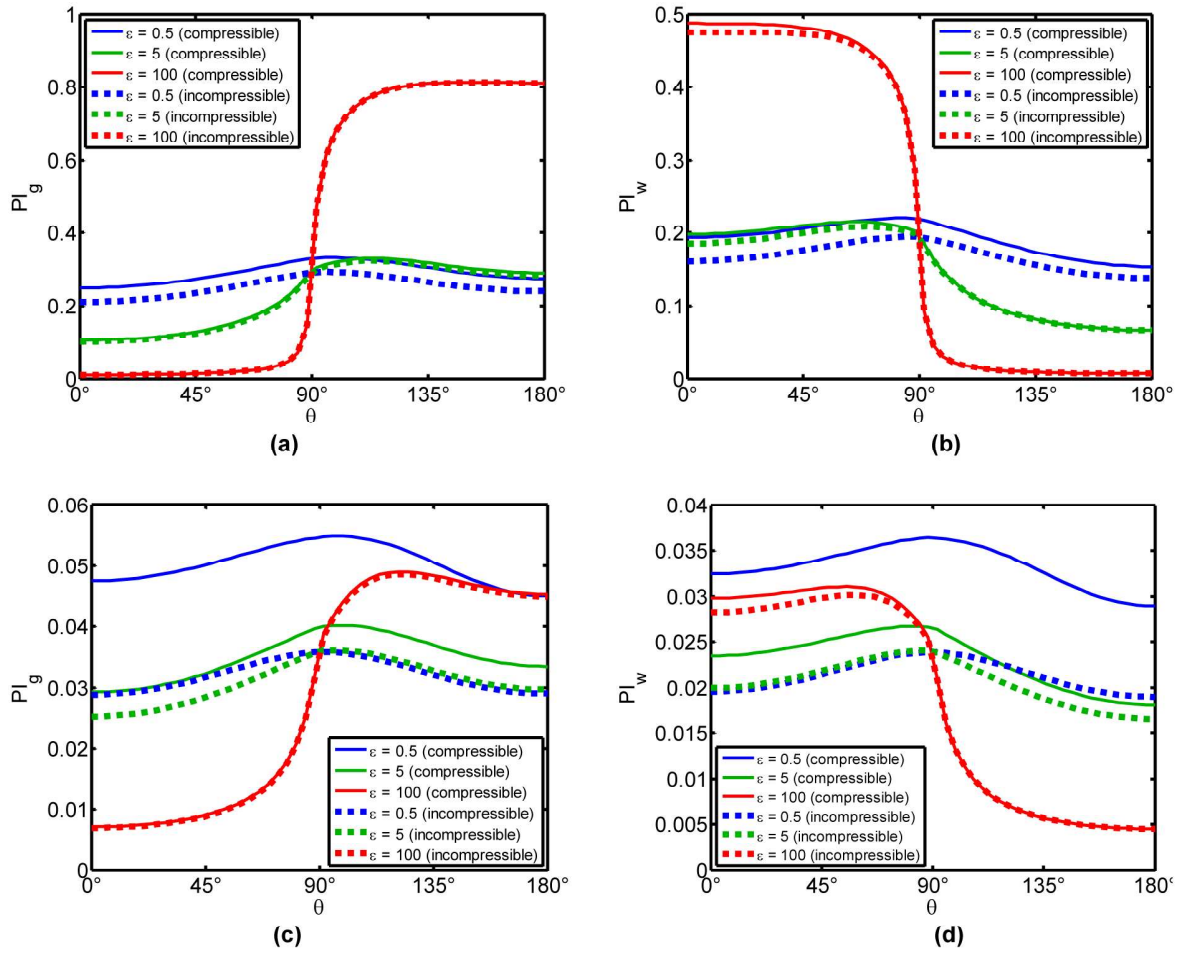

Figure 6—Productivity index versus contact angle at different capillary-viscous ratios under linear flow for (a) gas and (b) water and radial flow for (c) gas and (d) water. (Q_w = 0.4)

The tendency at low capillary viscous ratios is more complicated. At very low capillary viscous ratios, the capillary end effect is negligible and the productivity index is highly dependent on the saturation values determined at the inlet. Two effects occur when contact angle is increased. First, the water saturation determined at the inlet decreases; and second, the water phase occupies more space in larger pores. These two effects are competitive and cause the non-monotonic relationship between productivity index and contact angle (blue and green curves in Figs. 6a and b).

Linear flow in porous media with piecewise constant contact angle (core-fraction treatment)

Contact angle alteration has a direct consequence on the saturation profile and the productivity of each phase. However, if a contact angle alteration treatment is applied to a field, it is most likely that only a small region close to the wellbore or the fracture face will be altered. A fraction β is introduced which represents

the ratio of the altered region to the total core length. A piecewise constant relationship for the contact angle is used, where $\theta = \theta_1$ for $X < \beta$ and $\theta = \theta_2$ for $X > \beta$ (Fig. 7). In this case we assume $\theta_2 = 0$. When θ_1 is higher than zero, a second end effect occurs in the unaltered region (Fig. 7a). This second end effect is the result of capillary continuity between the altered and unaltered zone. The second end effect increases with θ_1, and the capillary viscous ratio.

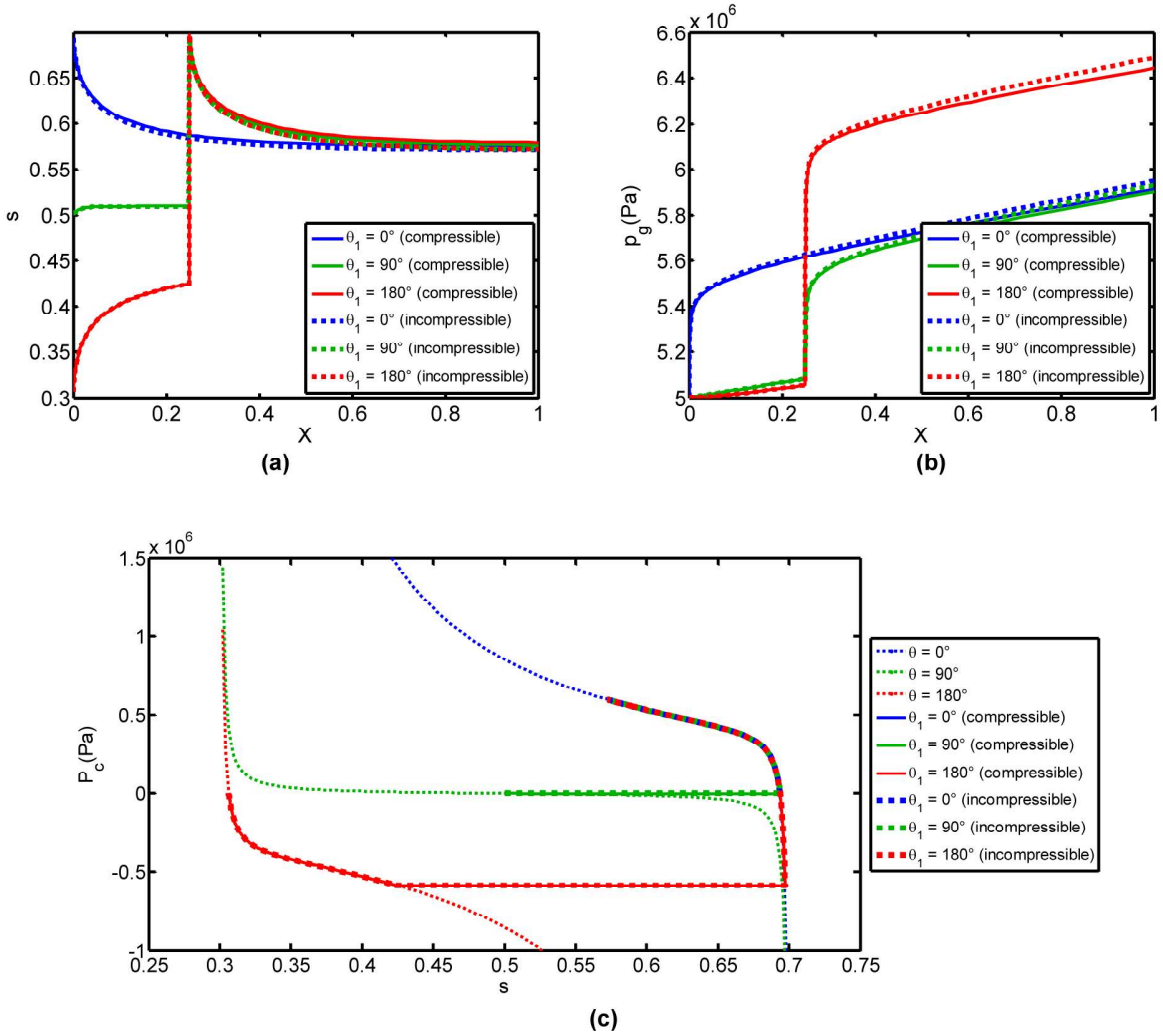

Figure 7—(a) Saturation, (b) gas pressure and (c) capillary pressure profiles at different θ_1 in linear flow with piecewise alteration of contact angle (Q_w = 0.4, β=0.25): ε = 5

The effect of θ_1 on pressure profile is shown in Fig. 7b. The pressure gradient is very high at X = 0 for $\theta_1 = 0$, but much lower for larger θ_1. At X = β, which corresponds to the contact angle discontinuity, the pressure gradient increases with the increase in θ_1. This is due to the reduction in capillary pressure in the region X > β, which can be reduced to below zero if $\theta_1 > 90°$.

The capillary pressure composition paths are shown in Fig. 7c. For $\theta_1 = 0°$, capillary pressure in the core increases from $P_c = 0$ at X = 0 to P_c (s_∞, 0) as $X \rightarrow \infty$. For $\theta_1 = 90°$ and 180°, the capillary pressure tends from $P_c = 0$ at X = 0 to P_c (s_∞, θ_1) as X increases. At X=β the saturation has an abrupt rise, while P_c remains constant. In the region X > β, the capillary pressure increases to P_c (s_∞, 0) as $s \rightarrow s_\infty$.

Figs. 8 a, b show the effects of contact angle on PI for gas and water in porous media with piecewise constant contact angle. The PI value is higher at $\theta_1 < 90°$ if compared to that at $\theta_1 > 90°$. This can be explained

by the increase in the water barrier at X = β with increase in θ_1. At very high θ_1, the pressure gradient at the discontinuity can be even higher than that at the wellbore. This causes PI to drop for very high θ_1 (Eq. (17)).

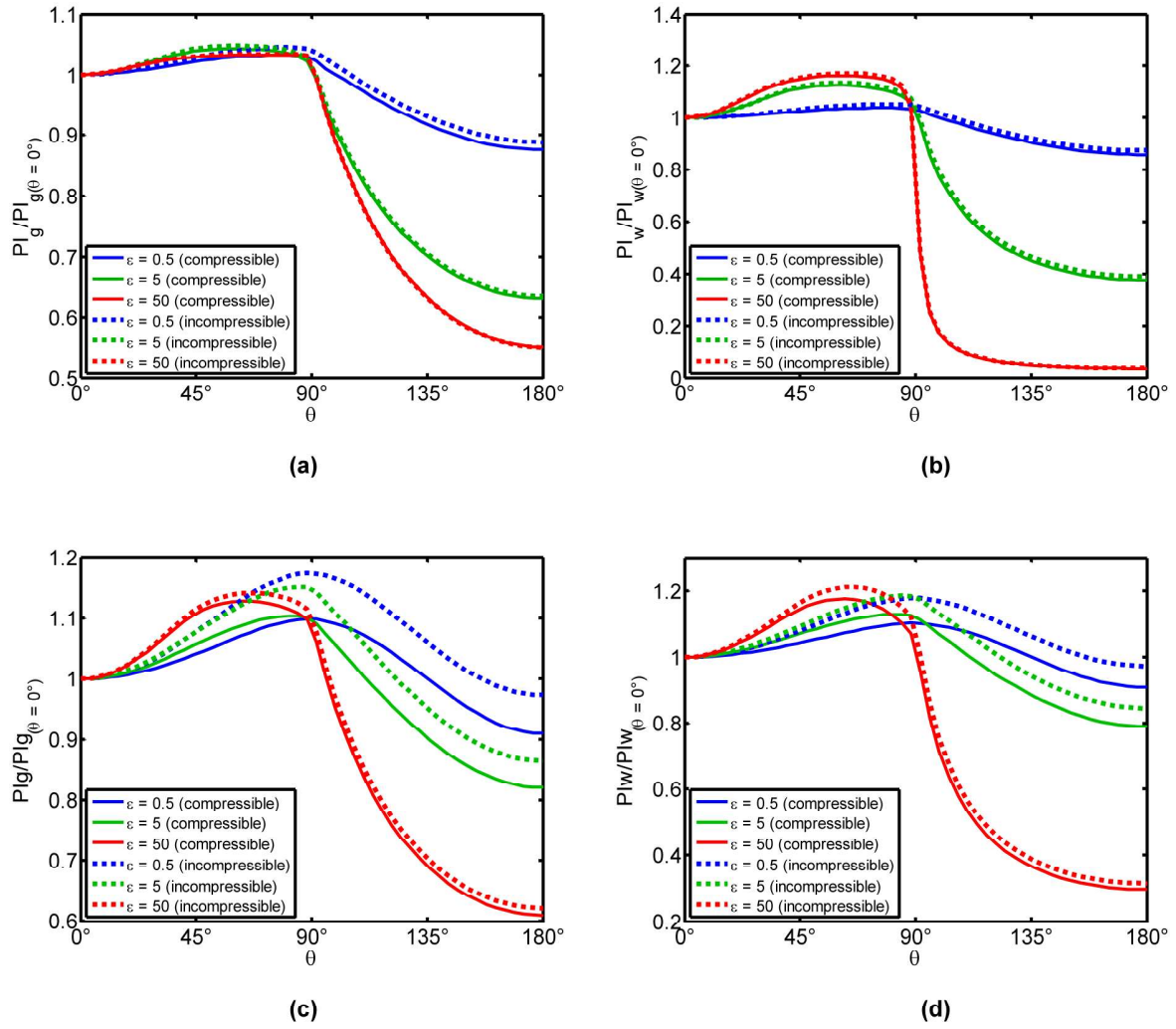

Figure 8—Productivity index at different θ_1 in linear flow (a, b), radial flow (c, d) with piecewise alteration of contact angle (Q_w = 0.4, β = 0.25)

Radial flow towards well with constant and piecewise constant contact angles

The PI for radial flow with constant contact angle follows the same trend as for linear flow. Figs. 6c and d present the effect of contact angle on PI values for gas and water, respectively. With the increase of contact angle, the water saturation decreases, while the relative permeability for water increases. These two competitive effects result in the non-monotonic function of PI(θ).

Compared to the incompressible gas case, the total mobility in the compressible case is higher (Eq. (15)), which causes lower pressure gradient and higher PI values in the compressible case (solid curves in Fig. 6c) than those in the incompressible case (dashed curves in Fig. 6c).

Figs. 8c and d present the relationship between PI and contact angle for the case of piecewise constant contact angles. The optimal contact angle corresponding to the maximum PI values for both gas and water are around 90°. Increase of the capillary viscous ratio leads to more significant end effect at the outer boundary of the treated zone, and smaller optimal contact angle (Figs. 8c, d).

Conclusions

The analytical modelling of steady-state gas-water flow in the rock with constant and piecewise-constant contact angles accounting for compressibility allows making the following conclusions:

- Non-monotonic saturation profile with steady-state commingled flow of gas and water for water-wet rocks is explained by the interplay between the capillary forces and gas compressibility.
- The saturation profile is non-monotonic if rock is water wet and capillary viscous ratio is low. Water saturation decreases with increasing distance close to the outlet due to capillary pressure increase, and increases at further distance due to gas compression.
- At high capillary-viscous ratios, increase in the contact angle results in an increase in the gas productivity index and a decrease in the water productivity index. When the capillary-viscous ratio is high, the flow is capillary dominated, leading to high saturations of the wetting phase, and hence, high productivity index of the wetting phase.
- At low capillary-viscous ratios, productivity indexes for both water and gas are non-monotonic functions of the contact angle. The reduction of contact angle leads to the decrease in saturation, while shifting water to occupy larger pores and increasing water relative permeability. The two competitive effects between saturation and relative permeability cause the non-monotonic dependence of productivity index on contact angle.
- An increase in the capillary-viscous ratio reduces the compressibility effect. The pressure drop reduces with the increase of capillary-viscous ratio, which decreases the effect of gas compressibility.
- Tuning of saturation profiles and pressure drop values in three tests exhibits close agreement between the experimental data and modelling results. The obtained values of Leveret J-function parameters C=0.09, α=3.95 vary in common intervals typical for two-phase flows in porous media.

Acknowledgements

Open Fund of State Key Laboratory of Oil and Gas Reservoir Geology and Exploitation (Chengdu University of Technology) (PLC201410) is gratefully acknowledged.

Nomenclature

b	Klinkenberg factor, Pa
C	capillary model coefficient
D	density-viscosity ratio
g	gas wet capillary fraction
J	leverett J function
k	permeability, m^2
k_{kg}	klinkenberg slip permeability correction factor
k_r	relative permeability
L	length scaling parameter, m
M	molar mass, kg/mol
P_c	capillary Pressure, Pa
p	pressure, Pa
P	Dimensionless pressure
q	mass rate, kg/m^2s
Q_w	water cut by mass
r	radius, m
R	Dimensionless radius

Z universal gas constant, 8.3144621 J/Mol·K
s water saturation
s_{gr} irreducible gas saturation
s_{wc} connate water saturation
S normalised saturation
T temperature, K
w capillary size, m
x distance, m
X dimensionless distance
z compressibility factor

Greek Letters

α Capillary model exponent
ε capillary viscous ratio
η tortuosity index
ϕ porosity
φ fraction of pore surface
μ viscosity, Pa·s
ρ density, kg/m^3
σ interfacial tension, N/m
θ macroscopic contact angle

Subscripts

g gas
w water (for productivity index and relative permeability) wetting (for saturation), well (for radius)
0 outlet
∞ inlet
1 treated reservoir
2 virgin reservoir

References

Al-Abduwani, F. A. H., Bedrikovetsky, P., Farajzadeh, R., Van Den Broek, W.M.G.T., Currie, P.K. (2005). External filter cake erosion: mathematical model and experimental study, in: SPE European Formation Damage Conference. Society of Petroleum Engineers, Sheveningen, The Netherlands.

Barenblatt, G.I., Entov, V.M., Ryzhik, V.M. (1990). Theory of Fluid Flows through Natural Rocks. Kluwer Academic Publishers, Dordrecht.

Bell, A. H. & Bond, D. C. (1974). Underground storage of natural gas in Illinois, Illinois State Geological Survey, Urbana, IL,

Bradford, S.A., Abriola, L.M., Leij, F.J., 1997. Wettability effects on two- and three fluid relative permeabilities. *J. Contam. Hydrol.* **28** (1-2), 171–191.

Brooks, R. H., Corey, A.T. (1964). Hydraulic Properties of Porous Media. Colorado State University, Hydraulic Papers.

Forst, W., Hoffmann, D. (2010). Optimization—Theory and Practice. Springer, New York.

Jones, F.O., Owens, W.W. (1980). A laboratory study of low-permeability gas sands. *J. Pet. Technol.* **32** (9), 1631–1640.

Mousavi, M. A., Hassanajili, S., Rahimpour, M. R. (2013). Synthesis of fluorinated nano-silica and its application in wettability alteration near-wellbore region in gas condensate reservoirs. *Applied Surface Science*, **273**, 205–214.

Morrow, N., Buckley, J. (2011). Improved oil recovery by low-salinity waterflooding. *J. Pet. Technol.* **63** (5), 106–113.

Mualem, Y. (1976). A new model for predicting the hydraulic conductivity of unsaturated porous media. *Water resources research*, **12** (3), 513–522.

Naik, S., You, Z., Bedrikovetsky, P. (2015). Rate enhancement in unconventional gas reservoirs by wettability alteration. *Journal of Natural Gas Science and Engineering*, **26**, 1573–1584.

Nasralla, R.A., Bataweel, M.A., Nasr-El-Din, H.A. (2013). Investigation of wettability alteration and oil-recovery improvement by low-salinity water in sandstone rock. *J. Can. Pet. Technol.* **52** (2), 144–154.

O'Carroll, D.M., Abriola, L.M., Polityka, C.A., Bradford, S.A., Demond, A.H. (2005). Prediction of two-phase capillary pressure-saturation relationships in fractional wettability systems. *J. Contam. Hydrol.* **77** (4), 247–270.

Peng, D. Y., Robinson, D. B. (1976). A new two-constant equation of state. *Industrial & Engineering Chemistry Fundamentals*, **15** (1), 59–64.

Pini, R., Benson, S.M. (2013). Simultaneous determination of capillary pressure and relative permeability curves from core-flooding experiments with various fluid pairs. *Water Resources Research*, **49** (6), 3516–3530.

Thungsuntonkhun, W., Engler, T.W. (2004). Applying NMR-hydraulic flow unit technique to estimate J-function and capillary pressure. In *SPWLA 45th Annual Logging Symposium*. Society of Petrophysicists and Well-Log Analysts.

Van Duijn, C.J., Molenaar, J., De Neef, M.J., 1995. The effect of capillary forces on immiscible two-phase flow in heterogeneous porous media. *Transp. Porous Media* **21** (1), 71–93.

Van Lingen, P.P., Bruining, J., Van Kruijsdijk, C.P.J.W., 1996. Capillary entrapment caused by small-scale wettability heterogeneities. *SPE Res. Eng.* **11** (2), 93–99.

Weiss, W.W., Xie, X. (2009). Field test of wettability alteration to increase the flow rate from aquifer gas storage wells. In SPE Eastern Regional Meeting. Society of Petroleum Engineers.

Xie, X., Liu, Y., Sharma, M., Weiss, W. W. (2009). Wettability alteration to increase deliverability of gas production wells. *Journal of Natural Gas Science and Engineering*, **1** (1), 39–45.

Yang, Y., Siqueira, F.D., Vaz, A.S.L., You, Z., Bedrikovetsky, P. (2016). Slow migration of detached fine particles over rock surface in porous media. *Journal of Natural Gas Science and Engineering*, **34**, 1159–1173.

You, Z., Bedrikovetsky, P., Badalyan, A. and Hand, M. (2015). Particle mobilization in porous media: temperature effects on competing electrostatic and drag forces. *Geophysical Research Letters*, **42**, 2852-2860.

You, Z., Yang, Y., Badalyan, A., Bedrikovetsky, P., Hand, M. (2016). Mathematical modelling of fines migration in geothermal reservoirs. *Geothermics*, **59**, 123–133.

Appendix A

Governing system for linear steady-state gas-water flow in homogeneous porous media

Consider steady-state flow of gas-water fluid in one dimension (Fig. 1). Mass fluxes for water q_w and gas q_g accounting for two-phase Darcy's flow are

$$q_w = -k\frac{k_{rw}(s,\theta)}{\mu_w}\rho_w\frac{dp_w}{dx} \tag{1}$$

$$q_g = -kk_{kg}(p_g)\frac{k_{rg}(s,\theta)}{\mu_g}\rho_g(p_g)\frac{dp_g}{dx} \tag{2}$$

where k is the permeability, s is the water saturation, θ (is the surface contact angle and k_{kg} is the Klinkenberg correction coefficient. The subscripts w and g in relative permeability k_{rw} and k_{rg}, viscosities μ_w and μ_g, densities ρ_w and ρ_g, and pressures p_w and p_g correspond to water and gas, respectively.

The capillary pressure p_c is the difference between the phase pressures, and is also proportional to the Leverett-J function J:

$$p_c = p_g - p_w = \frac{\sigma}{\sqrt{k/\phi}}J(s,\theta) \tag{3}$$

where σ is the interfacial tension, and ϕ is the porosity of the rock. The functions of capillary pressure and relative permeability are defined in Appendix D.

The mass fluxes for both water and gas are constant under steady state. We can then introduce the fraction of total flux for water as Q_w and the flux for gas as 1-Q_w:

$$Q_w = \frac{q_w}{q_g+q_w},\quad 1-Q_w = \frac{q_g}{q_g+q_w} \tag{4}$$

Let us introduce the following dimensionless variables and parameters:

$$P_i = \frac{k\rho_w}{(q_g+q_w)\mu_w L}p_i, i = w,g,\quad X = \frac{x}{L},\quad \varepsilon = \frac{\sigma\rho_w\sqrt{k\phi}}{(q_g+q_w)\mu_w L},\quad D(p_g) = \frac{\rho_g(p_g)\mu_w}{\rho_w\mu_g} \tag{5}$$

Here P is dimensionless pressure, X is dimensionless distance, and D is the density viscosity ratio. The capillary viscous ratio ε is the ratio between the reference capillary pressure and pressure drop across the core with single-phase water flow.

Substituting the dimensionless parameters (4-5) into Eqs. (1-3) yields

$$Q_w = -k_{rw}(s,\theta)\frac{dP_w}{dX} \tag{6}$$

$$1-Q_w = -k_{kg}(p_g)k_{rg}(s,\theta)D(p_g)\frac{dP_g}{dX} \tag{7}$$

$$P_g - P_w = \varepsilon J(s,\theta) \tag{8}$$

The equation for the gas flux (7) allows the gas pressure gradient to be expressed as

$$\frac{dP_g}{dX} = -\frac{1-Q_w}{k_{kg}\left(P_g\right)k_{rg}\left(s,\theta\right)D\left(P_g\right)} \tag{9}$$

The pressure gradients in both phases are expressed via the rates from (6, 7) and substituted into Eq. (8) as:

$$\varepsilon\frac{dJ\left(s\right)}{dX} = \frac{Q_w}{k_{rw}\left(s\right)} - \frac{1-Q_w}{k_{kg}\left(P_g\right)k_{rg}\left(s,\theta\right)D\left(P_g\right)} \tag{10}$$

We assume capillary pressure equals zero at the core outlet:

$$X=0:\ s=s_0,\ J\left(s_0\right)=0,\ P_g=P_0 \tag{11}$$

The system of two ordinary differential equations subject to the Cauchy conditions (11) determines the steady state profiles $s(x)$ and $P_g(x)$ for one-dimensional steady state gas-water flow.

In the particular case, where pressure drop across the core is significantly lower than the outlet pressure P_0, gas is considered to be incompressible. In this case Eq. (10) separates from Eq. (9) and allows for an implicit solution (Barenblatt et al, 1990):

$$X=\varepsilon\int_{s_0(\theta)}^{s}\frac{dJ\left(s,\theta\right)}{ds}\left[\frac{Q_w}{k_{rw}\left(s,\theta\right)} - \frac{1-Q_w}{k_{kg0}k_{rg}\left(s,\theta\right)D_0}\right]^{-1}ds \tag{12}$$

The solution to Eq. (12) is an asymptotic of that to (10) near the core outlet, where X⟶0.

Another particular case corresponds to negligible capillary pressure gradient, which is the asymptotic far away from the end effect zone:

$$\frac{dP_g}{dX} = \frac{dP_w}{dX} \tag{13}$$

The summation of Eqs. (6) and (7) accounting for (13) yields

$$-\frac{1}{\Lambda\left(s,\theta\right)} = \frac{dP_g}{dX} \tag{14}$$

where

$$\Lambda\left(s,\theta\right) = k_{rw}\left(s,\theta\right) + k_{rg}\left(s,\theta\right)k_{kg}\left(p_g\right)D\left(p_g\right) \tag{15}$$

is the total mobility.

After eliminating the pressure gradient terms with Eqs. (6-7) we obtain

$$\frac{Q_w}{1-Q_w} = \frac{k_{rw}\left(s,\theta\right)}{k_{rg}\left(s,\theta\right)k_{kg}\left(p_g\right)D\left(p_g\right)} \tag{16}$$

The dimensionless form for the productivity indexes for water and gas can be written as

$$PI_w = -\frac{Q_w}{\Delta P_w} \tag{17}$$

$$PI_g = -\frac{Q_g}{\Delta P_g} \tag{18}$$

Consider pressure and saturation profiles in long cores and the structure of the solution at X tending to infinity. For incompressible case, the limit saturation, s_∞, at X tending to infinity corresponds to condition where the mobility ratio equals the rate ratio

$$\frac{Q_w}{1-Q_w} = \frac{k_{rw}(s_\infty,\theta)}{k_{kg0}k_{rg}(s_\infty,\theta)}\frac{1}{D_0} \tag{19}$$

and pressure tends to infinity (Naik et. al, 2015). Assume that X tends to infinity with pressure tending to infinity, and gas density tends to a limit ρ_∞. The limit s_∞ corresponds to zero left hand side of Eq. (19), and satisfies the condition

$$\frac{Q_w}{1-Q_w} = \frac{k_{rw}(s_\infty,\theta)}{k_{rg}(s_\infty,\theta)}\frac{1}{D_\infty} \tag{20}$$

Graphical solution of Eq. (20) defining saturation at infinity is presented in Fig. 3.

Appendix B

Conditions at heterogeneity in linear steady-state gas-water flow in porous media with piecewise constant contact angle

The initial contact angle θ_2 has been changed to θ_1 in the fraction β of the core adjacent to the outlet:

$$\theta = \begin{cases} \theta_1, & 0 < X < \beta \\ \theta_2, & \beta < X < 1 \end{cases} \tag{21}$$

Continuity of pressure for both phases is assumed at the interface $X=\beta$:

$$X = \beta : P_g^- = P_g^+, P_w^- = P_w^+ \tag{22}$$

Therefore, capillary pressure is also continuous across the interface $X=\beta$.

Appendix C

Governing system for axisymmetric steady-state gas-water flow in homogeneous porous media

We discuss steady state fluxes of each phase under axisymmetric flow. As it follows from modified Darcy's law for each phase

$$q_w = -k2\pi r \frac{k_{rw}(s,\theta)}{\mu_w} \rho_w \frac{dp_w}{dr} \tag{23}$$

$$q_g = -k2\pi r k_{kg}(p_g) \frac{k_{rg}(s,\theta)}{\mu_g} \rho_g(p_g) \frac{dp_g}{dr} \tag{24}$$

Let us introduce the following dimensionless variables and parameters:

$$P_i = \frac{2\pi k \rho_w}{(q_w+q_g)\mu_w} p_i, \quad R = \frac{r}{r_e}, \quad \varepsilon = \frac{2\pi\sigma\rho_w\sqrt{k\phi}}{(q_w+q_g)\mu_w} \tag{24}$$

Here R is the dimensionless radius. Note that for the axisymmetric flow, the definitions of capillary viscous ratio and the dimensionless pressure (25) are different from those for the linear flow (5). However, the dimensionless term D is identical. Substituting dimensionless parameters (25) into eqs (23-24) yields

$$Q_w = -Rk_{rw}(s,\theta)\frac{dP_w}{dR} \tag{26}$$

$$1-Q_w = -RD(p_g)k_{kg}(p_g)k_{rg}(s,\theta)\frac{dP_g}{dR} \tag{27}$$

The equation for gas flux (27) allows the gas pressure gradient to be expressed as

$$\frac{dP_g}{dR} = -\frac{1-Q_w}{RD(p_g)k_{kg}(p_g)k_{rg}} \tag{28}$$

The capillary pressure equations in dimensional (3) and dimensionless (8) forms are identical under axisymmetric and linear flows. The pressure gradients in both phases can be expressed via the rates from (28-29) and substituted into Eq. (8). It yields:

$$\frac{ds}{dR} = \frac{1}{\varepsilon R \dfrac{dJ(s,\theta)}{ds}} \left[\frac{Q_w}{k_{rw}(s,\theta)} - \frac{1-Q_w}{D(p_g)k_{kg}(p_g)k_{rg}(s,\theta)} \right] \tag{29}$$

The capillary pressure equals zero at the wellbore:

$$R = R_w: \; s = s_0, \; J(s_0) = 0, \; P_g = P_0 \tag{30}$$

The system of two ordinary differential equations subject to Cauchy conditions (30) determines the steady state profiles $s(r)$ and $p_g(r)$ for axisymmetric steady state gas-water flow.

In the particular case, where pressure drop across the reservoir is significantly lower than the outlet pressure P_0, gas is considered to be incompressible. The functions k_{kg} and D become constant;

$$\Delta p << p, \quad \frac{ds}{dR} = \frac{1}{\varepsilon R \dfrac{dJ(s,\theta)}{ds}} \left[\frac{Q_w}{k_{rw}(s,\theta)} - \frac{1-Q_w}{D_0 k_{kg0} k_{rg}(s,\theta)} \right] \tag{31}$$

Solving the ordinary differential equation (31) by separation of variables and accounting for Cauchy conditions (28) yields:

$$R = R_w \exp\left(\varepsilon \int_{s_0(\theta)}^{s} \frac{dJ(s,\theta)}{ds} \left[\frac{Q_w}{k_{rw}(s,\theta)} - \frac{1-Q_w}{D_0 k_{kg0} k_{rg}(s,\theta)} \right]^{-1} ds \right) \tag{32}$$

The solution is asymptotic in the near-wellbore zone $R \to R_w$. Outside of this zone, where the capillary pressure gradient is negligible, Eq. (16) holds.

Now we consider pressure and saturation profiles and the structure of the solution at X tending to infinity, i.e. far away from the production well. By analogy with Eq. (19), the saturation s_∞ is determined by (20).

Appendix D

Functions of capillary pressure and relative Permeability

We define the normalized water saturation as

$$S(s)=\frac{s-s_{wc}}{1-s_{gr}-s_{wc}} \tag{33}$$

where s_{wc} and s_{gr} are connate and residual water saturations, respectively. The wetting saturation is defined as

$$S_w(s,\theta)=\begin{cases} S(s), \theta<90° \\ 1-S(s), \theta>90° \end{cases} \tag{34}$$

The Leveret-J function $J(s, \theta)$ is split into three fractions (O'Carroll et al., 2005)

$$J(s,\theta)=\varphi_1\cos(\theta)CS_w(s,\theta)^{-\frac{1}{\alpha}}+\varphi_2 CS(s)^{-\frac{1}{\alpha}}-\varphi_3 C(1-S(s)^{-\frac{1}{\alpha}}) \tag{35}$$

where the first fraction, φ_1, is affected by contact angle. The two remaining fractions, φ_2 and φ_3 represent a permanently water and permanently gas wet fraction. Parameters C and α are constants.

The relative permeability is defined as (Bradford et al., 1997)

$$k_{rw}(s,\theta)=(S(s))^{\eta}\frac{[1-g(\theta)]\int_0^S w^2(S)dS+g(\theta)\int_{1-S}^1 w^2(S)dS}{\int_0^1 w^2(S)dS} \tag{36}$$

$$k_{rg}(s,\theta)=(1-S(s))^{\eta}\frac{g(\theta)\int_0^{1-S} w^2(S)dS+[1-g(\theta)]\int_S^1 w^2(S)dS}{\int_0^1 w^2(S)dS} \tag{37}$$

where η represents tortuosity of the rock (Mualem, 1976).

The function $g(\theta)$ in Eq. (36) and Eq. (37) is an empirical function

$$g(\theta)=\frac{1}{2}\left[1-\cos(\theta)\right] \tag{38}$$

The pore size w in Eq. (36) and Eq. (37) is defined as

$$w(S)=\frac{S^{\frac{1}{\alpha}}}{C}\sqrt{\frac{k}{\phi}} \tag{39}$$

For low permeability rocks, any gas slippage effects can be included by multiplying gas relative permeability with the Klinkenberg coefficient (Jones and Owen, 1980)

$$k_{kg}(p_g)=\left(1+\frac{b}{p_g}\right),\ b=0.86k^{-0.33} \tag{40}$$

The density of gas can be calculated from the real gas law as (Peng and Robinson, 1976)

$$\rho_g = \frac{p_g M}{zRT} \tag{41}$$

where P_g is gas pressure, M is molar mass (kg/mol), R is gas constant (8.3144621 J/Mol·K), T is temperature, and z is compressibility factor.

5. Analytical modelling of the water block phenomenon in hydraulically fractured wells

Statement of Authorship

Title of Paper	Analytical modelling of the water block phenomenon in hydraulically fractured wells.
Publication Status	☑ Published ☐ Accepted for Publication ☐ Submitted for Publication ☐ Unpublished and Unsubmitted work written in manuscript style
Publication Details	Naik, S., Yang, S., Woolley, M. and Bedrikovetsky, P., 2019. Analytical modelling of the water block phenomenon in hydraulically fractured wells. Journal of Natural Gas Science and Engineering, 67, pp.56-70.

Principal Author

Name of Principal Author (Candidate)	Saurabh Naik		
Contribution to the Paper	Problem formulation, literature review, development of mathematical models, Implementation of mathematical solutions in Mat-lab, developing numerical simulation results for validation, creating figures, analysis of results, writing the manuscript		
Overall percentage (%)	90%		
Certification:	This paper reports on original research I conducted during the period of my Higher Degree by Research candidature and is not subject to any obligations or contractual agreements with a third party that would constrain its inclusion in this thesis. I am the primary author of this paper.		
Signature		Date	03/08/2019

Co-Author Contributions

By signing the Statement of Authorship, each author certifies that:

i. the candidate's stated contribution to the publication is accurate (as detailed above);

ii. permission is granted for the candidate in include the publication in the thesis; and

iii. the sum of all co-author contributions is equal to 100% less the candidate's stated contribution.

Name of Co-Author	Shuyan Yang		
Contribution to the Paper	Reviewing manuscript, editing manuscript		
Signature		Date	30/07/2019

Name of Co-Author	Matthew Woolley		
Contribution to the Paper	Providing field data, reviewing manuscript		
Signature		Date	30/07/19

Name of Co-Author	Pavel Bedrikovetsky
Contribution to the Paper	Reviewing manuscript
Signature	
Date	30/07/2019

Please cut and paste additional co-author panels here as required.

Journal of Natural Gas Science and Engineering 67 (2019) 56–70

Contents lists available at ScienceDirect

Journal of Natural Gas Science and Engineering

journal homepage: www.elsevier.com/locate/jngse

Analytical modelling of the water block phenomenon in hydraulically fractured wells

S. Naik[a], S. Yang[a], M. Woolley[b], P. Bedrikovetsky[a,*]

[a] The University of Adelaide, South Australia, Australia
[b] Santos Ltd, Adelaide, South Australia, Australia

ARTICLE INFO

Keywords:
Water blocking
Fractured well
Formation damage
Analytical model
End effect
Gas production

ABSTRACT

Hydraulic fracturing is a key technology which has enhanced the economic viability of the unconventional low permeability reservoirs by increasing their productivity. However, the high capillary forces associated with low permeability reservoirs can trap water near to the fracture face and impair the production of gas or oil. This phenomenon is commonly referred to as water block. In order to estimate how water blocking impairs well productivity, the model for well inflow performance must account for two phases, gas compressibility, gas-water capillary pressure, wettability, inertial flows, and pressure-dependent gas viscosity. In this paper, we derive an exact solution for the inflow performance of a fractured gas well during non-inertial flow. For inertial flow, an approximate analytical solution is obtained using the streamline method. The solutions account for immobile water, gas compressibility, gas-water capillary pressure, wettability, inertial flows, and pressure-dependent gas viscosity. A sensitivity analysis shows the essential role played by the Leverett *J* function, the relative permeability curves and the ratio between the capillary, viscous and inertial forces. The derived solutions are applied in a case study to determine that water block is a likely contributor to skin.

1. Introduction

Improving inflow performance is important in order to achieve commerciality of tight reservoirs, and one of the most common techniques to achieve this is hydraulic fracturing (Economides and Nolte, 1989; Yuan and Wood, 2015; Yuan et al., 2015).

For water-wet or mixed-wet rocks, the low capillary pressures in the hydraulic fracture result in high water saturations at the fracture face (Barenblatt et al., 1989; Jiang and Younis, 2016; Civan, 2015). This high water saturation creates a significant hydraulic resistance against flow of gas or oil. This phenomenon is referred to as water block, and is more problematic in tight reservoirs, where the capillary pressures in the rock is significantly higher than the fracture.

The extent of water block in a hydraulically fractured well is influenced by the compressibility of the gas, the flow convergence near to the well fracture and capillary, viscous and inertial forces. The inflow performance of the well can be calculated using numerical or analytical modelling.

Analytical models provide explicit or implicit formulae for skin. If compared with numerical models, this allows for significantly faster sensitivity studies and determination of model parameters from field data. Analytical models for oil or gas production permit clearer interpretation of the production history. As a result there have been many efforts to derive analytical solutions in different areas of reservoir and production engineering (Economides and Nolte, 1989; Bedrikovetsky, 2013; Lake et al., 2014; Huang et al., 2018).

Analytical solutions for one-dimensional (1D) flows accounting for two phase flows, gas compressibility, and capillary pressure have been published (Naik et al., 2015, 2018). However, for fractured wells the exact solution for 1D flow only corresponds to just the initial stage of production (Lee, 1982; Dake, 2013). When the pressure transient propagates far from the fracture, the deviation of the pressure distribution given by the linear flow model becomes significant due to curvilinear streamlines and singular flow near to the fracture tips.

Despite the high occurrence of water block in fractured wells in low permeability reservoirs (Bazin et al., 2010; Bahrami et al., 2011), the analytical solutions for fractured gas wells accounting for water block are not available. The present paper fills the gap.

The governing system of equations for gas-water flow with immobile water is well established. It consists of the mass balance equation for the gas phase, the momentum balance equation accounting for two phases (Darcy-Forchheimer's law), the equation for capillary pressure between the water and gas phase and the equation of state for gas (Dake, 2013; Towler, 2002).

* Corresponding author.
E-mail address: pavel@asp.adelaide.edu.au (P. Bedrikovetsky).

https://doi.org/10.1016/j.jngse.2019.04.018
Received 18 March 2019; Received in revised form 11 April 2019; Accepted 18 April 2019
Available online 24 April 2019
1875-5100/

The exact solutions for single-phase flow into fractured wells have been derived by reducing the governing system of equations to the Laplace equation (Bear, 2013). Similarly for two phase flow, we reduce the governing system of equations accounting for the gas and the immobile water to the Laplace equation, allowing for an exact solution. The exact formula for water block skin is then derived. The approximate solution accounting for inertial effects under high velocities near the fracture is obtained using the streamline method. The comparison of the solution with the numerical solution shows high accuracy of the approximate analytical solution. A sensitivity analysis determines that the most sensitive parameter affecting the skin is the pore size distribution index. The analytical models are used in a case study to determine if water block is a reasonable explanation for the increase of skin.

The text has the following structure. Section 2 derives the exact solution for the gas inflow performance with water blocking assuming Darcy's law. To validate the model proposed, Section 3 compares the analytical model to a numerical reservoir simulator. Section 4 develops a streamline method for gas flow accounting for capillary end-effects and the Darcy-Forchheimer law, and validates the analytical model numerically. Section 5 compares the plane parallel and radial flow solution to the analytical model derived. Section 6 performs a sensitivity study for the inflow performance accounting for non-inertial effects with respect to the modified capillary number and the dimensionless Forchheimer number. Section 7 provides the simplified analytical model for incompressible fluid, which corresponds to oil production. Section 8 applies the derived analytical models to a case study. Section 9 discusses the applications and the limitations of the models derived. Section 10 concludes the paper.

2. Derivation of gas inflow into a hydraulic fracture with immobile water

This section formulates assumptions for the model, presents basic equations and derives the exact solution for flow towards a fracture.

2.1. Assumptions of the model

Consider a vertical well which produces from a circular reservoir. The position of the well is given in Fig. 1. The reservoir has constant thickness and is isotropic and homogenous. The reservoir temperature is constant.

The well is hydraulically fractured. The fracture penetrates the entire thickness of the reservoir. This eliminates flow in the vertical direction. The pressure drop between the fracture tip and the wellbore is significantly smaller than the pressure drop between the reservoir and the wellbore. Therefore, the fracture is assumed to have infinite conductivity. The fracture half-length is less than half of the drainage radius.

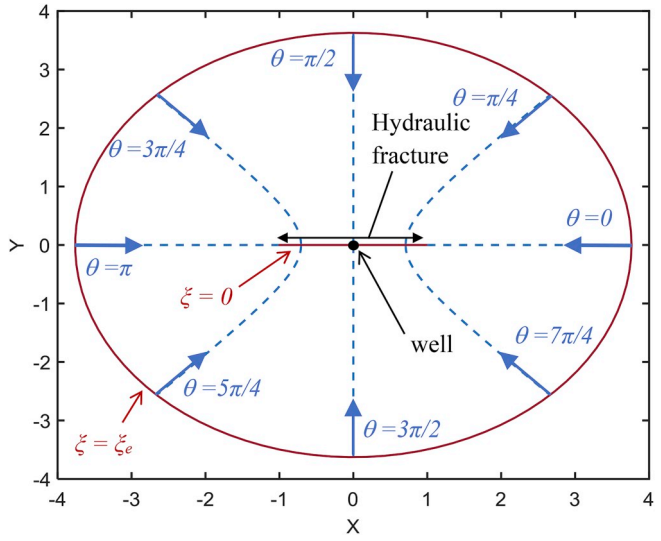

Fig. 1. Schematic of the elliptic coordinates used for the inflow performance model of a hydraulically fractured well.

Gas is produced under steady state and follows Darcy's law. There is no water production, however water is present in the reservoir.

2.2. Derivation of basic equations

The governing system for steady state gas flow with trapped water in a low-permeability porous medium consists of the mass balance equation for gas, Darcy's law for gas flow with Klinkenberg slip effects and the capillary pressure equation with constant water pressure:

$$\nabla \cdot u = 0 \tag{1}$$

$$\nabla p_g = u B_g(p_g) \frac{\mu_g(p_g)}{k k_{rg}(s) k_{kg}(p_g)} \tag{2}$$

$$p_g(s) = \frac{\sigma}{\sqrt{k/\phi}} J(s) + p_w \tag{3}$$

where u is the velocity at surface conditions, p is the pressure, B is the formation volume factor, k is the permeability, k_{rg} is the relative permeability to gas, s is the water saturation, k_{kg} is the Klinkenberg coefficient, μ is the viscosity, σ is the interfacial tension, ϕ is the porosity and J is the Leverett J function. The subscripts g and w represent gas and water at reservoir conditions, respectively.

The formation volume factor for gas, B_g, is defined as:

$$B_g(p_g) = \frac{p_{sc} z(p_g) T}{p_g z_{sc} T_{sc}} \tag{4}$$

where z is the compressibility factor, T is the temperature, and the subscript sc indicates surface conditions. The Klinkenberg coefficient k_{kg} (Jones and Owens, 1980) is defined as:

$$k_{kg}(p_g) = 1 + b/p_g, \quad b = 0.9735 k^{-0.33} \tag{5}$$

where b is an empirical constant. Since the fracture has infinite conductivity, the gas pressure is equal to the flowing bottom-hole pressure p_{wf} throughout the fracture. As the water is immobile, the water pressure is constant and can be evaluated from the bottom-hole flowing pressure:

$$p_w = p_{wf} - \frac{\sigma}{\sqrt{k/\phi}} J(s_{wf}) \tag{6}$$

where s_{wf} is the water saturation at the fracture face. The pore radius and permeability inside the hydraulic fracture are substantially higher than in the reservoir. As a result, the capillary pressure inside the fracture is negligible compared to the capillary pressure in the reservoir. The continuity in capillary pressure between the fracture and the reservoir rock causes the capillary pressure inside the reservoir rock to approach zero at the fracture face (Van Duijn et al., 1995). This means that for water wet cases, $s_{wf} = 1 - s_{gr}$, where s_{gr} is residual gas saturation. For gas wet cases $s_{wf} = s_{wirr}$, where s_{wirr} is the irreducible water saturation. For any other wettability, s_{wf} can be found from solving the equation $P_c(s_{wf}) = 0$. Let us define the potential Φ as:

$$\Phi(s) = \sigma \sqrt{k\phi} \int_{s_{wf}}^{s} \frac{k_{kg}(p_g(s))}{B_g(p_g(s))} \frac{k_{rg}(s) J'(s)}{\mu_g(p_g(s))} ds \tag{7}$$

This potential given by Eq. (7) satisfies the following equation:

$$\nabla \cdot u = \nabla^2 \Phi \tag{8}$$

2.3. Boundary conditions

Consider a set of Cartesian coordinates (x,y) such that the coordinate x is parallel to the hydraulic fracture and the coordinate y is perpendicular to the hydraulic fracture. The well is located at the origin of the axes (0,0). As $s = s_{wf}$ at the hydraulic fracture, the potential Φ is equal to zero at the hydraulic fracture. Therefore the inner boundary condition for potential is:

$$y = 0, -x_f < x < x_f: \Phi = 0 \tag{9}$$

where x_f is the fracture half-length. The outer boundary condition for potential is:

$$y^2 + x^2 = r_e^2: \Phi = \Phi(s_e) \tag{10}$$

where r_e is the drainage radius and s_e is the water saturation at the drainage radius which satisfies the following condition:

$$p_g(s_e) = p_e \tag{11}$$

where p_e is the pressure at the drainage radius. The function $p_g(s)$ is given by Eq. (3).

2.4. Flow equations under the streamline method

Prats (1961) and Hale and Evers (1981) used elliptic coordinates to describe the flow of fluid from a reservoir to a hydraulically fractured vertical well. The elliptic coordinates (ξ,θ) are defined by:

$$x(\xi, \theta) = x_f \cosh\xi \cos\theta$$
$$y(\xi, \theta) = x_f \sinh\xi \sin\theta \tag{12}$$

The dimensionless Cartesian coordinates can be obtained by dividing Eq. (12) by fracture half-length:

$$X = x/x_f$$
$$Y = y/x_f \tag{13}$$

The relationship between the dimensionless Cartesian coordinates and the elliptic coordinates is presented in Fig. 1. The gradient for potential under the new set of curvilinear coordinates is expressed as (Tang, 2007):

$$\nabla\Phi = \frac{\hat{e}_\xi}{h_\xi}\frac{\partial\Phi}{\partial\xi} + \frac{\hat{e}_\theta}{h_\theta}\frac{\partial\Phi}{\partial\theta} \tag{14}$$

where $\hat{e}_\xi$ and $\hat{e}_\theta$ are the unit vectors in direction ξ and θ respectively. The scale factors h_ξ and h_θ are:

$$h_\xi = \sqrt{\left(\frac{\partial x}{\partial\xi}\right)^2 + \left(\frac{\partial y}{\partial\xi}\right)^2}$$
$$h_\theta = \sqrt{\left(\frac{\partial x}{\partial\theta}\right)^2 + \left(\frac{\partial y}{\partial\theta}\right)^2} \tag{15}$$

The substitution of Eq. (12) into Eq. (15) results in:

$$h_\xi = h_\theta = x_f\sqrt{\sinh^2\xi + \sin^2\theta} \tag{16}$$

Let us assume that there is no flow in the θ direction. This gives the following equation:

$$u_\theta = 0, \frac{\partial\Phi}{\partial\theta} = 0 \tag{17}$$

The substitution of Eq. (16) and Eq. (17) into Eq. (14) results in:

$$\nabla\Phi = \frac{\hat{e}_\xi}{h_\xi}\frac{\partial\Phi}{\partial\xi} \tag{18}$$

2.5. Solution for potential

Using Eqs. (2) and (3) and the definition of the potential Eq. (7) we arrive at:

$$u = \nabla\Phi \tag{19}$$

From the substitution of Eqs. (16)–(18) into Eq. (19) we arrive at:

$$u_\xi = \frac{1}{x_f\sqrt{\sinh^2\xi + \sin^2\theta}}\frac{d\Phi}{d\xi} \tag{20}$$

where u_ξ is the velocity in direction ξ. The flow rate into the fracture is determined by integrating the normal component of velocity over any closed path around the fracture. If we choose an iso-potential line as the path to integrate on, the normal component of velocity will be u_ξ. The equation for gas flow rate is:

$$q_g = h\int_0^{2\pi} u_\xi\frac{\partial a}{\partial\theta}d\theta \tag{21}$$

where h is the formation height and a is the arc length. The arc length is defined as:

$$a = \int\sqrt{\left(\frac{\partial x}{\partial\theta}\right)^2 + \left(\frac{\partial y}{\partial\theta}\right)^2}d\theta \tag{22}$$

From the substitution of Eq. (12) into Eq. (22), we obtain:

$$\frac{\partial a}{\partial\theta} = x_f\sqrt{\sinh^2\xi + \sin^2\theta} \tag{23}$$

The substitution of Eq. (20) and Eq. (23) into Eq. (21) gives us the following equation for gas flow rate:

$$q_g = 2\pi h\frac{d\Phi}{d\xi} \tag{24}$$

The inner boundary condition (Eq. (9)) under the elliptic coordinates is:

$$\xi = 0: s = s_{wf}, \Phi = 0 \tag{25}$$

An important characteristic of the elliptic coordinates in Eq. (12) is that at large ξ ($\xi \gg 2$) they begin to resemble cylindrical coordinates with radius r (where $r = x_f\sinh\xi = x_f\cosh\xi$). A circular reservoir with boundary radius $r = r_e$ can be approximated by an elliptic reservoir with boundary $\xi_e = \ln(2r_e/x_f)$, as long as $r_e > > 2x_f$. Therefore, the outer boundary condition under elliptic coordinates is:

$$\xi = \xi_e = \ln(2r_e/x_f): \Phi = \Phi(s_e) \tag{26}$$

Finally, the solution for the potential is:

$$\Phi = \frac{\Phi(s_e)}{\xi_e}\xi \tag{27}$$

2.6. Analytical model for inflow performance

Substituting Eq. (3) into Eq. (24) and applying the chain rule to the resultant gives us:

$$q_g = 2\pi kh\frac{k_{kg}(p_g(s))}{B_g(p_g(s))}\frac{k_{rg}(s)}{\mu_g(p_g(s))}\frac{dp_g}{d\xi} \tag{28}$$

The definition of pseudo pressure ψ for reservoirs with Klinkenberg slip effects is:

$$\psi(p) = 2\int_0^p \frac{k_{kg}(p_g)p_g}{z(p_g)\mu_g(p_g)}dp_g \tag{29}$$

The substitution of Eq. (29) into Eq. (28) allows us to arrive at the inflow performance equation:

$$q_g = \pi kh\frac{z_{sc}T_{sc}}{p_{sc}T}\left[\frac{\psi(p_e) - \psi(p_{wf})}{\ln(r_e/r_w) + S_f + S_{wb}}\right] \tag{30}$$

where S_f is the skin for hydraulic fracture and S_{wb} is the skin for water block. They are expressed as:

$$S_f = \ln(2r_w/x_f) \tag{31}$$

$$S_{wb} = \int_0^{\xi_e} \left[\frac{1}{k_{rg}(s(\xi))} - 1 \right] d\xi \tag{32}$$

The saturation profile required for Eq. (32) can be found implicitly from applying the chain rule to Eq. (28):

$$\xi = \frac{1}{N_{mca}} \int_{s_{wf}}^{s(\xi)} \frac{k_{kg}(p_g(s))}{B_g(p_g(s))} \frac{\mu_g(p_{wf})}{\mu_g(p_g(s))} k_{rg}(s) J'(s) ds \tag{33}$$

where N_{mca} is the modified capillary number:

$$N_{mca} = \frac{q_g \mu_g(p_{wf})}{2\pi\sigma h \sqrt{k\phi}} \tag{34}$$

The modified capillary number is the ratio between the viscous and capillary forces on the pore scale (Barenblatt et al., 1989).

3. Comparison between the analytical model and the numerical reservoir simulator

This section formulates the input empirical model functions into the exact solution and validates the analytical model by comparison with a numerical reservoir simulator.

3.1. Forms of the relative permeability and capillary pressure curves

Any form of the Leverett J function and relative permeability can be used in the presented model. The Brooks-Corey capillary pressure model (Brooks and Corey, 1964) is applied in this study for the Leverett J function. The two parameters which define this model are the pore size distribution index λ and the dimensionless capillary entry pressure C. The Leverett J function has the form:

$$J(s) = C s_n(s)^{-\frac{1}{\lambda}} \tag{35}$$

where s_n is the normalised water saturation. It is expressed as:

$$s_n(s) = \frac{s - s_{wirr}}{1 - s_{gr} - s_{wirr}} \tag{36}$$

The Brooks-Corey-Mualem model (Mualem, 1976) for relative permeability is used in this paper and is defined as:

$$k_{rg}(s) = (1 - s_n(s))^{\eta} \left(1 - s_n(s)^{2+\frac{2}{\lambda}} \right) \tag{37}$$

where η is the tortuosity coefficient.

3.2. Numerical validation of the exact solution

The proposed analytical model was tested against the black oil reservoir simulator IMEX. The simulated reservoir contains a single hydraulically fractured production well in the centre. Input data for the simulated reservoir and the well is given in Table 1. The properties for the gas were generated with the Petroleum Experts' software PROSPER.

Table 1
Input data for validation test against reservoir simulator.

Parameter	Value
k (mD)	100
A (m^2)	1.225×10^5
x_f (m)	22.5
h (m)	6
ϕ	0.1
λ	1.5
η	2
σ (N/m)	0.05

Table 2
Gas composition.

Component	Mole precent
C_1	54.8
C_2	11.86
C_3	3.62
i-C_4	0.52
n-C_4	1.03
i-C_5	0.42
n-C_5	0.51
C_6	0.99
C_7	1.38
C_8+	0.93
CO_2	23.52
N_2	0.42

Table 3
Properties of component C_8+.

Parameter	Value
Critical Temperature (K)	594.6
Critical Pressure (MPa)	2.29
Acentric factor	0.4435

The compressibility factor was determined from the Peng and Robinson equation of state and the viscosity was determined from the Lohrenz, Bray and Clark gas viscosity correlation. The composition of the gas used is given in Table 2 and the combined properties of the larger components C_8+ is given in Table 3.

The model in the reservoir simulator has the following differences from the proposed model: the shape of the reservoir in the simulator is square instead of circular (the existence of a hydraulic fracture restricts the numerical model in IMEX to a Cartesian coordinate system), and the simulator does not have an infinite conductivity fracture. To accommodate the shape factor difference, the size of the reservoir is made much larger than the half-length of the fracture. To approximate an infinitely conductive fracture, the fracture in the simulator is given a permeability of 5000 Darcy and a width of 0.02 m.

Gas injectors are placed across the boundary of the reservoir. The total injection rate is the same as the production rate. The reservoir has an initial reservoir pressure of 13 MPa and water saturation of 0.1. The simulation is run until the bottom-hole pressure of the production well stabilizes and steady state is reached.

A total of 12 scenarios were investigated: 4 different values for production rate against 3 different values for dimensionless entry pressure C. The production rates q_g were 0.58, 0.81, 1.04 and 1.27 m^3/s. The modified capillary numbers N_{mca} for the given rates were 2.66×10^6, 3.72×10^6, 4.78×10^6 and 5.85×10^6, respectively. The values for C were 0.0375, 0.075 and 0.15.

The saturation profile for the proposed model is given by Eq. (33). The pressure for the model is given be Eq. (3) and the dimensionless pressure is given by:

$$P_g = \frac{\sqrt{k/\phi}}{\sigma} p_g \tag{38}$$

Fig. 2 shows the comparison between the saturation profiles and the dimensionless pressure profiles calculated by the proposed model and the reservoir simulator for the scenario where $C = 0.15$ and $N_{mca} = 4.78 \times 10^6$. The average coefficient of determination (R^2) for the saturation profiles is 0.94 and for the dimensionless pressure profiles is 0.99. The high water saturation at the fracture face causes a dramatic increase in pressure gradient close to the wellbore.

The bottom hole flowing pressure p_{wf} and the average reservoir pressure $\overline{p}$ from the numerical reservoir simulator allow us to calculate water block skin from the following equation (Ahmed and McKinney,

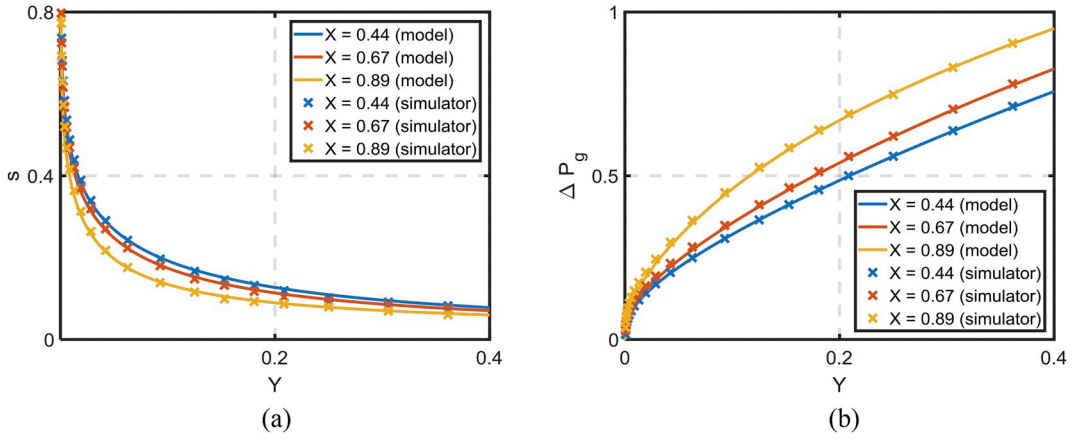

Fig. 2. Comparison between the proposed analytical model and the reservoir simulator at 3 different cross sections: (a) water saturation; (b) dimensionless pressure drop.

2005):

$$S_{wb} = \frac{\pi kh}{q_g}\frac{z_{sc}T_{sc}}{p_{sc}T}(\psi(\bar{p}) - \psi(p_{wf})) - \ln\left(\frac{r_e}{r_w}\right) + 0.75 - S_f \tag{39}$$

Fig. 3 shows the comparison between the skin values determined from the proposed analytical model and the reservoir simulator.

At low flow rates, the water block region will spread out closer to the edges of the reservoir and the difference in reservoir shape factor causes a deviation in skin value calculated. However, good agreement was achieved between the proposed model and the reservoir simulator. R^2 varied from 0.94 to 0.95 for all curves. The close agreement with skin, saturation profiles and pressure profiles validates the analytical model given by Eq. (27).

4. Non-Darcy flows at high production rates and inertial effects

This section derives the approximate analytical model for inertial flow using streamline method, and validates the solution by comparison with the numerical model.

4.1. Derivation of non-Darcy skin

The model presented in Section 2 considered slow, capillary dominated flow. However, at higher flow rates, inertial forces are large and non-Darcy flow can occur. The additional pressure drop due to the non-Darcy effect is accounted for by adding the Forchheimer term to Darcy's law. The Darcy-Forchheimer law is expressed as:

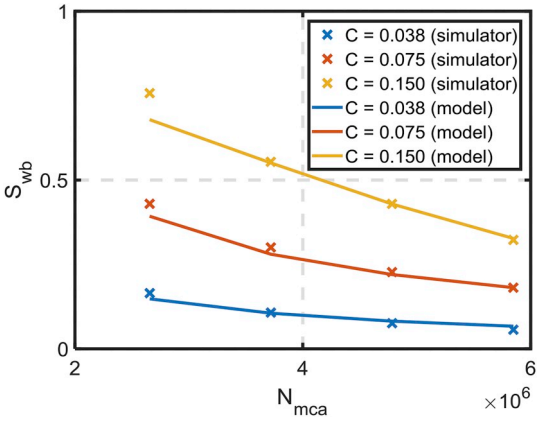

Fig. 3. Comparison of the water block skins calculated from the proposed analytical model and the reservoir simulator at 3 different dimensionless entry pressures.

$$\nabla p_g = uB_g(p_g)\left[\frac{\mu_g(p_g)}{kk_{rg}(s)k_{kg}(p_g)} + \beta|u|\frac{M}{R}\frac{p_{sc}}{z_{sc}T_{sc}}\right] \tag{40}$$

where β is the Forchheimer coefficient, M is the molar mass of the gas and R is the universal gas constant. From the streamline assumption (Eq. (17)), the modulus of velocity is:

$$|u| = u_\xi \tag{41}$$

From Eq. (21) and Eq. (23), we arrive at the modulus of velocity:

$$u_\xi = \frac{q_g}{h}\frac{G(\xi)}{x_f},\ G(\xi) = \left(\int_0^{2\pi}\sqrt{\sinh^2\xi + \sin^2\theta}\,d\theta\right)^{-1} \tag{42}$$

The quantity $G(\xi)/x_f$ is the inverse of the perimeter of the iso-potential line at the position ξ. As $\xi \to 0$, $G \to 1/4$ and Eq. (42) becomes the equation for velocity under linear flow. As $\xi \to \infty$, $G \to x_f/2\pi r$ and Eq. (42) becomes the equation for velocity under radial flow.

The streamline assumption (Eq. (17)) can reduce Eq. (40) to a single ordinary differential equation (ODE). The substitution of Eqs. (3), (41) and (42) the resultant ODE allows us to arrive at the following ODE:

$$\frac{ds}{d\xi} = N_{mca}\frac{B_g(p_g(s))}{J'(s)}\left[\frac{\mu_g(p_g(s))}{k_{rg}(s)k_{kg}(p_g(s))\mu_g(p_{wf})} + FG(\xi)\right] \tag{43}$$

where F is the dimensionless Forchheimer number:

$$F = \frac{q_g\beta k}{h\mu_g(p_{wf})x_f}\frac{M}{R}\frac{p_{sc}}{z_{sc}T_{sc}} \tag{44}$$

The boundary condition given by Eq. (25) can make the ODE (Eq. (43)) stiff. The implicit Klopfenstein –Shampine numerical differentiation formulae with quasi-constant step size (Shampine and Reichelt, 1997) are efficient at solving stiff ODEs, and are implemented into Matlab to solve Eq. (43).

The inflow performance equation accounting for the non-Darcy effects is:

$$q_g = \pi kh\frac{z_{sc}T_{sc}}{p_{sc}T}\left[\frac{\psi(p_e) - \psi(p_{wf})}{\ln(r_e/r_w) + S_f + S_{wb} + S_{nd}}\right] \tag{45}$$

where S_{nd} is the non-Darcy skin and is evaluated from:

$$S_{nd} = F\int_0^{\xi_e} G(\xi)k_{kg}(p_g(s(\xi)))\frac{\mu_g(p_{wf})}{\mu_g(p_g(s(\xi)))}d\xi \tag{46}$$

4.2. Numerical validation of the approximate analytical solution

The model accounting for non-Darcy effects (Eq. (43)) is compared

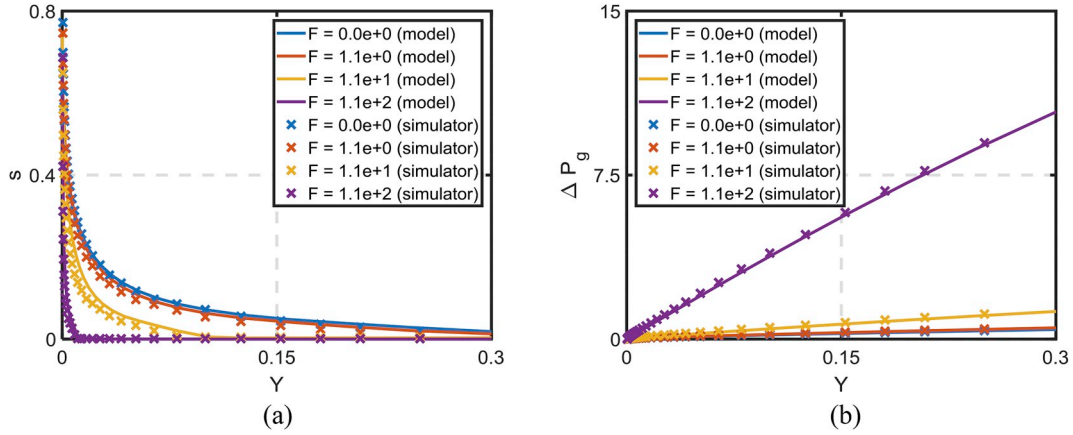

Fig. 4. Comparison between the proposed model and the reservoir simulator at the cross section $X = 0.44$ for 4 different dimensionless Forchheimer numbers: (a) water saturation; (b) dimensionless pressure drop.

to the numerical reservoir simulator IMEX. The reservoir has same characteristics as given in Section 3.1, and the technique used to validate the model is the same as given Section 3.1. The value for production rate and injection rate q_g was 0.58 m^3/s.

The sensitivity of saturation and pressure profile to F is given in Fig. 4. The blue curve represents Darcy flow, where $F = 0$. The value for the Forchheimer coefficient is determined from the empirical equation given by Pascal and Quillian (1980):

$$\beta = (1.0827 \times 10^{-5})k^{-1.176} \tag{47}$$

This equation gives a dimensionless Forchheimer number of $F = 9.4 \times 10^{-5}$. The crosses in Fig. 4 represent the numerical simulation results and the lines represent the model profile given by Eq. (43). The R^2 for all saturation and pressure profiles are within the range 0.97–0.99. The high agreement validates the semi-analytical model given by Eq. (43). The saturation gradient is influenced by both inertial and capillary forces. The inertial forces reduce the water saturation, and cause a reduction in water block.

The sum of water block and non-Darcy skin calculated by the numerical reservoir simulator and the proposed semi-analytic model for various dimensionless Forchheimer numbers is shown in Fig. 5. The close agreement ($R^2 = 0.99$) validates the semi-analytic model (Eq. (43)).

5. Comparison to linear and axisymmetric flow regimes

This section investigates the skin factor under the 1-D linear and radial flow regimes and compares it against the analytical model derived.

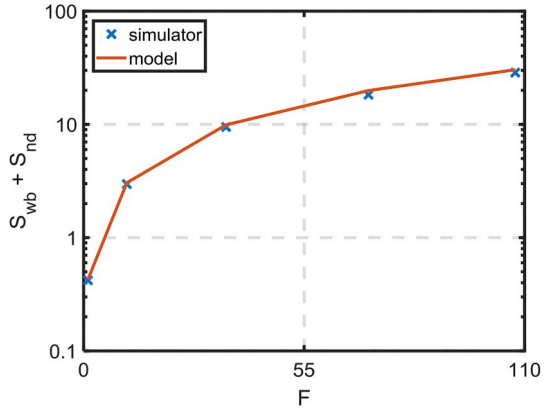

Fig. 5. Comparison between the sum of the water block skin and the non-Darcy skin calculated by the proposed model and the reservoir simulator.

5.1. Model for the linear flow regime

During the initial stage of production, the fractured well produces under a linear flow regime. The equations for saturation gradient ds/dx, water block skin S_{wb}, non-Darcy skin S_{nd} and the dimensionless drainage area A_d for linear flow are:

$$\frac{ds}{dx} = \frac{\pi N_{mca}}{2x_f}\frac{B_g(p_g(s))}{J'(s)}\left[\frac{\mu_g(p_g)}{k_{rg}(s)k_{kg}(p_g)\mu_g(p_{wf})} + \frac{F}{4}\right] \tag{48}$$

$$S_{wb} = \int_0^{L_e}\left[\frac{1}{k_{rg}(s(x))} - 1\right]dx \tag{49}$$

$$S_{nd} = \frac{\pi F}{8x_f}\int_0^{L_e} k_{kg}(p_g(s(x)))\frac{\mu_g(p_{wf})}{\mu_g(p_g(s(x)))}dx \tag{50}$$

$$A_d = \frac{4L_e}{x_f} \tag{51}$$

where L_e is the length from fracture face.

5.2. Model for the axisymmetric flow regime

When the pressure transient travels sufficiently far away from the fracture, the well flows under a radial flow regime. As it follows from Eqs. (1), (3) and (40) the equations for saturation gradient ds/dr, water block skin S_{wb}, non-Darcy skin S_{nd} and dimensionless drainage area A_d for radial flow are:

$$\frac{ds}{dr} = \frac{N_{mca}}{r}\frac{B_g(p_g(s))}{J'(s)}\left[\frac{\mu_g(p_g)}{k_{rg}(s)k_{kg}(p_g)\mu_g(p_{wf})} + \frac{Fx_f}{2\pi r}\right] \tag{52}$$

$$S_{wb} = \int_{x_f/2}^{r_e}\frac{1}{r}\left[\frac{1}{k_{rg}(s(r))} - 1\right]dr \tag{53}$$

$$S_{nd} = \frac{Fx_f}{2\pi}\int_{x_f/2}^{r_e}\frac{k_{kg}(p_g(s(r)))}{r^2}\frac{\mu_g(p_{wf})}{\mu_g(p_g(s(r)))}dr \tag{54}$$

$$A_d = \pi\left(\frac{r_e^2 - (x_f/2)^2}{x_f^2}\right) \tag{55}$$

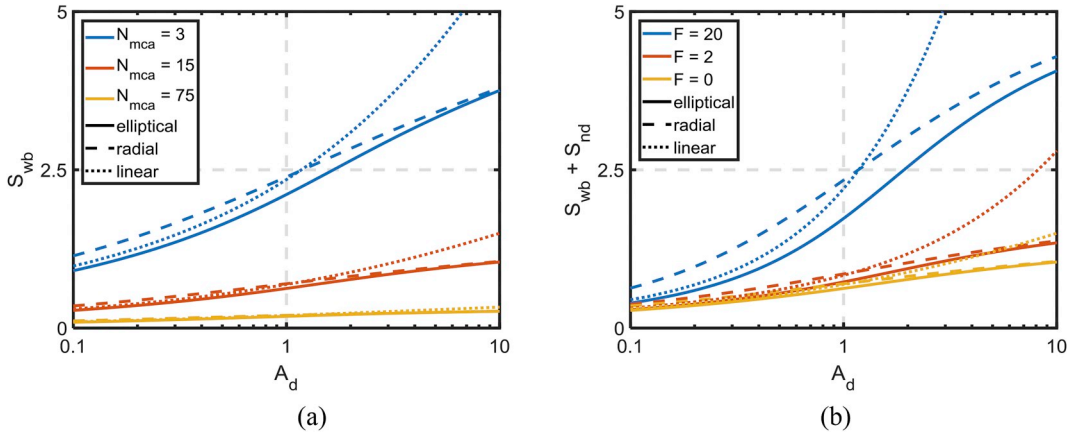

Fig. 6. Skin calculation comparison of for elliptical, radial and linear flows for varying dimensionless drainage area A_d: (a) the case of Darcy flow for different values of modified capillary number N_{mca}; (b) Non-Darcy flow at various dimensionless Forchheimer numbers F.

5.3. Comparison with the elliptic flow regime

In the intermediate of these two flow regimes, elliptic flow can occur. The dimensionless drainage area A_d for elliptic flow is:

$$A_d = \pi \sinh(\xi_e)\cosh(\xi_e) \tag{56}$$

Naik et al. (2018) provide the analytical models for radial and linear flows towards a well. Comparison of the presented model to the linear and radial flow models is provided in Fig. 6. Fig. 6a shows that the deviation between linear 1D flow and 2D flow towards fractured well increases as the drainage volume increases. However, at large drainage zones, where the fracture length is small in comparison with the drainage radius ($A_d > 10$), the flow towards the fracture converges to the radial flow. The higher is the modified capillary number N_{mca}, the higher is the rate, and the lower is the deviation between the three flows with different geometry.

Fig. 6b exhibits similar effect for non-Darcy flows: convergence of the fractured-well and axi-symmetric flows at large drainage areas, large deviation between the linear and fractured-well flows at large drainage areas, and high Forchheimer numbers.

6. Sensitivity analysis

This section investigates the sensitivity of the skin, and the radius of damage to various parameters which characterize the flow. The parameters investigated include the dimensionless Forchheimer number, modified capillary number, dimensionless capillary entry pressure, and the pore size distribution index.

6.1. Sensitivity of non-Darcy and water block skin with respect to inertial, viscous and capillary forces

This paper establishes a new semi-analytical model with consideration of inertial, viscous and capillary forces. The influence of the aforementioned forces on the inflow performance of a naturally fractured gas well is investigated. The physical characteristics of the reservoir which have been considered are given in Table 4. The dimensionless Forchheimer number F defines the ratio of inertial to viscous forces and the modified capillary number N_{mca} defines the ratio of viscous to capillary forces.

Fig. 7 shows the influence of increasing F on the saturation profile, at a fixed N_{mca}. The blue line represents the smallest value for F. When F is increased, the gas pressure increases and the gas phase becomes compressed. The result is that water saturation increase, as indicated by the red curve. However, at some point, the effect of the inertial forces will begin to reduce the saturation, as indicated by the yellow curve.

Table 4
Reservoir properties used for the sensitivity analysis.

Parameter	Value
k (mD)	0.1
p_{wf} (MPa)	5.5
C	0.15
λ	1.5
η	2
N_{mca}	1.5×10^2

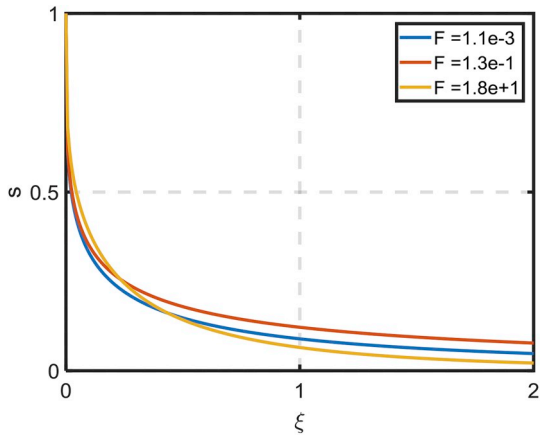

Fig. 7. Sensitivity of the saturation profile to the dimensionless Forchheimer number F. $N_{mca} = 1.5 \times 10^2$.

The final result is that there is some intermediate F where the saturation profile is largest.

Fig. 8 shows the sensitivity of S_{nd}, S_{wb} and their sum to N_{mca} and F. As expected S_{wb} is high when the N_{mca} is low. The non-monotonic relationship S_{wb} shares with F is the result of the competition between gas compression and inertial forces, as previously mentioned. Also, unsurprisingly, S_{nd} increases if F increases. However, the effect N_{mca} has on S_{nd} is not so straightforward. A decrease in N_{mca} causes a decrease in S_{nd}. This is due to the effect N_{mca} has on pressure drop. A decrease in N_{mca} causes an increase in pressure drop, which resultantly increases viscosity. The increase in viscosity is what reduces S_{nd}.

The sensitivity of S_{nd}, S_{wb} and their sum to C is presented in Fig. 9a. The Leverett J function and its derivative are proportional to C, which cause the water block skin to scale almost proportionally with C. Variation in C by ± 25% gives roughly 25% variance in water block skin.

The sensitivity of S_{nd}, S_{wb} and their sum to λ is presented in Fig. 9b.

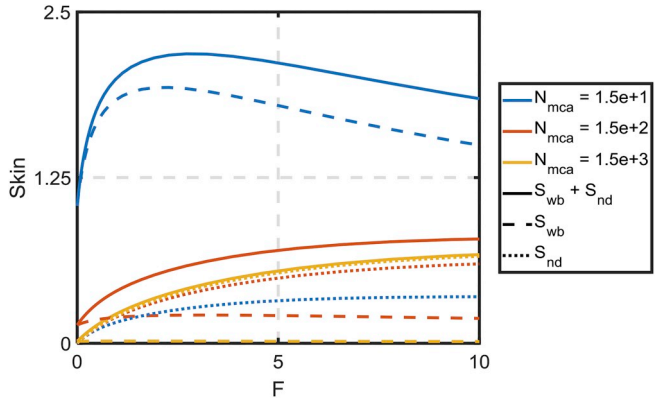

Fig. 8. Sensitivity of water block skin, non-Darcy skin and their sum to the dimensionless Forchheimer number and the modified capillary number.

A decrease in λ will increase the J function, which will increase S_{wb}. A decrease in λ by 25% can increase the skin by up to 80% and an increase in λ by 25% can decrease the skin up to 35%. Of the 2 parameters which define the forms of the Leverett J function, the skin due to water block is more dependent on the pore size distribution index λ. While the dimensionless parameters λ and C have a significant influence on the water block skin, they have a negligible influence on the non-Darcy skin.

6.2. Sensitivity of water block damage radius

Consider an iso-potential line given by ξ_D, such that 99% of skin due to water block results from water inside the region $\xi < \xi_D$:

$$0.99S_{wb} = \int_0^{\xi_D} \left[\frac{1}{k_{rg}(s(\xi))} - 1 \right] d\xi \tag{57}$$

Let us define the radius of a circle with the same cross sectional area as this ellipse as the water block damage radius r_D. It can be found from the following equation:

$$\frac{r_D}{x_f} = \sqrt{\frac{\sinh \xi_D}{2}} \tag{58}$$

The ratio r_D/x_f is called the dimensionless damage radius and is useful for estimating volumes of chemical treatment for water block clean up.

The sensitivity of r_D/x_f to F and N_{mca} is shown in Fig. 10a. The domination of capillary forces over viscous and inertial forces causes water saturation to spread over a larger distance and increase water block skin. This means that the affected area is larger when both the dimensionless Forchheimer number and the modified capillary number are low. For the cases investigated the radius of damage is generally around 2 times the fracture half-length, but can be as large as 2.5 times the fracture half-length.

Due to the nature of the water saturation profile, more of the damage is closer to the fracture. For the case of $N_{mca} = 1.5 \times 10^2$, 70% and 50% of the water block comes from a dimensionless damage radius of less than 1/2 and 1/3, respectively (Fig. 10b).

7. Simplified analytical model for a fractured oil well

Generally, for oil flow, the compressibility of oil in the reservoir is neglected and inertial effects are not considered. Viscosity can also be approximated by a constant. Under these assumptions the water block skin equation simplifies to:

$$S_{wb} = \int_{s_{wf}}^{s_e} \frac{J'(s)[1 - k_{ro}(s)]}{N_{mca} B_o} ds \tag{59}$$

where B_o is the formation volume factor for oil. The comparison of the model for oil to the model for gas is given in Fig. 11. Under the aforementioned assumptions, water block skin is only dependent on the ratio of capillary to viscous forces. Capillary forces are affected by the Leverett J function and the dimensionless capillary number N_{mca}. The water block skin calculated by the model for gas is larger than the model for oil due to the effects gas compression has on water saturation. Oil generally has higher viscosity than gas, which increases the capillary number. For this reason there is generally higher research into water blocking for gas wells than oil wells.

8. Case study: model application to production data

Using the analytical model developed in Section 4, here we aim to determine the relative permeability and Leverett J curves which replicate the skin observed in one hydraulically fractured gas well. This allows us to test whether water block is a reasonable explanation for the increasing skin observed in the aforementioned well.

8.1. Properties of the well and reservoir

Well C in the Cooper Basin was selected for this case study. It is a vertical well intersecting multiple production intervals. One of its primary zones is the Patchawarra sand. This zone was hydraulically fractured. The model was tuned to fit measured production data to investigate opportunities for enhancing gas rate. The result of the tuned parameter values and the goodness of fit can give insight into how

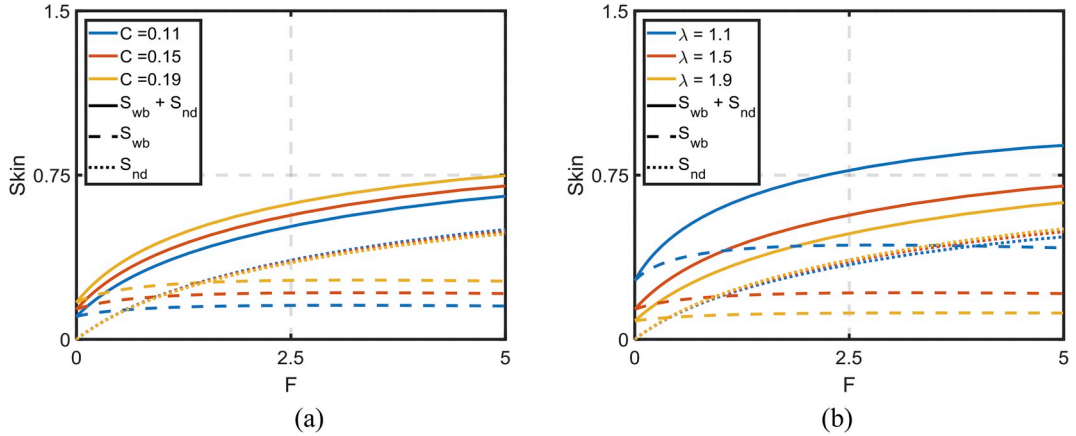

Fig. 9. Sensitivity of water block skin, non-Darcy skin and their sum to the dimensionless Forchheimer number and the Leverett J function parameters: (a) dimensionless entry pressure; (b) pore size distribution index.

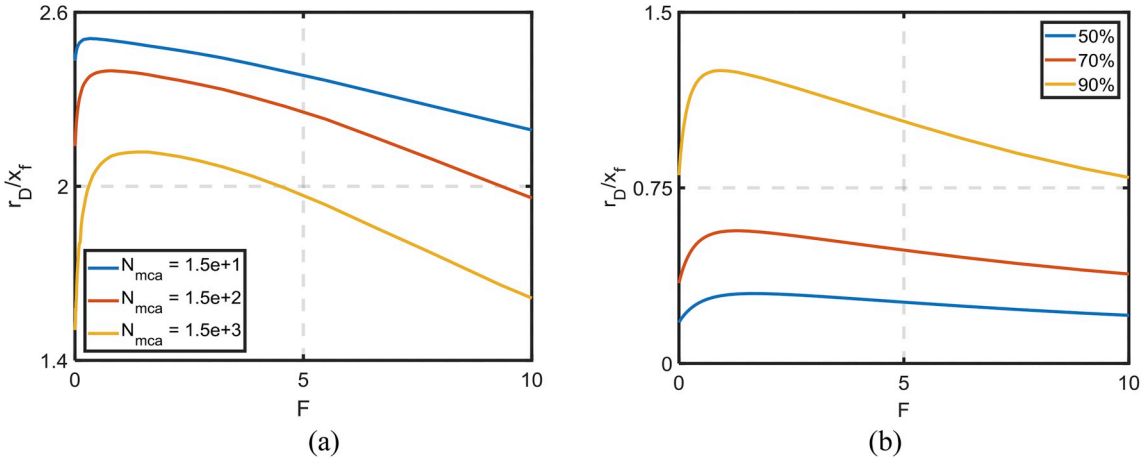

Fig. 10. Sensitivity of the dimensionless damage radius to the dimensionless Forchheimer number: (a) at varying modified capillary number; (b) for different percentages of water block.

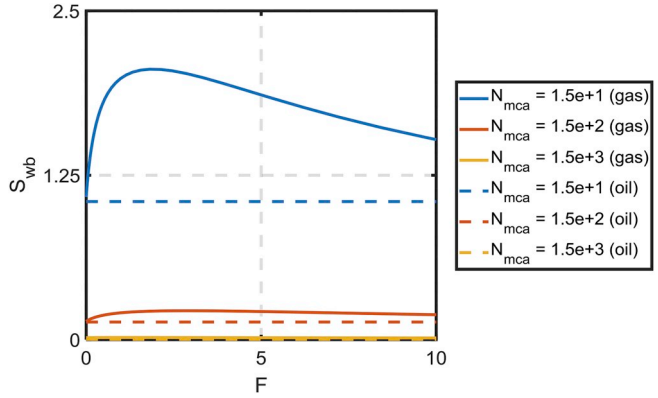

Fig. 11. Comparison of the water block skin calculated using the model for gas to the model for oil.

likely it is that water block is present.

After completion, a memory production logging tool (MPLT) test was performed. It gives the downhole measurements of pressure and rate during a short period of shut-in and production. The MPLT test is used to determine rate allocated to each production interval and is also used to give an indication of pressure drop during production of well life and shut in periods.

The well had a period where it was shut-in for a few days. The bottom-hole pressure during the shut-in is calculated from measured tubing head pressure and adding the same pressure drop determined from the MPLT shut-in test. The bottom-hole pressure during build-up is used to estimate initial reservoir pressure using pressure transient analysis equations implemented in the KAPPA software package Saphir. Pressure transient analysis equations are presented in Appendix A. The initial reservoir pressure determined was 14.7 MPa.

During the production period, the wellhead pressure and gas flow rate were measured every 4 h. The pressure drop from wellhead to the bottom-hole was calculated using Gray's correlation (Gray, 1974) implemented in Petroleum Experts' software PROSPER.

The production rate and bottom-hole flowing pressure data are used to calculate the permeability and drainage area using the rate transient analysis equations implemented in the KAPPA software Topaz. The rate transient analysis equations are presented in Appendix B. The determined interval permeability and drainage area were 0.0875 mD and 3.57×10^4 m^2 respectively.

The well has radius $r_w = 0.0787$ m and logging tools give porosity estimate of $\phi = 0.1$ and height $h = 6.1$ m. Since there is no well test to determine the fracture half-length of this particular interval, fracture half-length given from simulation results is used. Fracture stimulation simulation estimated an effective fracture half length of 17.4 m.

Core samples of the Patchawarra sand were taken from seven nearby wells. From these core samples mercury injection capillary (MICP) tests were performed. The Leverett *J* function was calculated for all of the cores.

8.2. Depletion model

The original gas in place (*OGIP*) is determined using initial reservoir pressure and drainage area from the following equation:

$$OGIP = Ah\phi(1 - s_{wi})\frac{p_i T_{sc} z_{sc}}{p_{sc} T z_i} \tag{60}$$

where A is the drainage area. The subscript i represents initial reservoir conditions. Volumetric drive with no water drive is assumed. The average reservoir pressure $\bar{p}$ is determined from the material balance equation:

$$\frac{\bar{p}}{\bar{z}} = \frac{p_i}{z_i}\left(1 - \frac{Q_p}{OGIP}\right) \tag{61}$$

where Q_p is the cumulative volume of gas produced. The measured gas flow rate q_g, calculated bottom-hole pressure p_{wf} and the calculated average reservoir pressure during the first year of production are given in Fig. 12a. The plot of $\bar{p}/\bar{z}$ against cumulative produced volume is given in Fig. 12b. The estimated depletion during the production period is given by the blue line.

8.3. Evaluating skin from production data

During the infinite acting radial flow regime the skin can be determined from (Bourdet, 2002):

$$S = \frac{1}{0.87}\left[\frac{2\pi kh}{q_g}\frac{z_{sc}T_{sc}}{p_{sc}T}(\psi(p_i) - \psi(p_{wf})) - \log\left(\frac{kt}{\phi\mu_g c_t r_w^2}\right) + 3.23\right] \tag{62}$$

where t is the production time and c_t is the total compressibility. The time for pseudo steady state to be reached is (Bourdet, 2002):

$$t_{PSS} = \frac{\phi\mu c_t r_e^2}{4k} \tag{63}$$

After pseudo steady state is reached, the equation for skin can be determined from (Ahmed and McKinney, 2005):

$$S = \frac{\pi kh}{q_g}\frac{z_{sc}T_{sc}}{p_{sc}T}(\psi(\bar{p}) - \psi(p_{wf})) - \ln\left(\frac{r_e}{r_w}\right) + 0.75 \tag{64}$$

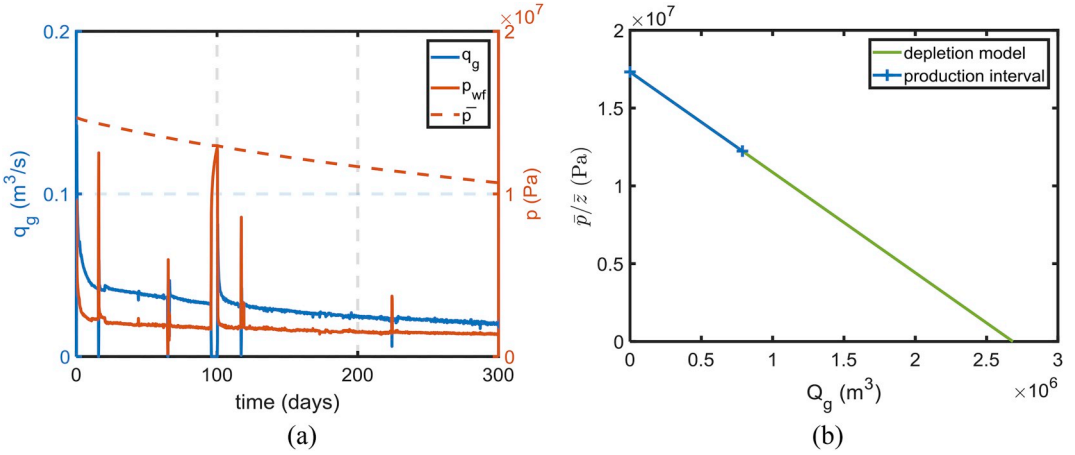

Fig. 12. Data from Cooper basin well and its estimated reservoir pressure: (a) measured gas flow rate, calculated bottom-hole pressure and calculated reservoir pressure; (b) The $\bar{p}/\bar{z}$ plot assuming volumetric depletion.

8.4. Tuning of well data by the analytical model

The model parameters C, λ and η are not known. With these parameters the model can give estimates of skin due to water block and non-Darcy flow. However, there can be more skin present due to other reasons, for example, drilling mud loss, proppant crushing and reservoir shape factor. When tuning the model to fit well production data, we added another constant, S_a, which represents the unaccounted for skin:

$$S = S_f + S_{wb} + S_{nd} + S_a \tag{65}$$

Parameters C, λ, η and S_a are tuned to fit the field estimate of skin. The results of tuning are presented in Fig. 13. Fig. 13a shows the comparison between modelled skin and calculated skin from production data and Fig. 13b shows comparison between tuned Leverett J function and the Leverett J function determined from mercury injection capillary pressure (MICP) tests.

Good fits were obtained for skin and the average J curve (i.e. $R^2 = 0.8$ for both cases) using the following parameter values: $C = 0.2$, $\lambda = 1.2$, $\eta = 13.95$, $S_a = 0.8$. The capillary pressure properties are within the same ranges as those in literature: C is between 0.01 and 0.6 (Desbarats, 1995; Thungsuntonkhun and Engler, 2004), and λ is between 0 and 7 (Leverett, 1941). For an irreducible water saturation range between 0 and 0.4, the empirical correlation given by Huet et al. (2005) gives C values between 0.11 and 0.17 and λ values between 0.85 and 0.9. These empirical values are not unreasonably far from the tuning results.

The tortuosity coefficient $\eta = 13.95$ is high compared to literature values, which are typically given as 0.5 or 2 (Mualem, 1976). However, when compared to the measured relative permeability in an analogous core, it has similar curvature, albeit a much smaller irreducible water saturation. The relative permeability comparison between the analogous core and the model is given in Fig. 13c.

9. Discussion

9.1. Discussion of the case study

The case study shows that water block can increase as the well depletes. As the gas flow rate decreases with well life, the modified capillary number and the dimensionless Forchheimer number will decrease, which can cause water block skin to increase. Thus, water block can be a reasonable explanation for the increase in skin. The water which forms the water block can come from more than one source, such as from the hydraulic fracturing operation or from the reservoir. During shut-in periods water from other intervals can also imbibe into the formation from the wellbore.

However, in order for water block skin to explain all of the increase in skin for the case study well, the tortuosity index in the relative permeability curve needs to be higher than that given in literature. This indicates that there may be additional skin effects not accounted for, such as scaling or depletion of other flow intervals, which can also contribute to the rise in skin. The existence of other factors contributing to skin is expected and the modelling results show that water block is a potential contributor.

Another explanation for the high tortuosity index is that the relative permeability model used does not account for any change in irreducible water saturation. Given that tight sands can sometimes exhibit sub-irreducible water saturations, they can be more sensitive to non-native water introduced from the fracture (Bennion and Thomas, 2005). Not accounting for this effect can cause the model to under-estimate water block skin if given a lower tortuosity index.

The case study does not conclusively prove that water block is the only cause of increasing skin. However, water block has been shown to be a potential explanation for this phenomenon. The model can be applied for estimating if the water block is significant enough to warrant intervention.

9.2. Applications of the models

In this paper we have converted the model for inflow of compressible gas with capillary entrapped water, given by Eqs. (1)–(3) to the Laplace equation. We have used the solution of the Laplace equation to calculate inflow performance of a fractured well in an ellipsoid reservoir. The method of conformal mapping and the Schwarz–Christoffel integral allow deriving the exact solutions for multiple well placement geometries and reservoir shape factors (Lavrentev and Shabat, 1977; Bedrikovetsky, 2013).

This work allows for estimating the improvement of productivity index from coreflood tests. Parvazdavani et al. (2014) presented the effect of nanoparticles which decrease the interfacial tension by 8 mN/m and improve relative permeability to oil. Results of the relative permeability measured before and after nano-fluid injection are presented in Fig. 14a. Substitution of the relative permeability curves and the interfacial tension values before and after treatment into Eq. (59) allow for the determination of skin improvement. Water block skin values for before and after treatment are presented in Fig. 14b.

The dimensionless numbers, F and N_{mca}, presented in this paper can be used as a screening criterion for well candidates in re-fracture treatments and chemical treatments. At high dimensionless Forchheimer numbers, re-fracturing can give the additional benefit of reducing non-Darcy skin on top of increasing half-length. Surfactant or

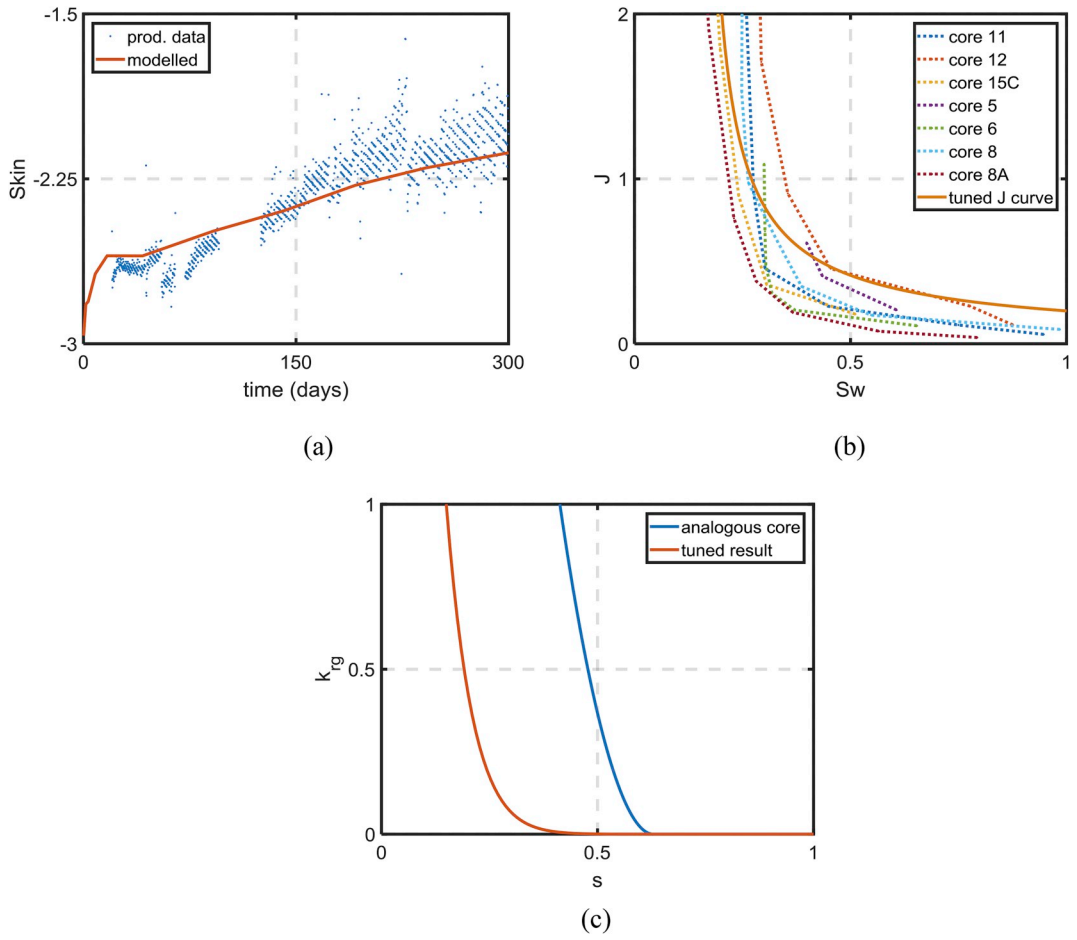

Fig. 13. Tuning the semi-analytical model to match the skin in fractured well: (a) skin for the well; (b) tuned Leverett *J* function curve; (c) comparison of relative permeability for the Cooper well to an analogous core.

nanoparticle treatment will reduce the capillary trapping of water (Towler et al., 2017; Xie et al., 2009; Ni et al., 2016), which is useful at low modified capillary numbers.

We show that the ratio of viscous to capillary forces and the magnitude of the Leverett *J* function control the water block skin. The values for the Leverett *J* function constants and the relative permeability tortuosity term can vary greatly and are the most important parameters to determine the likelihood of water block under steady flow. Generally in literature it has been reported that low permeability rocks can exhibit high skin due to water blockage (Bazin et al., 2010; Bahrami et al., 2011). This can be due to low permeability correlating with high dimensionless entry pressure and low pore size distribution index (Huet et al., 2005).

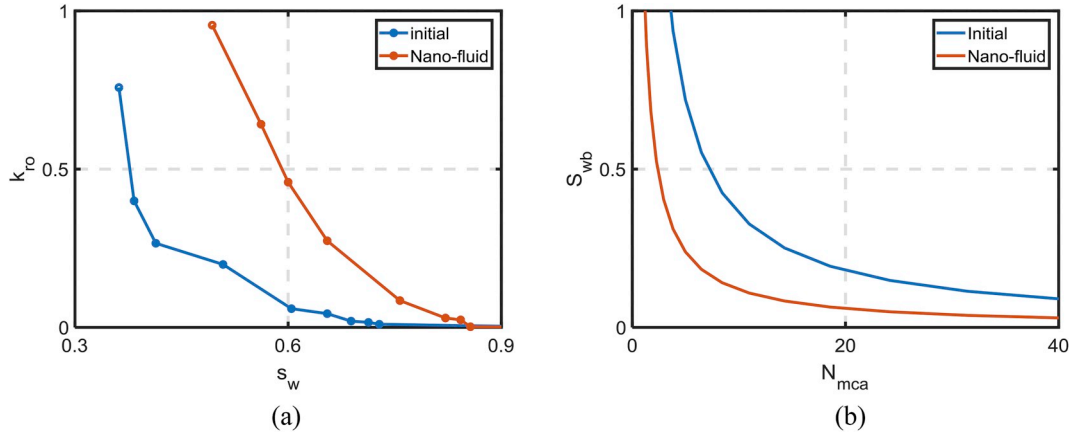

Fig. 14. Example case of core flood data used to estimate water block skin reduction: (a) measured relative permeability; (b) prediction of skin reduction due to application of Nano-fluid. Experimental data taken from Parvazdavani et al. (2014).

9.3. Limitations of the model

The model applied in this study (Eq. (43)) assumes infinite fracture conductivity and neglects pressure variation inside the fracture. The method of extending the model to account for hydraulic fracture conductivity can be found in the work of Economides and Nolte (1989).

The proposed model only considers steady state flow. However, the transient flow regime can be longer in low permeability reservoirs. The dynamic drainage area during transient flow and inflow performance equations during transient flow regime are given by Yuan et al. (2016). The current work can be extended to account for transient flow via conformal mapping to the dynamic drainage volume during the transient flow regime.

The model only considers homogeneous permeability. As permeability heterogeneity can affect capillary pressures near to the fracture face, water saturations near to the fracture will also be affected. The fracture flow back period and transient effects accounting for permeability heterogeneity and capillary pressure effects can be studied using a numerical reservoir simulator.

The model describes saturation distribution around the fractured production well and the skin factor accounting for capillary entrapped water. The model is not affected by the source of the water. However, the relative permeability and capillary pressure forms can be adjusted to account for the water source. In the case of fracture fluid leak off, fracture fluid first imbibes into the reservoir and then the gas will flow into the fracture. The gas inflow can be considered a secondary drainage process. The viscosity of the fracture fluid can change throughout this process. The hysteretic effects will need to be accounted for in the relative permeability and capillary-pressure curves.

After hydraulic fracturing, water block can be cleaned up from two dominant mechanisms; flow back and evaporation (Kamath and Laroche, 2003). Evaporative effects are dependent on flow rate, bottom hole flowing pressure and volatility of the gas. If the reservoir is completely dry, evaporative effects can remove the water film formed on the hydraulic fracture. This study neglects evaporative effects and is applicable for production after the clean-up of fracture fluid.

Adding energy conservation equation to the governing system (1–3) yield generalisation of this work for commingled production of water and steam from geothermal wells (Palabiyik et al., 2013; Tureyen et al., 2014).

The developed analytical model (30–33) does not account for fines migration, induced by shear from the fractured leak-off fluid, and consequent permeability decline (Bedrikovetsky et al., 2011, 2012). Another important permeability decline effect in fractured gas wells is the fracturing fluid leak-off containing suspended particles generated during fracture opening and propagation, yielding size exclusion, attachment and pore plugging (Bedrikovetsky et al., 2017).

Nomenclature

a	arc length, m
A	drainage area, m^2
A_d	dimensionless drainage area
b	Klinkenberg factor, Pa
B	formation volume factor
c_t	total compressibility, Pa^{-1}
C	dimensionless entry pressure
$\hat{e}$	unit vector
F	dimensionless Forchheimer number
G	inverse of dimensionless perimeter of ellipse
h	reservoir height, m
h_ξ	scale factor for the ξ coordinate
h_θ	scale factor for the θ coordinate
$OGIP$	original gas in place, m^3
J	Leverett J-function
k	permeability, m^2

Rock compressibility, which is very important for shale gas and oil reservoirs, can be implemented in the model by pressure-dependent porosity (Jiang and Younis, 2016; Huang et al., 2018).

10. Conclusions

This paper has extended the analytical models for 1D flow of compressible gas under the presence of capillary entrapped water derived by Naik et al. (2018) to 2D inertial and non-inertial flows around fractured wells. Besides revealing the saturation and pressure distribution around the fracture, the modelling was also able to unravel the impact of the interplay of capillary, viscous, inertial forces on the water block and non-Darcy skin. It allows us to conclude as follows:

1. The problem of 2-D non-inertial gas inflow towards a fractured well under the presence of capillary-trapped liquid allows for an exact solution. The explicit formulae for flow potential distribution is obtained by conformal mapping.
2. The solution defines implicit formulae for pressure and saturation distribution around the well. The skin as a result of water block around a hydraulic fracture is determined implicitly.
3. The competing effects of gas compression and inertial forces result in a non-monotonic relationship between water block skin and the dimensionless Forchheimer number.
4. Water block skin is sensitive to pore size distribution index λ and dimensionless entry pressure C. Skin due to water block can be small in low permeable formations despite high capillary pressure values if λ is large or if C is low.
5. The inflow-performance problem accounting for capillary-trapped fluid and gas inertia in the near-wellbore region can be solved using the stream-line method. Comparison with high-accuracy numerical solution exhibits high agreement ($R^2 = 0.97$).
6. There is a steep increase in water saturation close to the fracture face, which creates a major portion of the water block skin. The water block skin resulting from water inside some region close to the fracture face can be estimated implicitly from the model, which consequently provides an estimate for volume of chemical treatment required.

Acknowledgements

The authors would like to acknowledge the engineering students Emily Walker and Antreas Florentzou. Their honours research project assisted us in selecting the well candidate for the field case study. The authors are grateful to Eng. Mark Burgoyne (Santos Ltd) for the fruitful discussions. Many thanks are due to Dr. Themis Carageorgos and Mr. Thomas Russell for proofreading and providing feedback on the text.

k_{kg}	Klinkenberg correction coefficient
k_{rg}	relative permeability to gas
L_e	drainage boundary for linear flow model, m
M	molar mass, kg/mol
N_{mca}	modified capillary number
p	pressure, Pa
$\overline{p}$	average reservoir pressure, Pa
p_{ws}	bottom-hole shut-in pressure, Pa
P	dimensionless pressure, Pa
q_g	flow rate, m^3/s
Q_p	cumulative volume of gas produced, m^3
r	radius, m
r_w	wellbore radius, m
R	universal gas constant, 8.3144621 J/Mol·K
s	water saturation
s_n	normalised water saturation
s_e	boundary saturation\
s_{gr}	irreducible gas saturation
s_{wirr}	irreducible water saturation
S	skin
S_a	summation of the unaccounted skin
S_{wb}	water block skin
S_f	hydraulic fracture skin
S_{nd}	non-Darcy skin
t	time, s
t_{MB}	material balance time, s
t_{PSS}	beginning of pseudo-steady state time, s
t_{sup}	superposition time, s
T	temperature, K
u	velocity at surface conditions, m/s
x	Cartesian coordinate parallel to fracture, m
X	dimensionless Cartesian coordinate parallel to fracture
x_f	facture half length, m
y	Cartesian coordinate perpendicular to fracture, m
Y	dimensionless Cartesian coordinate perpendicular to fracture
z	compressibility factor

Greek Letters

β	Forchheimer coefficient, m^{-1}
η	tortuosity index
θ	elliptic coordinate which scales with the stream function
ϕ	porosity
λ	pore size distribution index
μ	viscosity, Pa·s
ξ	elliptic coordinate which scales with the potential
σ	interfacial tension, N/m
Φ	potential, m^2/s
ψ	modified pseudo-pressure, Pa/s

Subscripts

e	drainage boundary
D	water block damage boundary
i	initial reservoir conditions
g	gas
k	time period
o	oil
sc	standard conditions
w	water
wf	bottom-hole at flowing conditions
θ	in the direction of elliptic coordinate θ
ξ	in the direction of elliptic coordinate ξ

Appendix A. Pressure transient analysis equations

The build-up period can be preceded by multi-rate production. During build up, the difference between initial reservoir pseudo pressure, $\psi(p_i)$, and current static bottom-hole pseudo pressure $\psi(p_{ws})$, is given by (Bourdet, 2002):

$$\psi(p_i) - \psi(p_{ws}) = \frac{p_{sc}T}{z_{sc}T_{sc}}\frac{t_{\sup}}{2\pi kh} \tag{A-1}$$

where t_{sup} is the multi-rate superposition time expressed as:

$$t_{\sup} = \sum_{k=1}^{k=n} (q_k - q_{k-1})\log(t_c + \Delta t - t_{k-1}) \tag{A-2}$$

where q_k is flow rate during period k and t_k is time at end of period k.

Appendix B. Rate transient analysis equations

To identify flow regimes and characterize reservoir properties, production data can be plotted on a diagnostic plot. The diagnostic plot is a log-log plot of the derivative of the difference between the initial reservoir pseudo pressure ψ(pi) and the current flowing bottom hole pseudo pressure ψ(Pwf) against material balance time tMB. The usage of material balance allows for conversion of production data into an equivalent constant rate drawdown with rate qe (Ahmed and McKinney, 2005):

$$t_{MB} = \frac{Q_p}{q_e} \tag{B-1}$$

where Q_g is the cumulative volume of gas produced. Let us define the pseudo pressure drop derivative as:

$$\psi' = t_{MB}\frac{d(\psi(p_i) - \psi(p_{wf}))}{dt_{MB}} \tag{B-2}$$

From the diagnostic plot the pseudo radial flow regime can be determined from a constant value of the derivative plot (Ahmed and McKinney, 2005). The value of the constant can be used to determine permeability:

$$\log(\psi') = \log\left(\frac{1}{2\pi kh}\frac{p_{sc}T}{z_{sc}T_{sc}}\frac{1}{\ln(10)}\right) \tag{B-3}$$

References

Ahmed, T., McKinney, P., 2005. Advanced Reservoir Engineering. Elsevier, Burlington, MA.

Bahrami, H., Rezaee, M.R., Nazhat, D.H., Ostojic, J., Clennell, M.B., Jamili, A., 2011. Effect of water blocking damage on flow efficiency and productivity in tight gas reservoirs. In: Paper SPE-142283, Presented at the SPE Production and Operations Symposium, Oklahoma, USA, pp. 27–29 (March).

Barenblatt, G.I., Entov, V.M., Ryzhik, V.M., 1989. Theory of Fluid Flows through Natural Rocks. Springer, Amsterdam, The Netherlands.

Bazin, B., Peysson, Y., Lamy, F., Martin, F., Aubry, E., Chapuis, C., 2010. In-situ water-blocking measurements and interpretation related to fracturing operations in tight gas reservoirs. SPE Prod. Oper. 25 (4), 431–437.

Bear, J., 2013. Dynamics of Fluids in Porous Media. Dover Publications, New York.

Bedrikovetsky, P., 2013. Mathematical Theory of Oil and Gas Recovery: with Applications to Ex-USSR Oil and Gas Fields, vol. 4 Springer Science & Business Media.

Bedrikovetsky, P., Siqueira, F.D., Furtado, C., de Souza, A.L.S., 2011. Modified particle detachment model for colloidal transport in porous media. Journal of Transport in Porous Media 86, 353–383.

Bedrikovetsky, P., Zeinijahromi, A., Siqueira, F.D., Furtado, C., de Souza, A.L.S., 2012. Particle detachment under velocity alternation during suspension transport in porous media. Journal of Transport in Porous Media 91 (1), 173–197.

Bedrikovetsky, P., You, Z., Badalyan, A., Osipov, Yu, Kuzmina, L., 2017. Analytical model for straining-dominant large-retention depth filtration. Chem. Eng. J. 330, 1148–1159.

Bennion, D.B., Thomas, F.B., 2005. Formation damage issues impacting the productivity of low permeability, low initial water saturation gas producing formations. J. Energy Resour. Technol. 127 (3), 240–247.

Bourdet, D., 2002. Well Test Analysis – the Use of Advanced Interpretation Models. Elsevier, Amsterdam, The Netherlands.

Brooks, R.H., Corey, A.T., 1964. Hydraulic Properties of Porous Media. Hydrology Paper No. 3. Colorado State University, Fort Collins, Colorado, pp. 22–27.

Civan, F., 2015. Reservoir Formation Damage, third ed. Gulf Professional Publishing, Huston, TX.

Dake, L.P., 2013. The Practice of Reservoir Engineering, vol. 36 Elsevier, Amsterdam, The Netherlands.

Desbarats, A.J., 1995. Upscaling capillary pressure-saturation curves in heterogeneous porous media. Water Resour. Res. 31 (2), 281–288.

Economides, M.J., Nolte, K.G., 1989. Reservoir Stimulation, vol. 2 Prentice Hall, Englewood Cliffs, NJ.

Gray, H.E., 1974. Vertical Flow Correlation in Gas Wells. User Manual for API14B, Subsurface Controlled Safety Valve Sizing Computer Program.

Hale, B., Evers, J.F., 1981. Elliptical flow equations for vertically fractured gas wells. J. Pet. Technol. 33 (12), 2489–2497.

Huang, S., Ding, G., Wu, Y., Huang, H., Lan, X., Zhang, J., 2018. A semi-analytical model to evaluate productivity of shale gas wells with complex fracture networks. J. Nat. Gas Sci. Eng. 50, 374–383.

Huet, C.C., Rushing, J.A., Newsham, K.E., Blasingame, T.A., 2005. A modified purcell/burdine model for estimating absolute permeability from mercury-injection capillary pressure data. In: Presented at the International Petroleum Technology Conference, Doha, Qatar, pp. 21–23 (November).

Jiang, J., Younis, R.M., 2016. Compositional modeling of enhanced hydrocarbons recovery for fractured shale gas-condensate reservoirs with the effects of capillary pressure and multicomponent mechanisms. J. Nat. Gas Sci. Eng. 34, 1262–1275.

Jones, F.O., Owens, W.W., 1980. A laboratory study of low-permeability gas sands. J. Pet. Technol. 32 (9), 1631–1640.

Kamath, J., Laroche, C., 2003. Laboratory-based evaluation of gas well deliverability loss caused by water blocking. SPE J. 8 (01), 71–80.

Lake, L.W., Johns, R.T., Rossen, W.R., Pope, G.A., 2014. Fundamentals of Enhanced Oil Recovery. Society of Petroleum Engineers, Richardson, TX, USA.

Lavrentev, M.A., Shabat, B.V., 1977. Hydrodynamics Problems and Their Mathematical Models. Moscow, Russia.

Lee, J., 1982. Well Testing. Society of Petroleum Engineers, Richardson, TX, USA.

Leverett, M., 1941. Capillary behavior in porous solids. Transactions of the AIME 142 (01), 152–169.

Mualem, Y., 1976. A new model for predicting the hydraulic conductivity of unsaturated porous media. Water Resour. Res. 12 (3), 513–522.

Naik, S., You, Z., Bedrikovetsky, P., 2015. Rate enhancement in unconventional gas reservoirs by wettability alteration. J. Nat. Gas Sci. Eng. 26, 1573–1584.

Naik, S., You, Z., Bedrikovetsky, P., 2018. Productivity index enhancement by wettability alteration in two-phase compressible flows. J. Nat. Gas Sci. Eng. 50, 101–114.

Ni, G., Cheng, W., Lin, B., Zhai, C., 2016. Experimental study on removing water blocking effect (WBE) from two aspects of the pore negative pressure and surfactants. J. Nat. Gas Sci. Eng. 31, 596–602.

Palabiyik, Y., Tureyen, O.I., Onur, M., Deniz, M., 2013. February. A study on pressure and temperature behaviors of geothermal wells in single-phase liquid reservoirs. In: Proceedings of the Thirty-Eighth Workshop on Geothermal Reservoir Engineering.

Parvazdavani, M., Masihi, M., Ghazanfari, M.H., 2014. Monitoring the influence of dispersed nano-particles on oil–water relative permeability hysteresis. J. Pet. Sci. Eng. 124, 222–231.

Pascal, H., Quillian, R.G., 1980. Analysis of vertical fracture length and non-Darcy flow coefficient using variable rate tests. In: SPE Annual Technical Conference and Exhibition. Society of Petroleum Engineers.

Prats, M., 1961. Effect of vertical fractures on reservoir behavior-incompressible fluid case. Soc. Petrol. Eng. J. 1 (02), 105–118.

Shampine, L.F., Reichelt, M.W., 1997. The matlab ode suite. SIAM J. Sci. Comput. 18 (1), 1–22.

Tang, K.T., 2007. Mathematical Methods for Engineers and Scientists, vol. 1 Springer, New York.

Thungsuntonkhun, W., Engler, T.W., 2004. Applying NMR-hydraulic flow unit technique to estimate J-function and capillary pressure. In: Paper SPWLA-2004-EE, Presented at the SPWLA 45th Annual Logging Symposium, Noordwijk, Netherlands, pp. 6–9 (June).

Towler, B.F., 2002. Fundamental Principles of Reservoir Engineering. SPE Textbook Series, (8).
Towler, B.F., Lehr, H.L., Austin, S.W., Bowthorpe, B., Feldman, J.H., Forbis, S.K., Germack, D., Firouzi, M., 2017. Spontaneous imbibition experiments of enhanced oil recovery with surfactants and complex nano-fluids. J. Surfactants Deterg. 20 (2), 367–377.
Tureyen, O.I., Sarak, H., Gulgor, A., Erkan, B., Satman, A., 2014. February. A study on the production and reservoir performance of the Germencik geothermal field. In: Proceedings of the Thirty-Ninth Workshop on Geothermal Reservoir Engineering.
Van Duijn, C.J., Molenaar, J., De Neef, M.J., 1995. The effect of capillary forces on immiscible two-phase flow in heterogeneous porous media. Transport Porous Media 21 (1), 71–93.
Xie, X., Liu, Y., Sharma, M., Weiss, W.W., 2009. Wettability alteration to increase deliverability of gas production wells. J. Nat. Gas Sci. Eng. 1 (1–2), 39–45.
Yuan, B., Wood, D.A., 2015. Production analysis and performance forecasting for natural gas reservoirs: theory and practice (2011–2015). J. Nat. Gas Sci. Eng. (26), 1433–1438.
Yuan, B., Wood, D.A., Yu, W., 2015. Stimulation and hydraulic fracturing technology in natural gas reservoirs: theory and case studies (2012–2015). J. Nat. Gas Sci. Eng. (26), 1414–1421.
Yuan, B., Moghanloo, R.G., Shariff, E., 2016. Integrated investigation of dynamic drainage volume and inflow performance relationship (transient IPR) to optimize multistage fractured horizontal wells in tight/shale formations. J. Energy Resour. Technol. 138 (5).

6. Application of Percolation theory, Critical Path Theory and Effective Medium Theory for calculation of two phase relative permeability

Statement of Authorship

Title of Paper	Application of Percolation theory, Critical Path Theory and Effective Medium Theory for calculation of two phase relative permeability.
Publication Status	☐ Published ☐ Accepted for Publication ☐ Submitted for Publication ☑ Unpublished and Unsubmitted work written in manuscript style
Publication Details	

Principal Author

Name of Principal Author (Candidate)	Saurabh Naik		
Contribution to the Paper	Problem formulation, literature review, development of mathematical models, implementation of mathematical solutions in Mat-lab, creating figures, analysis of results, writing the manuscript		
Overall percentage (%)	80%		
Certification:	This paper reports on original research I conducted during the period of my Higher Degree by Research candidature and is not subject to any obligations or contractual agreements with a third party that would constrain its inclusion in this thesis. I am the primary author of this paper.		
Signature		Date	

Co-Author Contributions

By signing the Statement of Authorship, each author certifies that:

i. the candidate's stated contribution to the publication is accurate (as detailed above);

ii. permission is granted for the candidate to include the publication in the thesis; and

iii. the sum of all co-author contributions is equal to 100% less the candidate's stated contribution.

Name of Co-Author	Kirill Gerke		
Contribution to the Paper	developing numerical simulation results for validation, support on literature review, Reviewing manuscript, editing manuscript		
Signature		Date	31.07.2019

Name of Co-Author	Zhenjiang You		
Contribution to the Paper	reviewing manuscript, editing manuscript		
Signature		Date	1/8/19

Name of Co-Author	Pavel Bedrikovetsky		
Contribution to the Paper	reviewing manuscript		
Signature		Date	03/08/2019

Please cut and paste additional co-author panels here as required.

Application of Percolation theory, Critical Path Theory and Effective Medium Theory for calculation of two phase relative permeability

Saurabh Naik[a], Kirill M. Gerke[b], Zhenjiang You[c], Pavel Bedrikovetsky[a]

[a] The University of Adelaide, South Australia, Australia

[b] Schmidt's Institute of Physics of the Earth of Russian Academy of Sciences, Moscow, Russia

[c] Institute of Geosphere's Dynamics of Russian Academy of Sciences, Moscow, Russia

[d] Dokuchaev Soil Science Institute of Russian Academy of Sciences, Moscow, Russia

[e] Kazan Federal University, Kazan, Russia

[f] Moscow Institute of Physics and Technology, Dolgoprudny, Russia[g] The University of Queensland, Queensland, Australia

Keywords: Percolation theory; capillary pressure; relative permeability; effective medium theory; critical path theory; pore-network model.

Abstract

There has been active development of numerical pore network simulation models in recent years. These models allow for generation of capillary pressure and relative permeability curves which characterise two-phase immiscible flow in porous media. However, percolation models provide an efficient alternative, with reduced reliance on numerical techniques. Implementation of effective medium or critical path theory with the percolation model allows for evaluation of the relative permeability curves. This paper compares a percolation model with effective medium approximation and a percolation model with critical path approximation against a sophisticated pore network simulator during the drainage of water by oil. Both approximations failed to match the irreducible water saturation for water relative permeability. While the effective medium approximation poorly matches the pore network simulator, the critical path approximation is shown to match the result of the oil relative permeability. Despite the difference in end points, there is qualitative agreement between critical path approximation and the pore network simulator. Moreover, observed differences are not necessarily a drawback due to important boundary effects as discussed in the paper. Our results indicate that percolation theory made predictions have a potential to become an efficient tool for upscaling by computing multi-phase flow properties for numerous porosity sub-domains.

1. Introduction

Prediction of the porous media flow properties is important in numerous disciplines, notable examples include hydrocarbon extraction (Sahimi, 2011; Blunt, 2017) and the design of fluid injection programs for underground reservoirs (Zeinijahromi et al., 2013; Godinho et al., 2016). The relative permeability curves play essential roles in parameterizing continuum media models and simulating large scale flow and transport phenomena.

In particular, in reservoirs which contain large changes in permeability or capillary pressure, the forms of the capillary pressure and relative permeability curves will have strong impact on the performance of the extraction or injection program. Close to the wellbore, there can be a large reduction in capillary pressure. The saturation and pressure profile close to the wellbore can be highly affected by the aforementioned curves.

Such curves will be influenced by the physical characteristics of the pore network, the surface of the solid walls and the interfacial properties of the two phases. To appropriately model the influence of interfacial tension reduction or contact angle alteration, so-called pore-scale modelling techniques are invaluable as, unlike laboratory measurement, they allow to perform numerous experiments using the same digital pore structure model. The latter can be obtained using X-ray computed tomography (XCT) (Cnudde and Boone, 2013), stochastic reconstructions (Adler et al., 1990; Yeong and Torquato, 1998; Jiao and Chawla, 2014; Gerke et al., 2014; Thovert and Adler, 2011; Tahmasebi et al., 2012) or their superposition (Li et al., 2014; Li et al., 2017).

A variety of computational methods exist to simulate single and multiphase fluid flow within heterogeneous pore spaces. Among the most popular are the: 1) Lattice Boltzmann method (Khirevich et al., 2015; Dashtian et al., 2019); 2) finite element, finite volume and volume of fluid methods (Raeini et al., 2012; Bilger et al., 2017); 3) smoothed particle hydrodynamics (Holmes et al., 2016); 4) finite-difference and Laplace Stokes equation solvers (Shabro et al., 2012; Gerke et al., 2018); 5) level set (Bilger et al., 2017; Verma et al., 2018); 6) phase-field (Frank et al., 2018; Rokhforouz and Amiri, 2017) and density functional theory based (Demianov et al, 2011) methods. While debates about the advantages and downsides of each approach are far from settling down, even with modern parallelized computations and hardware, all these methods are extremely computationally intensive. This limits the size of the simulation domain that can be evaluated to a very limited volume of usually $300\text{-}700^3$ voxels, while the time needed with high performance computing (HPC) resources easily reaches several weeks. For complex and hierarchical porous media, the problem is exacerbated due to the need to work on as large as possible 3D pore geometries to capture the REV of a porous medium or to work on fused 3D structure models resulting from a number of multiscale images for samples such as shales (Gerke et al., 2015; Tahmasebi, 2018), carbonates (Bultreys et al., 2015) or soils (Karsanina et al., 2018). It is safe to conclude that such direct pore-scale modelling techniques are too computationally expensive to routinely process REVs of real rock samples.

To make pore-scale simulations for complex hierarchical porous media practical one can utilize indirect modelling methods such as pore-network models (PNM) (Fatt, 1956a,b,c; Xiong et al., 2016; Gostick et al., 2016). There have been classical pore-network simulation models developed by Oren, et al. (1997) and Valvatne and Blunt (2004) which can calculate the relative permeability and capillary pressure curves accounting for wettability and interfacial tension effects in the quasi static regime. While significantly reducing the complexity of the simulations, PNMs can suffer minimal accuracy reductions if parameterized using abovementioned direct pore-scale simulations (Miao et al., 2017; Raeini et al., 2017). Although PNMs allow a very efficient computational framework to simulate single-, two- and even three-phase (Pereira et al., 1996; Van Dijke and Sorbie, 2002; Piri and Blunt, 2005) flow, if one fuses macro and micro XCT scans with stochastic reconstructions (Karsanina and Gerke, 2018; Chen et al., 2019) based on SEM or FIB-SEM images it is easy to hit more than 10^{10} pore-network elements where even PNM simulations can get prohibitive.

Another alternative to simulate flow properties even faster than PNM would be percolation models. The critical parameters which are required to analytically evaluate the network properties in percolation models only depend on the lattice type and the dimension of the network. Given that we have a reasonable estimate of a lattice which represents natural porous media and that the critical parameters have already been evaluated, properties such as the percolation threshold, and infinite cluster strength can be evaluated analytically. This allows for an analytical evaluation of the capillary pressure curve, as shown in Heiba et al. (1992) and Larson et al. (1981).

However, the calculation of relative permeability is more challenging. While there are analytical expressions for network conductivity, they are for Bethe lattices (Heiba, et al., 1983), which are not representative of natural porous media. Blunt et al. (1992) provided an analytical expression for relative permeability, assuming saturation as equal to site occupancy and applying the percolation expression for conductivity. However, the conductivity calculated using the percolation expression does not account for variability in the bond conductivity distribution. Natural porous media have a variety of pore throat sizes, and consequently a variety of values for conductivity. A more complicated approach is required when bond conductance is disordered.

One approach for disordered media is effective medium theory (EMT). Kirkpatrick (1973) presents the numerical validation of the EMT and shows that it accurately describes the conductivity of the bond percolation problem, except close to the percolation threshold. There have been numerous publications on the application of effective medium theory for calculation of relative permeability. However, the application of effective medium theory has had varying degrees of success.

Ghanbarian, et al. (2016) apply EMT but replace bond occupation directly with saturation. Close to threshold they use the percolation expression instead of EMT to calculate relative permeability. They find percolation exponents by fitting to capillary pressure data. Under this approach, they achieve good results for 14 out of 21 of the laboratory samples. They discuss that the deviation can occur from neglecting corner & film flow. Ghanbarian and Hunt (2017) improved on this work by incorporating pore-solid interface roughness effects in the hydraulic conductance of bonds. However, the model still under predicted the unsaturated hydraulic conductivity.

The aim of this paper is to build upon previous knowledge and improve percolation models to determine the efficacy of effective medium theory for calculation of two-phase relative permeability as verified by comparison against conventional pore-network model. Bond percolation models previously developed have required some correction to the relationship bond radius shared with volume and conductivity by some empirical term (Heiba, et al., 1983; Heiba, et al., 1992) in order to achieve realistic relative permeability curves. The SEM or FIB-SEM techniques used to generate pore network models create distributions for pore bodies and pore throats. In order to properly for the difference in pore body and pore throat distributions a more sophisticated percolation model is developed. For the first time we apply bond-site percolation to describe two-phase immiscible flow. This allows us to account for variability in pore body and throat sizes, without utilizing empirical parameters. Irregularity of the pore shape is accounted for by including corner flow in the pore bodies and pore throats. The effective medium approximation is applied for calculation of relative permeability for both phases. Hunt (2001) mentioned that critical path theory may be superior for calculation of networks with highly disordered conductivity distributions. Critical path theory is also presented as an alternative approach for calculation of relative permeability.

This paper presents a new fast and robust percolation theory-based model to simulate single and two-phase flow within porous media with known pore size distributions. The model is presented in section 2. The generation of the input functions for the percolation model is described in section 3. A pore network simulator is compared to the percolation effective medium approach and the percolation critical path approach. The network simulator is described in section 4. The results of the comparison are presented in section 5. The discussion of the results is provided in section 6. Finally, the conclusions of the paper are presented in section 7.

2. Percolation model for oil-water drainage

Let us represent a porous medium as a simple cubic network. The network is composed of sites. Each site centre is separated by a distance l to the next adjacent site in each of the three dimensions of the Cartesian coordinate system. Each site is connected to the six nearest sites by a bond. Each site represents a pore body and each bond represents a pore throat. The pore bodies are modelled as cubes and the pore throats as triangular capillaries. The porous medium is assumed to be initially filled by water.

2.1. Calculation of the entry pressure and meniscus curvature

In order for oil to enter into a water wet pore body or throat it must displace the water. The interfacial energy between water and a water wet surface will be lower than oil and the water wet surface. The difference in interfacial energy represents the amount of work that must be done for the oil to displace the water. The pressure of the oil phase must be large enough for this work to be done. The pressure at which the oil phase will overcome the work required is called the entry pressure. The entry pressure can be calculated using the MS-P Method. The MS-P method involves equating the terminal meniscus curvature and the arc meniscus curvature to find the radius at which the displacing phase can enter the pore throat (Mason and Morrow, 1991).

During piston like displacement, the terminal meniscus curvature is defined by:

$$\frac{P_c}{\sigma_{ow}} = \frac{1}{r_d} \tag{1}$$

where p_c is capillary pressure, σ_{ow} is the interfacial tension between oil and water and r_d is the radius of curvature during drainage. The arc meniscus curvature during piston like displacement and under thermodynamic equilibrium is (Lago and Araujo, 2001):

$$\frac{P_c}{\sigma_{ow}} = \frac{L_{ow} + L_{os}\cos\theta}{A_{eff}} \tag{2}$$

where L_{ow} is the perimeter of the oil-water contact, L_{os} is the perimeter of the oil-solid contact, θ is contact angle and A_{eff} is the effective cross-sectional area of the oil. Substitution of (1) into (2) results in:

$$\frac{1}{r_d} = \frac{L_{ow} + L_{os}\cos\theta}{A_{eff}} \tag{3}$$

The cross section of a triangular capillary during MS-P displacement is given in Fig. 1.

2.2. Equations for arbitrary triangular capillaries

The dimensionless shape factor G is defined as the ratio between the area A, and the perimeter L squared (Mason and Morrow, 1991):

$$G = \frac{A}{L^2} \tag{4}$$

It can be calculated from the relationship between the three half-angles β_i (i=1,2,3) which make up the triangle:

$$G = \frac{1}{4\sum_{i=1}^{i=3} \cot \beta_i} \tag{5}$$

The perimeter of triangle can be calculated from the inscribed radius r_{in} and the shape factor:

$$L = \frac{r_{in}}{2G} \tag{6}$$

The area of the triangle can also be derived from the inscribed radius and the shape factor:

$$A = \frac{r_{in}^{\ 2}}{4G} \tag{7}$$

During the displacement of water by oil in a triangular capillary, the area and perimeter terms for arbitrary triangles are given by Øren et al., (1997):

$$A_{eff} = A - r_d^{\ 2} \sum_{i=1}^{i=3} \left[\frac{\cos\theta \cos(\theta + \beta_i)}{\sin \beta_i} + \theta + \beta_i - \frac{\pi}{2} \right] \tag{8}$$

$$L_{ow} = 2r_d \sum_{i=1}^{i=3} \left[\frac{\pi}{2} - \beta - \theta \right] \tag{9}$$

$$L_{os} = L - 2r_d \sum_{i=1}^{i=3} \left[\frac{\cos(\theta + \beta_i)}{\sin(\beta_i)} \right] \tag{10}$$

After substitution of Eqs. (4 - 10) into Eq. (3), the quadratic solution for r_d is:

$$r_d = \frac{r_{in} \cos\theta \left(-1 \pm \sqrt{1 + 4GD / \cos^2 \theta} \right)}{4GD} \tag{11}$$

where D is constant. The equation to calculate D is:

$$D = \sum_{i=1}^{i=3} \left[\frac{\cos\theta \cos(\theta + \beta_i)}{\sin \beta_i} + \theta + \beta_i - \frac{\pi}{2} \right] - 2\cos\theta \sum_{i=1}^{i=3} \left[\frac{\cos(\theta + \beta_i)}{\sin(\beta_i)} \right] + 2\sum_{i=1}^{i=3} \left[\frac{\pi}{2} - \beta - \theta \right] \tag{12}$$

2.3. Threshold radius for bonds and sites

Let us assume that all bonds and all sites are completely water wet, with θ = 0°. The smallest bond which can be entered by oil will have an inscribed radius which satisfies the following condition:

$$r_b = \frac{\sigma_{ow}}{P_c D_r} \tag{13}$$

where r_b is the inscribed radius of the bond and D_r is a constant. It is derived using MS-P theory:

$$D_r = \frac{-1 \pm \sqrt{1 + 4GD}}{4GD} \tag{14}$$

The smallest site which can be entered by oil will have an inscribed radius which satisfies the following condition:

$$r_s > \frac{2\sigma_{ow}}{P_c} \tag{15}$$

where r_s is the inscribed radius of the site.

2.4. Hydraulic conductance

The flow rate of the oil or water phase through a pore throat or pore body will depend on the shape, cross sectional area of the phase and the pressure drop. The velocity of each phase is proportional to pressure drop for that phase. The constant of proportionality is called the conductance.

The bonds are modelled as equilateral triangles. The conductance of an equilateral triangle g_b, is given by Patzek and Silin (2001). Their equation is applied for bond conductance g_b:

$$g_b = 0.6 G_t A^2 \tag{16}$$

where G_t is the shape factor for a triangle. Sites are modelled as cubes. The conductance of a square is given by Patzek and Silin (2001). Their equation is applied for the calculation of site conductance g_s:

$$g_s = 0.5623 G_s A^2 \tag{17}$$

where G_s is the shape factor for a triangle. The conductance of oil in centre of triangle is given by Øren et al., (1997). Their equation is used for the calculation of conductance to oil in bonds g_{ob}:

$$g_{ob} = 0.6 G_t A_{eff}^2 \tag{18}$$

The conductance of oil in centre of square is given by Øren et al., (1997). Their equation is used for the calculation of conductance to oil in sites g_{os}:

$$g_{os} = 0.5623 G_s A_{eff}^2 \tag{19}$$

During displacement, water will gather in corners. The area of water in each corner A_{wc} can be calculated by:

$$A_{wc}(\theta, r, \beta) = r_d{}^2 \left(\theta + \beta - \frac{\pi}{2} + \frac{\cos\theta \cos(\theta + \beta)}{\sin\beta} \right) \tag{20}$$

The shape factor for water in the corner G_{wc} is:

$$G_{wc}(\theta, r, \beta) = \frac{A_{wc}}{4\left(\frac{r_d \cos(\theta_i + \beta)}{\sin\beta} \right)^2 \left(1 - \frac{\sin\beta}{\cos(\theta_i + \beta)} \left(\theta_i + \beta - \frac{\pi}{2} \right) \right)^2} \tag{21}$$

Assuming that there is no slip condition at the water-oil boundary, the corner water conductance g_{wc} can then be calculated by (Valvatne and Blunt, 2004):

$$g_{wc} = CA_{wc}^2 G_{wc} \tag{22}$$

where the constant C is:

$$C = 0.364 + 0.28\frac{\sin\beta\cos\beta}{4G_{wc}\left(1+\sin\beta\right)^2} \tag{23}$$

To calculate the conductance of the corner water through a site (g_{wcs}) or bond (g_{wcb}), take the corner conductance multiplied by the number of corners. For sites the half-length is $\beta = \pi/8$ and the number of corners is 4. For bonds $\beta = \pi/6$ and the number of corners is 3.

To calculate the conductance from one site to another, we use the equation for a set of conductors in series:

$$\frac{l}{g} = \frac{r_{ins1}}{g_{s1}\left(r_{ins1}\right)} + \frac{l_b}{g_b\left(r_{inb}\right)} + \frac{r_{ins2}}{g_{s2}\left(r_{ins2}\right)} \tag{24}$$

where l is the distance between two adjacent site centres, g is the conductance from one site to the other, r_{ins1} and r_{ins2} are the inscribed radius of the first and second site respectively, g_{s1} and g_{s2} are the conductance for the first and second sites respectively, g_b is bond conductance and l_b is the bond length.

The lengths must satisfy the following equation:

$$l_b = l - r_{ins1} - r_{ins2} \tag{25}$$

2.5. Pore filling during drainage

During drainage, the proportion of bonds available to be filled by oil p_{bo} can be calculated by:

$$p_{bo} = \int_{r_b}^{r_{b\max}} f_b\left(r_{in}\right) dr_{in} \tag{26}$$

where r_b is the inscribed radius of the smallest bond available to oil. It is defined by:

$$r_b = \frac{\sigma_{ow}}{P_c D_r} \tag{27}$$

The proportion of sites available to be filled by oil p_{so} can be found from:

$$p_{so} = \int_{r_s}^{r_{s\max}} f_s\left(r_{in}\right) dr_{in} \tag{28}$$

where r_s is the inscribed radius of the smallest site available to oil. It is defined by:

$$r_s = \frac{2\sigma_{ow}}{P_c} \tag{29}$$

The porosity made up of sites ϕ_s is calcaulated by:

$$\phi_s = \frac{1}{l^3} \int_{r_{s\min}}^{r_{s\max}} f_s\left(r_{ins}\right) 8 {r_{ins}}^3 dr_{ins} \tag{30}$$

The volume of oil in the site V_{so} is approximated by:

$$V_{so}\left(r_{in}, r_d\right) = 8 {r_{in}}^3 - 24 r_{in} A_{wc}\left(\theta, r, \beta\right) \tag{31}$$

This equation does not properly take into account water volumes in the corner. However, the same equation is used in the pore network simulator, which allows for the percolation model results to be compared with the pore network simulator.

The oil saturation in the sites s_{so} is calculated by:

$$S_{so} = \frac{p_{s\infty}\left(p_{so}, p_{bo}\right)}{p_{so}\phi_s} \int_{r_s}^{r_{b\max}} f_s\left(r_{in}\right) V_{so}\left(r_{in}, r_d\right) dr_{in} \tag{32}$$

where $p_{s\infty}$ is the proportion of sites occupied by oil. The porosity made up of bonds ϕ_b is calculated by:

$$\phi_b = \frac{Z}{2} \int_{r_{s\min}}^{r_{s\max}} \int_{r_{s\min}}^{r_{s\max}} \int_{r_{b\min}}^{r_{b\max}} f_b\left(r_{inb}\right) f_s\left(r_{ins1}\right) f_s\left(r_{ins2}\right) A_b\left(r_{inb}\right) l_b\left(r_{ins1}, r_{ins2}\right) dr_{inb} dr_{ins1} dr_{ins2} \tag{33}$$

The oil saturation from bonds S_{bo} is calculated by:

$$S_{bo} = \frac{p_{b\infty}\left(p_{so}, p_{bo}\right)}{{p_{so}}^2 p_{bo}\phi_b} \int_{r_{s\min}}^{r_{s\max}} \int_{r_{s\min}}^{r_{s\max}} \int_{r_b}^{r_{b\max}} f_b\left(r_{inb}\right) f_s\left(r_{ins1}\right) f_b\left(r_{ins2}\right) A_{bo}\left(r_{in}, r_c, \theta\right) l_b\left(r_{ins1}, r_{ins2}\right) dr_{inb} dr_{ins1} dr_{ins2} \tag{34}$$

where $p_{b\infty}$ is proportion of bonds occupied by oil. The total water saturation S_w is then calculated by

$$S_w = 1 - \left(S_{so}\phi_s + S_{bo}\phi_b\right) \tag{35}$$

The functions $p_{b\infty}$ and $p_{s\infty}$ are calculated numerically using code developed in house in numerical computing environment MATLAB®. Results of numerical calculation are presented in Fig. 2.

2.6. Effective Medium Theory

Effective media theory (EMT) is used to approximate the conductance of a network. It approximates a network with some distribution of bond conductance g_p with an equivalently conductive network where each bond conductance is equal to the effective medium conductance g_e. It can also be called the effective medium approximation (EMA). Kirkpatrick (1973) derived the equation of effective conductance as:

$$\int_0^\infty h\left(g_p\right) \frac{g_p - g_e}{g_p + \left(\frac{Z}{2} - 1\right) g_e} dg_p = 0 \tag{36}$$

where h is the frequency of conductance g_p in the network, and Z is the coordination number. Given our distribution of bond sizes and site sizes, Monte Carlo simulation can be used to quickly obtain the conductance distribution. The probability of a site or bond can be found from the site or bond size distribution, respectively.

The distribution for oil can be generated, by assigning all sites smaller than r_s and all bonds smaller than r_b to have no oil conductance. The probability distribution used for the Monte Carlo simulation is:

$$P(r_{ins}) = \begin{cases} 0 & , r_{ins} < r_s \\ f_s(r_{ins})/p_s & , r_{ins} > r_s \end{cases}$$
$$P(r_{inb}) = \begin{cases} 0 & , r_{inb} < r_b \\ f_b(r_{inb})/p_b & , r_{inb} > r_b \end{cases} \quad (37)$$

The conductance to oil from one site to the next, g_o, is calculated in the following equation:

$$\frac{l}{g_o} = \frac{r_{ins1}}{g_{os}(r_{ins1})} + \frac{l_b}{g_{ob}(r_{inb})} + \frac{r_{ins2}}{g_{os}(r_{ins2})} \quad (38)$$

The integral of the distribution of oil conductivities h_o, should be equal to the number of bonds available to oil. Therefore, the normalized distribution generated by the Monte Carlo simulation is multiplied by p_b to get the conductance distribution h_o. Finally the oil conductance, g_o, can be calculated by:

$$\frac{-(1-p_b)}{\left(\frac{Z}{2}-1\right)} + \int_0^\infty h_o(g_o)\frac{g_o - g_e}{g_o + \left(\frac{Z}{2}-1\right)g_e}dg_o = 0 \quad (39)$$

The EMA for water is more complex. There are six possible configurations that can exist between two sites and a bond. Diagram for each configuration is given in Fig. 3. C_1 to C_3 are configurations with oil in the bond. C_1 is the configuration with oil in both sites, C_2 is the configuration with oil in one site and C_3 is the configuration with oil in no sites. The configurations C_4 to C_6 are configurations with water in the bond. C_4 is the configuration with oil in both sites, C_5 is the configuration with oil in one site and C_6 is the configuration with oil in no sites. The conductance for configurations C1 to C6 are g_{w1} to g_{w6}. They are calculated by:

$$\frac{l}{g_{w1}} = \frac{r_{ins1}}{g_{wcs}} + \frac{l_b}{g_{wcb}} + \frac{r_{ins2}}{g_{wcs}} \quad (40)$$

$$\frac{l}{g_{w2}} = \frac{r_{ins1}}{g_s(r_{ins1})} + \frac{l_b}{g_{wcb}} + \frac{r_{ins2}}{g_{wcs}} \quad (41)$$

$$\frac{l}{g_{w3}} = \frac{r_{ins1}}{g_s(r_{ins1})} + \frac{l_b}{g_{wcb}} + \frac{r_{ins2}}{g_s(r_{ins2})} \quad (42)$$

$$\frac{l}{g_{w4}} = \frac{r_{ins1}}{g_{wcs}} + \frac{l_b}{g_b(r_{inb})} + \frac{r_{ins2}}{g_{wcs}} \quad (43)$$

$$\frac{l}{g_{w5}} = \frac{r_{ins1}}{g_s(r_{ins1})} + \frac{l_b}{g_b(r_{inb})} + \frac{r_{ins2}}{g_{wcs}} \quad (44)$$

$$\frac{l}{g_{w6}} = \frac{r_{ins1}}{g_s\left(r_{ins1}\right)} + \frac{l_b}{g_b\left(r_{inb}\right)} + \frac{r_{ins2}}{g_s\left(r_{ins2}\right)} \tag{45}$$

The probability that a bond or site with inscribed radius r_{inb} or r_{ins} has oil in the centre is given by Eq. (37). The probability distribution that a bond or site with inscribed radius r_{inb} or r_{ins} only contains water is given by:

$$\begin{aligned} P\left(r_{ins}\right) &= \begin{cases} f_s\left(r_{ins}\right)/\left(1-p_s\right) & , r_{ins} < r_s \\ 0 & , r_{ins} > r_s \end{cases} \\ P\left(r_{inb}\right) &= \begin{cases} f_b\left(r_{ins}\right)/\left(1-p_b\right) & , r_{inb} < r_b \\ 0 & , r_{inb} > r_b \end{cases} \end{aligned} \tag{46}$$

Given these probability distributions, the distribution of conductances made up by each of the configurations h_{wi} can be calculated using Monte-Carlo simulation. Fig. 4 shows a schematic for frequency of bonds which make up each configuration. The total of all of the frequencies gives the bond size distribution. The probabilities of configurations 1 to 6 are p_1... p_6. The probabilities depend on the proportion of sites and bonds available to the invading phase. They are calculated numerically using code developed in house in numerical computing environment MATLAB®. The results are given in Fig. 5. The total distribution for water conductance, h_w can be calculated by:

$$h_w\left(g_w\right) = \sum_{i=1}^{i=6} p_i h_{wi}\left(g_{wi}\right) \tag{47}$$

The conductance to water g_w is calculated by solving the following equation:

$$\int_0^\infty h_w\left(g_w\right) \frac{g_w - g_e}{g_w + \left(\frac{Z}{2} - 1\right) g_e} dg_o = 0 \tag{48}$$

2.7. Critical Path Theory

A method of estimating the conductance of a disordered network was developed by Ambegaoker et al. (1971). The conductance of a set of parallel conductors is controlled by the largest conductor. The conductance of a set of conductors in series is controlled by the smallest conductor. They divide the network into two sets of conductors; small and large conductors. The smallest conductor of the large set is called the critical conductance g_c. All conductors greater than g_c are reduced to g_c and all conductors smaller than g_c are set to zero. The theory is called critical path theory (CPT) the resultant equation for conductance as given by Sahimi (1993) is:

$$g_e = c_{cpt} g_c \left(p_{cpt}\left(g_c\right) - p_{bth}\right)^{\mu} \tag{49}$$

where c_{cpt} is a constant, μ is the percolation exponent for conductance (Sahimi 1993, gives a value of μ = 2 for 3 dimensional networks) and p_{bth} is the bond percolation threshold. The probability p_{cpt} is the probability that a bond conductance is greater than or equal to some critical conductance g_c :

$$p_{cpt}\left(g_c\right) = \int_{g_c}^{\infty} h(g) dg \tag{50}$$

The correct critical conductance g_c to use is the conductance which maximises g_e (Sahimi 1993). To calculate the correct threshold to use during bond-site percolation, we will need the thresholds for site and bond percolation. Galam and Mauger (1996) proposed the following expression for percolation threshold:

$$p_{th}^{*} = \Upsilon_0 \left[(d-1)(Z-1) \right]^{-a_1} d^{a_2} \tag{51}$$

where for sites; $\Upsilon_0 = 1.2868$, $a_1 = 0.6160$ and $a_2 = 0$ and for bonds $\Upsilon_0 = 0.7541$, $a_1 = 0.9346$ and $a_2 = a_1$. The calculated values for a simple cubic lattice with Z = 6 were $p^*_{bth} = 0.2448$ and $p^*_{sth} = 0.3115$. The percolation threshold for bonds in a bond-site network, p_{bth}, is dependent on the proportion of sites which can also contribute to the infinite cluster $p_{s\infty}$. Yanuka and Englman (1990) obtained the following expression for the bond percolation threshold during bond-site percolation:

$$p_{bth}\left(p_{s\infty}\right) = \left(p_{bth}^{*}\right)^{\left(1-\alpha_s(p_s)\right)} \tag{52}$$

where

$$\alpha_s\left(p_s\right) = \frac{\log\left(p_s\right)}{\log\left(p_{sth}^{*}\right)} \tag{53}$$

3. Infinite cluster and configuration proportion during the bond-site percolation

The in–house code in Matlab® is developed for calculation of the percolation process across a 40x40x40 simple cubic lattice. One face of the network is designated as the entry for the invaded phase. Any bond or site available to this face will become part of the invading cluster. The algorithm is as follows: A proportion of sites is made available to the infinite cluster. None of the bonds in the network are initially available to the invading cluster. One random bond is made available to the invading cluster. Then the proportions $p_{b\infty}$, $p_{s\infty}$ and p_1 to p_6 are calculated. Then another random bond is made available and the calculation of proportions $p_{b\infty}$, $p_{s\infty}$ and p_1 to $p_6$is repeated. This process is repeated until all the bonds are available to the invading phase. The proportions $p_{b\infty}$, $p_{s\infty}$ and p_1 to p_6 are calculated for 120 simulations for 32 different values of p_s. Figs. 2. And 5. Show the average result of these simulations.

The calculation of $p_{b\infty}$ is given in Fig. 2a. When all the sites are available, the infinite cluster strength for bonds follows the bond percolation process. As the proportion of available sites is reduced, $p_{b\infty}$ decreases. When the proportion of available sites drops below the site percolation threshold, the invading cluster can no longer form an infinite cluster.

The calculation of $p_{s\infty}$ is given in Fig. 2b. Similar to the previous figure, the proportion of sites in the infinite cluster will decrease as the number of bonds decrease. However, one difference is that if $p_b > 0.64$, all sites can be connected to the infinite cluster. If $p_b < 0.64$, there will be some proportion of sites which will be separate to the infinite cluster. This proportion will decrease as p_b decreases, and drop to zero once p_b is below the bond percolation threshold.

The probability of configuration C_1 will always monotonically increase as the number of bonds and sites available to be filled by oil increases (Fig. 5a). When all the sites are available to oil ($p_s = 1$), the probability p_1 is the same as the infinite cluster strength during bond percolation. The probability of configuration p_2 will monotonically increase as the number of bonds to be filled by oil increases (Fig. 5b). There exists some maximum for p_2 at some intermediate value for p_s. If there are no sites available

to oil or if all the sites are available to oil, configuration C_2 cannot exist. Configuration C_2 only exists at some intermediate value for p_s. Configuration C_3 does not exist during the drainage process (Fig. 5c).

The probabilities p_4 and p_5 share a non-monotonic relationship with p_b (Fig. 5d & 5e). If p_b is too low, no enough sites will become part of the infinite cluster. Otherwise, if p_b is too high, there will be less bonds occupied by the wetting phase. Proportion p_6 will monotonically decrease with increase in either p_b or p_s (Fig. 5f).

4. Pore network simulator

As the target of all pore network simulations is a direct comparison against solutions obtained based on percolation theory, all physics mechanisms and parameters of the pore network simulator are tuned to be the same as the percolation model.

At first, we construct a lattice-based pore-network model with prescribed pore-body and pore-throat size distributions. Given the distance in between the pore-bodies, we place them at the nodes of the lattice by randomly sampling from the size distribution. Next, we loop through each of the pore-bodies and pore throat and assign the radii from the prescribed distribution. For the case where Z = 3, the number of throats attached to the given pore-body is randomized. While placing throats we also perform body-throat partitioning that will define local element's conductance according to Eq. (24). The length of throat is defined as in Eq. (25). The shape factors for all pore bodies and pore throats are assigned to equal that of the square and the equilateral triangle, respectively. The construction procedure as described above ensures that resulting characteristics of the constructed network are the same as those for percolation theory simulations (and no correlations exist between pore and throat placement as assumed in all PM computations) and for PNS on lattices with more than 10^3 throats the differences for pore, throat, length and Z distributions are virtually negligible. This is observable in the comparison of the distributions used for the PM and the histogram of the elements for the PNS in Fig. 6.

After construction the pore-network is saved into so-called Statoil format and is also visualized using the open-source software VTK. All processing is performed using in-house C++ code imbedded within the credible pore-network extraction framework (Miao et al., Gerke et al., 2019a) and the size of all models was 40^3 lattice units (totalling to 64×10^3 pore-bodies and 19.2×10^4 pore-throats for Z = 6). The examples of visualizations for PNS with Z = 6 is presented in Fig. 7a and for Z = 3 in Fig. 7b. For single and two-phase flow simulations the constructed pore-network is passed into Valvatne's code (Valvane and Blunt, 2004), which utilized the same physics as described for PM in sections 2.1-2.4. The flow was simulated in a single direction along one of major orthogonal axes. The contact angles within the network are assigned to 0° to represent fully water-wet conditions. The fluid properties for simulations using both theoretical and modelling approaches were chosen to represent a typical water-oil system with the surface tension of 30 mN/m. The simulated network permeability, capillary curves and relative permeability curves for drainage from a network initially saturated with water were saved for comparison against PM results.

5. Comparison between percolation model and Pore network simulator

The percolation model (PM) developed in Section 2 is compared against the pore network simulator (PNS) described in Section 4. Four different distributions for bond inscribed radius and site inscribed radius were used. The probability density function for each of the site-bond distributions is shown in Fig. 8. They density functions are normalized lognormal distributions with an upper limit of 29 μm. The distance between adjacent sites is l = 60 μm. There are two kinds of lattices used; a simple cubic lattice with coordination number Z = 6 and a simple cubic lattice with half the bonds turned off, resulting

in average coordination number Z = 3. The bond percolation threshold for the second lattice is p^*_{bth} = 0.4896. In total 8 cases are compared.

The capillary pressure curves obtained from the percolation model show very high agreement with those from the pore-network simulator (PNS) for all 8 cases (Fig. 9). However, there is deviation in relative-permeability curves.

Fig. 10. Shows the comparison of pore network simulator with the percolation model with EMT and CPT for calculation of relative permeability for lattice with Z = 6. Fig. 11. Shows the same comparison but for the second lattice, where Z = 3. In all the cases, EMT deviates from the PNS.

Water relative permeability matches at very high water saturations but the pore network simulator diverges from the convex trend at lower water saturations. Generally, the PNS predicts higher water relative permeability. The CPT and EMT calculations for water relative permeability are similar. Both EMT and CPT can be treating the oil clusters as if they are randomly distributed throughout the network as opposed to a penetrating backbone cluster with many branches. They can therefore predict that more water pathways are broken than what is actually occurring. CPT predicts slightly lower water relative permeability to EMT in some cases. This is due to one of the assumptions associated with CPT. It assumes that the conductance for a set of conductors is in series and the overall conductance is equal to the smallest conductor in that set. The set is made up of a distribution of conductance, and if that set has a wide distribution this assumption can be accurate. But if that distribution has low variance, the assumption will under predict the overall conductance.

The oil relative permeability curve modelled by CPT matches the PNS much more closely than the other models. The reason could be that the penetrating cluster of oil could be bottlenecked by the smallest conductors in the set, which is more suitably calculated by CPT. The oil relative permeability curve modelled by EMT usually always terminates at lower water saturation than the pore network simulator. This is not uncommon, EMT has been reported in literature to underestimate permeability close to the threshold.

6. Discussion

The end point values for relative permeability; connate water saturation, residual oil saturation, water relative permeability at residual oil and oil relative permeability at connate water saturation are important parameters for calculation of water flood efficiency. The comparison shows large deviation using either EMT or CPT for the prediction of the relative permeability end points for all cases except for s_{or} at Z = 6.

The percolation model predicts that water becomes immobile at saturation less than 0.5 for cases where Z = 6 and 0.7 for the cases where Z = 3. The relative permeability calculated by the percolation model shows either very small or almost no window of two-phase flow for the networks with Z = 6. For the networks with Z = 3, the percolation model calculates no window of saturation where both phases are mobile. The values of end point saturation and two-phase flow windows are unrealistic compared to natural porous media. The reason for these high values is that the percolation threshold is high.

For more realistic two-phase saturation windows and end point values, one option is to use higher coordination numbers. There are analytical expressions already available for percolation threshold by Galam and Mauger (1996) and infinite cluster strength by Bedrikovetsky. and Bruining (1995) for bond percolation, so for this reason we investigate the end point value dependence on coordination number

using just bond percolation. The end point values are determined from where the relative permeability calculated by CPT become 1×10^{-3}.

End point saturation values are given in fig. 12a for values of from Z = 3 up to Z = 12 for three different values of coefficient of variation (c_v) in inscribed bond radius. The irreducible water saturation s_{wc} and the residual oil saturation s_{or} reduce as Z increases dues to the reduction in percolation threshold.

Increases in c_v cause an increase in the tail end of the lognormal distribution. As the area of the bond will scale to the power of 2 with the inscribed radius, the oil saturation will increase more than the water saturation when there is an increase in c_v. For this reason, increase in c_v results in decrease in s_{wc} and an increase in s_{or}. s_{wc} is more sensitive to c_v and Z than s_{or}. This is due to the distribution of smaller bonds being more affected by changes in c_v in a lognormal distribution.

The end point relative permeability values are shown in Fig. 12b. The relative permeability to water at residual oil saturation k_{rwor} and the relative permeability to oil at irreducible water saturation k_{rowc} both increase as Z increases because the percolation threshold decreases. The conductivity of the bond will scale to the power of 4 with the inscribed radius, so increase in c_v will cause dramatic increase in k_{rowc}. The window for two phase flow is presented in Fig. 13. As there is decrease in both end point saturations with Z, the window will increase with Z.

However, the coordination numbers observed in sandstones aren't on average that much higher than 6. Rabbani et al. (2016) calculates average coordination number for several sandstones in the range 1.75 to 6.75. In natural porous media, the larger pore bodies will have larger pore throats. This would cause the network to have correlation between available sites and bonds. Correlated bond-site percolation can give lower thresholds and be more appropriate for future developments. Moreover, direct simulations of percolation on pore-networks extracted from 3D pore geometries of real porous media can serve as a much more accurate basis for percolation theory based models as discussed here.

While the comparison against PNS was made on the assumption that it provides a solid base for verification, it is possible to speculate that PM actually provides more accurate results. It was recently shown that boundary conditions can significantly affect obtained flow properties (Gerke et al., 2019b) and closed walls boundary conditions on the walls of the modelling domain, as utilized in PNS, may not be appropriate for upscaling. Contrary to PNS, PM assumes infinite porous media domain, which is arguably a more plausible assumption for homogenization to continuum scale, as for example, is needed for multi-scale PNS (Bultreys et al., 2015).

7. Conclusions

Our new method to utilize percolation theory to simulate two-phase flow properties based on pore-size distribution. It provides a fast and robust computational framework which can be immediately used for intensive pore-scale simulations, which include upscaling for highly heterogeneous pore scale media such as shales, carbonates and soils. While we utilise a relatively simple lattice-based pore-network construction approach, the extension to more complex pore-networks with highly heterogeneous connections is possible based on pore-network simulations for such media. The new method allows the following conclusions to be drawn:

1. Critical path theory is superior for calculation of oil relative permeability over effective medium theory in all cases studied.
2. Effective medium theory shows deviation from pore network simulator close to threshold.

3. There is no simultaneous two-phase flow at small coordination number. This is due to the high percolation threshold which occurs at small coordination numbers.
4. There is good agreement between percolation model and the pore network simulator capillary pressure curves.
5. Despite the large difference in relative permeability end points, critical path theory shows qualitative agreement with the relative permeability curves generated by the pore network simulator.

Nomenclature

A	cross sectional area
A_{wc}	cross sectional are for corner water
A_{eff}	effective cross sectional area of the oil
C	configuration
c_{cpt}	constant for critical path equation
G	dimensionless shape factor
G_{wc}	dimensionless shape factor for corner water
g	conductivity
g_c	critical conductance
g_e	effective medium conductance
g_b	bond conductance
g_{ob}	conductance for oil in bond
g_{os}	conductance for oil in site
g_{wc}	conductance for water in corner
g_{wcb}	conductance for corner water in bond
g_{wcs}	conductance for corner water in site
g_{wi}	conductance for water in configuration i
g_s	site conductance
h	frequency of conductance
h_o	frequency of conductance to oil
h_w	frequency of conductance to water
L	perimeter
L_{ow}	perimeter of the oil-water contact
L_{os}	perimeter of the oil-solid contact
l	distance between two adjacent site centres
l_b	length of bond
P_c	capillary pressure
p_{bo}	proportion of bonds available to oil
p_{bth}	bond percolation threshold
$p_{b\infty}$	proportion of bonds occupied by oil
p_{cpt}	proportion of conductance greater than the critical conductance
p_i	probability of configuration i
p_{so}	proportion of sites available to oil
$p_{s\infty}$	proportion of sites occupied by oil
p^*_{bth}	percolation threshold for bonds
p^*_{sth}	percolation threshold for sites
r_d	radius of curvature during MS-P drainage
r_b	inscribed radius of smallest bond available to oil
r_{bmax}	inscribed radius of largest bond

r_s inscribed radius of smallest site available to oil
r_{smax} inscribed radius of largest site
r_{in} inscribed radius
r_{inb} inscribed radius of bond
r_{ins} inscribed radius of site
S_{bo} oil saturation from bonds
S_{so} oil saturation from sites
S_w water saturation
V_{so} volume of oil in site
Z coordination number

Greek letters

β half angle of corner
ϕ_b porosity from bonds
ϕ_s porosity from sites
μ critical exponent for conductivity
σ_{ow} interfacial tension between oil and water
θ contact angle

Acknowledgements

This work was supported with supercomputing resources provided by the Phoenix HPC service at the University of Adelaide. This research was supported by the Russian Science Foundation grant 17-17-01310 (K.M.G.).

References

Ambegaokar, V., Halperin, B.I. and Langer, J.S., 1971. Hopping conductivity in disordered systems. Physical review B, 4(8), p.2612.

Bedrikovetsky, P. and Bruining, J., 1995, May. A percolation based upscaling technique for viscous force dominated waterflooding in uncorrelated heterogeneous reservoirs. In IOR 1995-8th European Symposium on Improved Oil Recovery.

Blunt, M., King, M.J. and Scher, H., 1992. Simulation and theory of two-phase flow in porous media. Physical Review A, 46(12), p.7680.

Bultreys, T., Van Hoorebeke, L., & Cnudde, V. (2015). Multi-scale, micro-computed tomography-based pore network models to simulate drainage in heterogeneous rocks. Advances in Water Resources, 78, 36-49.

Galam, S. and Mauger, A., 1997. Universal formulas for percolation thresholds. II. Extension to anisotropic and aperiodic lattices. Physical Review E, 56(1), p.322.

Gerke, K. M., Sizonenko, T. O., Karsanina, M. V., Lavrukhin E.V., Abashkin V.V., Korost D.V., 2019a Improving watershed-based pore-network extraction method using maximum inscribed ball pore-body positioning. Advances in Water Resources (in revision).

Gerke K.M., Karsanina, M. V., Katsman R., 2019b. Calculation of tensorial flow properties on pore level: exploring the influence of boundary conditions on permeability of 3D stochastic reconstructions. Physical Review E (in revision).

Ghanbarian, B. and Hunt, A.G., 2017. Improving unsaturated hydraulic conductivity estimation in soils via percolation theory. Geoderma, 303, pp.9-18.

Ghanbarian, B., Sahimi, M. and Daigle, H., 2016. Modeling relative permeability of water in soil: Application of effective-medium approximation and percolation theory. Water Resources Research, 52(7), pp.5025-5040.

Heiba, A.A., Davis, H.T. and Scriven, L.E., 1983, January. Effect of wettability on two-phase relative permeabilities and capillary pressures. In SPE annual technical conference and exhibition. Society of Petroleum Engineers.

Heiba, A.A., Sahimi, M., Scriven, L.E. and Davis, H.T., 1992. Percolation theory of two-phase relative permeability. SPE Reservoir Engineering, 7(01), pp.123-132.

Hunt, A.G., 2001. Applications of percolation theory to porous media with distributed local conductances. Advances in Water Resources, 24(3-4), pp.279-307.

Kirkpatrick, S., 1973. Percolation and conduction. Reviews of modern physics, 45(4), p.574.

Lago, M. and Araujo, M., 2001. Threshold pressure in capillaries with polygonal cross section. Journal of colloid and interface science, 243(1), pp.219-226.

Larson, R. G., Scriven, L. E., and Davis, H. T., 1981. Percolation theory of two phase flow in porous media. Chemical Engineering Science, 36(1), 57-73.

Mason, G. and Morrow, N.R., 1991. Capillary behavior of a perfectly wetting liquid in irregular triangular tubes. Journal of Colloid and Interface Science, 141(1), pp.262-274.

Miao, X., Gerke, K. M., & Sizonenko, T. O., 2017. A new way to parameterize hydraulic conductances of pore elements: A step towards creating pore-networks without pore shape simplifications. Advances in Water Resources, 105, 162-172.

Oren, P.E., Bakke, S. and Arntzen, O.J., 1997, January. Extending predictive capabilities to network models. In SPE Annual Technical Conference and Exhibition. Society of Petroleum Engineers.

Patzek, T.W. and Silin, D.B., 2001. Shape factor and hydraulic conductance in noncircular capillaries: I. One-phase creeping flow. Journal of colloid and interface science, 236(2), pp.295-304.

Rabbani, A., Ayatollahi, S., Kharrat, R. and Dashti, N., 2016. Estimation of 3-D pore network coordination number of rocks from watershed segmentation of a single 2-D image. Advances in water resources, 94, pp.264-277.

Sahimi, M., 1993. Flow phenomena in rocks: from continuum models to fractals, percolation, cellular automata, and simulated annealing. Reviews of modern physics, 65(4), p.1393.

Valvatne, P.H. and Blunt, M.J., 2004. Predictive pore-scale modelling of two-phase flow in mixed wet media. Water resources research, 40(7).

Yanuka, M. and Englman, R., 1990. Bond-site percolation: empirical representation of critical probabilities. Journal of Physics A: Mathematical and General, 23(7), p.L339.

Khirevich, S., Ginzburg, I., Tallarek, U., 2015. Coarse-and fine-grid numerical behavior of MRT/TRT lattice-Boltzmann schemes in regular and random sphere packings. J. Comput. Phys. 281, 708–742.

Dashtian, H., Bakhshian, S., Hajirezaie, S., Nicot, J. P., & Hosseini, S. A. (2019). Convection-diffusion-reaction of CO2-enriched brine in porous media: A pore-scale study. Computers & Geosciences, 125, 19-29.

Bilger, C., Aboukhedr, M., Vogiatzaki, K., & Cant, R. S. (2017). Evaluation of two-phase flow solvers using Level Set and Volume of Fluid methods. Journal of Computational Physics, 345, 665-686.

Raeini, A.Q., Blunt, M.J., Bijeljic, B., 2012. Modelling two-phase flow in porous media at the pore scale using the volume-of-fluid method. J. Comput. Phys. 231, 5653–5668.

Raeini, A. Q., Bijeljic, B., & Blunt, M. J. (2017). Generalized network modeling: Network extraction as a coarse-scale discretization of the void space of porous media. Physical Review E, 96(1), 013312.

Fatt, I. (1956a) The network model of porous media I. Capillary pressure characteristics. Petrol. Trans. AIME 207, 144-159.

Fatt, I. (1956b) The network model of porous media II. Dynamic properties of a single size tube network. Petrol. Trans. AIME 207, 160-163.

Fatt, I. (1956c) The network model of porous media III. Dynamic properties of networks with tube radius distribution. Petrol. Trans. AIME 207, 164-181.

Xiong, Q., Baychev, T., Jivkov, A. (2016) Review of pore network modelling of porous media: experimental characterisations, network constructions and applications to reactive transport. Journal of Contaminant Hydrology, 192, 101-117.

Thovert, J.F., Adler, P.M., 2011. Grain reconstruction of porous media: Application to a Bentheim sandstone. Phys. Rev. E - Stat. Nonlinear, Soft Matter Phys. 83, 056116.

Shabro, V., Torres-Verdín, C., Javadpour, F., Sepehrnoori, K., 2012. Finite-Difference Approximation for Fluid-Flow Simulation and Calculation of Permeability in Porous Media. Transp. Porous Media 94, 775–793.

Gerke K.M., Vasilyev R.V., Khirevich S., Karsanina M.V., Collins D., Sizonenko T., Korost D.V., Lamontagne S., Mallants D. Finite-difference method Stokes solver (FDMSS) for 3D pore geometries: Software development, validation and case studies. Computers & Geosciences, 2018, 114: 41-58.

Verma, R., Icardi, M., & Prodanović, M. (2018). Effect of wettability on two-phase quasi-static displacement: Validation of two pore scale modeling approaches. Journal of contaminant hydrology, 212, 115-133.

Rokhforouz, M. R., & Akhlaghi Amiri, H. A. (2017). Phase-field simulation of counter-current spontaneous imbibition in a fractured heterogeneous porous medium. Physics of Fluids, 29(6), 062104.

Holmes, D.W., Williams, J.R., Tilke, P., Leonardi, C.R., 2016. Characterizing flow in oil reservoir rock using SPH : Absolute permeability. Comput. Part. Mech. 3, 141–154.

Frank, F., Liu, C., Scanziani, A., Alpak, F. O., & Riviere, B. (2018). An energy-based equilibrium contact angle boundary condition on jagged surfaces for phase-field methods. Journal of colloid and interface science, 523, 282-291.

Demianov, A., Dinariev, O., & Evseev, N. (2011). Density functional modelling in multiphase compositional hydrodynamics. The Canadian Journal of Chemical Engineering, 89(2), 206-226.

Gerke, K.M., Karsanina, M. V, Mallants, D., 2015b. Universal Stochastic Multiscale Image Fusion : An Example Application for Shale Rock. Sci. Rep. 5, 15880.

Karsanina M.V., Gerke K.M., 2018. Hierarchical Optimization: Fast and Robust Multiscale Stochastic Reconstructions with Rescaled Correlation Functions. Physical Review Letters, 121(26), 265501.

Karsanina M.V., Gerke K.M., Skvortsova E.B., Ivanov A.L., Mallants D. Enhancing image resolution of soils by stochastic multiscale image fusion. Geoderma, 2018, 314: 138-145.

Tahmasebi, P. (2018). Nanoscale and multiresolution models for shale samples. Fuel, 217, 218-225.

Pereira, G. G., Pinczewski, W. V., Chan, D. Y. C., Paterson, L., & Øren, P. E. (1996). Pore-scale network model for drainage-dominated three-phase flow in porous media. Transport in Porous media, 24(2), 167-201.

Van Dijke, M. I. J., & Sorbie, K. S. (2002). Pore-scale network model for three-phase flow in mixed-wet porous media. Physical Review E, 66(4), 046302.

Piri, M., & Blunt, M. J. (2005). Three-dimensional mixed-wet random pore-scale network modeling of two-and three-phase flow in porous media. I. Model description. Physical Review E, 71(2), 026301.

Cnudde, V. and Boone, M.N. (2013) High-resolution X-ray computed tomography in geosciences: A review of the current technology and applications. Earth-Science Reviews 123, 1-17.

Godinho, J.R., Gerke, K.M., Stack, A.G. and Lee, P.D. (2016) The dynamic nature of crystal growth in pores. Scientific Reports 6, 33086.

Gostick, J., Aghighi, M., Hinebaugh, J., Tranter, T., Hoeh, M. A., Day, H., Spellacy B., Sharqawy M.H., Bazylak A., Burns A., Lehnert, W., Putz A. (2016). OpenPNM: a pore network modeling package. Computing in Science & Engineering, 18(4), 60-74.

Chen, P. E., Xu, W., Chawla, N., Ren, Y., & Jiao, Y. (2019). Hierarchical n-Point Polytope Functions for Quantitative Representation of Complex Heterogeneous Materials and Microstructural Evolution. Acta Materialia 179: 317-327.

Yeong, C., Torquato, S., 1998. Reconstructing random media. II. Three-dimensional media from two-dimensional cuts. Phys. Rev. E 58, 224–233.

Adler, P.M., Jacquin, C.G., Quiblier, J.A., 1990. Flow in simulated porous media. Int. J. Multiph. Flow 16, 691–712.

Gerke, K.M., Karsanina, M. V., Vasilyev, R. V., Mallants, D., 2014. Improving pattern reconstruction using directional correlation functions. EPL (Europhysics Lett.) 106, 66002.

Jiao, Y., Chawla, N., 2014. Modeling and characterizing anisotropic inclusion orientation in heterogeneous material via directional cluster functions and stochastic microstructure reconstruction. J. Appl. Phys. 115, 093511.

Li, H., Chen, P. E., & Jiao, Y. (2017). Accurate Reconstruction of Porous Materials via Stochastic Fusion of Limited Bimodal Microstructural Data. Transport in Porous Media, 1-18.

Li, H., Chawla, N., & Jiao, Y. (2014). Reconstruction of heterogeneous materials via stochastic optimization of limited-angle X-ray tomographic projections. Scripta Materialia, 86, 48-51.

Tahmasebi, P., & Sahimi, M. (2012). Reconstruction of three-dimensional porous media using a single thin section. Physical Review E, 85(6), 066709.

Sahimi, M. (2011). Flow and transport in porous media and fractured rock: from classical methods to modern approaches. John Wiley & Sons.

Blunt, M. J. (2017). Multiphase flow in permeable media: A pore-scale perspective. Cambridge University Press.

Zeinijahromi, A., Nguyen, T. K. P., & Bedrikovetsky, P. (2013). Mathematical model for fines-migration-assisted waterflooding with induced formation damage. Spe Journal, 18(03), 518-533.

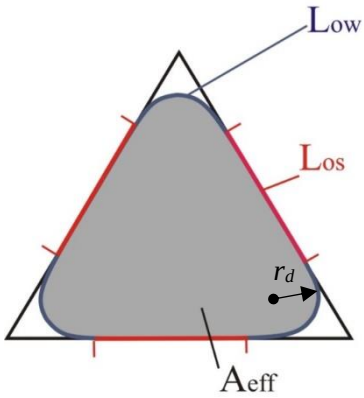

Fig. 1. Cross section of a triangular capillary during Mayer, Stowe and Princep (MS-P) displacement.

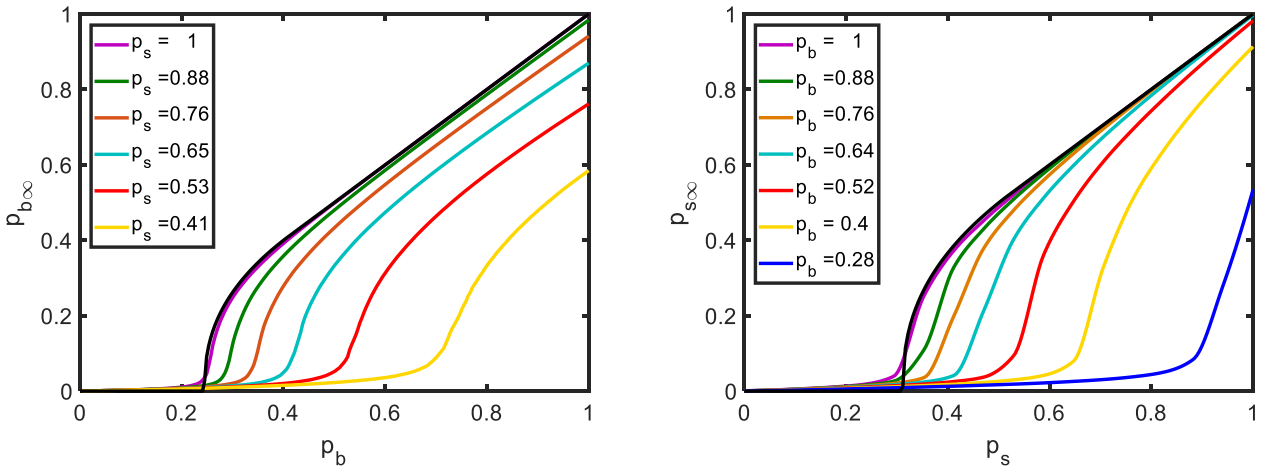

(a) (b)

Fig. 2. Numerical calculation of the infinite cluster strength during the site-bond percolation process on a simple cubic lattice: (a) bonds forming an infinite cluster ($p_{b\infty}$) against available bonds (p_b) for different proportion of available sites (p_s) compared to the analytical model (in black) during bond percolation; (b) sites forming an infinite cluster ($p_{s\infty}$) against available sites at for different proportion of available bonds compared to the analytical model (in black) during site percolation.

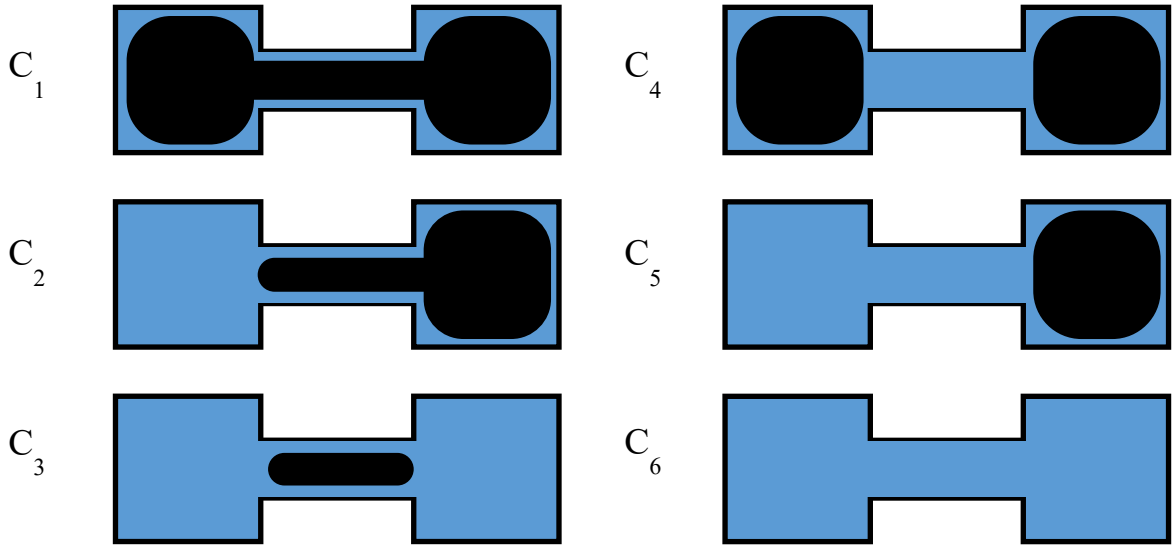

Fig. 3. Configurations of oil (in black) and water (in blue) which can exist in between two connected sites and a bond.

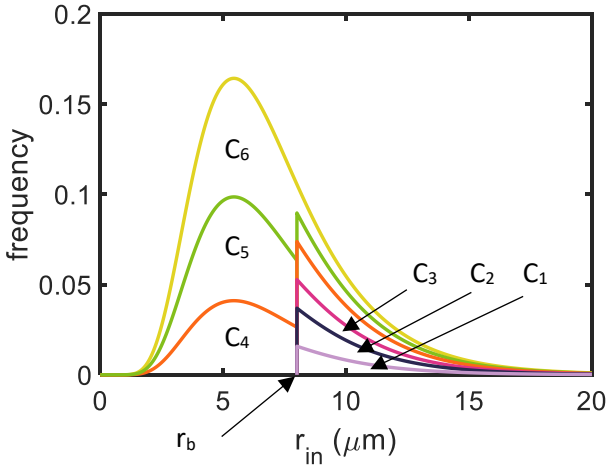

Fig. 4. Frequency of each configuration occurring at any given bond with inscribed radius r_{in}. The radius r_b is the inscribed radius of the smallest bond which can be penetrated by oil via capillary forces.

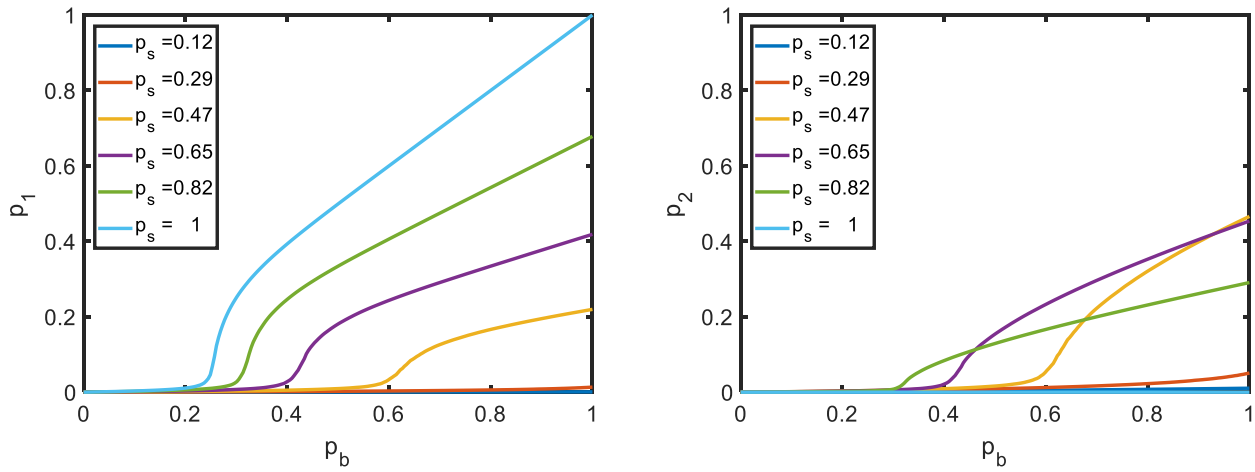

(a)

(b)

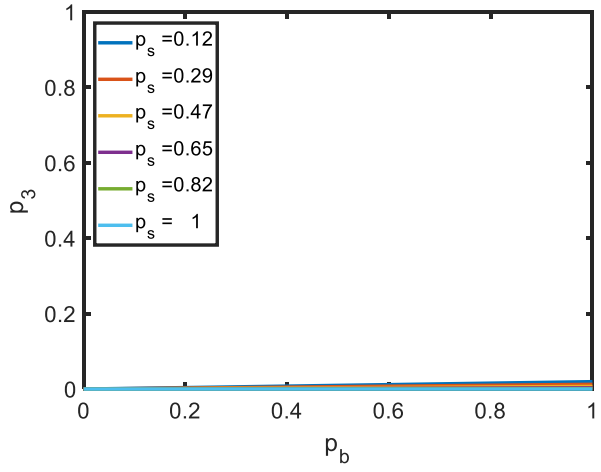

(c)

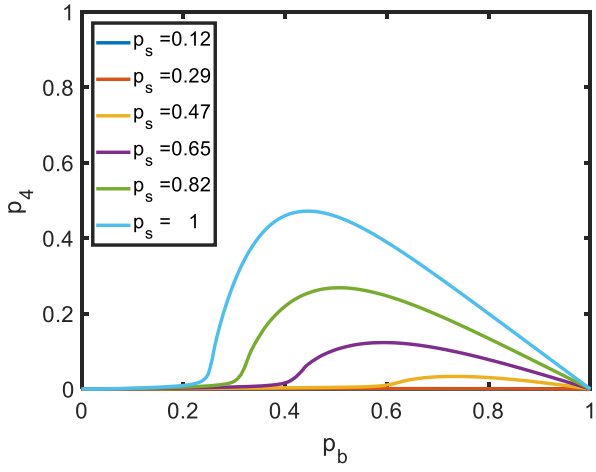

(d)

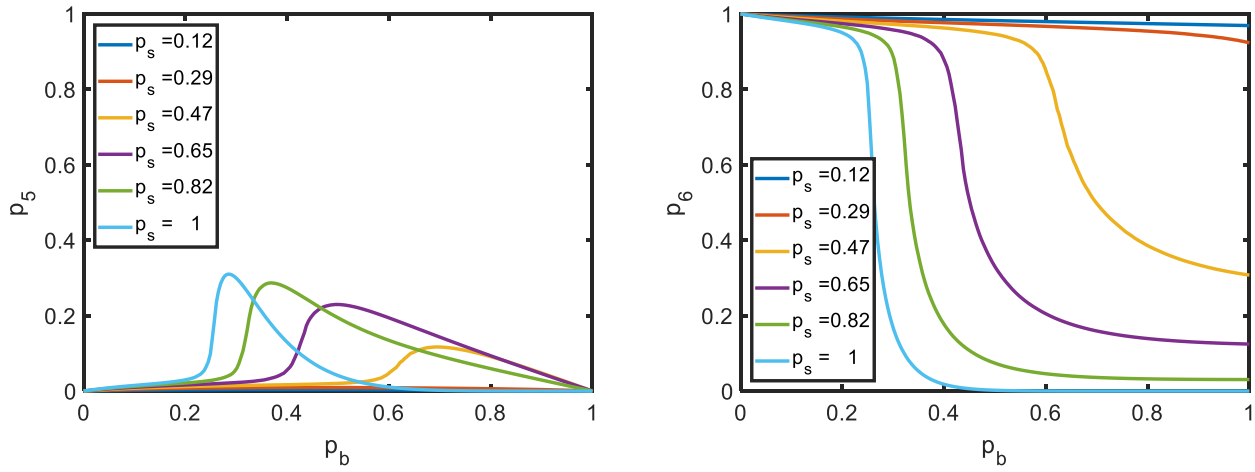

(e) (f)

Fig. 5. Numerical calculation of the probability of the configurations (as given in Fig. 3) existing: (a) C_1; (b) C_2; (c) C_3; (d) C_4; (e) C_5; (f) C_6.

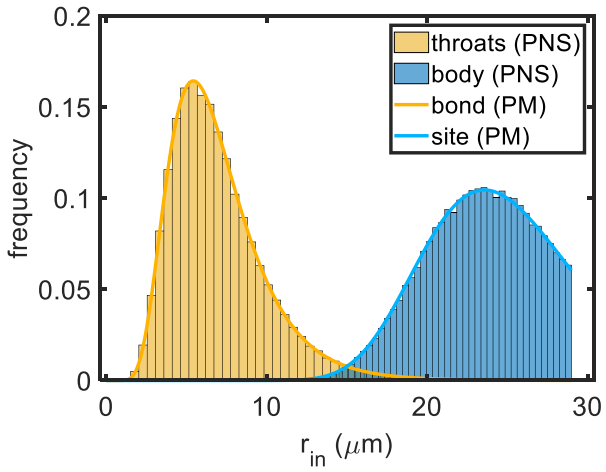

Fig. 6. Comparison of the site/bond size distributions used in percolation model (PM) compared against throat/body distributions used in pore network simulator (PNS).

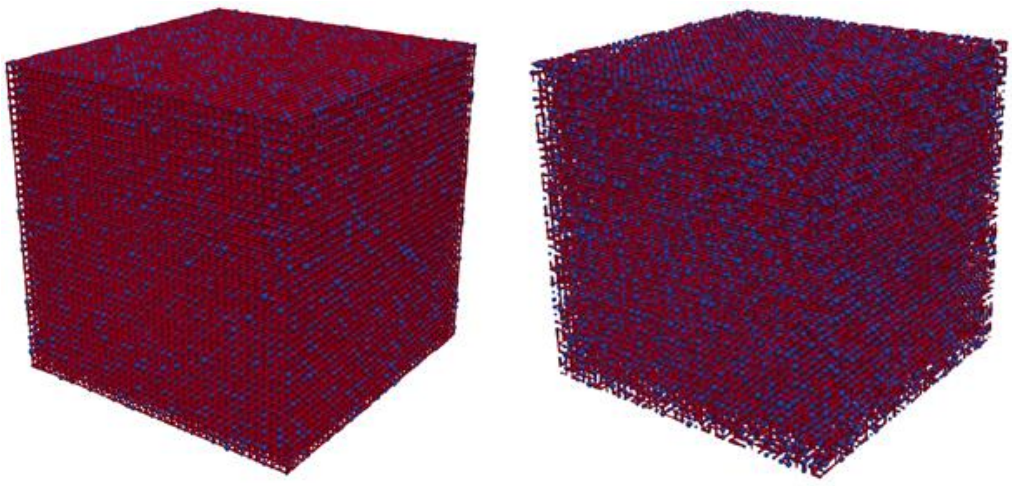

(a) (b)

Fig. 7. Visualization of the pore network used in simulation: (a) Z = 6; (b) Z = 3.

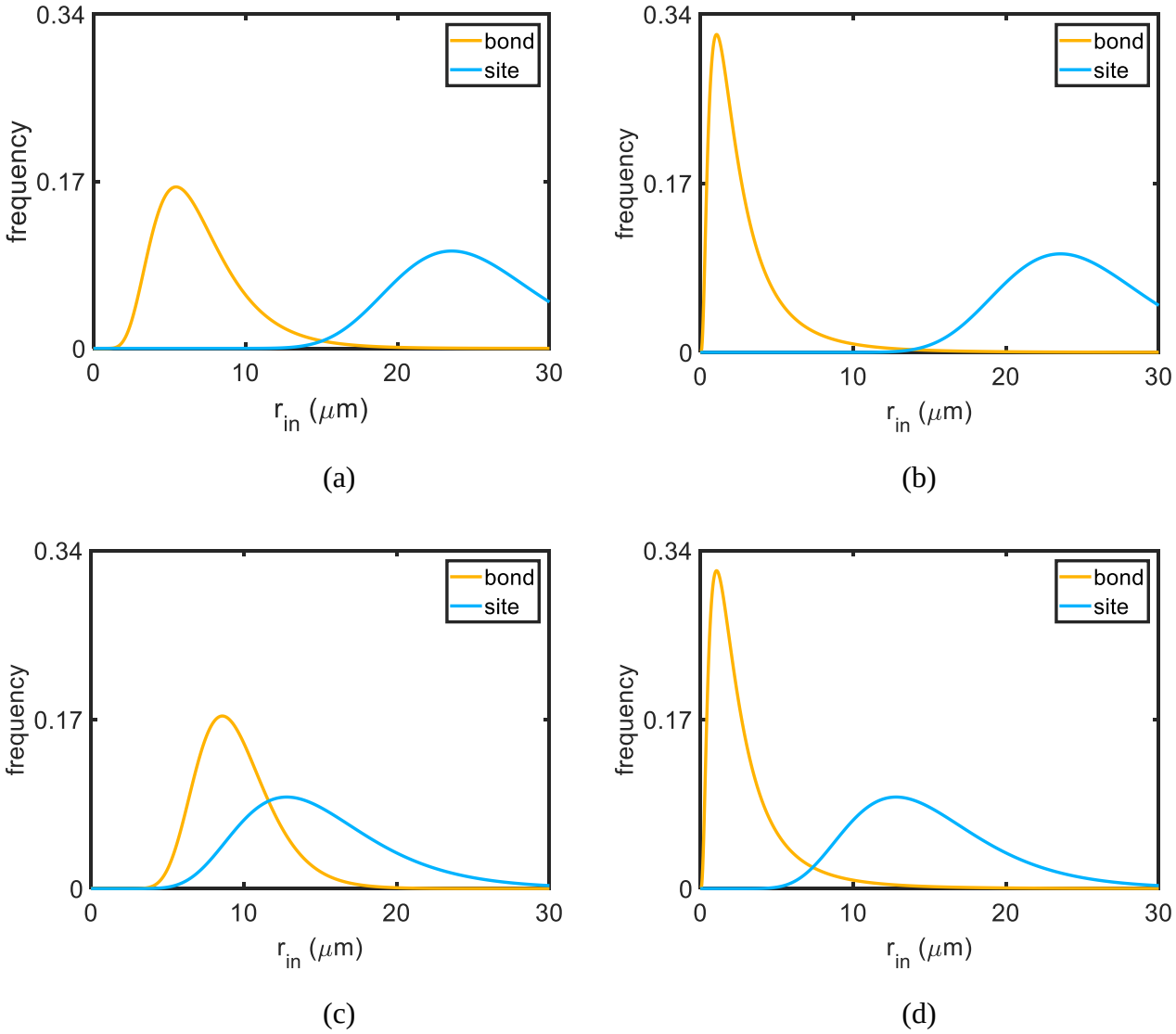

Fig. 8. Frequency of bonds and sites with inscribed radius r_{in} for: (a) distribution A; (b) distribution B; (c) distribution C; (d) distribution D.

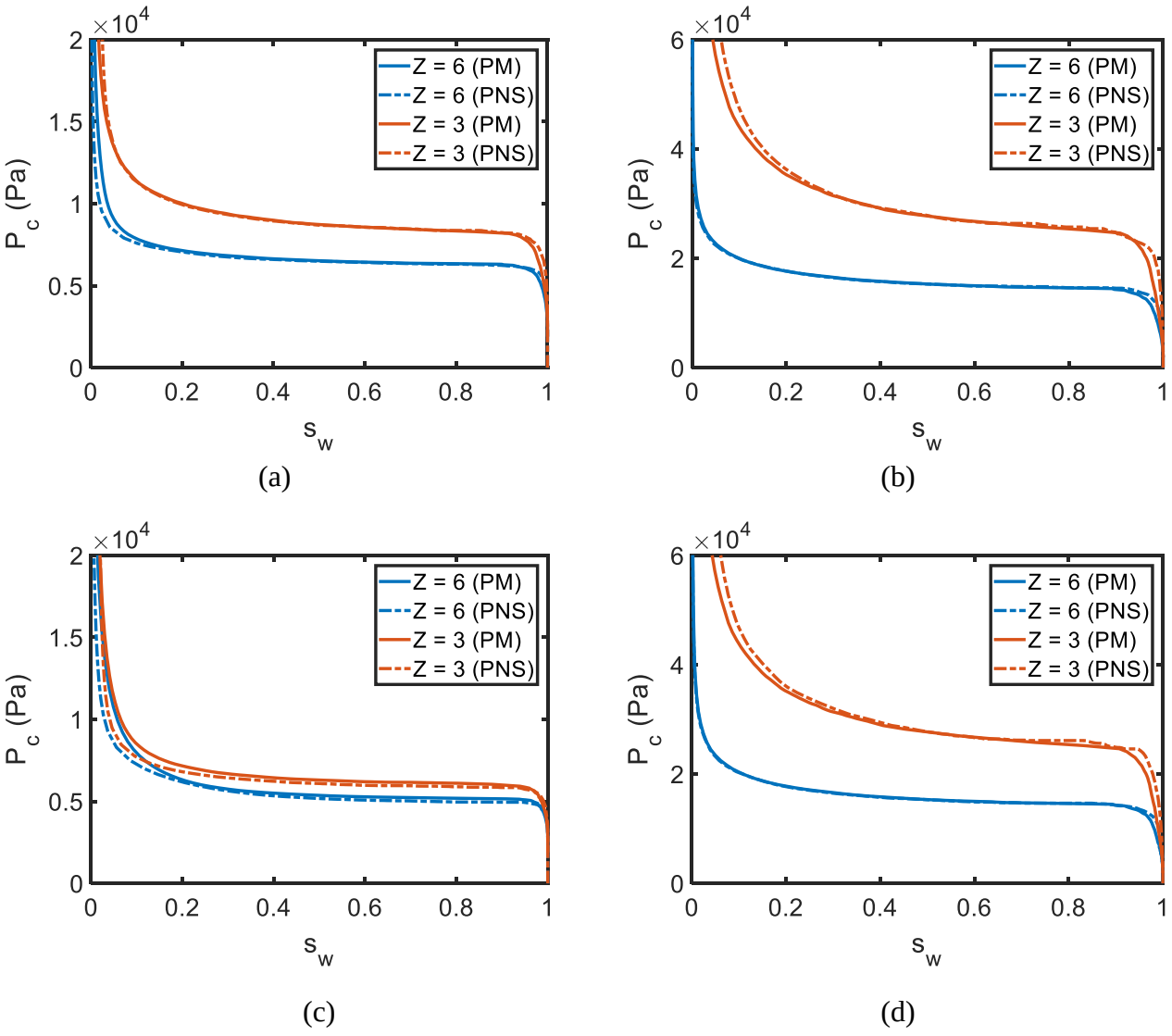

Fig. 9. Comparison between capillary pressures calculated via the pore network simulator (PNS) and via the percolation model (PM) at coordination number (Z) 3 and 6: (a) distribution A; (b) distribution B; (c) distribution C; (d) distribution D.

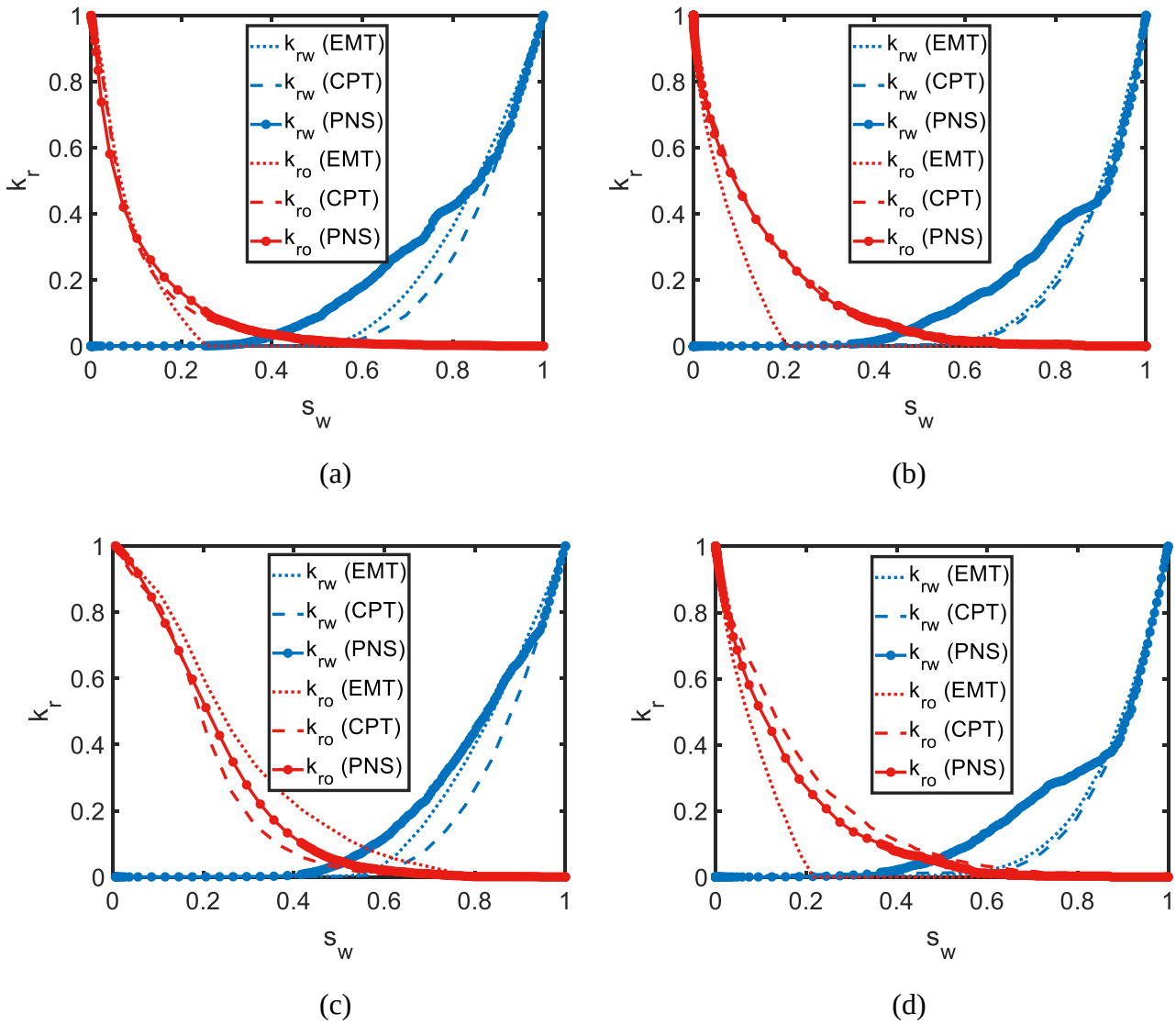

Fig. 10. Comparison between the relative permeability curves calculated via the pore network simulator (PNS) and via the bond-site percolation model with effective medium theory (EMT), with an average network coordination number Z = 6: (a) distribution A; (b) distribution B; (c) distribution C; (d) distribution D.

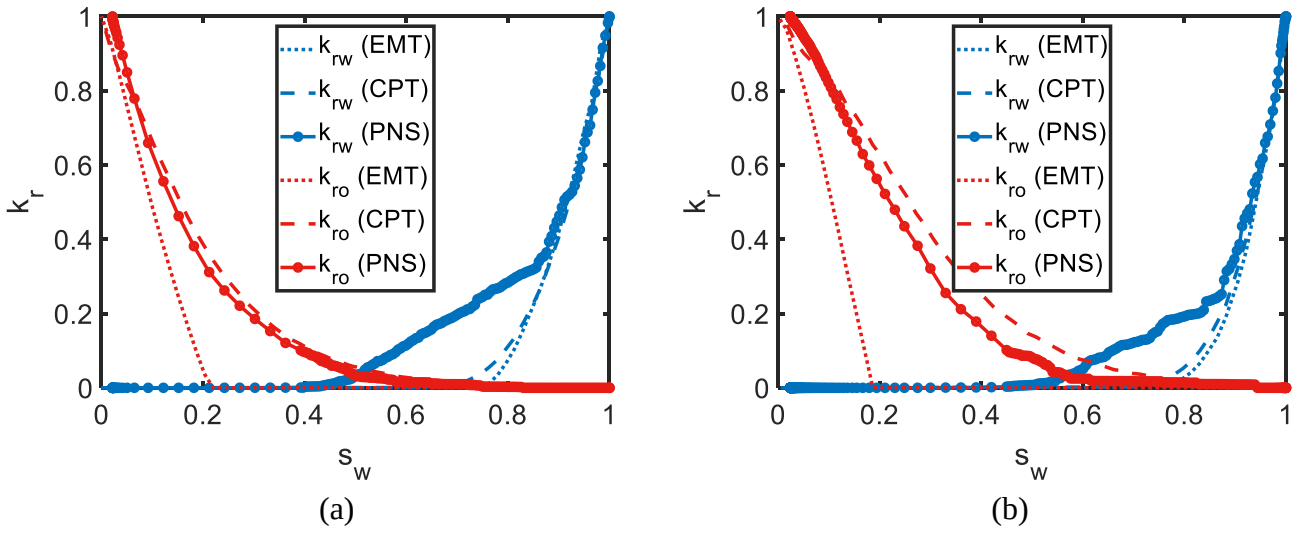

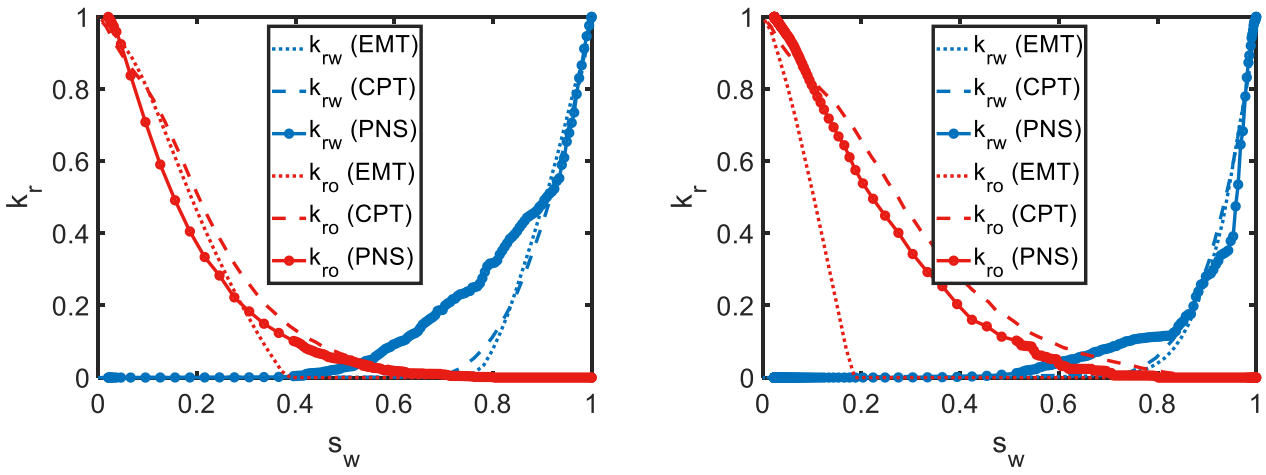

Fig. 11. Comparison between the relative permeability curves calculated via the pore network simulator (PNS) and via the bond-site percolation model with effective medium theory (EMT), with an average network coordination number Z = 3: (a) distribution A; (b) distribution B; (c) distribution C; (d) distribution D.

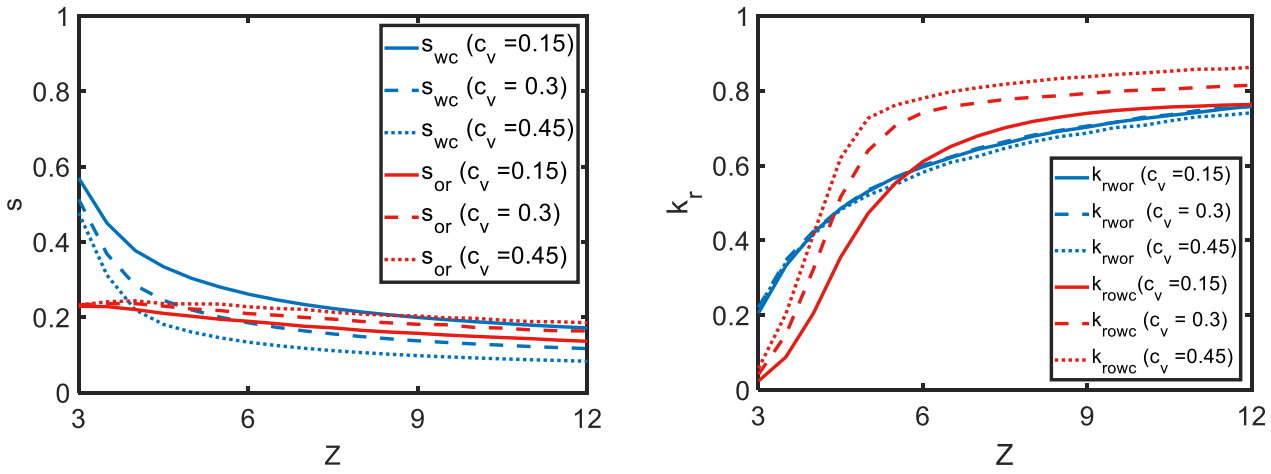

Fig. 12. Sensitivity of the end point values to coordination number as calculated by bond percolation & CPT for different coefficients of variation in bond inscribed radius: (a) end point saturations; (b) end point relative permeability.

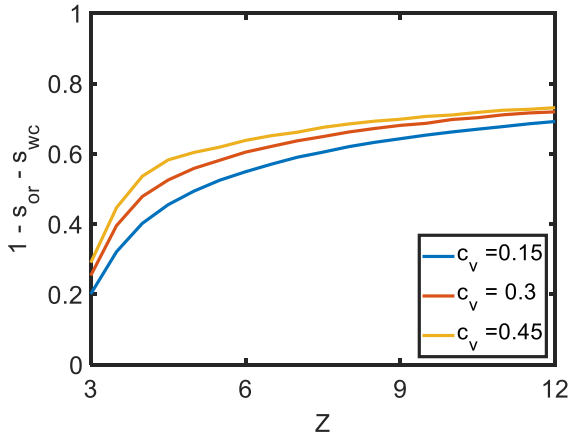

Fig. 13. Two phase saturation window as calculated by bond percolation & CPT. Sensitivity to the coordination number and the coefficient of variation for the bond radii.

7. Discussion

7.1. Summary

The thesis presented new novel analytical models for the evaluation of skin due to water block in oil and gas wells. The analytical models have been validated by comparison to experimental and numerical results, and applied for the evaluation of production and storage well inflow performance.

The third chapter was the first chapter which involved the novel aspects of the thesis. It investigated the impact of altering the contact angle on inflow performance of gas and oil wells. Altering contact angle simultaneously impacted both the capillary pressure and the relative permeability curves, which was not considered in previous publications. The first analytical model for two phase flow accounting for contact angle dependence in the capillary pressure and relative permeability curves was developed in the thesis. The model showed that the contact angle dependence on these curves will give existence to an optimal contact angle for gas and oil production. The optimal contact angle was influenced by the forms of the relative permeability curves and the capillary pressure curve. However the capillary pressure curve was only as influential as the ratio of the capillary forces over the other forces present. The third chapter only investigated when viscous and capillary forces were present. When capillary forces dominated over viscous forces, the optimal contact angle was hydrophobic. When viscous forces dominated over capillary forces, the optimal contact angle was at some intermediate value and was influenced by the forms of the water and gas relative permeability curves and the water cut.

The fourth chapter developed the analytical model incorporating gas compressibility. The effect of gas compression gives rise to a non-monotonic saturation profile. The gas phase expands as it approaches the wellbore due to pressure decline, which causes the water saturation to decrease. However, the capillary pressure also declines as it approaches the wellbore, which can cause water saturation to increase. The shape of this profile depends on the capillary-viscous ratio, relative permeability curves, water cut and the capillary pressure curve. The models allow for the design of treatment strategies of water blocked gas wells. There are many surfactant/chemical treatments in the market for reduction of interfacial tension or

alteration of contact angle of gas reservoirs. The treatment of gas wells with these chemicals will result in the alteration of the contact angle of the near wellbore region. The developed models were applied for the evaluation of the impact of piecewise-alteration of the contact angle. They show that a second capillary end effect can appear at the end of the treated zone, which negatively impacts the flow of hydrocarbon and reduces the optimal contact angle.

The results of the previous chapters are shown to be applicable to hydraulically fractured wells. Chapter five shows that when the pressure drop in the hydraulic fracture is negligible compared to the pressure drop from the reservoir to the fracture, there exists an analytical solution for water block skin under steady state flow. Two models are developed in Chapter 5. The first is the explicit model for Darcy gas-water flow into a highly conductive hydraulically fractured well, the second is a semi-analytical model for non-Darcy flow into a highly conductive hydraulically fractured well. The models show that there is a steep increase in water close to the hydraulic fracture. The percentage of skin as a result of water block can be implicitly calculated for a region around the hydraulic fracture, which can then be used for the evaluation of volume of treatment fluid required. Inertial forces are shown to reduce the water block but give rise to non-Darcy skin.

The forms of relative permeability and capillary pressure are very important in determining the optimal contact angle for gas and oil production. The forms of these curves are the result of the wettability, the pore network topology and the distribution of pore sizes. Chapter six developed the percolation model which can take into account pore network topology and size distributions. The model incorporated the impact of corner water film, network coordination number, and pore throat and pore body size distribution. The model showed that at low coordination numbers there does not exist simultaneous flow of both phases. Two methods for calculation of relative permeability were compared to pore network simulation. The first was the effective medium theory and the second was the critical path theory. Critical path theory was shown to be a better match the relative permeability curves generated by the pore network simulator.

7.2. Limitations & Future Outlook

Some of the models supplied are semi-analytical, particularly for compressible gas, where two ordinary differential equations need to be solved simultaneously in order to evaluate saturation and pressure profile. As this method is not fully explicit it limits the applicability of the model.

For all the analytical solutions supplied, the steady state assumption is invoked. This assumption does limit the application to flow periods after the pressure transient has reached the reservoir boundaries. Ultra-low permeability reservoirs can be in the transient flow regime for longer than months, which can misevaluate the impact of water blocking on well production performance. The problem can be solved numerically, however there can be future work to investigate if there exists any analytical or semi- analytical solutions for the water block problem including transient flow.

Rock compressibility was not considered but can be very important for shale and coal reservoirs and can be implemented in the model by pressure-dependent porosity.

The literature review has shown that low permeability rocks are more susceptible to water block. The literature review also shows that in ultra-low permeability rocks such as shales, molecular interactions of the pore walls can influence the capillary curvature. The Young Laplace equation needs to be modified to account for this effect. It will cause a change in the capillary entry pressure for small pore throats, which will change the capillary pressure and relative permeability curves.

At low pore throat sizes and low pressures the Hagen-Poiseuille equation breaks down and the assumption of zero flow at the pore walls is no longer valid. The thesis has incorporated a simple empirical model to account for gas slip at the pore walls with the empirical klinkenberg slip relationship, but further work can be done to account for Knudsen diffusive flux.

The capillary pressure and relative permeability models used in the first 4 chapters were capillary bundle models with fractional wettability assumed. The capillary bundle model is not representative of porous media. While work in this thesis later develops a percolation model which takes into account network topology, the

fractional wettability of the network was not considered. The future opportunity of this work can be in developing a sophisticated percolation model for evaluation of the relative permeability and capillary pressure which accounts for fractional wettability. This percolation model can be applied in the analytical models derived previously to study impacts of pore size distribution, pore network coordination number and wettability on water block skin.

The percolation model presented in this thesis utilizes the results of numerical calculation to calculate the infinite cluster density during site bond percolation. Empirical expressions for the infinite cluster density can be developed for site-bond percolation in simple cubic lattices, which can allow for analytical expressions for capillary pressure developed from site bond percolation models.

Currently none of the percolation models developed take into account imbibition. The imbibition process can be used to describe fracture fluid, drill fluid or completion fluid loss into a hydrocarbon bearing reservoir. The introduction of foreign waters to reservoir can cause high water block. The modelling of the imbibition of foreign water into the reservoir can be used to evaluate skin due to water block before steady state conditions.

The thesis has covered analytical solutions for water block under steady state conditions. The areas for future work in the area of water-block evaluation:

1. Development of analytical or semi-analytical models for non-steady flow accounting for capillary entrapment of water close to the hydraulic fracture and/or wellbore.
2. Development of percolation model accounting for wettability, pore network topology, pore size distributions and imbibition for calculation of capillary pressure and relative permeability curves.
3. Incorporation of nano-scale effects such as gas slip, Knudsen-diffusive flow and molecular interactions on the capillary curvature in the aforementioned models.
4. Incorporation of rock compressibility into the aforementioned models.

8. Conclusions

The analytical modelling of the water block phenomenon during two phase steady state flow allow to make the following conclusions:

1. There exists an optimal contact angle for maximising oil or gas production during steady state commingled production of oil and water or gas and water. The optimal contact angle will depend on factors such as the initial rock wettability, ratio of capillary to viscous forces, forms of the Leverett J function, and forms of the relative permeability curves.
2. The optimal contact angle for maximising oil or gas production will increase as the ratio of capillary to viscous forces increases. When the capillary forces are negligible, the optimal contact angle will be determined by the competition between the viscosity ratio of the two phases, the forms of the relative permeability curves, and the water cut.
3. Piece-wise alteration of wettability causes the existence of a second capillary end effect outside the altered zone. This second end effect can negatively impact gas flow. For this reason, the optimal contact angle for gas production is lower in the piece-wise altered case than for the case where the wettability is changed in the entire reservoir.
4. The competition between the capillary forces and the expansion of a compressible gas phase close to the wellbore can result in a non-monotonic saturation profile. This effect is more prominent when the capillary-viscous ratio is low.
5. When there is no water production, alteration of wettability to completely hydrophobic can remove the water block. For intermediate values of water cut, the optimal contact angle will be some intermediate value.
6. There is explicit formulae for Darcy flow of gas towards a hydraulically fractured vertical well accounting for capillary trapped liquid. The saturation and pressure values can be determined implicitly.
7. The competing effects of gas compression and inertial forces result in a non-monotonic relationship between water block skin and the dimensionless Forchheimer number.
8. The oil relative permeability calculated by critical path theory matches the relative permeability modelled by pore network simulation better than effective medium theory. The assumptions of critical path theory are more suitable for the highly heterogeneous distribution of conductivity which is typical for natural porous media.
9. There is no simultaneous two phase flow when the average coordination number of the pore network is small. This is due to the high percolation threshold which occurs at small coordination numbers.